

DYNAMIC LOADS IN LAYERED HALFSPACES

by

Sandra Hull Seale

B.S.E., Princeton University
(1981)

S.M., Massachusetts Institute of Technology
(1983)

SUBMITTED TO THE DEPARTMENT OF CIVIL
ENGINEERING IN PARTIAL FULFILLMENT OF THE
REQUIREMENTS FOR THE DEGREE OF

DOCTOR OF PHILOSOPHY

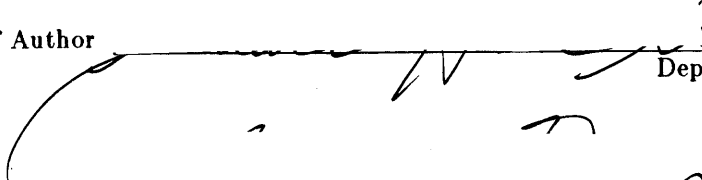
at the

MASSACHUSETTS INSTITUTE OF TECHNOLOGY

September 1985

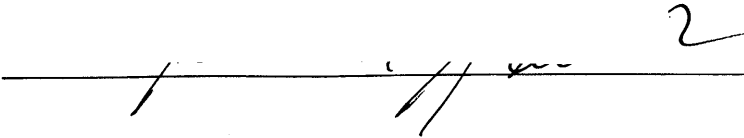
Copyright © 1985 M.I.T.

Signature of Author



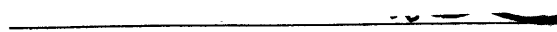
Department of Civil Engineering
September 18, 1985

Certified by



Eduardo A. Kausel
Thesis Supervisor

Accepted by



François M. M. Morel

MASSACHUSETTS INSTITUTE
OF TECHNOLOGY

Chairman, Department Committee on Graduate Students

JAN 02 1986

ARCHIVES

LIBRARIES

Dynamic Loads in Layered Halfspaces

by

Sandra Hull Seale

Submitted to the Department of Civil Engineering on September 18, 1985 in partial fulfillment of the requirements for the degree of Doctor of Philosophy.

Abstract

An approximate solution of Lamb's problem of vibrations in an elastic halfspace is presented. The stiffness method of Kausel and Roësset (1981) is used to model a layered soil stratum. The layers are represented by stiffness matrices that are algebraic in the frequency-wavenumber domain. The global stiffness matrix for the soil system is obtained by overlapping the layer matrices at common degrees of freedom. Once the stiffness matrix is inverted with a spectral decomposition, displacements are computed by means of an inverse transform that exists in closed form. The stiffness matrix for an elastic halfspace is derived by taking the Taylor series expansion of the true stiffness about the horizontal wavenumber. The solution for static loads in layered halfspaces is derived by examining the limit of the dynamic case when frequency goes to zero. Modifications of the stiffness matrices for cross-anisotropic materials are presented. Anisotropy is found to cause only changes to the stiffness matrices themselves and not to the underlying mathematics of the displacement calculations.

Examples of displacements for dynamic and static loads are computed and compared to analytic solutions (when they exist). Comparisons show that the discrete stiffness method gives very accurate results with a relatively small ($\simeq 10$) number of sublayers in the overlying stratum. A discussion of the limitations of this method and its application to future research topics is presented.

Thesis Supervisor: Eduardo A. Kausel
Title: Associate Professor

Acknowledgments

I wish to thank Professor Eduardo Kausel, who was superb in his role of advisor. He was generous with his time and inspired in his guidance. I thoroughly enjoyed working and exercising with Professor Kausel.

My financial support for the past three years has been provided by an Exxon Teaching Fellowship.



Mr Clevver he says to Eusa, 'Thats a guvner lot of knowing youre inputting in to that box parbly theres knowing a nuff in there for any kynd of thing.'

Eusa says, 'Thats about it. I dont think theres many things you cudnt do with that knowing. You cud do any thing at all you cud make boats in the air or you cud blow the worl a part.'

Mr Clevver says, 'Scatter my datter that cernly is intersting. Eusa tel me some thing tho. Whyd you input all that knowing out of your head in to that box? Whynt you keap it in your head wunt it be safer there?'

Eusa says, 'Wel you see I cant jus keap this knowing in my head Ive got things to do with it Ive got to work it a roun. Ive got to work the E qwations and the low cations Ive got to comb the nations of it. Which I cant do all that oansome in my head thats why I nead this box its going to do the hevvy head work for my new projeck.'

Table of Contents

Abstract	2
Acknowledgments	3
Table of Contents	4
List of Figures	7
List of Tables	9
1. Introduction	10
2. Review of Previous Work	14
2.1 Geometry and Material Properties	14
2.2 The Stiffness Method	17
2.2.1 In-plane Motion	17
2.2.2 Anti-plane Motion	19
2.2.3 Development of the Stiffness Method	20
2.3 Green's Functions for a Layered Stratum	23
2.3.1 Algebraic Stiffness Matrix	23
2.3.2 Solution for Displacements	29
3. Dynamic Loads in Layered Halfspaces	34
3.1 Derivation of the Paraxial Approximation	35
3.2 Characteristics of the Paraxial Approximation	36
3.2.1 Anti-plane Case	36
3.2.2 In-plane Case	40
3.3 Computation of Displacements	53
3.3.1 Examples	53
3.3.2 Variation of Physical Parameters	53
4.	68
The Limiting Case: Static Loads in Layered Halfspaces	
4.1 Introduction	68
4.2 Anti-plane Case	69
4.2.1 Eigenvalue Problem	69
4.2.2 Eigenvalues	74
4.2.3 Loading	75
4.3 In-plane Case	78
4.3.1 Eigenvalue Problem	78
4.3.2 Eigenvalues	83
4.3.3 Loading	83
4.4 Displacements due to Static Point Loads	85
4.4.1 Horizontal Point Load	86

4.4.2 Vertical Point Load	88
4.4.3 Examples	90
4.5 Displacements due to Static Disk Loads	100
4.6 Conclusions	106
5.	109
Dynamic Loads in Cross-Anisotropic Layered Halfspaces	
5.1 Introduction	109
5.2 Wave Propagation in Cross-Anisotropic Halfspaces	111
5.2.1 Anti-plane Motion	113
5.2.2 In-plane motion	114
5.3 Algebraic Stiffness Matrices	119
5.3.1 Layer Matrices	119
5.3.2 Halfspace Matrices	120
5.4 Dynamic Displacements	123
5.5 Static Loads in Cross-Anisotropic Layered Halfspaces	133
6. Conclusions	139
Appendix A.	142
Proof that Orthogonality Conditions and Flexibilities For the Static Halfspace Reduce to Those of the Rigid Base Case	
A.1 Anti-plane Case	142
A.2 In-plane case	144
Appendix B.	147
Static Eigenvalues for the Anti-plane Case of a Homogeneous Stratum on an Elastic Halfspace	
B.1 Discrete Case	147
B.1.1 Roots of the Eigenvalue Problem	147
B.1.2 Real Roots	153
B.2 Continuum Solution	161
B.2.1 Eigenvalues	161
B.2.2 Modal Shapes for $\gamma < 1$	164
Appendix C. Solution of the Discrete Static Eigenvalue Problem	165
C.1 Iteration for Proximal and/or Complex Conjugate Pairs of Eigenvalues	165
C.2 Cleaning Eigenvectors	168
C.2.1 Distinct Eigenvalues	169
C.2.2 Complex Conjugate Eigenvalues	171
C.2.3 One Complex Conjugate Eigenvalue and One Distinct Eigenvalue	173
C.3 The Static Eigenvalue Problem	174

Appendix D. Solutions of Integrals for Static Displacements	177
D.1 Integrals for Static Point Loads	177
D.1.1 Solution of I_{2l}	178
D.1.2 Solution of I_{3l}	179
D.1.3 Solution of I_{1l}	179
D.2 Approximations of Integrals for Static Disk Loads	180
Appendix E.	182
Numerical Evaluation of Struve and Neumann Functions	
E.1 Struve Functions	182
E.1.1 Ascending Series	183
E.1.2 Asymptotic Expansion	185
E.1.3 Analytic Continuation	186
E.2 Neumann Functions	188
E.2.1 Ascending Series	188
E.2.2 Asymptotic Expansion	194
E.3 Hankel Functions	195
Appendix F. Calculation of the Paraxial Approximation	196
F.1 Anti-plane Case	196
F.2 In-plane Case	197
Appendix G.	203
Proof that the Paraxial Approximation is Consistent with the Clayton-Engquist Approximation	
G.1 Anti-plane Case	203
G.1.1 Clayton-Engquist Method	203
G.1.2 Stiffness Method	204
G.2 In-plane Case	205
G.2.1 Clayton-Engquist Method	205
G.2.2 Stiffness Method	207
References	209

List of Figures

Figure 2-1:	Geometry of a Layered Halfspace	15
Figure 2-2:	Geometry of a Layer	16
Figure 3-1:	Real Part of the True Anti-plane Stiffness	38
Figure 3-2:	Imaginary Parts of the True and the Approximate Anti-plane Stiffness	39
Figure 3-3:	Real Part of k_{11}	42
Figure 3-4:	Imaginary Part of k_{11}	43
Figure 3-5:	Real Part of k_{12}	44
Figure 3-6:	Imaginary Part of k_{12}	45
Figure 3-7:	Real Part of k_{22}	46
Figure 3-8:	Imaginary Part of k_{22}	47
Figure 3-9:	Rayleigh Wave Roots for the True and Approximate Stiffness	49
Figure 3-10:	Spurious Root of the Approximation	50
Figure 3-11:	Determinant of the Imaginary Part of the Stiffness for $\nu = 1/4$	51
Figure 3-12:	Determinant of the Imaginary Part of the Stiffness for $\nu = 1/3$	52
Figure 3-13:	Real Part of the Vertical Displacement at $\rho = 0$	54
Figure 3-14:	Imaginary Part of the Vertical Displacement at $\rho = 0$	55
Figure 3-15:	Real Part of the Vertical Displacement at $\rho = 1.0$	56
Figure 3-16:	Imaginary Part of the Vertical Displacement at $\rho = 1.0$	57
Figure 3-17:	Real Part of the Horizontal Displacement at $\rho = 0$	58
Figure 3-18:	Imaginary Part of the Horizontal Displacement at $\rho = 0$	59
Figure 3-19:	Real Part of the Horizontal Displacement at $\rho = 1.0$	60
Figure 3-20:	Imaginary Part of the Horizontal Displacement at $\rho = 1.0$	61
Figure 3-21:	True and Approximate Solutions for Vertical Displacements at the Origin	63
Figure 3-22:	Displacements Calculated with the Paraxial Approximation for Different Layer Depths	64
Figure 3-23:	Displacements Calculated with the Paraxial Approximation for Different Poisson Ratios	65
Figure 4-1:	Eigenvalues of Anti-plane Modes for $N = 1$ to 12	76
Figure 4-2:	Eigenvalues of In-Plane Modes for $N = 12$	84
Figure 4-3:	Geometry of Homogeneous Halfspace Subjected to Static Point Loads	92
Figure 4-4:	Radial Displacements due to Radial Point Load at the Surface	94
Figure 4-5:	Tangential Displacements due to Radial Point Load at the Surface	95
Figure 4-6:	Vertical Displacements due to Vertical Point Load at the Surface	96
Figure 4-7:	Radial Displacements due to Vertical Point Load at the Surface	97
Figure 4-8:	Vertical Displacements due to Vertical Buried Point Load	98
Figure 4-9:	Radial Displacements due to Radial Buried Point Load	99
Figure 4-10:	Displacements at the Surface due to Vertical Point Load, $G_r = 2.0$	101
Figure 4-11:	Displacements at the Surface due to Radial Point Load, $G_r = 2.0$	102
Figure 4-12:	Displacements at the Surface due to Vertical Point Load, $G_1 = 2.0$	103
Figure 4-13:	Displacements at the Surface due to Radial Point Load, $G_1 = 2.0$	104
Figure 4-14:	Vertical Displacements versus Depth	107
Figure 5-1:	Real Part of the Vertical Displacement at $\rho = 0$, Anisotropic Stratum	125
Figure 5-2:	Real Part of the Horizontal Displacement at $\rho = 0$, Anisotropic Stratum	126
Figure 5-3:	Real Part of the Vertical Displacement at $\rho = 1$, Anisotropic Stratum	127
Figure 5-4:	Real Part of the Horizontal Displacement at $\rho = 1$, Anisotropic Stratum	128

Figure 5-5:	Real Part of the Vertical Displacement at $\rho = 0$, Anisotropic Halfspace	129
Figure 5-6:	Real Part of the Horizontal Displacement at $\rho = 0$, Anisotropic Halfspace	130
Figure 5-7:	Real Part of the Vertical Displacement at $\rho = 1$, Anisotropic Halfspace	131
Figure 5-8:	Real Part of the Horizontal Displacement at $\rho = 1$, Anisotropic Halfspace	132
Figure 5-9:	Horizontal Displacement due to Static Horizontal Point Load at the Surface	137
Figure 5-10:	Vertical Displacement due to Static Vertical Point Load at the Surface	138
Figure B-1:	Homogenous Layer Overlying an Elastic Halfspace	148
Figure B-2:	The Root α of Equation B-31 and kh versus α	155
Figure B-3:	The Root of Equation B-49	159
Figure B-4:	Wavenumber kh	160
Figure B-5:	Wavenumber kh versus γ	162
Figure E-1:	Mapping z from the Right Half Plane to the Left	187
Figure E-2:	The Functions $F_0(z)$ and $F_1(z)$ for Real Argument	189
Figure E-3:	Contours of the Real Part of $F_0(z)$	190
Figure E-4:	Contours of the Imaginary Part of $F_0(z)$	191
Figure E-5:	Contours of the Real Part of $F_1(z)$	192
Figure E-6:	Contours of the Imaginary Part of $F_1(z)$	193

List of Tables

Table 2-I:	Algebraic Layer Stiffness Matrices A and B	24
Table 2-II:	Algebraic Layer Stiffness Matrices G and M	25
Table 2-III:	Integrals Used to Compute Dynamic Displacements	32
Table 4-I:	Integrals Used to Compute Static Displacements	91
Table 5-I:	Algebraic Layer Stiffness Matrices A , B and G	121

Chapter 1

Introduction

The area of geodynamics concerning displacements in an elastic halfspace due to transient loading is known as "Lamb's problem", after the classic work of Lamb (1904). Much work has been done in this field, most of it by seismologists who were interested in describing the propagation of seismic waves in the Earth's crust. These solutions are usually not applicable to engineering problems because of restrictions on the geometry of the soil. The most well known example is the solution of Lamb's problem developed by Cagniard (1962). This method obtains time-dependent displacements due to a transient point source within a solid composed of two semi-infinite homogeneous media in welded contact. When one of these media is assumed to be a vacuum, the solution for a halfspace results.

An examination of the Cagniard method illustrates the features of the transient solution that are important to the study of seismology. The application of this technique starts with the Laplace transforms with respect to time of the wave equation, the boundary conditions and the source. The homogeneous and particular solutions are derived in the transform domain and the boundary conditions are applied. The inverse Laplace transform is not performed, as this would be impossible to do in closed form for most cases. Rather, the variables of the solutions are changed so that the solution takes the form of a Laplace transform, and the inverse transform can be extracted by inspection. This change of variables usually requires several applications of conformal mapping and contour integration, which render the mathematics of Cagniard's method formidable. Dix (1954) presented a simple application of Cagniard's technique to the solution of the scalar wave generated by a point source in an infinite medium. Dix also explained how the solution for a general transient load can be obtained by applying the Duhamel integral to the solution for a step load. deHoop (1962) modified the method of Cagniard by applying Fourier transforms to the

spatial variables as well as a Laplace transform with respect to time. The inverse Fourier transforms are then manipulated with changes of variables into a Laplace transform and the solution is extracted by inspection. deHoop also applied his method to the solution of a scalar wave in an infinite medium.

Johnson (1974) presented the full three-dimensional solution, derived with the Cagniard-deHoop method, for displacements in a halfspace due to a unit pulse. In this work, the advantages of this technique to the study of seismology become clear. The solution for displacements is given as the sum of six wave forms: incident P and S waves and reflected PP, SS, PS, and SP waves. Thus the progress of a particular wave can easily be examined by separating this wave from the displacement solutions. Although the solution method tends to lose physical meaning during the multiple integrals performed in the complex plane, the final result for displacements is expressed in terms of normal modes of wave propagation that are easily understood. The references cited above give examples of displacement solutions that exist in closed form for special cases (e.g. at the surface). The general solution given by Johnson contains an integral which must be evaluated numerically. The fact that the Cagniard-deHoop method is restricted to a homogeneous halfspace and requires numerical integration makes it less practical for engineering applications where displacements in layered soils are desired.

Another solution for dynamic loads in a homogeneous halfspace was developed by Pinney (1954). Integral solutions for layered halfspaces have been given by Bouchon (1981), Luco and Apsel (1983) and Apsel and Luco (1983). Alekseyev and Mikhaylenko (1976/1977) developed a procedure that can be used in a finite difference formulation and Whittaker and Christiano (1979) employ the integral Green's function of the halfspace in a finite element method for flexible plates. All of the above methods require numerical integrations of improper integrals. This is a difficult problem, since the integrands involve transcendental functions which themselves must be evaluated numerically and the kernels may be "wavy", leading to high computational effort for proper resolution of the integrals.

Transfer matrix techniques are another approach to the problem of displacements in layered halfspaces subjected to dynamic loads. Thomson (1950) and Haskell (1953) developed a transfer matrix that relates the state vector (the stresses and displacements on an interface) of a layer to the state of the layer above it. The elements of the matrix are transcendental functions of the frequency ω , wavenumber k and layer properties. Since the matrix is written in the frequency-wavenumber domain, integral transforms are required to obtain displacements in the space-time domain. Applications of the transfer matrix method have been presented by Harkrider (1964), Haskell (1964), Knopoff (1964) and Dunkin (1965). Although the matrix method simplifies the problem of layering, numerical integration is still required to obtain displacements.

The starting point for the solution method described in this paper is a stiffness matrix derived from the Haskell-Thomson transfer matrix by Kausel and Roësset (1981). Elements of the transfer matrix are rearranged so that stresses on two adjacent interfaces are related to displacements on the interfaces via the stiffness matrix. Then stiffness matrices of the individual layers are overlapped to form a global stiffness matrix for the soil system. The stiffness method is analogous to the matrix techniques applied to problems in structural dynamics. Displacements are computed with numerical integration. Details of the method are presented in Chapter 2.

When the thicknesses of the layers in the soil are small compared to the wavelengths of interest, the transcendental functions in the stiffness matrix can be simplified to algebraic functions of the wavenumber k . This is accomplished by making the assumption that the displacements are piecewise linear in the vertical direction. The algebraic stiffness matrices which result were first presented by Lysmer and Waas (1972). Waas (1972) and Kausel (1974) also derived these matrices. The matrices have been used to represent the behavior of semi-infinite boundaries in finite element analyses by Drake (1972), Schlue (1979), and Tassoulas (1981).

The algebraic stiffness matrices have also been applied by Kausel and Peek (1982b) to obtain Green's function solutions of layered soils resting on a rigid base and subjected to dynamic loads. The method described here and in the above reference is a specialization of the one presented by

Kausel (1981). The global stiffness matrix of the stratum is assembled and the harmonic applied load is transformed into the wavenumber domain. The stiffness matrix is inverted with a spectral decomposition in terms of the natural wavenumbers and propagation modes (the eigenvalues and eigenvectors of the stiffness matrix). The inverse integral transform is then performed to yield displacements. The principal advantage of this method is that the inverse transforms exist in *closed form*, thus increasing the speed and accuracy of the procedure. This method was applied by Kausel and Peek (1982a) to obtain Green's functions for use in a boundary integral method for layered soils.

The technique described above has been limited to cases of a soil stratum resting on a rigid base, since no thin layer approximation can be made to a halfspace. This paper describes an extension of the method to dynamic problems of layered soils resting on a viscoelastic halfspace. The algebraic expression of the halfspace stiffness is obtained by taking a Taylor series expansion of the true transcendental stiffness. Then a solution for static loads in layered halfspaces is obtained by evaluating the dynamic case in the limit when the frequency w goes to zero. Finally, an extension of the method for anisotropic media with as many as five elastic constants is presented.

This method for computing displacements due to dynamic loads in layered halfspaces is an engineering solution to a well known problem. The accuracy and speed of the solution method make it useful for a variety of engineering problems which are described in this paper.

Chapter 2

Review of Previous Work

In this chapter the assumptions and the mathematics leading to the Green's function solution of the stratum are presented. For more detailed theory on the propagation of waves in elastic media, the reader is referred to Aki (1980), Båth (1979), Graff (1975), Love (1944), Love (1967), Bullen (1963) and Pao (1983). Studies of the propagation of waves in layered media can be found in Brekhovskih (1980), Ewing et. al. (1952) and Roësset and Kausel (1980). The essential mathematics, distilled from the above references, are given below.

2.1 Geometry and Material Properties

The geometry of the halfspace is shown in Figure 2-1. The surface of the halfspace, where $z = 0$, is the x - y plane in Cartesian coordinates, or the ρ - θ plane in cylindrical coordinates. The cross-section of the halfspace, in Figure 2-1 is the z - x or z - ρ plane. The stratum resting on the halfspace has total depth H and is subdivided into N parallel layers. The layers are numbered sequentially with layer 1 being at the surface and layer N being above the halfspace. The layers are in "welded" contact such that displacements and stresses are continuous across the layer interfaces. Figure 2-2 shows the geometry of an individual layer with loads and displacements at the interfaces. Each layer i has depth h_i and the interface elevations are z_i and z_{i+1} .

The individual layers are homogeneous. Each layer i has mass density denoted by ρ_i . For isotropic layers (see Chapter 5 for a discussion of anisotropic materials), each layer has Lamé constants λ_i and G_i , with the corresponding Poisson ratio ν_i and elastic modulus E_i . To model the dissipative behavior of soils, we use the complex Lamé moduli

Figure 2-1: Geometry of a Layered Halfspace

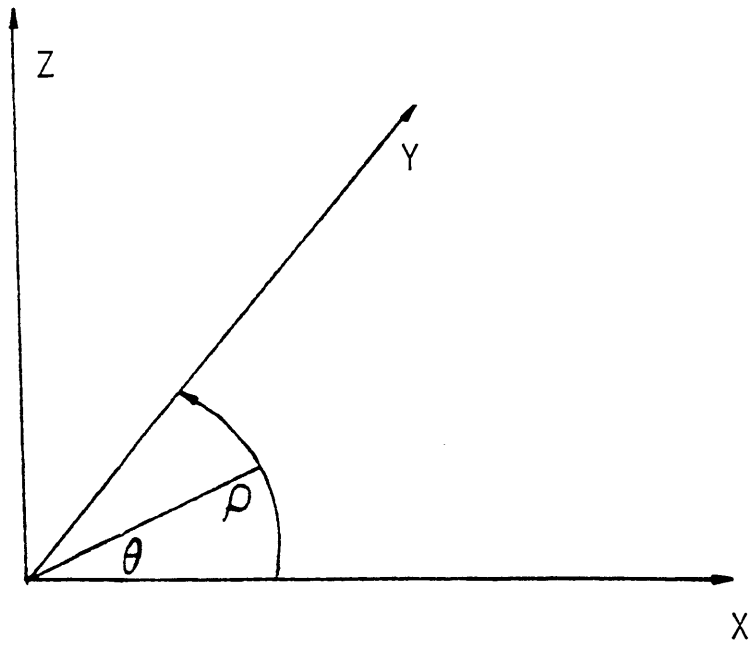
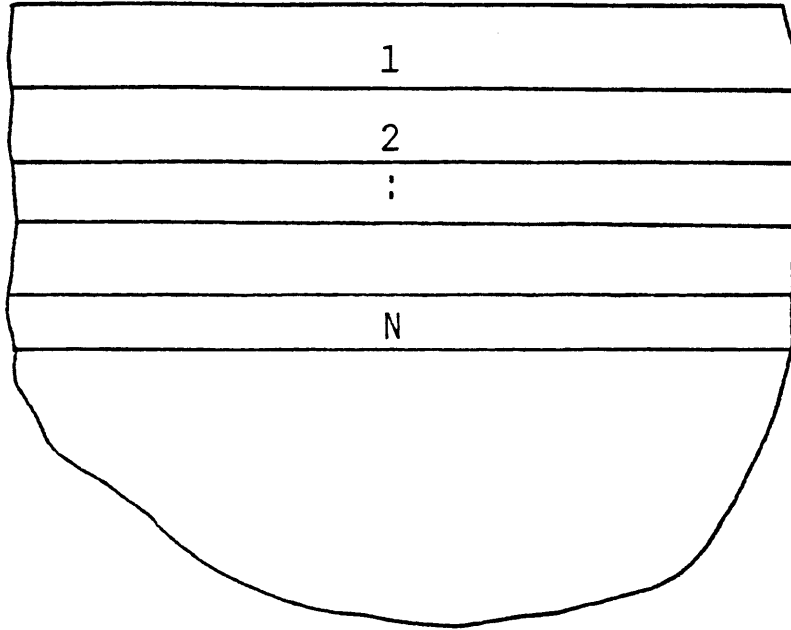
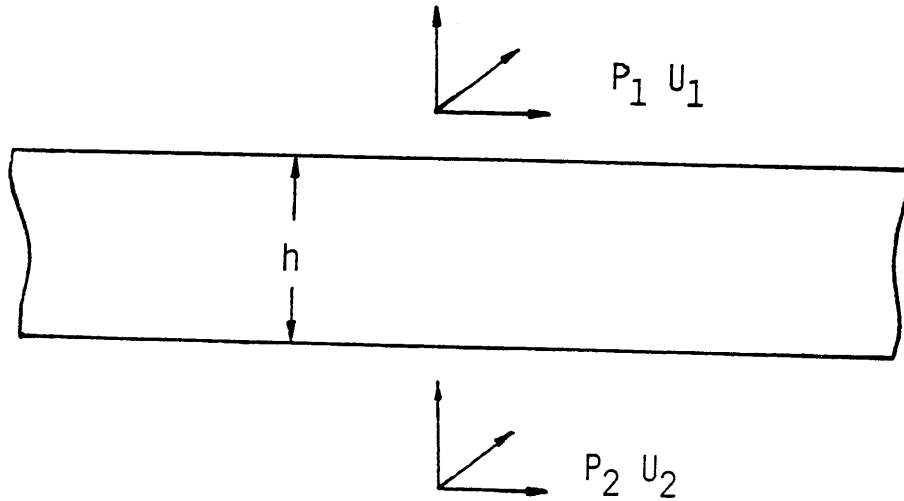


Figure 2-2: Geometry of a Layer



$$\begin{aligned}\lambda^c &= (1 + 2i\beta)\lambda \\ G^c &= (1 + 2i\beta)G\end{aligned}$$

2-1

where β is the fraction of critical damping. For $\omega > 0$, β is also positive. Since the damping coefficient is independent of frequency, damping is hysteretic in nature. For more details on hysteretic damping, see Kausel (1974). Using complex moduli to represent a linearly viscoelastic material does not alter the derivations presented for a linearly elastic material. Thus the complex moduli can be substituted for λ and G when dissipative behavior is required. The use of complex moduli in cases of dynamic loading insures that no singular displacements (at resonance) are obtained.

2.2 The Stiffness Method

2.2.1 In-plane Motion

Consider a stratum in plane strain subjected to a harmonic load. The displacement vector in Cartesian coordinates is

$$\begin{bmatrix} u(x,z) \\ 0 \\ w(x,z) \end{bmatrix} e^{i\omega t} \quad 2-2$$

where ω is the frequency of the forcing function. Motion is restricted to the x - z plane and is independent of the y coordinate. In layer i , the wave equations are

$$(\lambda_i + 2G_i) \frac{\partial^2 u}{\partial x^2} + \lambda_i \frac{\partial^2 w}{\partial x \partial z} + G_i \left[\frac{\partial^2 u}{\partial z^2} + \frac{\partial^2 w}{\partial x \partial z} \right] + \rho_i \omega^2 u = 0 \quad 2-3$$

$$(\lambda_i + 2G_i) \frac{\partial^2 w}{\partial z^2} + \lambda_i \frac{\partial^2 u}{\partial x \partial z} + G_i \left[\frac{\partial^2 w}{\partial x^2} + \frac{\partial^2 u}{\partial x \partial z} \right] + \rho_i \omega^2 w = 0$$

The stresses are given by

$$\sigma_x = (\lambda_i + 2G_i) \frac{\partial u}{\partial x} + \lambda_i \frac{\partial w}{\partial z}$$

$$\tau_{xz} = G_i \left[\frac{\partial w}{\partial x} + \frac{\partial u}{\partial z} \right] \quad 2-4$$

$$\sigma_z = (\lambda_i + 2G_i) \frac{\partial w}{\partial z} + \lambda_i \frac{\partial u}{\partial x}$$

We look for solutions by separating the x and z dependence of the displacements

$$\begin{aligned} u(x,z) &= U(z) f(x) \\ w(x,z) &= W(z) f(x) \end{aligned} \quad 2-5$$

Substituting 2-5 into the differential equations 2-3 gives

$$\frac{d^2 f}{dx^2} + k^2 f = 0 \quad 2-6$$

where k is a constant (the wavenumber). Thus the displacements are given by

$$\begin{aligned} u(x,z) &= U(z) e^{-ikx} \\ w(x,z) &= W(z) e^{-ikx} \end{aligned} \tag{2-7}$$

Now write u and w as

$$u = \frac{\partial \phi}{\partial x} - \frac{\partial \psi}{\partial z} \tag{2-8}$$

$$w = \frac{\partial \phi}{\partial z} + \frac{\partial \psi}{\partial x}$$

where ϕ and ψ are potential functions. When 2-8 are substituted into the wave equation 2-3, we obtain

$$\frac{\partial^2 \phi}{\partial x^2} + \frac{\partial^2 \phi}{\partial z^2} = -\frac{\omega^2}{C_{pi}^2} \phi \tag{2-9}$$

$$\frac{\partial^2 \psi}{\partial x^2} + \frac{\partial^2 \psi}{\partial z^2} = -\frac{\omega^2}{C_{si}^2} \psi$$

where C_{si} and C_{pi} are the shear and pressure wave velocities, given by

$$C_{si} = \sqrt{\frac{G_i}{\rho_i}} \tag{2-10}$$

$$C_{pi} = \sqrt{\frac{\lambda_i + 2G_i}{\rho_i}}$$

We want to find solutions to 2-9 of the form

$$\begin{aligned} \phi(x,z) &= \Phi(z) e^{-ikx} \\ \psi(x,z) &= \Psi(z) e^{-ikx} \end{aligned} \tag{2-11}$$

Substituting 2-11 into 2-9 gives

$$\frac{d^2 \Phi}{dz^2} + r_i^2 \Phi = 0 \tag{2-12}$$

$$\frac{d^2 \Psi}{dz^2} + s_i^2 \Psi = 0$$

where

$$r_i^2 = \frac{\omega^2}{C_{pi}^2} - k^2 \quad 2-13$$

$$s_i^2 = \frac{\omega^2}{C_{si}^2} - k^2$$

Then the solution for the potential functions is

$$\Phi(z) = A_{1i} \cos (r_i z) + A_{2i} \sin (r_i z) \quad 2-14$$

$$\Psi(z) = A_{3i} \cos (s_i z) + A_{4i} \sin (s_i z)$$

Substituting 2-14 into 2-11 and then applying 2-8, we obtain

$$U = -ik\Phi - \frac{d\Psi}{dz} \quad 2-15$$

$$W = \frac{d\Phi}{dz} - ik\Psi$$

The amplitudes $A_{1i}, A_{2i}, A_{3i}, A_{4i}$ for each layer i can be expressed as functions of $U(z_i), W(z_i), U(z_{i+1}), W(z_{i+1})$ and also as functions of $\sigma_z(z_i), \tau_{xz}(z_i), \sigma_z(z_{i+1}), \tau_{xz}(z_{i+1})$. This is the basis of the transfer matrix. The state vector, $Z_{i+1} = \{u(z_{i+1}), w(z_{i+1}), \tau_{xz}(z_{i+1}), \sigma_z(z_{i+1})\}^T$ is obtained in terms of the amplitudes A . Then the amplitudes are obtained in terms of the state vector Z_i . This amplitude vector is then substituted into the expression for Z_{i+1} to yield

$$Z_{i+1} = H_i Z_i \quad 2-16$$

where H_i is the local transfer matrix. The elements of the transfer matrix can be found in Haskell (1953).

2.2.2 Anti-plane Motion

Consider a stratum in anti-plane shear subjected to a harmonic load. The displacement vector is

$$\begin{bmatrix} 0 \\ v(x, z) \\ 0 \end{bmatrix} e^{i\omega t} \quad 2-17$$

Motion is in the y direction and planar (independent of the y coordinate). The equation of motion in layer i is

$$G_i \left[\frac{\partial^2 v}{\partial x^2} + \frac{\partial^2 v}{\partial z^2} \right] - \rho_i \omega^2 v = 0 \quad 2-18$$

The shear stresses are given by

$$\tau_{yz} = G_i \frac{\partial v}{\partial z} \quad 2-19$$

$$\tau_{yx} = G_i \frac{\partial v}{\partial x}$$

Separation of variables gives a solution of the form

$$v(x, z) = V(z) e^{-ikx} \quad 2-20$$

From the differential equation 2-18, we obtain the function

$$V(z) = A_{1i} \cos (s_i z) + A_{2i} \sin (s_i z) \quad 2-21$$

where

$$s_i^2 = \frac{\omega^2}{C_{si}^2} - k^2$$

Again, A_{1i} and A_{2i} can be removed from the expressions for $v(z_i)$, $v(z_{i+1})$, $\tau_{yz}(z_i)$, $\tau_{yz}(z_{i+1})$ so that v and τ_{yz} at z_{i+1} are linear functions of v and τ_{yz} at z_i .

2.2.3 Development of the Stiffness Method

In this section, a summary of the technique developed by Kausel and Roësset (1981) is presented. The reader is referred to that reference for more details. Adopting the notation of Kausel and Roësset, we write the state vector as

$$Z = \{ \bar{u}_x, \bar{u}_y, i\bar{u}_z, \bar{\tau}_{xz}, \bar{\tau}_{yz}, i\bar{\sigma}_z \}^T = \begin{bmatrix} \bar{U} \\ \bar{S} \end{bmatrix} \quad 2-22$$

in Cartesian coordinates and

$$Z = \{ \bar{u}_\rho, \bar{u}_\theta, \bar{u}_z, \bar{\tau}_{\rho z}, \bar{\tau}_{\theta z}, \bar{\sigma}_z \}^T = \left[\frac{\bar{U}}{\bar{S}} \right] \quad 2-23$$

in cylindrical coordinates. The superscript bar indicates that these quantities are functions of z only. In Cartesian coordinates, for a stratum in plane strain, the true state vector is

$$\begin{bmatrix} U \\ S \end{bmatrix} = \begin{bmatrix} \bar{U} \\ \bar{S} \end{bmatrix} e^{i(\omega t - kx)} \quad 2-24$$

where ω is the harmonic frequency of the forcing function and k is the horizontal wavenumber.

In cylindrical coordinates, the dependence of the displacements and stresses on the azimuthal direction is given by multiplying $\bar{u}_\rho, \bar{u}_z, \bar{\tau}_{\rho z}, \bar{\sigma}_z$ by $\cos \mu\theta$ and $\bar{u}_\theta, \bar{\tau}_{\theta z}$ by $-\sin \mu\theta$ if the displacements and stresses are symmetric with respect to the z axis, or by $\sin \mu\theta$ and $\cos \mu\theta$ if they are antisymmetric. The integer μ is a Fourier index which is described below. The variation in the radial direction is given by multiplying \bar{V} and \bar{S} by the matrix C_μ , which is the same for all layers

$$\begin{bmatrix} U \\ S \end{bmatrix}_\mu = \begin{bmatrix} C_\mu \bar{U} \\ C_\mu \bar{S} \end{bmatrix} = \begin{bmatrix} C_\mu & \\ & C_\mu \end{bmatrix} \begin{bmatrix} \bar{U} \\ \bar{S} \end{bmatrix} \quad 2-25$$

where

$$C_\mu = \begin{bmatrix} \frac{d}{d(k\rho)} J_\mu & \frac{\mu}{k\rho} J_\mu & 0 \\ \frac{\mu}{k\rho} J_\mu & \frac{d}{d(k\rho)} J_\mu & 0 \\ 0 & 0 & -J_\mu \end{bmatrix} \quad 2-26$$

and J_μ are Bessel functions. Thus the displacements and stresses are decomposed into a Fourier series in the θ direction and into cylindrical functions in the ρ direction.

The transfer matrix for layer j relates the state vectors

$$Z_{j+1} = H_j Z_j \quad 2-27$$

where now the vectors contain all three displacements and continuous stresses. In plane strain, the in-plane motions are uncoupled from the anti-plane motions, as described in the section above. The transfer matrix for cylindrical symmetry is the same as that for plane strain. The transfer matrix is not a function of the Fourier index μ .

Now we consider equilibrium of a single layer. The layer has load $\bar{P}_1 = \bar{S}_1$ on the upper interface and $\bar{P}_2 = -\bar{S}_2$ on the lower interface. Then, substituting in 2-27, we obtain

$$\begin{bmatrix} \bar{U}_2 \\ -\bar{P}_2 \end{bmatrix} = \begin{bmatrix} H_{11} & H_{12} \\ H_{21} & H_{22} \end{bmatrix} \begin{bmatrix} \bar{U}_1 \\ \bar{P}_1 \end{bmatrix} \quad 2-28$$

where H_{ij} are submatrices of H_j obtained by partitioning. Rearranging terms so that loads are on the left hand side of the equation gives

$$\begin{bmatrix} \bar{P}_1 \\ \bar{P}_2 \end{bmatrix} = \begin{bmatrix} -H_{12}^{-1}H_{11} & H_{12}^{-1} \\ H_{22}H_{12}^{-1}H_{11}-H_{21} & -H_{22}H_{12}^{-1} \end{bmatrix} \begin{bmatrix} \bar{U}_1 \\ \bar{U}_2 \end{bmatrix} \quad 2-29$$

or

$$\bar{P} = K \bar{U}$$

where K is the symmetric layer stiffness matrix, \bar{P} is the load vector and \bar{U} is the displacement vector. The global stiffness matrix for a layered soil system is formed by overlapping the layer matrices at common degrees of freedom. The global load vector consists of tractions applied at the layer interfaces. The techniques applied to solve for displacements are analogous to those of structural dynamics. The elements of the K matrix are complicated transcendental functions. The K matrices for zero and non-zero values of k and ω are given by Kausel and Roësset (1981).

2.3 Green's Functions for a Layered Stratum

In this section, the algebraic stiffness matrix is presented and it is applied to the solutions of displacements in layered stratum subjected to dynamic loads. The material in this section is taken from Kausel and Peek (1982b).

2.3.1 Algebraic Stiffness Matrix

When the soil layers are thin compared to the significant wavelengths, the layer stiffness matrix can be approximated as

$$K_j = A_j k^2 + B_j k + G_j - \omega^2 M_j \quad 2-30$$

These layer matrices are computed by assuming that displacements are piecewise linear in the z direction and then applying finite element energy balance techniques. The displacements in layer j are

$$\bar{U} = \frac{z_{j+1} - z}{h} \bar{U}_j + \frac{z - z_j}{h} \bar{U}_{j+1} \quad 2-31$$

Each layer is a one-dimensional finite element in the z direction. The layer stiffness matrices A_j and B_j are presented in Table 2-I, G_j and M_j are presented in Table 2-II. Note that the 2nd and 5th rows and columns of these matrices, corresponding to the anti-plane degrees of freedom, are uncoupled from the in-plane degrees of freedom.

The global stiffness matrix is assembled by overlapping the layer stiffness matrices at common degrees of freedom. For the stratum resting on a rigid base, the three degrees of freedom at the interface of the rigid rock are set to zero and removed from the eigenproblem. Note that when the wavenumber k is zero (no propagation in the z direction), the stiffness matrix $G - \omega^2 M$ is that of a vibrating shear beam modeled with finite elements and a consistent mass matrix. Thus the layered stratum has the same resonant frequencies as a shear beam with a fixed base.

Table 2-I: Algebraic Layer Stiffness Matrices A and B

$$A_j = \frac{h}{6} \begin{bmatrix} 2(\lambda+2G) & & & \lambda+2G & & \\ & 2G & & & G & \\ & & 2G & & & G \\ \lambda+2G & & & 2(\lambda+2G) & & \\ & G & & & 2G & \\ & & G & & & 2G \end{bmatrix}$$

$$B_j = \frac{1}{2} \begin{bmatrix} & \lambda-G & & & & -(\lambda+G) \\ \lambda-G & & & \lambda+G & & \\ & & \lambda+G & & & -(\lambda-G) \\ & & & & & \\ -(\lambda+G) & & & -(\lambda-G) & & \end{bmatrix}$$

In principle, for a vector of prescribed external loadings \bar{P} , we wish to obtain the displacements \bar{U} by inverting the stiffness matrix

$$\bar{U} = K^{-1} \bar{P} \qquad 2-32$$

This inversion is performed with a spectral decomposition of the stiffness matrix. In order to obtain the wavenumbers and modes of propagation, we must solve the quadratic eigenvalue problem

Table 2-II: Algebraic Layer Stiffness Matrices G and M

$$G_j = \frac{1}{h} \begin{bmatrix} G & & & -G & & \\ & G & & & & -G \\ & & \lambda+2G & & & -(\lambda+2G) \\ -G & & & G & & \\ & -G & & & G & \\ & & -(\lambda+2G) & & & \lambda+2G \end{bmatrix}$$

$$M_j = \frac{\rho h}{6} \begin{bmatrix} 2 & & & & & 1 \\ & 2 & & & & 1 \\ & & 2 & & & 1 \\ 1 & & & 2 & & \\ & 1 & & & 2 & \\ & & 1 & & & 2 \end{bmatrix}$$

$$K \phi = 0$$

For a stratum of N layers, the solution of this problem yields $2N$ eigenvalues for the anti-plane case and $4N$ eigenvalues for the in-plane case. The wavenumbers k_j occur in pairs of $\pm k_j$, which correspond to waves that travel from the origin and decay towards infinity and waves that travel from infinity and decay towards the origin. The details of the eigenvalue problem and physical significance of the wavenumbers are explained in detail by Waas (1972). We select the $3N$ eigenvalues k_j with negative imaginary part for complex k_j and positive real part for real k_j . These

correspond to waves that propagate away from the origin or decay towards the origin.

The quadratic eigenvalue problem can be expressed as a linear eigenvalue problem of double dimension, which requires all $6N$ eigenmodes for decomposition. The special structure of the matrices in this case allows the quadratic eigenvalue problem to be expressed as a linear problem of the same dimension. Rearranging the rows and columns of the stiffness matrix by degree of freedom, we obtain the eigenproblem with right and left vectors

$$\overline{K} Z_j = (\overline{A} k_j^2 + \overline{C}) Z_j = 0 \quad 2-34$$

$$Y_j^T \overline{K} = Y_j^T (\overline{A} k_j^2 + \overline{C}) = 0$$

where

$$\overline{A} = \begin{bmatrix} A_x & & \\ B_{xz}^T & A_z & \\ & & A_y \end{bmatrix} \quad 2-35$$

$$\overline{C} = \begin{bmatrix} C_x & B_{xz} & \\ & C_z & \\ & & C_y \end{bmatrix}$$

and the submatrices are all tridiagonal. For a given frequency ω , $C = G - \omega^2 M$. The left and right eigenvectors are

$$Y_j = \begin{bmatrix} k_j \phi_{xj} \\ \phi_{zj} \\ \phi_{yj} \end{bmatrix} \quad Z_j = \begin{bmatrix} \phi_{xj} \\ k_j \phi_{zj} \\ \phi_{yj} \end{bmatrix} \quad 2-36$$

In matrix form, the eigenvalue problem is

$$\overline{A} Z K^2 + \overline{C} Z = 0 \quad 2-37$$

$$\overline{A}^T Y K^2 + \overline{C}^T Y = 0$$

where

$$Y = \begin{bmatrix} \Phi_x K_R \\ \Phi_z \\ \Phi_y \end{bmatrix}$$

$$Z = \begin{bmatrix} \bar{\phi}_x \\ \bar{\phi}_z K_R \\ \bar{\phi}_y \end{bmatrix} \quad 2-38$$

$$K = \begin{bmatrix} K_R \\ K_L \end{bmatrix} = \begin{bmatrix} \text{"Rayleigh" modes} \\ \text{"Love" modes} \end{bmatrix}$$

Kausel and Roësset (1981) derived the group velocities (velocities at which energy is transferred into the medium) of the natural modes of propagation from the eigenvalue problem. The left and right eigenvectors satisfy orthogonality with respect to \bar{A} and \bar{C} . The normalization is

$$Y^T \bar{A} Z = \begin{bmatrix} K_R \\ I \end{bmatrix} = J \quad 2-39$$

$$Y^T \bar{C} Z = - \begin{bmatrix} K_R \\ K_L^2 \end{bmatrix} = -JK^2$$

From 2-39, we know that \bar{A} and \bar{C} can be inverted when no eigenvalues are zero. The results of inverting \bar{A} and \bar{C} are given by Kausel and Peek (1982b). The equilibrium equation 2-29 in the wavenumber domain is

$$\bar{K} \bar{U} = (\bar{A} k^2 + \bar{C}) \bar{U} = \bar{P} \quad 2-40$$

where

$$\bar{U} = \begin{bmatrix} \bar{U}_x \\ k\bar{U}_z \\ \bar{U}_y \end{bmatrix} \quad \bar{P} = \begin{bmatrix} \bar{P}_x \\ k\bar{P}_z \\ \bar{P}_y \end{bmatrix} \quad 2-41$$

We premultiply 2-4 by Y^T and postmultiply by $Z Z^{-1} = I$ to obtain

$$Y^T (\bar{A} k^2 + \bar{C}) Z Z^{-1} \bar{U} = Y^T \bar{P} \quad 2-42$$

Applying the orthogonality relations 2-39 to 2-42 yields

$$(J k^2 - JK^2) Z^{-1} \bar{U} = Y^T \bar{P} \quad 2-43$$

Solving for displacements \overline{U} in the wavenumber domain gives

$$\overline{U} = Z J^{-1} (k^2 I - K^2)^{-1} Y^T \overline{P} \quad 2-44$$

Expanding 2-44 yields the flexibility (the inverse of the stiffness) matrix

$$\begin{bmatrix} \overline{U}_x \\ \overline{U}_z \\ \overline{U}_y \end{bmatrix} = \begin{bmatrix} \frac{1}{k} \phi_x D_R \phi_x^T & k \phi_x K_R^{-1} D_R \phi_z^T & \\ \frac{1}{k} \phi_z K_R D_R \phi_x^T & \phi_z D_R \phi_z^T & \\ & & \phi_y D_L \phi_y^T \end{bmatrix} \begin{bmatrix} \overline{P}_x \\ \overline{P}_z \\ \overline{P}_y \end{bmatrix} \quad 2-45$$

where

$$D_R = (k^2 I - K_R^2)^{-1} \quad 2-46$$

$$D_L = (k^2 I - K_L^2)^{-1}$$

It can be proven that this flexibility matrix is symmetric. We define the $N \times N$ submatrices

$$F_{xx} = \{ f_{xx}^{mn} \} = \phi_x D_R \phi_x^T \quad m, n = 1, \dots, N$$

$$F_{xz} = \{ f_{xz}^{mn} \} = \begin{cases} k \phi_x K_R^{-1} D_R \phi_z^T \\ \frac{1}{k} \phi_z K_R D_R \phi_x^T \end{cases} \quad 2-47$$

$$F_{zx} = F_{xz}^T$$

$$F_{zz} = \{ f_{zz}^{mn} \} = \phi_z D_R \phi_z^T$$

$$F_{yy} = \{ f_{yy}^{mn} \} = \phi_y D_L \phi_y^T$$

The elements of the flexibility matrix for displacements at the m^{th} elevation due to loads at the n^{th} elevation are

$$F^{mn} = \begin{bmatrix} f_{xx}^{mn} & 0 & f_{xz}^{mn} \\ 0 & f_{yy}^{mn} & 0 \\ f_{zx}^{mn} & 0 & f_{zz}^{mn} \end{bmatrix} \quad 2-48$$

The matrices of eigenvectors are

$$\phi_x = \{ \phi_x^{ml} \} \quad m = 1, \dots, N \quad l = 1, \dots, 2N$$

$$\Phi_z = \{ \phi_z^{ml} \} \quad m = 1, \dots, N \quad l = 1, \dots, 2N \quad 2-49$$

$$\Phi_y = \{ \phi_y^{ml} \} \quad m = 1, \dots, N \quad l = 1, \dots, N$$

Substituting 2-49 and 2-46 into 2-47 yields the individual elements of the flexibility matrix

$$\begin{aligned} f_{xz}^{mn} &= \sum_{l=1}^{2N} \phi_x^{nl} \phi_x^{ml} a_l^R \\ f_{xz}^{mn} &= \sum_{l=1}^{2N} \phi_x^{ml} \phi_x^{nl} b_l^R = \sum_{l=1}^{2N} \phi_z^{ml} \phi_z^{nl} c_l^R \\ f_{zz}^{mn} &= \sum_{l=1}^{2N} \phi_z^{ml} \phi_z^{nl} a_l^R \\ f_{yy}^{mn} &= \sum_{l=1}^N \phi_y^{ml} \phi_y^{nl} a_l^L \end{aligned} \quad 2-50$$

where

$$a_l = \frac{1}{k^2 - k_l^2} \quad b_l = \frac{1}{k_l (k^2 - k_l^2)} \quad c_l = \frac{k_l}{k (k^2 - k_l^2)} \quad 2-51$$

Now that we have obtained the inverse of the stiffness matrix, we can proceed to solve for displacements.

2.3.2 Solution for Displacements

At this point, we make a switch to cylindrical coordinates. As stated previously, the transfer matrix, and therefore the stiffness and flexibility matrices, is the same for plane strain and cylindrical coordinates. The stress and displacement vectors are

$$\overline{S} = \begin{bmatrix} \overline{\tau}_{\rho z} \\ \overline{\tau}_{\theta z} \\ \overline{\sigma}_z \end{bmatrix} \quad \overline{U} = \begin{bmatrix} \overline{u}_\rho \\ \overline{u}_\theta \\ \overline{u}_z \end{bmatrix} \quad 2-52$$

The Hankel transforms between the wavenumber and the spatial domains are

$$U = \sum_{\mu=0}^{\infty} T_\mu \int_0^{\infty} k C_\mu \overline{U}_\mu dk \quad 2-53$$

$$\bar{U}_\mu = a_\mu \int_0^\infty \rho C_\mu \int_0^{2\pi} T_\mu U d\theta d\rho \quad 2-54$$

where μ is the Fourier index, C_μ is the matrix of Equation 2-26 and T_μ is a diagonal matrix containing the terms $\cos \mu\theta$ and $\sin \mu\theta$ according to the symmetry of the loading, as described in Section 2.2.3. The orthogonalization factor a_μ is

$$a_\mu = \begin{cases} \frac{1}{2\pi} & \text{for } \mu = 0 \\ \frac{1}{\pi} & \text{for } \mu \neq 0 \end{cases} \quad 2-55$$

The time dependence of the loads is the constant factor $e^{i\omega t}$.

By applying the results of the previous section, we obtain the displacements at elevation m due to a load applied at elevation n

$$U^{mn} = \sum_{\mu=0}^{\infty} T_\mu \int_0^\infty k C_\mu F^{mn} \bar{P}_\mu dk \quad 2-56$$

where \bar{P}_μ is the load vector in the wavenumber domain,

$$\bar{P}_\mu = a_\mu \int_0^\infty \rho C_\mu \int_0^{2\pi} T_\mu P d\theta d\rho \quad 2-57$$

The advantage that the method presented above has over the ones cited in Chapter 1 is that the transforms of Equation 2-56 are computed in closed form.

Consider a horizontal and a vertical disk load. The components in cylindrical coordinates of uniform loads q over a disk of radius R are

$$P_H = q \begin{bmatrix} \cos \theta \\ -\sin \theta \\ 0 \end{bmatrix} \quad P_V = q \begin{bmatrix} 0 \\ 0 \\ 1 \end{bmatrix} \quad 0 \leq \rho \leq R \quad 2-58$$

The transform of the horizontal load, from 2-57, is

$$\bar{P}_1 = q \begin{bmatrix} 1 \\ 1 \\ 0 \end{bmatrix} \frac{R}{k} J_1(kR) \quad 2-59$$

$$\overline{P}_\mu = 0 \quad \mu \neq 1$$

The transform of the vertical load is

$$\overline{P}_0 = -q \begin{bmatrix} 0 \\ 0 \\ 1 \end{bmatrix} \frac{R}{k} J_1(kR) \quad 2-60$$

$$\overline{P}_\mu = 0 \quad \mu \neq 0$$

Substituting 2-59 into 2-56, we obtain the displacements due to a horizontal disk load

$$\begin{aligned} u_\rho^{mn} &= qR \left[\sum_{l=1}^{2N} \phi_x^{ml} \phi_x^{nl} \frac{d}{d\rho} I_{3l}^R + \sum_{l=1}^N \phi_y^{ml} \phi_y^{nl} \frac{1}{\rho} I_{3l}^L \right] (\cos \theta) \\ u_\theta^{mn} &= qR \left[\sum_{l=1}^{2N} \phi_x^{ml} \phi_x^{nl} \frac{1}{\rho} I_{3l}^R + \sum_{l=1}^N \phi_y^{ml} \phi_y^{nl} \frac{d}{d\rho} I_{3l}^L \right] (-\sin \theta) \\ u_z^{mn} &= -qR \left[\sum_{l=1}^{2N} \phi_z^{ml} \phi_z^{nl} I_{3l}^R k_l^R \right] (\cos \theta) \end{aligned} \quad 2-61$$

Likewise, substituting 2-60 into 2-56, we obtain the displacements due to a vertical disk load

$$\begin{aligned} u_\rho^{mn} &= -qR \left[\sum_{l=1}^{2N} \phi_x^{ml} \phi_z^{nl} \frac{1}{k_l} \frac{d}{d\rho} I_{1l}^R \right] \\ u_\theta^{mn} &= 0 \\ u_z^{mn} &= qR \left[\sum_{l=1}^{2N} \phi_z^{ml} \phi_z^{nl} I_{1l}^R \right] \end{aligned} \quad 2-62$$

The integrals I_{1l} , I_{2l} and I_{3l} , representing the inverse transforms, are given in Table 2-III (from Kausel and Peek (1982b)). Note that stresses can be obtained from this solution for displacements. Derivatives can be taken in the z direction once, and the solution is continuous in the ρ direction. Thus stresses can be obtained at the center of each layer.

The computation of these Green's functions is a simple procedure: 1. Assemble the global stiffness matrix. 2. Extract eigenvalues and eigenvectors. 3. Evaluate the formulas in 2-61 and 2-62.

Table 2-III: Integrals Used to Compute Dynamic Displacements

$$I_{1l} = \int_0^\infty \frac{J_0(k\rho)J_1(kR)dk}{k^2 - k_l^2} = \begin{cases} \frac{\pi}{2ik_l} J_0(k_l\rho) H_1^{(2)}(k_l R) - \frac{1}{Rk_l^2} & 0 \leq \rho \leq R \\ \frac{\pi}{2ik_l} J_1(k_l R) H_0^{(2)}(k_l\rho) & R \leq \rho \end{cases}$$

$$I_{2l} = \int_0^\infty \frac{kJ_1(k\rho)J_1(kR)dk}{k^2 - k_l^2} = \begin{cases} \frac{\pi}{2i} J_1(k_l\rho) H_1^{(2)}(k_l R) & 0 \leq \rho \leq R \\ \frac{\pi}{2i} J_1(k_l R) H_1^{(2)}(k_l\rho) & R \leq \rho \end{cases}$$

$$I_{3l} = \int_0^\infty \frac{J_1(k\rho)J_1(kR)dk}{k(k^2 - k_l^2)} = \begin{cases} \frac{\pi}{2ik_l^2} J_1(k_l\rho) H_1^{(2)}(k_l R) - \frac{\rho}{2Rk_l^2} & 0 \leq \rho \leq R \\ \frac{\pi}{2ik_l^2} J_1(k_l R) H_1^{(2)}(k_l\rho) - \frac{R}{2\rho k_l^2} & R \leq \rho \end{cases}$$

Notes: Integrals valid for $\text{Im}(k_l) < 0$

$$I_{2l} = -\frac{dI_{1l}}{d\rho} \quad I_{1l} = \frac{1}{\rho} I_{3l} + \frac{d}{d\rho} I_{3l}$$

Displacements computed with this procedure are compared to those computed with numerical integration of the transcendental stiffness in Kausel and Peek (1982b). Plots of displacement versus frequency at different radii are presented. For the stratum, very accurate results are obtained with a relatively small number of layers (≈ 12). The resonant properties of the stratum at its shear beam frequencies are well reproduced. It is also shown that the discrete solution diverges when waves with wavelength λ less than $4h$ dominate the motion. The discrete solution is shown to save great computational effort over the continuum solution for situations where the

stratum has many layers with different properties or when loads are applied at several elevations.

Chapter 3

Dynamic Loads in Layered Halfspaces

Two approaches to the solution for dynamic displacements in layered media have been discussed in this paper. The most widely employed techniques involve integral transforms which must be evaluated numerically. In Chapter 2, a method developed by Kausel was described where the transforms exist in closed form. However, this method is restricted to situations where the soil layers rest on a rigid base. Davies and Banerjee (1983) presented a review of several of these techniques applied to the solution of dynamic displacements in a halfspace. They used Kausel's method to study a halfspace by modeling the soil deposit with a very large depth so that the rigid base had little influence on the displacements near the surface. The relatively large depths of the bottom layers introduced numerical inaccuracies in the solution. The accuracy of the solution improved as the number of layers was increased.

An alternate approach is to derive algebraic approximations for the impedance of the halfspace itself. The contribution of the halfspace stiffness to the bottom interface can then be added directly to the global stiffness matrix of the layered soil system. Thereafter, the procedure for calculating the Green's functions is exactly the same as for the rigid base case described in Chapter 2. The procedure given below has been presented by Hull and Kausel (1984) in an abbreviated form.

The approximation to the halfspace stiffness is called a "paraxial" approximation because it is valid for paraxial waves, or waves that propagate within a cone of the z axis. A paraxial approximation of the wave equation that is used as an absorbing boundary in a finite difference scheme was presented by Clayton and Engquist (1977). They employed the approximation to absorb the energy of incident waves on the boundary of the finite difference grid.

3.1 Derivation of the Paraxial Approximation

A second-order paraxial approximation to the halfspace stiffness is obtained by calculating the first three terms in the Taylor series expansion of the exact impedances:

$$K(k) \simeq K(0) + k K'(0) + \frac{1}{2} k^2 K''(0) \quad 3-1$$

where the primes indicate derivatives with respect to the wavenumber k . The exact impedances are given by Kausel and Roësset (1981). For the anti-plane case,

$$K = k s G \quad 3-2$$

And for the in-plane case,

$$K = 2 k G \left[\frac{1-s^2}{2(1-rs)} \begin{bmatrix} r & 1 \\ 1 & s \end{bmatrix} - \begin{bmatrix} 0 & 1 \\ 1 & 0 \end{bmatrix} \right] \quad 3-3$$

where G is the shear modulus of the halfspace. The parameters r and s are defined as

$$r = \sqrt{1 - (\omega/k C_p)^2} \quad 3-4$$

$$s = \sqrt{1 - (\omega/k C_s)^2}$$

where ω is the frequency of excitation. The mathematical details of obtaining derivatives and evaluating them at $k=0$ are presented in Appendix F. For the anti-plane case, the paraxial approximation is

$$K(k) \simeq i \frac{G \omega}{C_s} - i \frac{G C_s}{2 \omega} k^2 \quad 3-5$$

For the in-plane case, the paraxial approximation is

$$K(k) \simeq i \omega \rho C_s \begin{bmatrix} 1 & \\ & 1/\alpha \end{bmatrix} + G \frac{(1-2\alpha)}{\alpha} k \begin{bmatrix} 1 & \\ & 1 \end{bmatrix} + i \frac{G C_s}{2 \alpha \omega} k^2 \begin{bmatrix} -(2-\alpha) & \\ & (1-2\alpha)/\alpha^2 \end{bmatrix} \quad 3-6$$

where $\alpha = \frac{C_s}{C_p}$ is the ratio of the s-wave speed to the p-wave speed.

These paraxial approximations to the stiffness of the halfspace are shown, in Appendix G, to

be equivalent to the paraxial approximations to the wave equation developed by Clayton and Engquist (1977) (actually, there is a sign error in the Clayton-Engquist approximation which is discussed in Appendix G). In the approximation 3-6, the terms in k^0 and k^2 fall on the diagonal and the terms in k^1 fall on the off-diagonal. Thus, when these matrices are added to the global stiffness, the structures of A , B and C remain the same as in the stratum case. All of the techniques described by Waas (1972) can still be applied to solve the eigenvalue problem.

The stiffness matrix as a function of $k = 0$ represents the behavior of the halfspace when displacements are functions of frequency only, i.e. during standing waves. The $i\omega$ term indicates that the halfspace acts as a dashpot, absorbing energy in the form of radiation damping. The other terms in the paraxial approximation do not have straightforward physical interpretations. The behavior of the approximation as a whole is investigated below.

3.2 Characteristics of the Paraxial Approximation

3.2.1 Anti-plane Case

Clayton and Engquist (1977) show that the range of acceptable wave velocities for the scalar wave equation is $C < C_s$. For wave velocities greater than the shear wave speed of the material, evanescent waves are obtained. This dissipative property is not physically possible in the undamped halfspace. We define the dimensionless parameter λ

$$\lambda = \frac{C_s k}{\omega} = \frac{C_s}{C} \tag{3-7}$$

In terms of λ , the exact halfspace stiffness is

$$K(\lambda) = \omega \rho C_s \sqrt{\lambda^2 - 1} \tag{3-8}$$

The paraxial approximation is

$$K(\lambda) \simeq i \omega \rho C_s \left[1 - \frac{1}{2} \lambda^2 \right] \tag{3-9}$$

Expanding in Taylor series about small k has the same effect as expanding about small λ , so we expect the paraxial approximation to best represent the true stiffness when λ is small. Figures 3-1 and 3-2 show the real and imaginary parts of the anti-plane stiffness. It is clear from 3-8 that the true stiffness is real when $\lambda > 1$, which is outside of the range of interest. The real component for $\lambda > 1$ is shown in Figure 3-1. From 3-9, we can see that the approximation of the stiffness is always imaginary. The plot of the approximation and the imaginary part of 3-8 is shown in Figure 3-2. For values of λ less than 1, the agreement with the true stiffness is excellent.

Another test of the quality of the approximation is an investigation of the roots of the stiffness matrix. By setting the determinant of the stiffness matrix to zero, we obtain the velocities at which waves will propagate parallel to the traction-free surface of the medium. For the anti-plane case, this reduces to setting $K(\lambda)$ to zero. From 3-8, we see that $K(\lambda)$ is zero when $\lambda = 1$. In other words, anti-plane shear waves propagate parallel to the surface of a halfspace at the shear speed of the soil. The approximation 3-9, on the other hand, has one root at $\lambda = \sqrt{2}$. Thus, in the algebraic model, shear waves propagate at approximately 1.41 times the material shear speed.

The energy absorbing characteristics of the approximation are important for deciding how well it models a halfspace. Waas (1972) showed that the energy transmitted by propagating waves in a layered soil is (in the most general case)

$$E = \frac{\omega}{2} \text{Im} \{ u^* K u^T \} \tag{3-10}$$

where the $*$ indicates the complex conjugate transpose of the displacement vector. This is a quadratic Hermitic form involving a complex, symmetric matrix. Hence, its imaginary part, for arbitrary complex u , is only a function of the imaginary part of K . In particular, the determinant of the imaginary part of K should be greater than zero in order to insure positive definiteness of the quadratic form, i.e., to guarantee a positive energy transmission for arbitrary displacements u . In matrix form, this is

$$\det \{ \text{Im} (K) \} > 0 \tag{3-11}$$

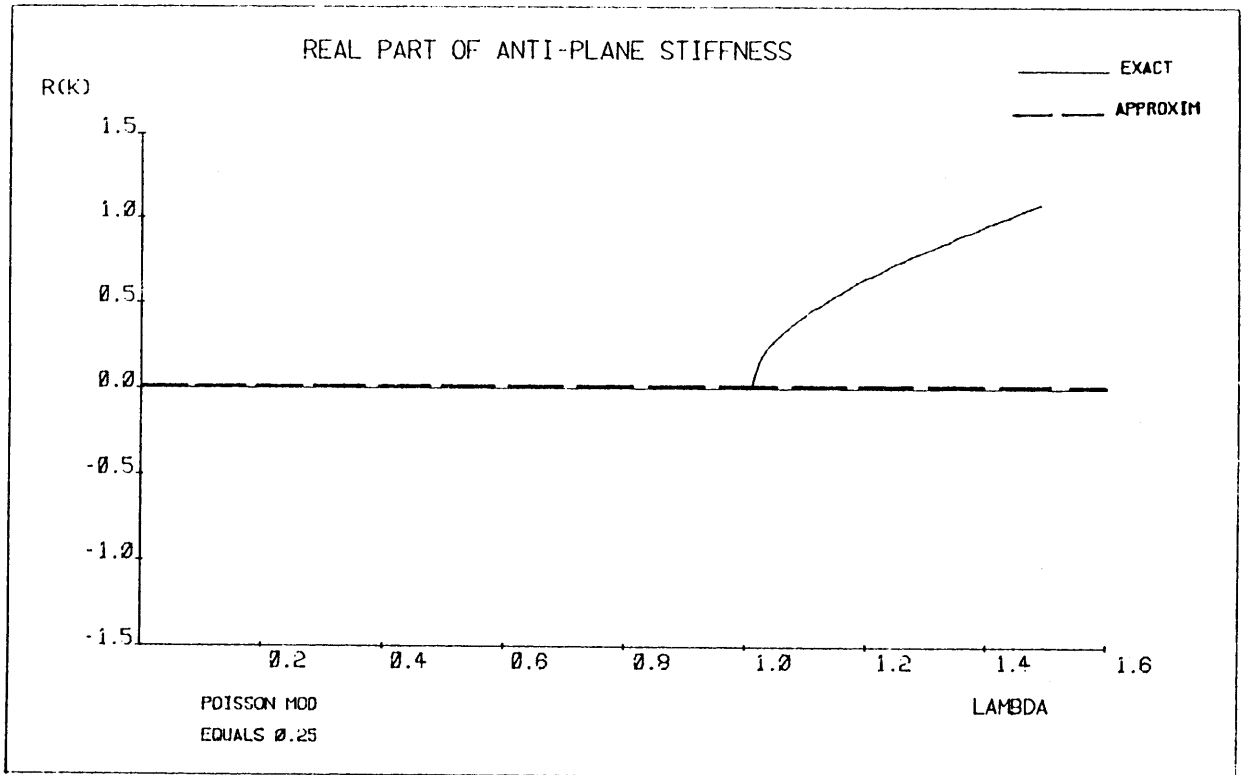


Figure 3-1: Real Part of the True Anti-plane Stiffness

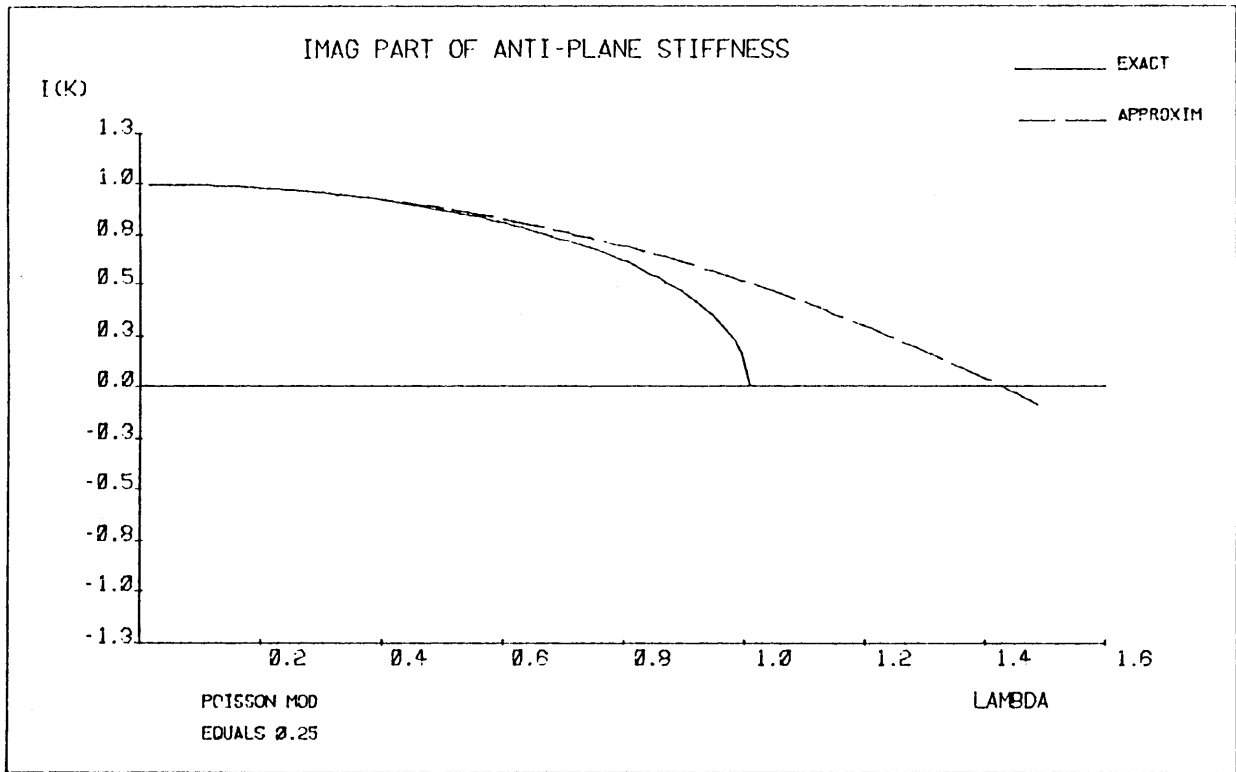


Figure 3-2: Imaginary Parts of the True and the Approximate Anti-plane Stiffness

For $\lambda < 1$, the imaginary part of $K(\lambda)$ is

$$\omega \rho C_s \sqrt{1 - \lambda^2} \quad 3-12$$

which is always positive (frequencies are understood to be positive). The imaginary part of the approximation is

$$\omega \rho C_s \left[1 - \frac{1}{2} \lambda^2 \right] \quad 3-13$$

which is positive for $\lambda^2 < \sqrt{2}$. In the range of interest, $\lambda < 1$, the imaginary part of the paraxial approximation is indeed positive. Thus the paraxial approximation absorbs energy from the waves as does the elastic halfspace.

The dispersion relation, obtained from the wave equation, for the anti-plane case is

$$k_x^2 + k_z^2 = \frac{\omega^2}{C_s^2} \quad 3-14$$

Clayton and Engquist (1977) show that the paraxial approximation best matches Equation 3-14 for small values of k_x . This means that for small values of k_x , the paraxial approximation behaves most like the wave equation. The advantages of this attribute are not evident for the present application.

3.2.2 In-plane Case

In terms of λ , the exact stiffness matrix for the in-plane case is

$$K(\lambda) = \omega \rho C_s \lambda \left[\frac{1-s^2}{1-rs} \begin{bmatrix} r & 1 \\ 1 & s \end{bmatrix} - \begin{bmatrix} 0 & 2 \\ 2 & 0 \end{bmatrix} \right] \quad 3-15$$

where

$$s = \sqrt{1 - \frac{1}{\lambda^2}} \quad 3-16$$

$$r = \sqrt{1 - \frac{\alpha^2}{\lambda^2}} \quad \text{where } \lambda = \frac{C_s k}{\omega} = \frac{C_s}{C}$$

The paraxial approximation is

$$K(\lambda) = \omega \rho C_s \left[i \begin{bmatrix} 1 \\ 1/\alpha \end{bmatrix} + \lambda \frac{(1-2\alpha)}{\alpha} \begin{bmatrix} 1 \\ 1 \end{bmatrix} + \frac{i}{2\alpha} \omega \rho C_s \lambda^2 \begin{bmatrix} -(2-\alpha) \\ (1-2\alpha)/\alpha^2 \end{bmatrix} \right] \quad 3-17$$

The general form of these stiffness matrices is

$$K(\lambda) = \omega \rho C_s \begin{bmatrix} k_{11}(\lambda) & k_{12}(\lambda) \\ k_{12}(\lambda) & k_{22}(\lambda) \end{bmatrix} \quad 3-18$$

Figures 3-3 through 3-8 show the elements of the stiffness matrix as a function of λ for the exact and the approximate cases. The elements are computed for a Poisson's modulus ν equal to 0.25 ($\alpha \simeq 0.57735$). Figure 3-3 shows the real part of k_{11} and Figure 3-7 shows the real part of k_{22} . Figure 3-4 shows the imaginary part of k_{11} and Figure 3-8 shows the imaginary part of k_{22} . From Equation 3-14, we can see that the approximations of k_{11} and k_{22} are always imaginary and k_{12} is always real. For $\lambda < \alpha$, r and s are imaginary and the exact k_{11} and k_{22} are purely imaginary. When $\alpha < \lambda < 1$, r becomes real and s is imaginary. In this range, the exact k_{11} and k_{22} are complex. For $\lambda > 1$, r and s are both real and the exact k_{11} and k_{22} are both real. Thus in the range $\lambda < \alpha$, the paraxial approximation matches the exact k_{11} and k_{22} very well. For $\lambda > 1$, the paraxial approximation does not match the exact terms at all.

Figure 3-5 shows the real part of k_{12} and Figure 3-6 shows the imaginary part of k_{12} . For $\lambda < \alpha$, the exact k_{12} is purely real. In the range $\alpha < \lambda < 1$, k_{12} is complex. When $\lambda > 1$, k_{12} is purely real again. The approximation is close to the exact stiffness in the real ranges (except near $\lambda = \alpha$ and $\lambda = 1$). In the range where k_{12} is complex, the approximation remains real.

Again, we can investigate the roots of the characteristic equation of the stiffness matrix. The exact stiffness has one real root λ^2 for each value of ν , and this is the Rayleigh wave. The characteristic equation of the paraxial approximation is

$$-(2-\alpha)(1-2\alpha)\lambda^4 + 2\alpha(1-\alpha)(1-\alpha-8\alpha^2)\lambda^2 + 4\alpha^3 = 0 \quad 3-19$$

Since Equation 3-19 is a quadratic in λ^2 , for every value of α there are *two* roots of λ^2 . Thus the

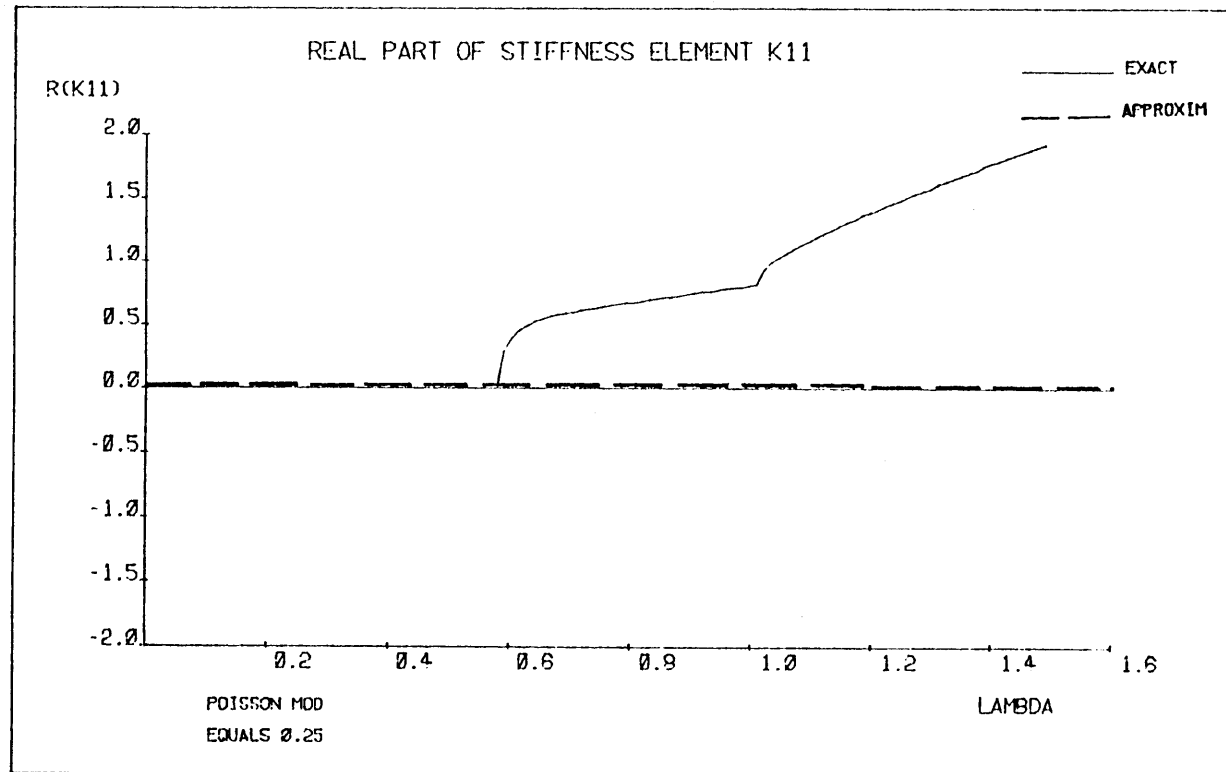


Figure 3-3: Real Part of k_{11}

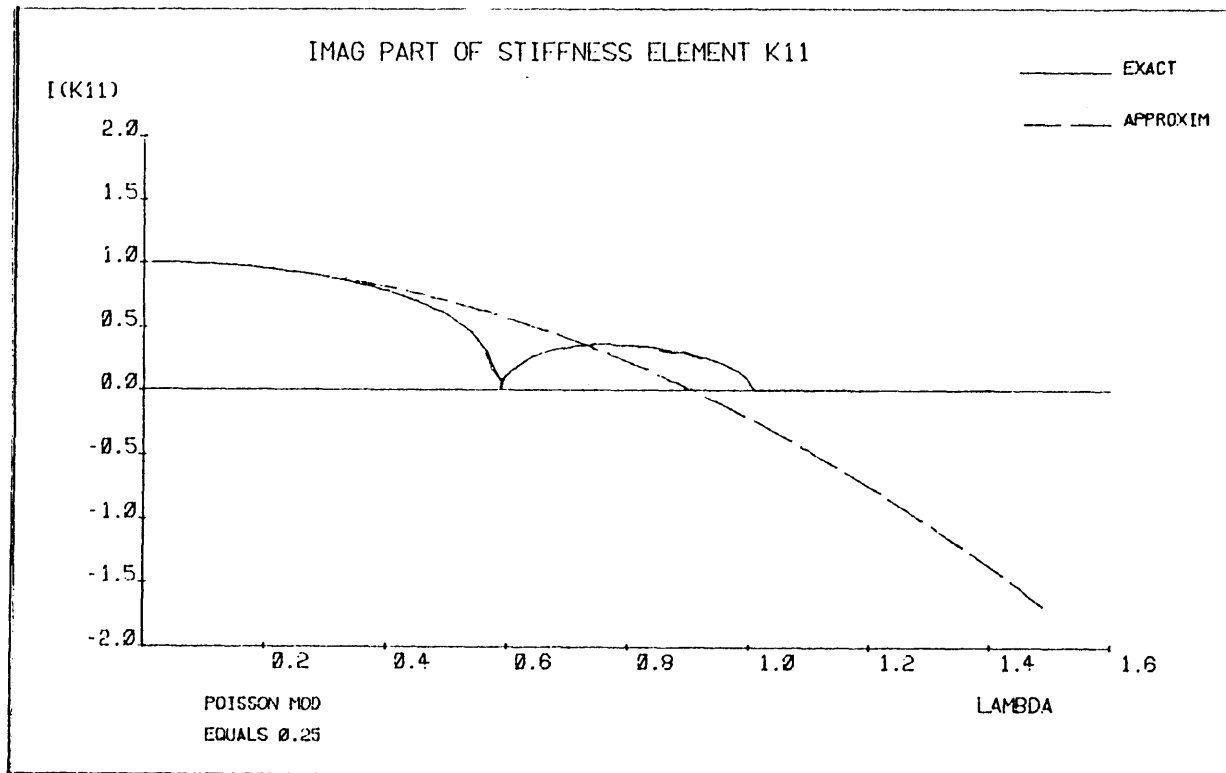


Figure 3-4: Imaginary Part of k_{11}

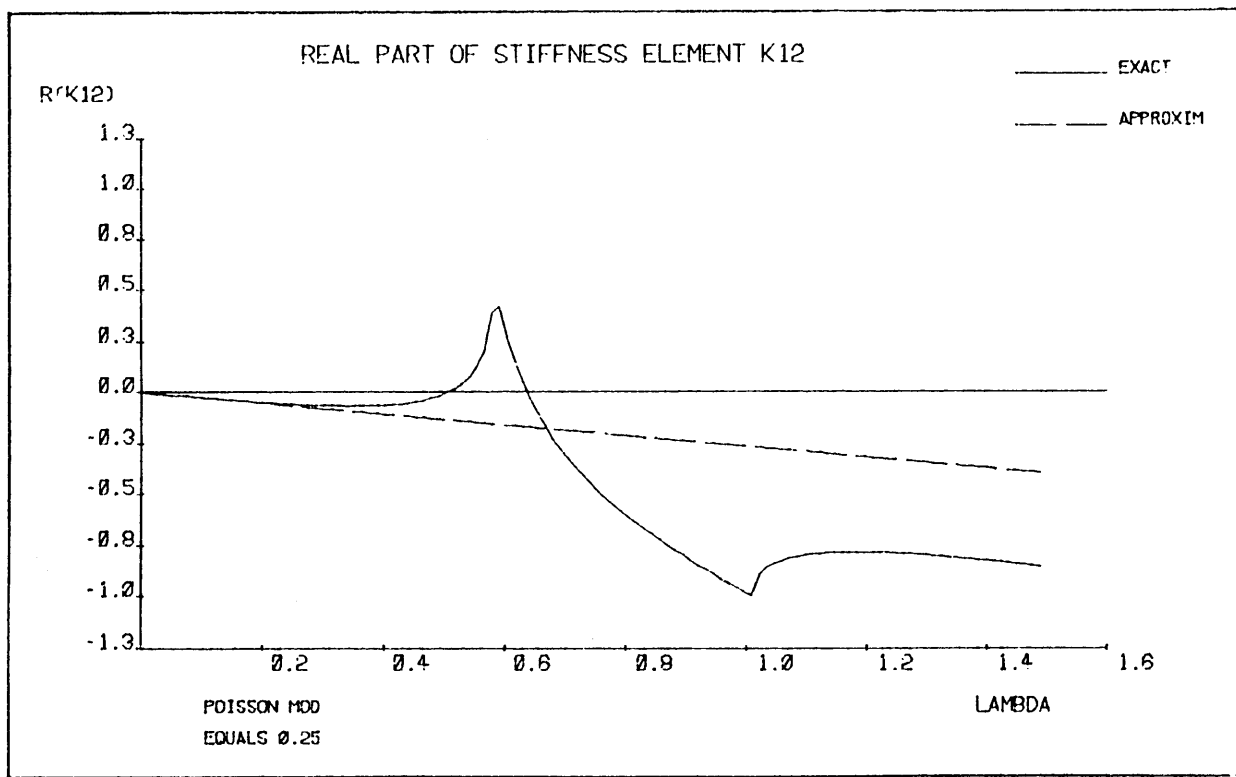


Figure 3-5: Real Part of k_{12}

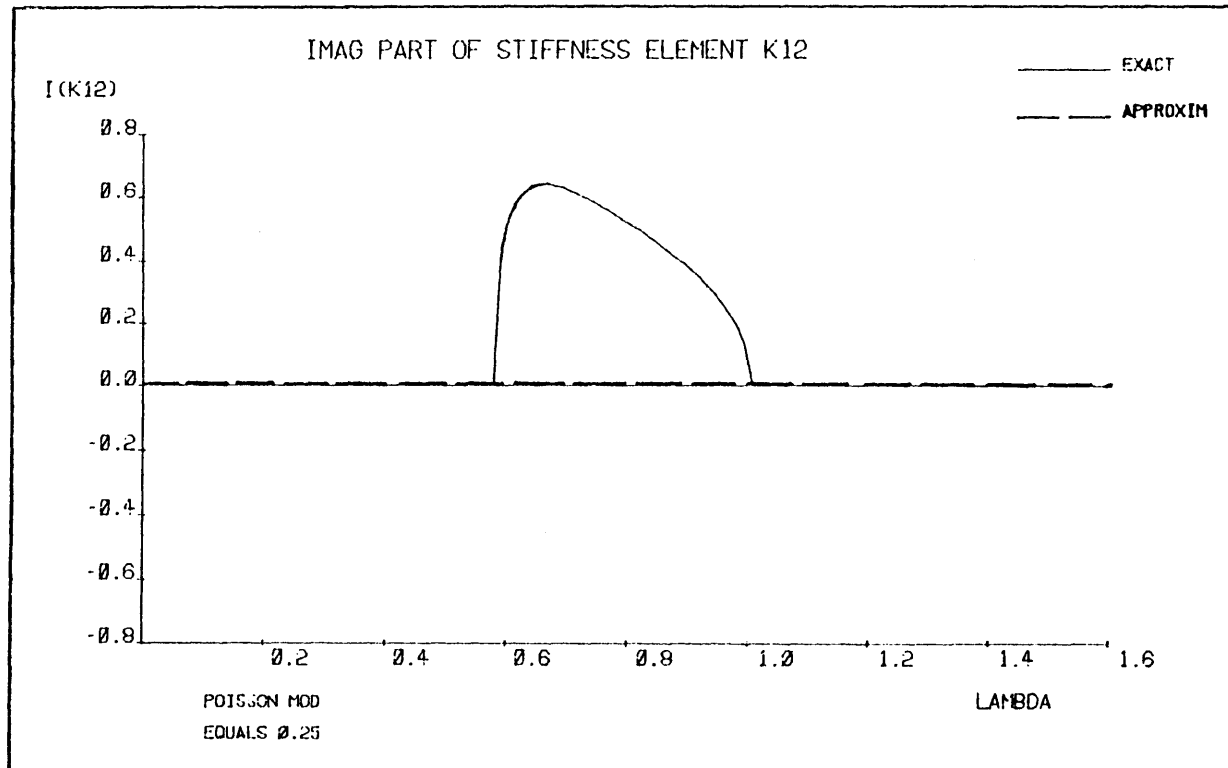


Figure 3-6: Imaginary Part of k_{12}

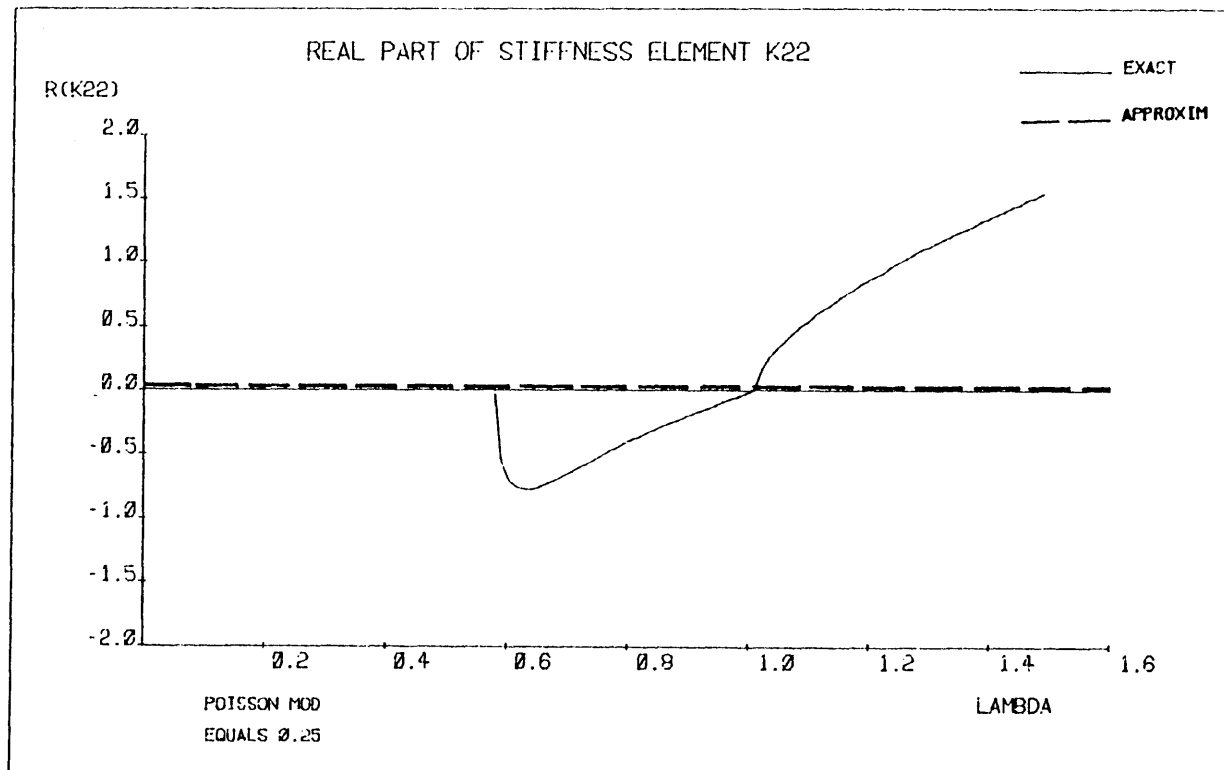


Figure 3-7: Real Part of k_{22}

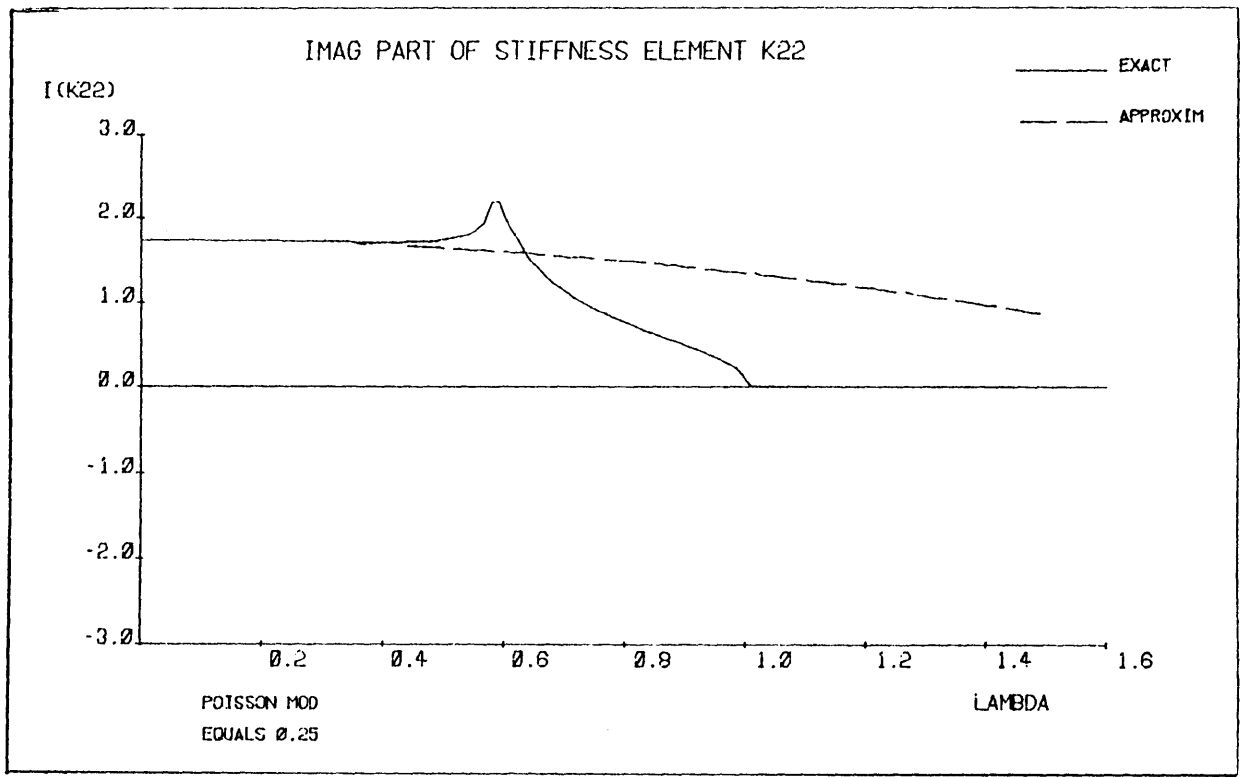


Figure 3-8: Imaginary Part of k_{22}

paraxial approximation introduces a spurious root (propagation mode) into the eigenvalue problem. Another feature of 3-19 is that when $\alpha = \frac{1}{2}$ ($\nu = \frac{1}{3}$), the coefficient of λ^4 vanishes and the second root goes through infinity. For $g(a) < \frac{1}{2}$ ($\nu > \frac{1}{3}$), the coefficient of λ^4 is negative and the second root is also negative. This has the effect of causing the halfspace to be too stiff. This phenomenon is described in greater detail in Section 3.3 below.

For $\nu < 0.110394$ ($\alpha > 0.66178$), the two roots of Equation 3-19 are complex, implying evanescent wave modes. Therefore, the paraxial approximation should deteriorate for Poisson's ratios below this limit. The true Rayleigh wave velocity and the approximate velocity obtained from 3-19 are plotted as a function of Poisson's ratio in Figure 3-9 (for $\nu \geq 0.125$). For the lower values of ν , the approximation is better than for values close to the incompressible case of $\nu = 0.5$. The spurious root is plotted in Figure 3-10.

To investigate the energy-absorbing characteristics of the paraxial approximation, we again examine the determinant of the imaginary part of the stiffness matrix. The determinant of the imaginary parts of the true and the approximate in-plane stiffnesses are plotted in Figure 3-11 for $\nu = \frac{1}{4}$, and in Figure 3-12 for $\nu = \frac{1}{3}$. The behavior of these curves is similar to that of the anti-plane case. The determinant of the true stiffness is positive until $\lambda^2 = \alpha^2$, the value of λ at which the vertical wavenumber becomes imaginary, and is zero thereafter. The determinant of the paraxial approximation is positive in this range (following the shape of the true curve) and remains close to zero for $\lambda^2 > \alpha^2$.

Finally, Clayton and Engquist (1977) plot the dispersion relation for the paraxial approximation along with the true dispersion relation. Again, the parabolic curves of the approximation match the circles of the dispersion relation best when k_x is small.

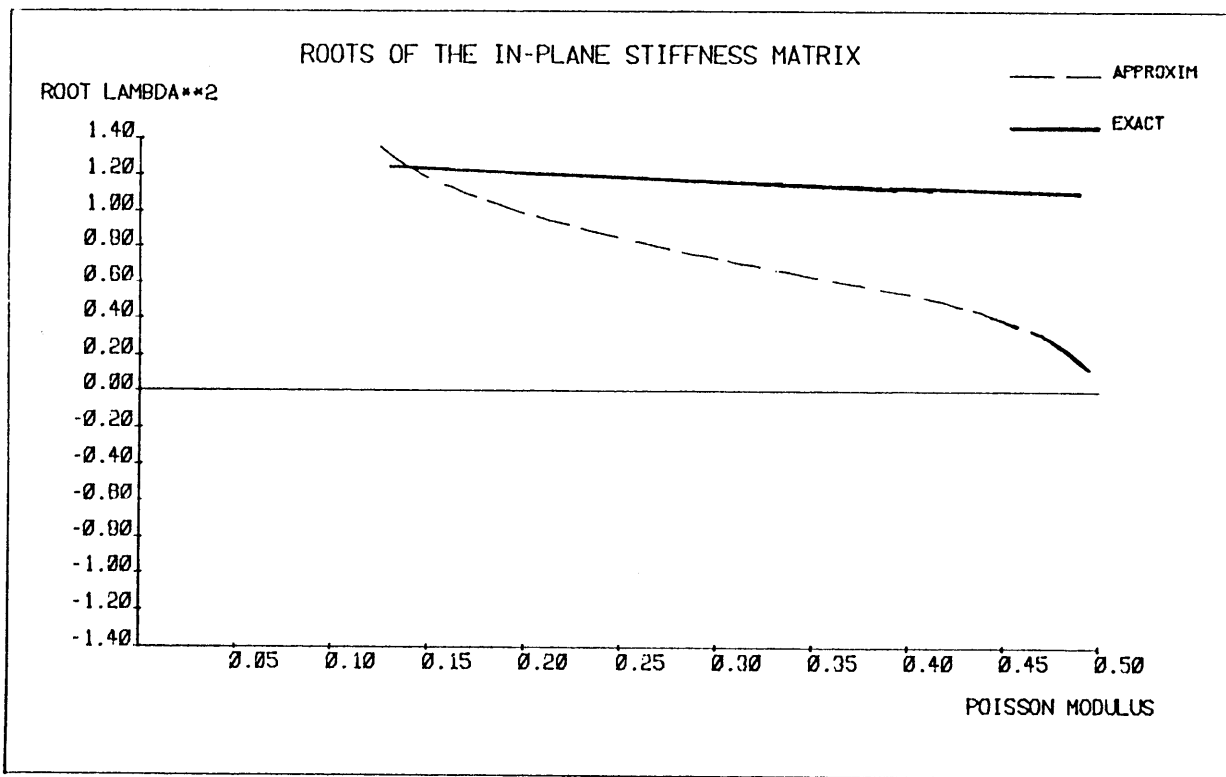


Figure 3-9: Rayleigh Wave Roots for the True and Approximate Stiffness

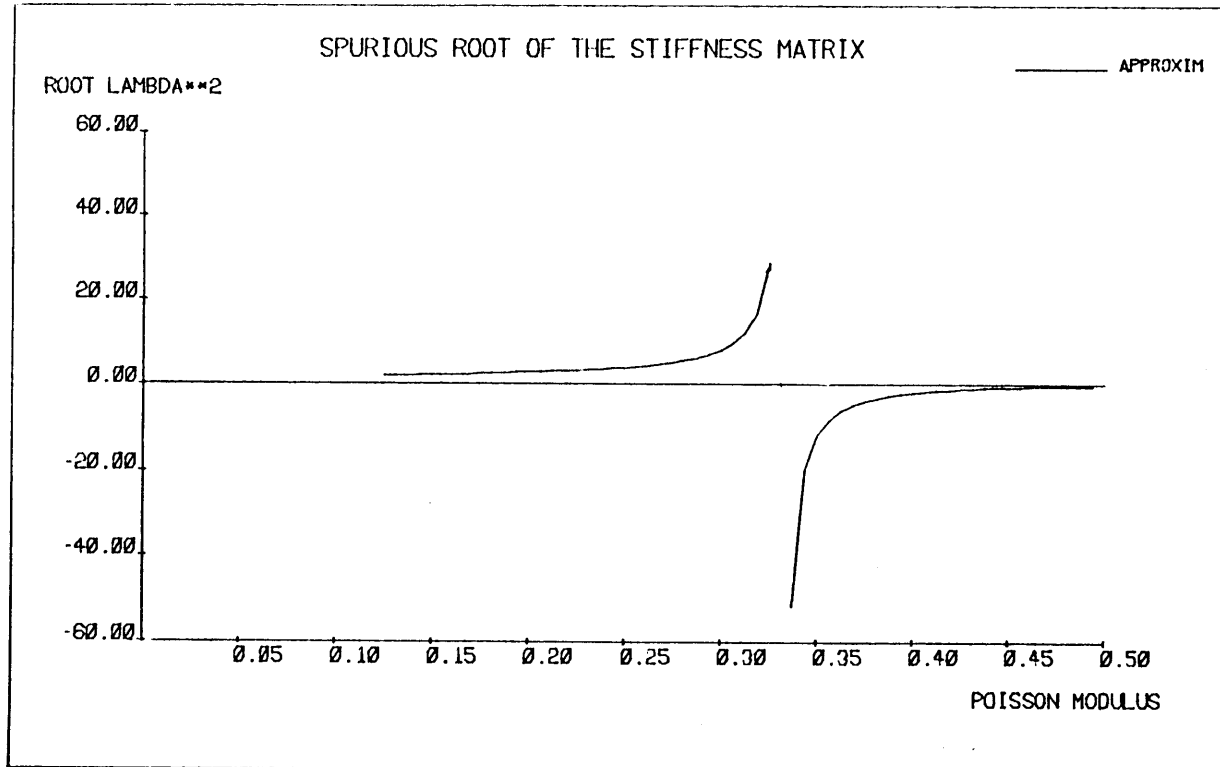


Figure 3-10: Spurious Root of the Approximation

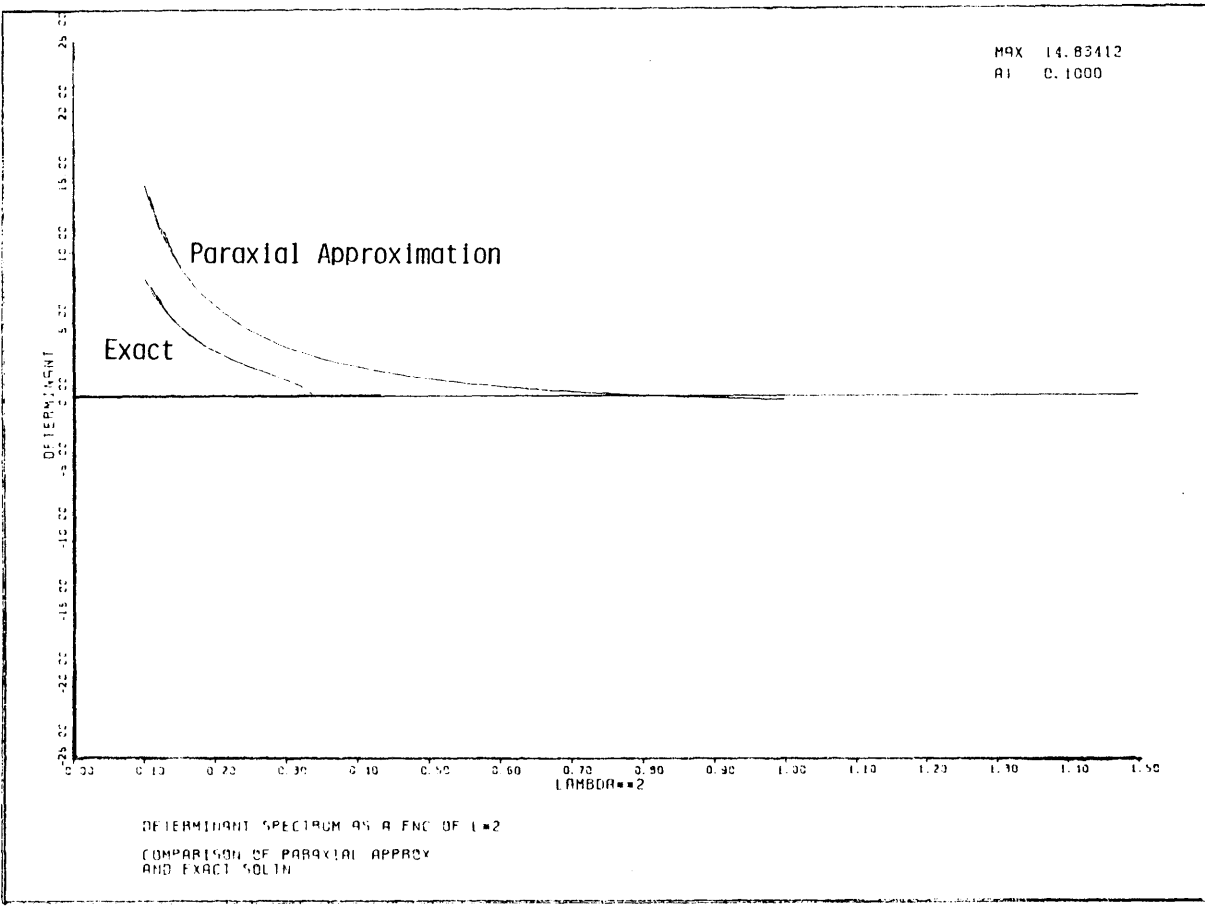
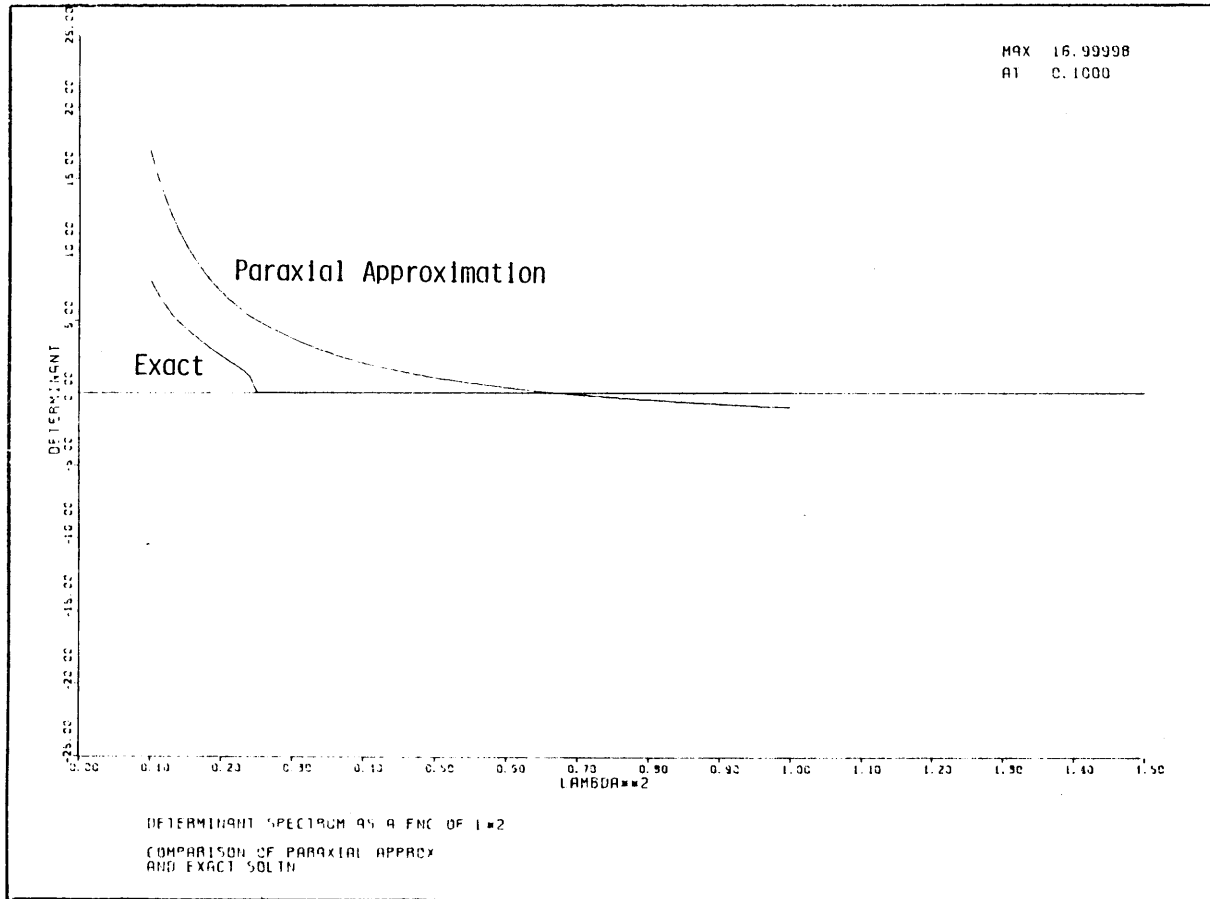


Figure 3-11: Determinant of the Imaginary Part of the Stiffness for $\nu = 1/4$

Figure 3-12: Determinant of the Imaginary Part of the Stiffness for $\nu = 1/3$



3.3 Computation of Displacements

3.3.1 Examples

Dynamic displacements computed with the paraxial approximation are plotted in Figures 3-13 to 3-20. These plots show displacements at the surface in a homogeneous halfspace where $C_s = \lambda = G = \rho = H = 1.0$, $\beta = 0.05$ and H is the depth of the overlying layer. The radius of the disk load is $R = 0.25$. Displacements are plotted versus dimensionless frequency $f_0 = fH/C_s$, beginning at $f_0 = 0.10$. Since the expansion of the terms in the stiffness is valid for small λ , it is not valid for small frequencies ω . Each plot has four curves, one is the true displacements of a halfspace computed with numerical integration and the other three correspond to displacements computed with the discrete method where the overlying layer is divided into 1, 4 and 12 sublayers.

Figures 3-13 and 3-14 show the real and imaginary parts of the vertical displacements at the origin $\rho = 0$ due to a vertical disk load. As the number of layers is increased, the approximation solution approaches the true solution. The 12 layer case shows excellent agreement with the true solution. Figures 3-15 and 3-16 show the real and imaginary parts of the vertical displacement at $\rho = 1.0$ due to a vertical disk load. At this distance from the origin, the displacements oscillate with frequency. The 12 layer case again shows excellent agreement with the true solution.

Figures 3-17 through 3-20 show the real and imaginary parts of the horizontal displacement due to a horizontal disk load at $\rho = 0$ and $\rho = 1.0$. In all four plots, the 12 layer case is almost identical to the true solution.

3.3.2 Variation of Physical Parameters

The examples above use standard physical properties. The influence of altering some of these parameters is investigated in this section. For the purpose of comparison, Figure 3-21 presents the true and the approximate solutions for vertical displacements in a halfspace at the origin due to a vertical disk load. The physical properties are those used in the examples above, but the

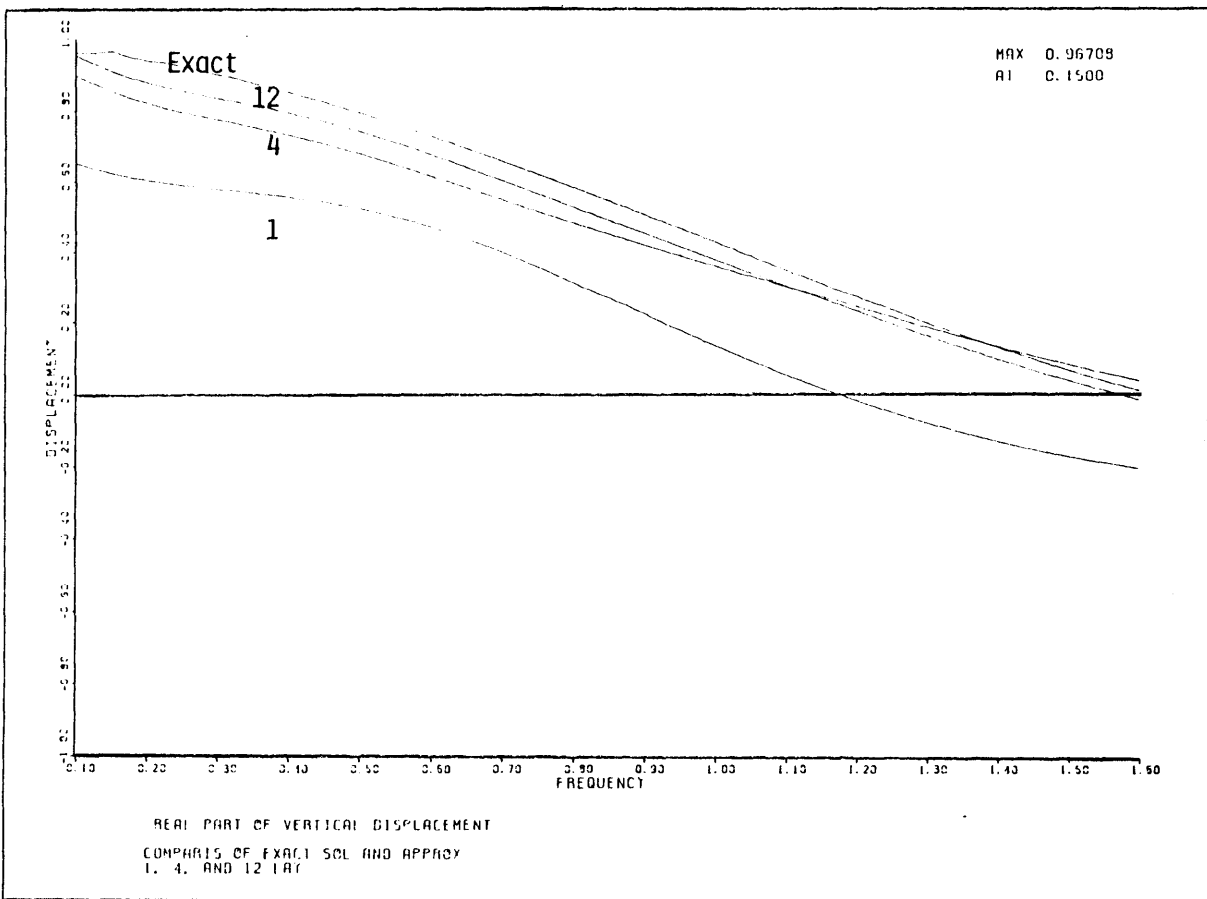


Figure 3-13: Real Part of the Vertical Displacement at $\rho = 0$

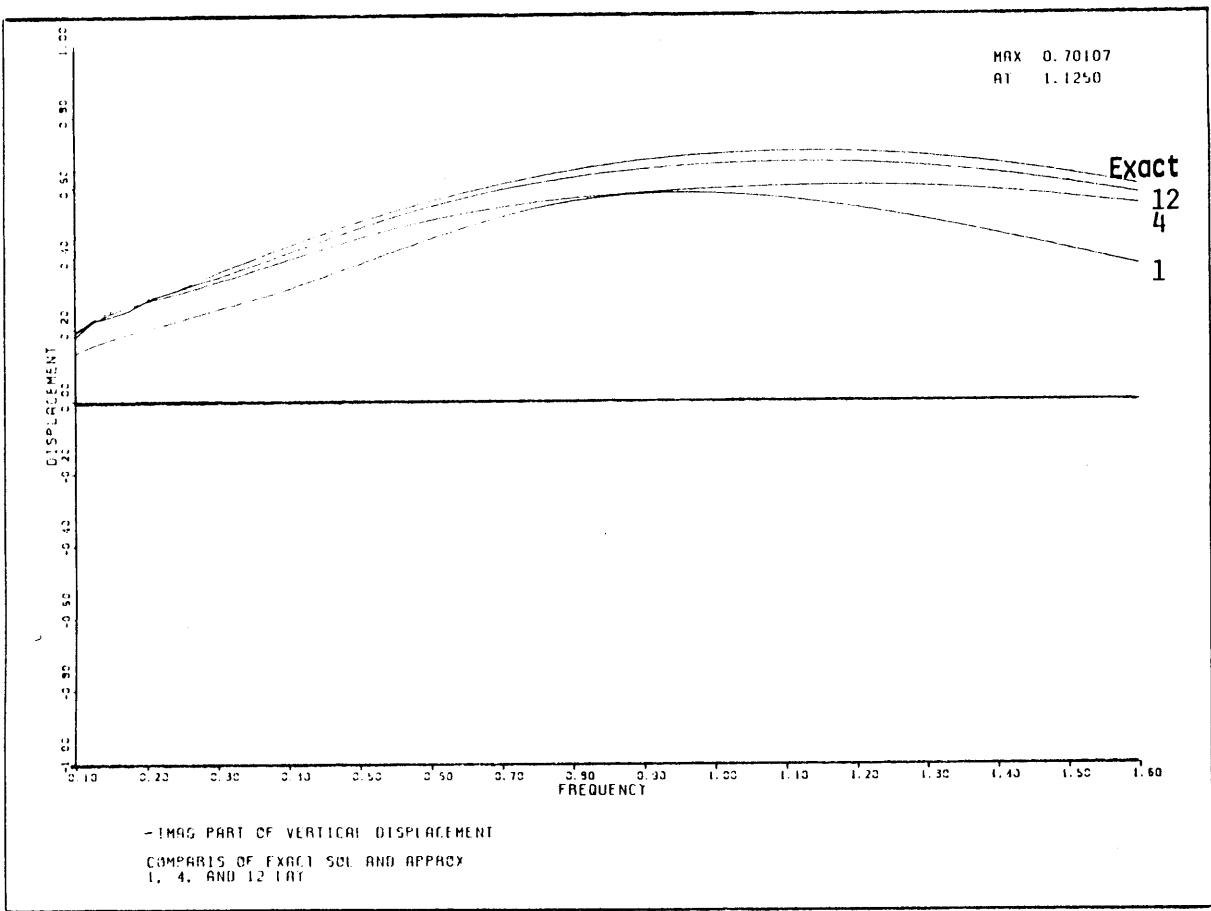


Figure 3-14: Imaginary Part of the Vertical Displacement at $\rho = 0$

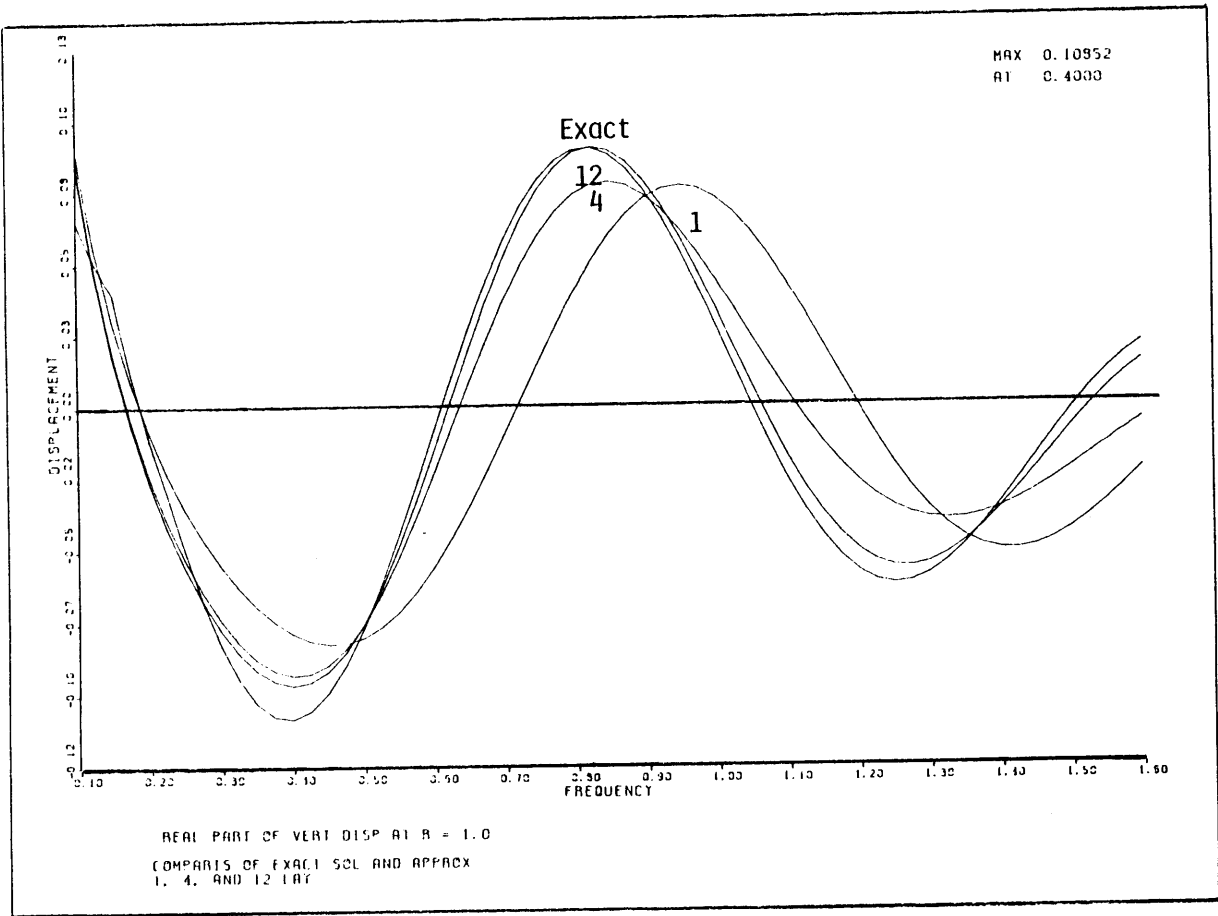


Figure 3-15: Real Part of the Vertical Displacement at $\rho = 1.0$

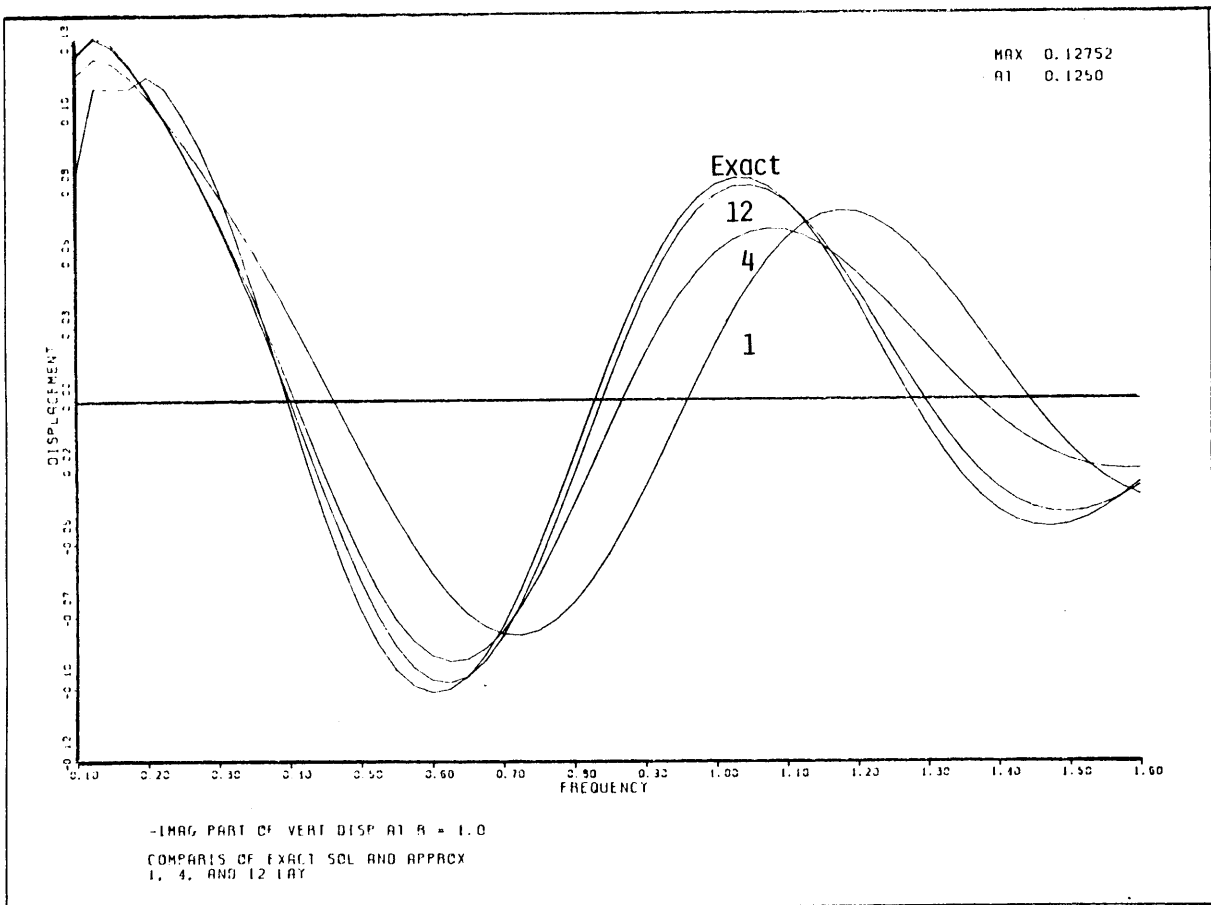


Figure 3-16: Imaginary Part of the Vertical
 Displacement at $\rho = 1.0$

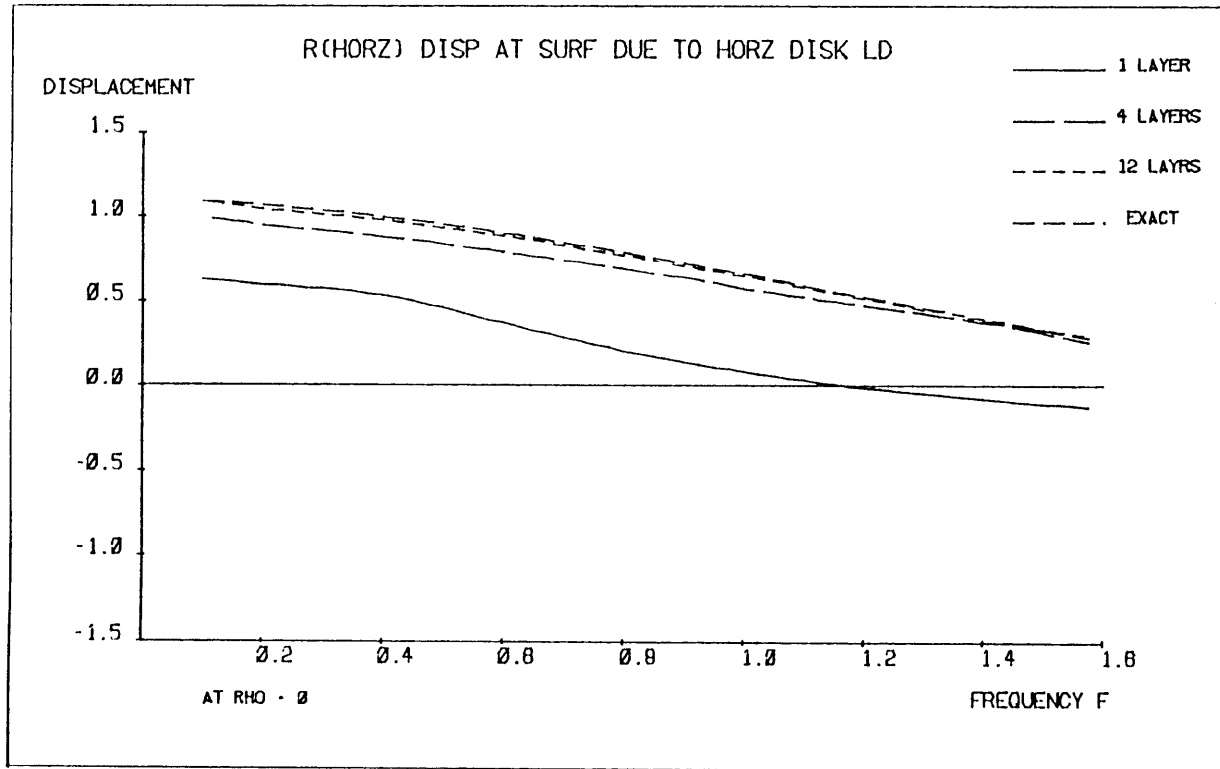


Figure 3-17: Real Part of the Horizontal
Displacement at $\rho = 0$

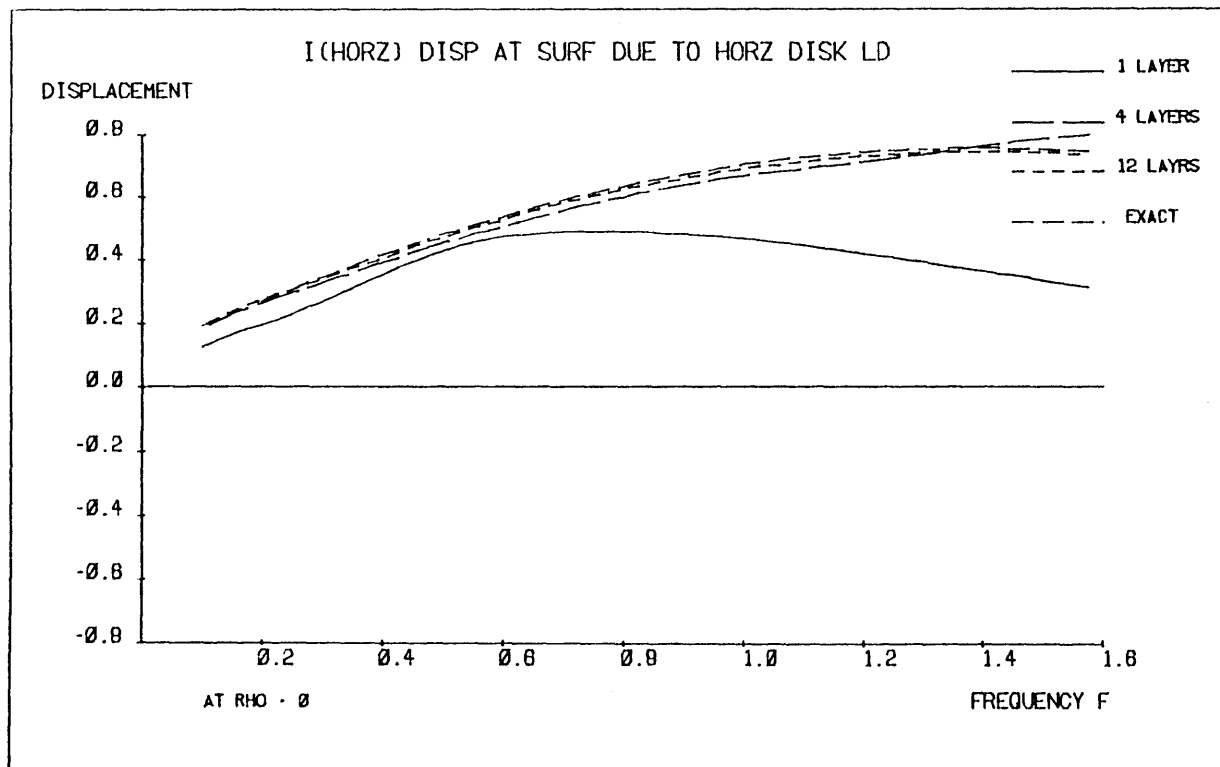


Figure 3-18: Imaginary Part of the Horizontal
Displacement at $\rho = 0$

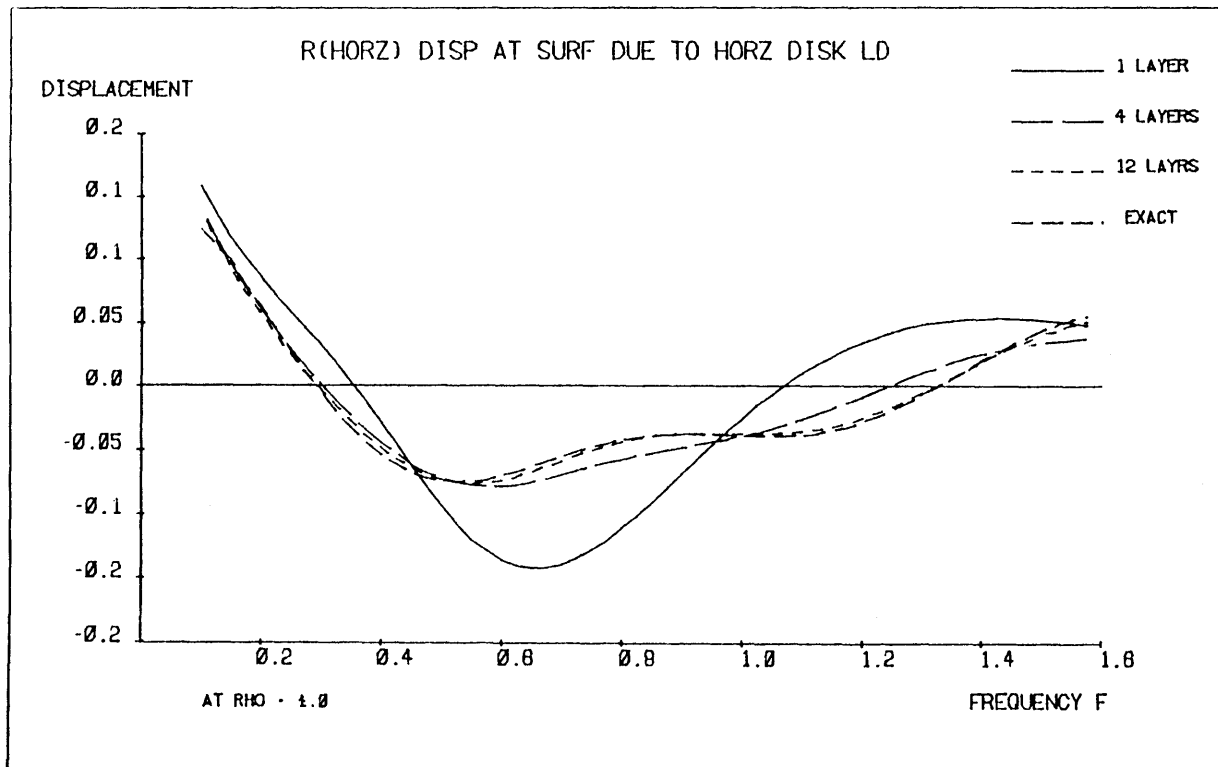


Figure 3-19: Real Part of the Horizontal
Displacement at $\rho = 1.0$

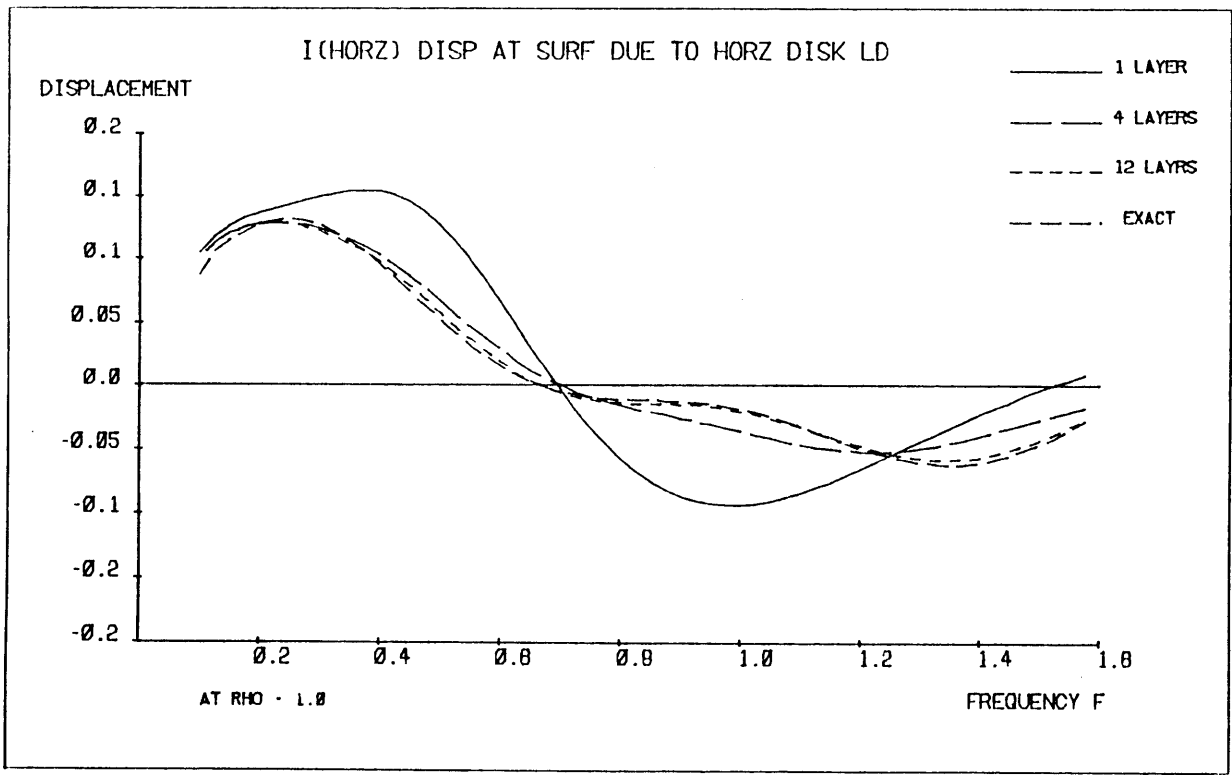


Figure 3-20: Imaginary Part of the Horizontal
Displacement at $\rho = 1.0$

approximation is applied with no overlying layers. It is clear from Figure 3-21 that the paraxial approximation by itself is not a good representation of the halfspace.

The addition of a single layer improves displacement calculations. Figure 3-22 shows the vertical displacements at the origin for the true case and for the paraxial approximation of a halfspace with one overlying layer. The three approximation curves correspond to three values for the depth of the layer, $H = 0.1, 0.25$ and 1.0 . The thin layer ($H = 0.1$) curve naturally resembles the results obtained from the halfspace approximation alone. The thick layer ($H = 1.0$) curve has the same shape as the true displacement curve but has a lower absolute value, indicating that this approximation is too stiff. The best results are obtained when the depth of the layer is equal to the radius of the disk load ($H = R = 0.25$). The displacement curve resembles that of the approximation alone at lower frequencies where it falls off suddenly. This is the influence of the $\frac{1}{\omega}$ term in the paraxial approximation which dominates at low frequencies.

The paraxial approximation is also somewhat sensitive to the value of Poisson's ratio. A plot of vertical displacements at the origin due to a vertical disk load computed with the paraxial approximation itself and various Poisson's ratios is shown in Figure 3-23. The four curves are for Poisson's ratios $\nu = 0.15, 0.25, 0.35$ and 0.45 . For $\nu < \frac{1}{3}$, as ν approaches $\frac{1}{3}$, the waviness of the displacements is more pronounced. For $\nu \geq \frac{1}{3}$, the displacements are essentially zero, due to the influence of the negative spurious root discussed above. The paraxial approximation presented in this chapter gives poor results when $\nu \geq \frac{1}{3}$. If displacements are desired for larger values of ν , the approximation itself should be altered. In particular, one would need to change the coefficients in the matrices so that the second root of Equation 3-19 would be positive for the chosen value of ν . The functional form of the approximation may remain the same, but the coefficients themselves must be altered. Of course, this alteration changes the behavior of the paraxial approximation as a whole and one would have to experiment with the new coefficients to determine the frequency range where the displacements are most accurate. In particular, the change of coefficient described above may cause an exaggeration of the drop in displacements at low frequencies, so that more

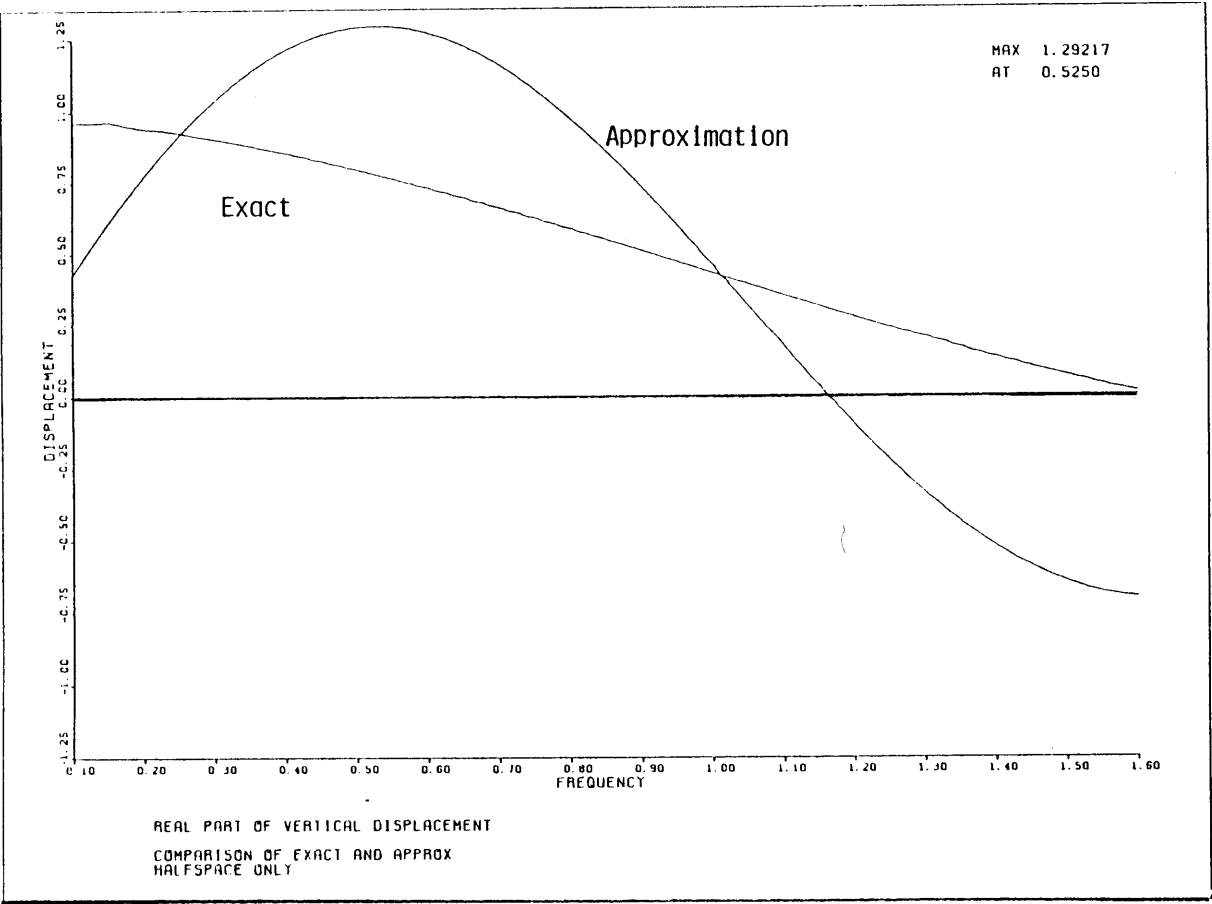


Figure 3-21: True and Approximate Solutions for Vertical Displacements at the Origin

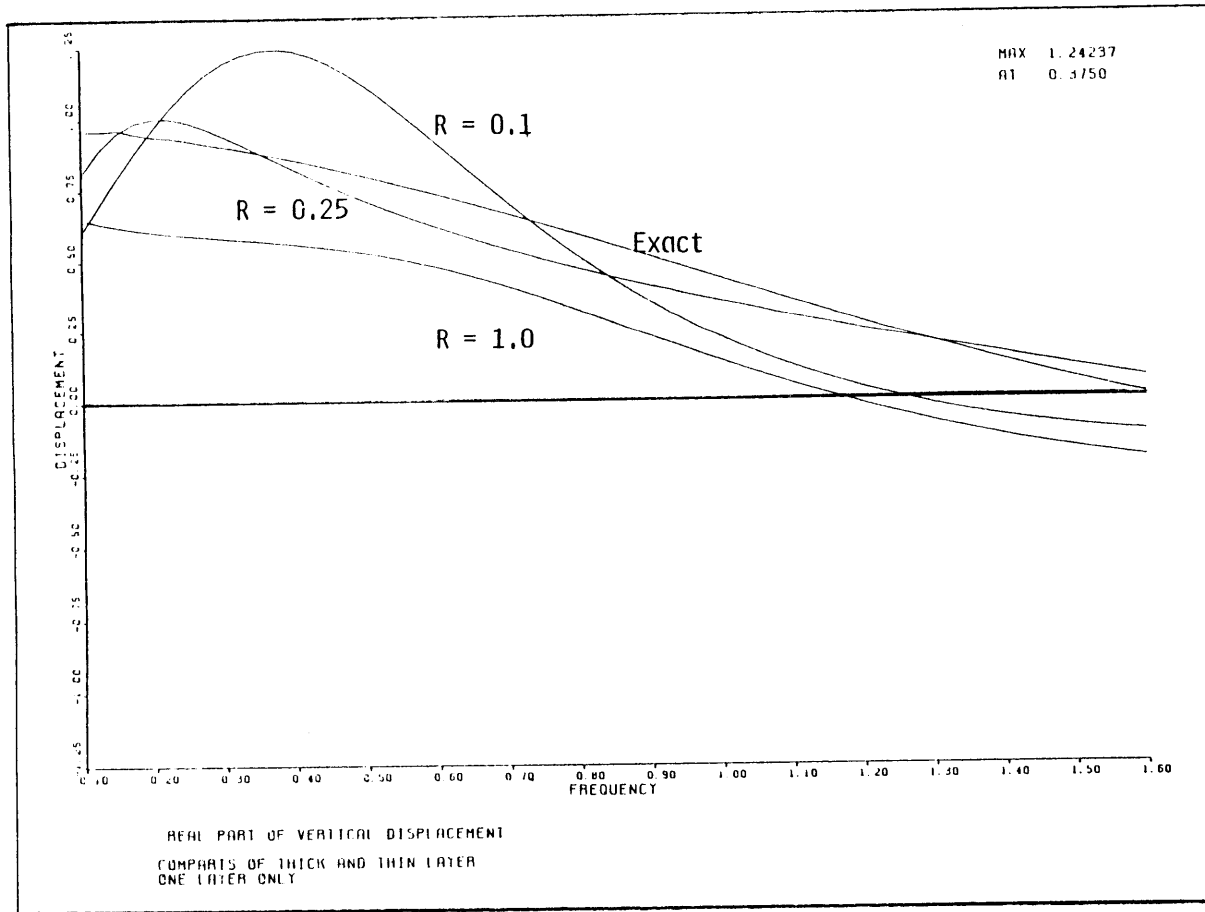


Figure 3-22: Displacements Calculated with the Paraxial Approximation for Different Layer Depths

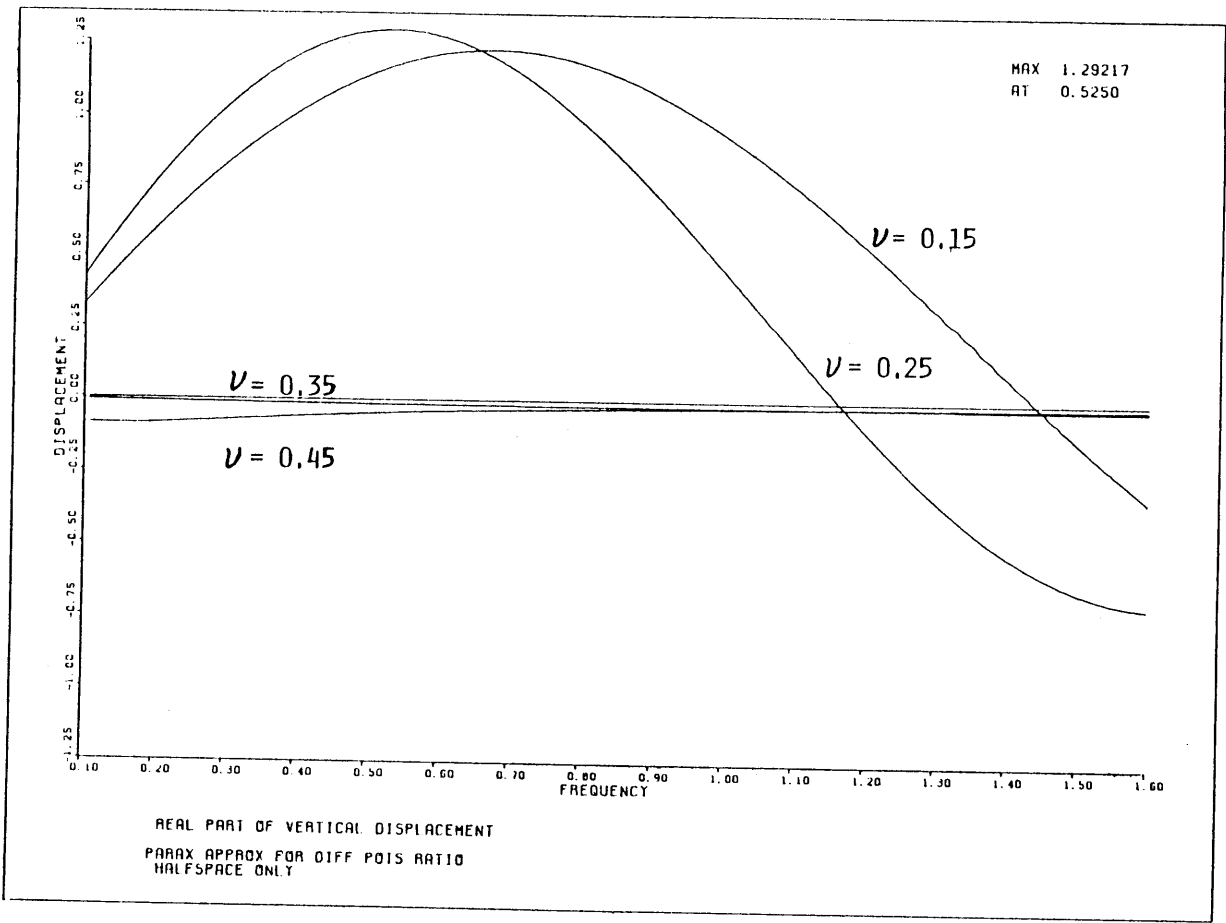


Figure 3-23: Displacements Calculated with the Paraxial Approximation for Different Poisson Ratios

layers may be required for sufficiently accurate results in that range.

Experience with the paraxial approximation has shown that at low frequencies (and with low Poisson's ratios), real values of the wavenumber k are obtained in the quadratic eigenvalue problem. For the halfspace with damping, real wavenumbers are physically impossible since they represent waves that do not attenuate with distance. Thus the occurrence of a real wavenumber indicates that the paraxial approximation is poor in the region of low frequencies.

The real wavenumber occurs at a particular frequency ω_p . As ω increases from zero towards ω_p , the wavenumber k approaches the real axis from below (only wavenumbers with negative imaginary parts are chosen). At a frequency just greater than ω_p , the wavenumber has crossed the real axis and become k^* (the sign of the imaginary part has changed). When this occurs, the negative of k is chosen for the solution. Thus at ω_p , the contributing wavenumber k suddenly becomes $-k^*$. A wavenumber k approaching the real axis in the third quadrant moves to the fourth quadrant for $\omega > \omega_p$ and a wavenumber in the fourth quadrant moves to the third quadrant. This sudden jump in the wavenumber at ω_p induces a change in the shape of the corresponding eigenvector. For every k, ϕ pair, k and $\bar{\phi}$ (the adjoint) are also solutions of the eigenvalue problem. However, for $-k^*, \phi^*$ is not a solution, since the stiffness matrix itself is complex. Thus the eigenvector takes a different shape at ω_p and this causes an abrupt change in the computed displacements.

It is difficult to detect "bad" modes that occur before ω_p . The only way to locate ω_p itself is by observing the sudden change in displacements at that frequency. The application of energy propagation principles described by Waas (1972) allows the energy contribution for each mode to be computed separately. There is the possibility that a "bad mode" would cause a negative energy contribution. However, Equation 3-10 implies that the stiffness matrix K has certain characteristics based on the physics of the problem. In particular, when damping is zero, the matrix A is positive definite. In our case, A has complex elements from the paraxial approximation and is therefore not positive definite. Thus we cannot select only those modes that have positive propagation energy.

A general rule of thumb is that for the the physical properties used in this chapter ($\nu < \frac{1}{3}$, normalized shear modulus G and density $\rho \simeq 1$), there will be no real poles for dimensionless frequency f_0 greater than 0.2.

Aki (1980) described a Rayleigh-Ritz method for obtaining approximate eigenvalues and eigenvectors. Shape functions are chosen to model displacements in a layered halfspace. When these functions are substituted into energy integrals and stationarity is applied, an algebraic matrix equation results. The choice of a shape function that decays exponentially with depth yields a matrix of coefficients that can reproduce the propagation of surface waves. This approach, however, would not be suitable for the purposes described in this paper, where loads applied at the surface generate waves that travel into the halfspace. Thus the ability of the halfspace approximation to model the energy absorbed from incident waves is more important for the loading case than its ability to model surface waves.

Many other variations of the paraxial approximation were tested in the course of this research. Attempts were made to choose algebraic functions that better resembled the true stiffness elements. Also, matrices were chosen that matched the properties of the layer matrices (positive definiteness, etc.). In all cases, it was found that the matrices obtained with the Taylor series expansion gave the best results for displacements for the most wide varieties of geometrical configurations and material properties. Of course, any engineer who is interested in a particular configuration could refine the paraxial approximation to best model that case.

Chapter 4

The Limiting Case: Static Loads in Layered Halfspaces

4.1 Introduction

The stiffness matrix method can be applied in the solution for displacements due to static loads in a layered soil resting on an elastic halfspace. Solutions for displacements due to point loads acting within, or on the surface of, a homogeneous semi-infinite solid can be found in the famous works of Kelvin (1843), Boussinesq (1878), Cerutti (1882) and Mindlin (1936). More complicated situations, such as layered soils, require numerical integration; these solutions are restricted to solids with a small number of layers. A solution for solids with up to three layers has been presented by Burminster (1945) and investigated experimentally by Ueshita and Meyerhof (1967). For a review of Integral Transform techniques, see Davies and Banerjee (1978). The stiffness matrix method presented below is a new approach to these problems, in that the integral transform is computed in closed form, thereby avoiding the difficulties inherent in numerical integration. The dynamic stiffness matrix for a halfspace is approximated by the algebraic stiffness matrix described in Chapter 3. The static stiffness matrix for a halfspace does not need to be approximated, since the transcendental functions reduce to algebraic functions of the wavenumber k when frequency ω is zero.

To solve for static displacements, we follow the same procedure for the dynamic case, outlined in Chapter 2; and we customize the stiffness method for ω equal to zero. As in the dynamic case, the anti-plane, or "Love", modes are uncoupled from the in-plane "Rayleigh" modes. In the static case, the stiffness matrices are real, as the material properties do not include damping. Thus the roots of the quadratic eigenvalue problem are either real numbers or complex conjugate pairs.

There are also three rigid body modes, one corresponding to each cartesian direction. The contribution of the rigid body modes to the flexibility of the layered soil profile is exactly the halfspace flexibility. On the other hand, the real and complex eigenvalues and their corresponding eigenvectors are mathematical artifacts and do not represent true deflection modes.

The addition of the halfspace stiffness to the global stiffness matrix destroys the special structure of the in-plane quadratic eigenvalue problem that allowed reducing it to a linear eigenvalue problem of the same dimension. Thus, the quadratic eigenvalue problem must be expressed as a linear eigenvalue problem of double dimension, and all of the eigenvalues and eigenvectors are required to invert the stiffness matrix.

4.2 Anti-plane Case

4.2.1 Eigenvalue Problem

From Kausel (1981), the anti-plane stiffness of a halfspace with zero frequency and non-zero wavenumber is

$$K = |k|G_r \quad 4-1$$

where G_r is the shear modulus of the halfspace. Since in the cylindrical formulation we work with only non-negative wavenumbers k , we can drop the absolute value sign and write the stiffness as

$$K = kG_r \quad 4-2$$

The eigenvalue problem for the anti-plane case of $N - 1$ layers resting on a halfspace becomes

$$(Ak_j^2 + Bk_j + C)X_j = 0 \quad 4-3$$

where A , B and C are of dimension $N \times N$. The A matrix is the same as in the stratum case of Chapter 2. In the stratum case, there is no B matrix, whereas for the halfspace case Equation 4-2 contributes one term to this matrix. Hence

$$B = \text{diag} (0 , 0 , \dots , G_r) \quad 4-4$$

C is the matrix G from Chapter 2, since ω is zero. The G matrix by itself is singular, which leads to an interesting characteristic of the static problem. Consider the case where $k_j = 0$. The eigenvalue problem reduces to

$$C X_j = 0 \quad 4-5$$

By inspection, we select a vector of dimension N , satisfying Equation 4-5, of the form

$$X_j = E \equiv \{1, 1, \dots, 1\}^T \quad 4-6$$

in which every element is 1. This vector of equal displacements is a rigid body mode of the layered soil system. In this mode, no force is required to maintain a uniform displacement in the anti-plane direction everywhere in the soil. The presence of the rigid body mode is not a surprise. In the static problem, there are no constraints to prevent displacement of the system as a whole.

The quadratic eigenvalue problem can be written in the form of a linear eigenvalue problem of dimension $2N$ as

$$k_j \begin{bmatrix} 0 & A \\ A & B \end{bmatrix} \begin{bmatrix} k_j X_j \\ X_j \end{bmatrix} + \begin{bmatrix} -A & 0 \\ 0 & C \end{bmatrix} \begin{bmatrix} k_j X_j \\ X_j \end{bmatrix} = \begin{bmatrix} 0 \\ 0 \end{bmatrix} \quad 4-7$$

We define these $2N \times 2N$ matrices

$$\overline{A} = \begin{bmatrix} 0 & A \\ A & B \end{bmatrix} \quad \overline{C} = \begin{bmatrix} -A & 0 \\ 0 & C \end{bmatrix} \quad 4-8$$

Note that \overline{C} is singular because the submatrix C is singular. \overline{A} is positive definite and its inverse is given by

$$\overline{A}^{-1} = \begin{bmatrix} -A^{-1}BA^{-1} & A^{-1} \\ A^{-1} & 0 \end{bmatrix} \quad 4-9$$

We then define the eigenmatrix

$$Z = \begin{bmatrix} XK \\ X \end{bmatrix} \quad Z_j = \begin{bmatrix} X_j k_j \\ X_j \end{bmatrix} \quad 4-10$$

where X is the $N \times 2N$ matrix of eigenvectors and K is the $2N \times 2N$ diagonal matrix of eigenvalues. The linear eigenvalue problem is written as

$$k_j \overline{A} Z_j + \overline{C} Z_j = 0 \quad 4-11$$

Since both \overline{A} and \overline{C} are symmetric, the eigenvectors must satisfy the standard orthogonality conditions. The first condition is

$$Z_i^T \overline{C} Z_j = \begin{cases} 0 & \text{if } k_i \neq k_j \\ \text{arbitrary constant} & \text{if } k_i = k_j \end{cases} \quad 4-12$$

Expanding equation 4-12 gives

$$(k_i X_i^T \ X_i^T) \begin{bmatrix} -A & 0 \\ 0 & C \end{bmatrix} \begin{bmatrix} k_j X_j \\ X_j \end{bmatrix} = \quad 4-13$$

$$-k_i k_j X_i^T A X_j + X_i^T C X_j$$

We choose the normalization

$$k_i k_j X_i^T A X_j - X_i^T C X_j = \begin{cases} 0 & \text{if } i \neq j \\ 2k_j^2 & \text{if } i = j \end{cases} \quad 4-14$$

In matrix form the normalization is

$$K X^T A X K - X^T C X = 2K^2$$

or

$$Z^T \overline{C} Z = -2K \quad 4-15$$

This normalization is also satisfied by the rigid body mode where $k_j = 0$. The procedure so far parallels that of the rigid base case. Proof that this normalization reduces to that of the rigid base case, when $G_r \rightarrow \infty$, is given in Appendix A.

Now consider the orthogonality condition

$$Z_i^T \overline{A} Z_j = \begin{cases} 0 & \text{if } i \neq j \\ q_j & \text{if } i = j \end{cases} \quad 4-16$$

Expanding Equation 4-16 gives

$$(k_i X_i^T \quad X_i^T) \begin{bmatrix} 0 & A \\ A & B \end{bmatrix} \begin{bmatrix} k_j X_j \\ X_j \end{bmatrix} = \quad 4-17$$

$$(k_i + k_j) X_i^T A X_j + X_i^T B X_j$$

We must determine the q_j . From the eigenvalue problem, Equation 4-11, we have

$$Z_i^T \overline{A} Z_j + Z_i^T \overline{C} Z_j = 0 \quad 4-18$$

Let $i = j$ and apply the orthogonality conditions 4-14 and 4-16. Then 4-18 becomes

$$k_j q_j - 2k_j^2 = 0 \quad 4-19$$

or

$$k_j (q_j - 2k_j) = 0$$

If $k_j \neq 0$, then $q_j = 2k_j$. When $k_j = 0$, q_j can have any value. Let the rigid body mode, for which $k_j = 0$, have the index $j = 1$. Substituting the eigenvector E , from Equation 4-6, into Equation 4-17 gives

$$q_1 = 0 \cdot E^T A E + E^T B E = G_r \quad 4-20$$

Then the q_j are given by

$$q_1 = G_r \quad 4-21$$

$$q_j = 2k_j \quad j \neq 1$$

We define the modified spectral matrix \overline{K} to be

$$\overline{K} = \text{diag} \left[\frac{1}{2} G_r, k_2, k_3, \dots, k_{2N} \right] = \quad 4-22$$

$$K + \frac{1}{2}G_r J$$

where $J = \text{diag}(1, 0, \dots, 0)$. The second orthogonality condition in matrix form is

$$Z^T \overline{A} Z = 2 \overline{K} \tag{4-23}$$

or

$$KX^TAX + X^TAXK + X^TBX = 2 \overline{K}$$

Since we know that \overline{A} and \overline{K} are not singular (from 4-9 and 4-22), it follows from Equation 4-23 that

$$\det(Z) \cdot \det(\overline{A}) \cdot \det(Z) = \det(2 \overline{K}) \neq 0 \tag{4-24}$$

Thus $\det(Z) \neq 0$ and Z is not singular. Therefore, Z spans the full $2N$ space and can be inverted. From Equation 4-23 we obtain

$$\overline{A} = 2Z^{-T} \overline{K} Z^{-1} \tag{4-25}$$

We then can invert \overline{A}

$$\overline{A}^{-1} = \frac{1}{2} Z \overline{K}^{-1} Z^T \tag{4-26}$$

Expanding 4-26 gives

$$\overline{A}^{-1} = \frac{1}{2} \begin{bmatrix} XK \\ X \end{bmatrix} \overline{K}^{-1} (KX^T \ X^T) = \tag{4-27}$$

$$\frac{1}{2} \begin{bmatrix} XK \overline{K}^{-1} KX^T & XK \overline{K}^{-1} X^T \\ X \overline{K}^{-1} KX^T & X \overline{K}^{-1} X^T \end{bmatrix}$$

These expressions can be simplified by noting that

$$K \bar{K}^{-1} = M = I - J = \text{diag} (0 , 1 , 1 , \dots , 1) \quad 4-28$$

and

$$K \bar{K}^{-1} K = K$$

Then

$$\bar{A}^{-1} = \frac{1}{2} \begin{bmatrix} X K X^T & X M X^T \\ X M X^T & X \bar{K}^{-1} X^T \end{bmatrix} \quad 4-29$$

Matching terms in 4-29 with terms in 4-9, we obtain

$$\begin{aligned} A^{-1} &= \frac{1}{2} X M X^T & 4-30 \\ A^{-1} B A^{-1} &= -\frac{1}{2} X K X^T \\ 0 &= X \bar{K}^{-1} X^T \end{aligned}$$

Proof that these expressions are consistent with the rigid base case is provided in Appendix A.

4.2.2 Eigenvalues

Eigenvalues in the static case are either real or complex conjugate pairs. For the anti-plane case, there is a total of $2N$ eigenvalues: $N - 1$ complex conjugate pairs, one real and one zero. Since static loads produce real displacements, the complex modes have no physical meaning and must be regarded as mathematical artifacts. Furthermore, the single real mode is the mathematical equivalent of a buckling mode, yet it is also devoid of physical significance as its associated eigenvalue violates Equation 4-1. Although the modes may not be meaningful individually, their aggregate contribution to displacements is indeed a real number (see Section 4.4), since the complex conjugate parts cancel each other out.

A plot of eigenvalues k_j for the homogeneous halfspace is presented in Figure 4-1. The material properties are $\rho = \lambda = G = C_s = 1$ and the overlying layer has depth $H = 1$. There are 12 curves for which eigenvalues are plotted, corresponding to subdivisions of the layer into 1 to 12

sublayers. The plot shows only one branch of the complex conjugate pairs. The real parts of the eigenvalues are always negative and decrease in absolute value as the imaginary parts increase. The shape of the eigenvalue curve varies with changes in material properties and sublayer depths.

Kausel derived the analytical solution for eigenvalues in both the continuum and the discrete anti-plane cases of a layer over a halfspace subjected to static loads. These solutions are presented in Appendix B. Both solutions are restricted to the case of a homogeneous stratum overlying an elastic halfspace. In the discrete case, the analytical solution would be difficult to solve numerically.

Roots of the eigenvalue problem are computed with an algorithm that uses direct iteration to find complex conjugate pairs of eigenvalues. The scheme is efficient in that it takes advantage of the symmetric banded form of the matrices and performs no complex arithmetic. Details of the algorithm are presented in Appendix C.

4.2.3 Loading

Consider the equilibrium equation in the wavenumber domain

$$(Ak^2 + Bk + C)U = P \quad 4-31$$

In linear form, this is

$$\left[k \begin{bmatrix} 0 & A \\ A & B \end{bmatrix} + \begin{bmatrix} -A & 0 \\ 0 & C \end{bmatrix} \right] \begin{bmatrix} kU \\ U \end{bmatrix} = \begin{bmatrix} 0 \\ P \end{bmatrix} \quad 4-32$$

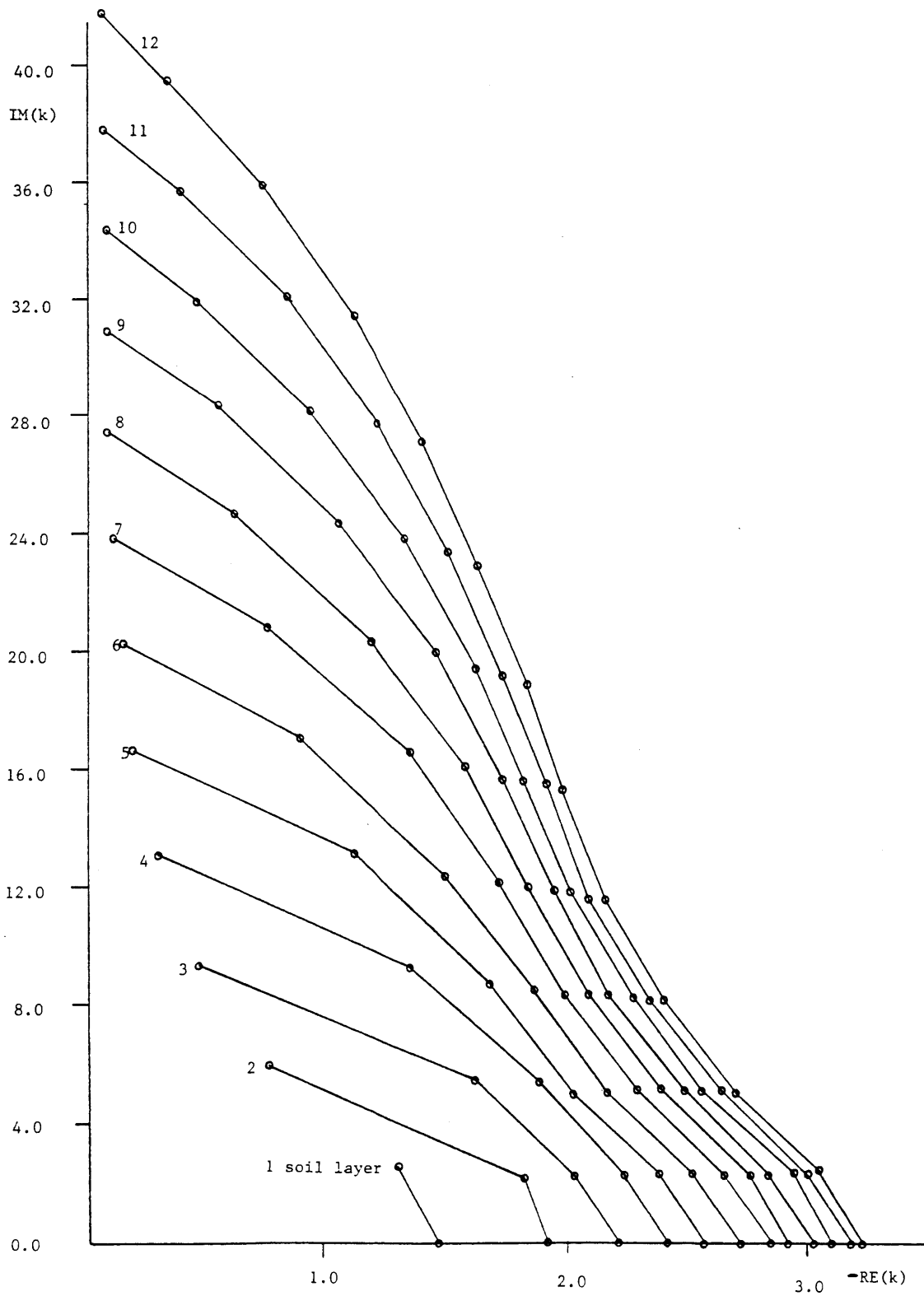
or

$$(\overline{A}k + \overline{C})\overline{U} = \overline{P}$$

Expand \overline{U} in terms of the modes

$$\overline{U} = Z\Gamma = \sum_{j=1}^{2N} \gamma_j Z_j \quad 4-33$$

Figure 4-1: Eigenvalues of Anti-plane Modes for $N = 1$ to 12



or

$$U = X\Gamma$$

where the γ_j are the participation factors. Substituting 4-33 into 4-32 gives

$$(\overline{A}k + \overline{C})Z\Gamma = \overline{P} \quad 4-34$$

Multiply by Z^T

$$Z^T(\overline{A}k + \overline{C})Z\Gamma = Z^T\overline{P} = X^TP = Q \quad 4-35$$

Now apply the orthogonality conditions 4-15 and 4-23

$$(2\overline{K}k - 2K^2)\Gamma = Q \quad 4-36$$

or

$$2\overline{K}(kI - K)\Gamma = Q$$

Solving for Γ gives

$$\Gamma = \frac{1}{2}(kI - K)^{-1}\overline{K}^{-1}Q \quad 4-37$$

Substituting 4-37 into 4-33 yields

$$U = \frac{1}{2}X(kI - K)^{-1}\overline{K}^{-1}X^TP \quad 4-38$$

Again, this is consistent with the rigid base case, as is shown in Appendix A. Equation 4-38 can be written as

$$U = FP \quad 4-39$$

where $F = \{f^{mn}\}$ is the matrix of flexibility coefficients at the m^{th} elevation due to unit loads at the n^{th} elevation (the inverse of the stiffness matrix). Changing to the notation of Chapter 2, the

elements of this matrix are

$$f_{yy}^{mn} = \frac{1}{G_r k} + \sum_{l=2}^{2N} \phi_y^{ml} \phi_y^{nl} \frac{1}{2k_l^L(k - k_l^L)} \quad 4-40$$

where the subscript L stands for Love modes.

The term $\frac{1}{G_r k}$ arises because $\phi_y^{m1} = \phi_y^{n1} = 1$ (the m^{th} and n^{th} elements of E) and $\frac{1}{2(k-0)} \times \frac{2}{G_r} = \frac{1}{G_r k}$. This term is the contribution of the rigid body mode to the flexibility matrix of the system. Note that it is the inverse of the halfspace stiffness 4-2. We define the coefficient

$$a_l = \frac{1}{2k_l(k - k_l)} \quad 4-41$$

Then the flexibility becomes

$$f_{yy}^{mn} = \frac{1}{G_r k} + \sum_{l=2}^{2N} \phi_y^{ml} \phi_y^{nl} a_l^L \quad 4-42$$

4.3 In-plane Case

4.3.1 Eigenvalue Problem

The procedure followed here parallels that of the anti-plane case. From Kausel (1981), the stiffness of the halfspace with zero frequency and non-negative wavenumber is

$$K = \frac{2kG_r}{(1 + \alpha_r^2)} \begin{bmatrix} 1 & -\alpha_r^2 \\ -\alpha_r^2 & 1 \end{bmatrix} \quad k \geq 0 \quad 4-43$$

where α_r and G_r are properties of the halfspace. The eigenvalue problem for the in-plane case is

$$(Ak_j^2 + Bk_j + C)X_j = 0 \quad 4-44$$

where A , B and C are of dimension $2N \times 2N$. Here the A matrix is the same as in Chapter 2 and the C matrix is the G matrix of Chapter 2. The B matrix is now the sum of the halfspace and the stratum contributions

$$B = B_{layers} + B_{halfspace} \quad 4-45$$

where B_{layers} is the B matrix from Chapter 2 and $B_{halfspace}$ is

$$B_{halfspace} = \frac{2G_r}{(1 + \alpha_r^2)} \begin{bmatrix} 1 & -\alpha_r^2 \\ -\alpha_r^2 & 1 \end{bmatrix} \quad 4-46$$

for the last two degrees of freedom. For the dynamic or stratum cases, we can rearrange the degrees of freedom so that the stiffness matrices have these structures

$$A = \begin{bmatrix} A_x \\ A_z \end{bmatrix} \quad B = \begin{bmatrix} B_{xz}^T & B_{xz} \end{bmatrix} \quad C = \begin{bmatrix} C_x \\ C_z \end{bmatrix} \quad 4-47$$

Then the quadratic eigenvalue problem can be expressed as a linear eigenvalue problem of dimension $2N$ (Kausel (1982b)). With the addition of the halfspace, the structure of B becomes

$$B = \begin{bmatrix} B_x & B_{xz} \\ B_{xz}^T & B_z \end{bmatrix} \quad 4-48$$

where

$$B_x = B_z = \text{diag} \left[0, 0, \dots, \frac{2G_r}{(1 + \alpha_r^2)} \right] \quad 4-49$$

It is now necessary to express the quadratic eigenvalue problem as a linear eigenvalue problem of dimension $4N$. As in the anti-plane case, the C matrix is singular. When we set k_j to zero we obtain

$$\begin{bmatrix} C_x \\ C_z \end{bmatrix} \begin{bmatrix} X_{xj} \\ X_{zj} \end{bmatrix} = \begin{bmatrix} 0 \\ 0 \end{bmatrix} \quad 4-50$$

Both C_x and C_z are singular. Thus there are two solutions to 4-50

$$X_j = \begin{bmatrix} E \\ 0 \end{bmatrix} \quad \text{and} \quad X_j = \begin{bmatrix} 0 \\ E \end{bmatrix} \quad 4-51$$

There are two rigid body modes and $k_j = 0$ is a repeated root. The actual rigid body modes are linear combinations of the ones given by 4-51

$$X_j = c_1 \begin{bmatrix} E \\ 0 \end{bmatrix} + c_2 \begin{bmatrix} 0 \\ E \end{bmatrix} \quad 4-52$$

where the coefficients c_1 and c_2 must be determined from orthogonality conditions.

Using the same notation as in the anti-plane case, the linear eigenvalue problem is

$$(\overline{A} k_j + \overline{C})Z_j = 0 \quad 4-53$$

where relationships 4-8, 4-9 and 4-10 are the same, but everything is twice the size (K is $4N \times 4N$, X is $2N \times 4N$, Z is $4N \times 4N$). The orthogonality condition 4-15 is again the same for this case, as is the normalization. The condition is satisfied by both rigid body modes where $k_j = 0$. The orthogonality condition is consistent with the rigid base case, which is shown in Appendix A.

Let the rigid body modes have indices 1 and 2, i.e. they are the first two modes. Consider the second orthogonality condition

$$(k_i + k_j)X_i^T A X_j + X_i^T B X_j = \begin{cases} 0 & \text{if } i \neq j \\ q_j & \text{if } i = j \end{cases} \quad 4-54$$

For $i = j$ this becomes

$$k_j(q_j - 2k_j) = 0 \quad 4-55$$

For $k_j \neq 0$, $q_j = 2k_j$. For $k_j = 0$, q_j must be determined. The rigid body modes must be chosen so that the orthogonality condition 4-54 is satisfied

$$X_1^T B X_2 = 0 \quad 4-56$$

We choose $X_1 = \{E, E\}^T$ and $X_2 = \{E, cE\}^T$ where c must be evaluated. Substitute X_1 and X_2 into 4-54

$$\begin{aligned} (E^T \ E^T) \begin{bmatrix} B_{xz l.} + B_{xz h.s.} & B_z \\ B_{xz l.}^T + B_{xz h.s.}^T & \end{bmatrix} \begin{bmatrix} E \\ cE \end{bmatrix} \\ = E^T B_x E + cE^T B_{xz l.} E + cE^T B_{xz h.s.} E + E^T B_{xz l.}^T E + E^T B_{xz h.s.}^T E + cE^T B_z E \end{aligned} \quad 4-57$$

$$= (1 + c) \frac{2G_r(1 - \alpha_r^2)}{1 + \alpha_r^2} = 0$$

Thus

$$c = -1$$

Then

$$X_1 = \begin{bmatrix} E \\ E \end{bmatrix} \quad \text{and} \quad X_2 = \begin{bmatrix} E \\ -E \end{bmatrix} \quad 4-58$$

In the first rigid body mode, the displacements in the x and z degrees of freedom are equal. In the second rigid body mode, the displacements are equal in magnitude yet opposite in sign. In the first mode the displacements are in phase, in the second mode they are out of phase. Now we can solve for q_1 and q_2 .

$$q_1 = X_1^T B X_1 = \frac{4G_r(1 - \alpha_r^2)}{1 + \alpha_r^2} \quad 4-59$$

$$q_2 = X_2^T B X_2 = 4G_r$$

Then the q_i are given by

$$q_1 = \frac{4G_r(1 - \alpha_r^2)}{1 + \alpha_r^2}$$

$$q_2 = 4G_r \quad 4-60$$

$$q_j = 2k_j \quad \text{for } j \neq 1, 2$$

We define the modified spectral matrix \overline{K}

$$\overline{K} = \text{diag} \left[\frac{2G_r(1 - \alpha_r^2)}{(1 + \alpha_r^2)}, 2G_r, k_3, \dots, k_{4N} \right] = \quad 4-61$$

$$K + \text{diag} \left[\frac{q_1}{2}, \frac{q_2}{2}, 0, \dots, 0 \right] J$$

where $J = \text{diag}(1,1,0, \dots, 0)$.

Then the second orthogonality condition in matrix form is

$$Z^T \overline{A} Z = 2 \overline{K} \tag{4-62}$$

Following the same logic as in the anti-plane case, we can prove that Z is not singular and therefore can be inverted. The inverse of \overline{A} is the same as for the anti-plane case

$$\begin{aligned} A^{-1} &= \frac{1}{2} X M X^T \\ A^{-1} B A^{-1} &= -\frac{1}{2} X K X^T \\ 0 &= X \overline{K}^{-1} X^T \end{aligned} \tag{4-63}$$

where here $M = I - J = \text{diag}(0,0,1, \dots, 1)$. If we rearrange A and B by degrees of freedom and let $X = \{\phi_x, \phi_z\}^T$, then the following expressions are obtained

$$\begin{aligned} A_x^{-1} &= \frac{1}{2} \phi_x M \phi_x^T \\ A_z^{-1} &= \frac{1}{2} \phi_z M \phi_z^T \\ 0 &= \phi_x M \phi_z^T \\ \\ A_x^{-1} B_x A_x^{-1} &= -\frac{1}{2} \phi_x K \phi_x^T \\ A_x^{-1} B_{xz} A_z^{-1} &= -\frac{1}{2} \phi_x K \phi_z^T \\ A_z^{-1} B_z A_z^{-1} &= -\frac{1}{2} \phi_z K \phi_z^T \\ \\ 0 &= \phi_x \overline{K}^{-1} \phi_x^T \\ 0 &= \phi_x \overline{K}^{-1} \phi_z^T \\ 0 &= \phi_z \overline{K}^{-1} \phi_z^T \end{aligned} \tag{4-64}$$

Proof that these equations are consistent with the rigid base case is given in Appendix A.

4.3.2 Eigenvalues

For the in-plane case, there are a total of $4N$ eigenvalues: two are zero, two are real, and there are $2N - 2$ complex conjugate pairs. Again, the real and complex modes are mathematical artifacts and do not have physical meaning. Eigenvalues k_j for the homogeneous halfspace of Section 4.2.2, where the overlying layer is divided into 12 sublayers, are plotted in Figure 4-2. The eigenvalues for the in-plane case are plotted as circles. The dotted line connects eigenvalues for the 12 layer anti-plane case. Note that the in-plane eigenvalues form two distinct groups. Half of the eigenvalues fall on a curve not unlike that of the anti-plane case, except that the absolute values of the k_j are larger. The other half is clustered nearer to the smaller real root. Again, the real parts are always negative. The anti-plane eigenvalues divide the quadrant between the two groups. Although we have not proven it, our experience indicates that the anti-plane eigenvalues always fall between these two groups of in-plane eigenvalues in the complex quadrant. The significance of this observation is that the real anti-plane root lies between the two real in-plane roots. Thus the real anti-plane root can be used as a starting point in a search for the real in-plane roots. Roots of the eigenvalue problem for the in-plane case are computed with the algorithm described in Appendix C.

4.3.3 Loading

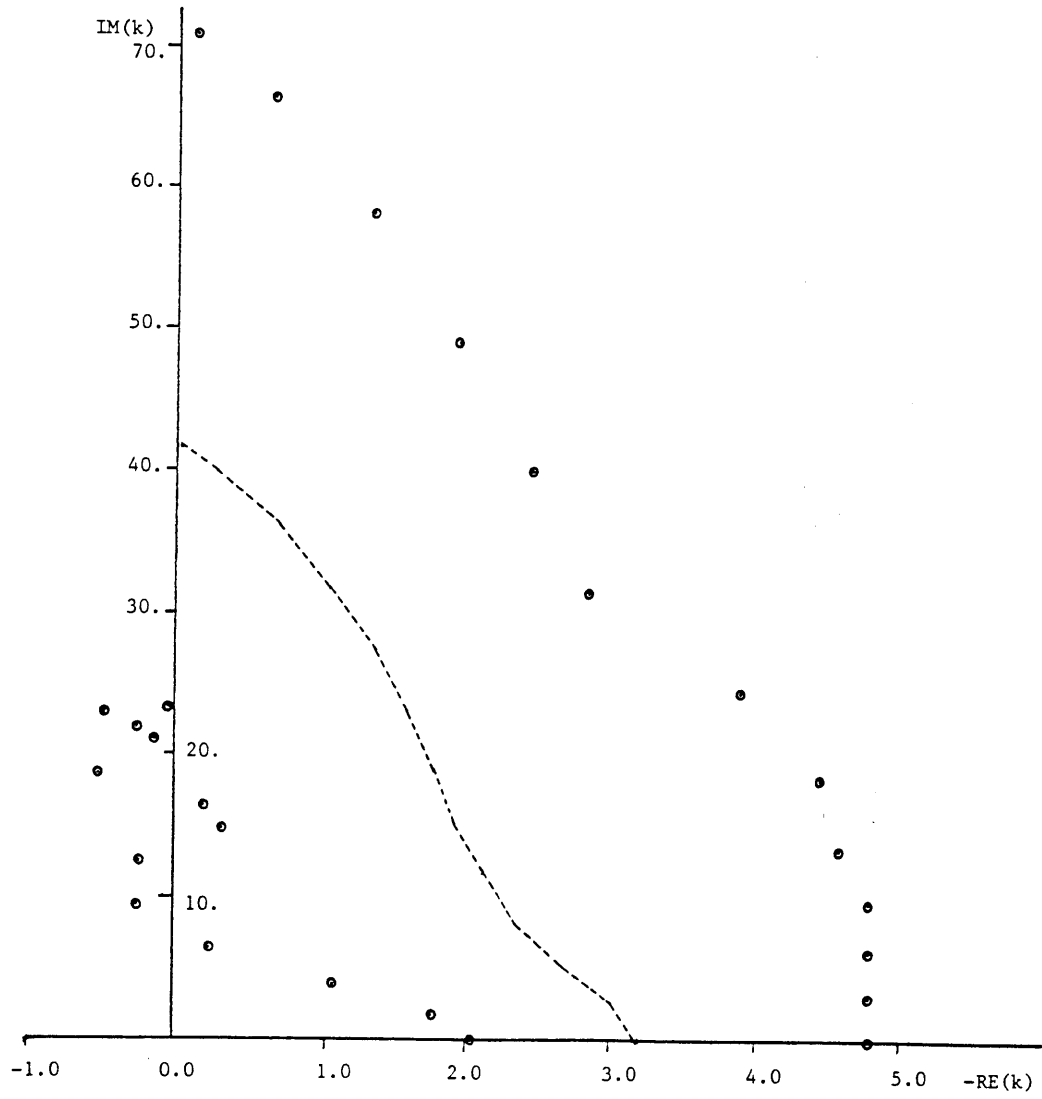
Following the same procedure as for the anti-plane case (Equations 4-31 through 4-38), we obtain the flexibility matrix

$$F = \frac{1}{2}X(kI - K)^{-1}\overline{K}^{-1}X^T \quad 4-65$$

where the matrices X , K , and \overline{K} are those defined in Section 4.3.1. To obtain the flexibilities by degree of freedom, we partition X

$$X = \begin{bmatrix} \Phi_x \\ \Phi_z \end{bmatrix} = \begin{bmatrix} \phi_{1x} & \phi_{2x} & \phi_{3x} & \dots \\ \phi_{1z} & \phi_{2z} & \phi_{3z} & \dots \end{bmatrix} \quad 4-66$$

Figure 4-2: Eigenvalues of In-Plane Modes for $N = 12$



Then the submatrices are

$$\begin{aligned}
 F_{xx} &= \frac{1}{2} \left[\frac{(1 + \alpha_r^2)}{2kG_r(1 - \alpha_r^2)} \phi_{1x} \phi_{1x}^T + \frac{1}{2kG_r} \phi_{2x} \phi_{2x}^T + \frac{1}{k_3(k - k_3)} \phi_{3x} \phi_{3x}^T + \dots \right] \\
 F_{xz} &= \frac{1}{2} \left[\frac{(1 + \alpha_r^2)}{2kG_r(1 - \alpha_r^2)} \phi_{1x} \phi_{1z}^T + \frac{1}{2kG_r} \phi_{2x} \phi_{2z}^T + \frac{1}{k_3(k - k_3)} \phi_{3x} \phi_{3z}^T + \dots \right] \\
 F_{zz} &= \frac{1}{2} \left[\frac{(1 + \alpha_r^2)}{2kG_r(1 - \alpha_r^2)} \phi_{1z} \phi_{1z}^T + \frac{1}{2kG_r} \phi_{2z} \phi_{2z}^T + \frac{1}{k_3(k - k_3)} \phi_{3z} \phi_{3z}^T + \dots \right] \\
 F_{zx} &= \frac{1}{2} \left[\frac{(1 + \alpha_r^2)}{2kG_r(1 - \alpha_r^2)} \phi_{1z} \phi_{1x}^T + \frac{1}{2kG_r} \phi_{2z} \phi_{2x}^T + \frac{1}{k_3(k - k_3)} \phi_{3z} \phi_{3x}^T + \dots \right]
 \end{aligned} \tag{4-67}$$

The individual components of each flexibility matrix are given by

$$\begin{aligned}
 F_{xx}^{mn} &= \frac{1}{2kG_r(1 - \alpha_r^2)} + \sum_{l=3}^{4N} \phi_x^{ml} \phi_x^{nl} a_l^R \\
 F_{xz}^{mn} &= \frac{\alpha_r^2}{2kG_r(1 - \alpha_r^2)} + \sum_{l=3}^{4N} \phi_x^{ml} \phi_z^{nl} a_l^R \\
 F_{zz}^{mn} &= \frac{1}{2kG_r(1 - \alpha_r^2)} + \sum_{l=3}^{4N} \phi_z^{ml} \phi_z^{nl} a_l^R \\
 F_{zx}^{mn} &= \frac{\alpha_r^2}{2kG_r(1 - \alpha_r^2)} + \sum_{l=3}^{4N} \phi_z^{ml} \phi_x^{nl} a_l^R
 \end{aligned} \tag{4-68}$$

where a_l^R is the coefficient defined in 4-41 for the Rayleigh modes. The contribution of the rigid body modes to the flexibilities is the inverse of the halfspace stiffness 4-43. Proof that these flexibilities reduce to the rigid base case is given in Appendix A.

4.4 Displacements due to Static Point Loads

Given the flexibilities 4-40 and 4-68, we can obtain displacements due to static loads. We use the same procedure that Kausel (1982b) did for dynamic loads. The displacement vector in cylindrical coordinates is

$$\bar{U} = \begin{bmatrix} \bar{u}_\rho \\ \bar{u}_\theta \\ \bar{u}_z \end{bmatrix} \quad 4-69$$

where the superscript bar refers to the frequency-wave number domain. \bar{U} is related to U , the vector of displacements in the spatial domain, by the transforms 2-54 and 2-53 of Chapter 2. The displacements at the m^{th} elevation are given by Equation 2-56, where \bar{P}_μ is the transform of the loads applied at the n^{th} interface given by Equation 2-57.

When the applied static load is a point load, the transforms of Equation 2-56 can be computed analytically. A point load is a singularity in the spatial domain. To find the transform of a point load, we begin with a uniform load q distributed over a disk of radius R . After computing the transform of the disk load 2-57, we take the limit of \bar{P}_μ as $R \rightarrow 0$.

4.4.1 Horizontal Point Load

The components in cylindrical coordinates of a uniform load q distributed over a disk of radius R are

$$P = q \begin{bmatrix} \cos \theta \\ -\sin \theta \\ 0 \end{bmatrix} \quad 0 \leq \rho \leq R \quad 4-70$$

Applying Equation 2-57, we obtain

$$\bar{P}_1 = q \begin{bmatrix} 1 \\ 1 \\ 0 \end{bmatrix} \frac{R}{k} J_1(kR) \quad 4-71$$

$$\bar{P}_\mu = 0 \quad \mu \neq 1$$

For a disk load q with a total magnitude of 1,

$$q = \frac{1}{\pi R^2} \quad 4-72$$

From the series expansion for $J_1(x)$, we obtain $\lim_{x \rightarrow 0} \frac{J_1(x)}{x} = \frac{1}{2}$. Then the limit of \bar{P}_1 as $R \rightarrow 0$ is

$$\overline{P}_1 = \frac{1}{2\pi} \begin{bmatrix} 1 \\ 1 \\ 0 \end{bmatrix} \quad 4-73$$

The global flexibility matrix F^{mn} is given by Equation 2-48. The product $F^{mn} \overline{P}_1$ is

$$F^{mn} \overline{P}_1 = \frac{1}{2\pi} \begin{bmatrix} f_{xx}^{mn} \\ f_{yy}^{mn} \\ f_{zx}^{mn} \end{bmatrix} \quad 4-74$$

Substituting 4-74 into the integral 2-56 yields the displacement vector

$$\begin{aligned} u_\rho^{mn} &= \frac{1}{2\pi} \left[\frac{d}{d\rho} \int_0^\infty J_1(k\rho) f_{xx}^{mn} dk + \frac{1}{\rho} \int_0^\infty J_1(k\rho) f_{yy}^{mn} dk \right] \\ u_\theta^{mn} &= \frac{1}{2\pi} \left[\frac{1}{\rho} \int_0^\infty J_1(k\rho) f_{xx}^{mn} dk + \frac{d}{d\rho} \int_0^\infty J_1(k\rho) f_{yy}^{mn} dk \right] \\ u_z^{mn} &= \frac{1}{2\pi} \left[- \int_0^\infty k J_1(k\rho) f_{zx}^{mn} dk \right] \end{aligned} \quad 4-75$$

The following integrals occur with the rigid body terms

$$\begin{aligned} \int_0^\infty \frac{J_1(k\rho)}{k} dk &= 1 \\ \int_0^\infty J_1(k\rho) dk &= \frac{1}{\rho} \\ \int_0^\infty J_0(k\rho) dk &= \frac{1}{\rho} \end{aligned} \quad 4-76$$

Substituting the flexibilities 4-40 and 4-68 into 4-75 and applying the integrals 4-76 gives the displacement vector

$$\begin{aligned} &\frac{1}{2\pi} \left[\frac{1}{\rho G_r} + \sum_{l=3}^{4N} \phi_x^{ml} \phi_x^{nl} \frac{d}{d\rho} \int_0^\infty a_l^R J_1(k\rho) dk + \sum_{l=2}^{2N} \phi_y^{ml} \phi_y^{nl} \frac{1}{\rho} \int_0^\infty a_l^L J_1(k\rho) dk \right] \\ &\frac{1}{2\pi} \left[\frac{1}{2\rho G_r (1 - \alpha_r^2)} + \sum_{l=3}^{4N} \phi_x^{ml} \phi_x^{nl} \frac{1}{\rho} \int_0^\infty a_l^R J_1(k\rho) dk + \sum_{l=2}^{2N} \phi_y^{ml} \phi_y^{nl} \frac{d}{d\rho} \int_0^\infty a_l^L J_1(k\rho) dk \right] \end{aligned} \quad 4-77$$

$$-\frac{1}{2\pi} \left[\frac{\alpha_r^2}{2\rho G_r(1-\alpha_r^2)} + \sum_{l=3}^{4N} \phi_z^{ml} \phi_x^{nl} \int_0^\infty a_l^R k J_1(k\rho) dk \right]$$

We define these integrals (see Table 4-I).

$$I_{3l} = \int_0^\infty a_l J_1(k\rho) dk \quad 4-78$$

$$I_{2l} = \int_0^\infty a_l k J_1(k\rho) dk$$

$$I_{1l} = \int_0^\infty a_l k J_0(k\rho) dk$$

Then the expressions in 4-77 simplify to

$$\begin{aligned} u_\rho^{mn} &= \frac{1}{2\pi} \left[\frac{1}{\rho G_r} + \sum_{l=3}^{4N} \phi_x^{ml} \phi_x^{nl} \frac{d}{d\rho} I_{3l}^R + \sum_{l=2}^{2N} \phi_y^{ml} \phi_y^{nl} \frac{1}{\rho} I_{3l}^L \right] (\cos \theta) \\ u_\theta^{mn} &= \frac{1}{2\pi} \left[\frac{1}{2\rho G_r(1-\alpha_r^2)} + \sum_{l=3}^{4N} \phi_x^{ml} \phi_x^{nl} \frac{1}{\rho} I_{3l}^R + \sum_{l=2}^{2N} \phi_y^{ml} \phi_y^{nl} \frac{d}{d\rho} I_{3l}^L \right] (-\sin \theta) \\ u_z^{mn} &= -\frac{1}{2\pi} \left[\frac{\alpha_r^2}{2\rho G_r(1-\alpha_r^2)} + \sum_{l=3}^{4N} \phi_z^{ml} \phi_x^{nl} I_{2l}^R \right] (\cos \theta) \end{aligned} \quad 4-79$$

The constant terms in the displacements are the Cerutti solutions for displacements on the surface of a halfspace due to a horizontal point load on the surface. Thus our method of integral transforms for the point load is consistent in that we recover the Cerutti solution when there are no layers resting on the halfspace.

4.4.2 Vertical Point Load

We follow the same procedure to obtain displacements due to a vertical point load as we did for the horizontal point load. The components in cylindrical coordinate of a uniform vertical load q distributed over a disk of radius R are

$$P = q \begin{bmatrix} 0 \\ 0 \\ 1 \end{bmatrix} \quad 0 \leq \rho \leq R \quad 4-80$$

Substituting 4-80 into Equation 2-57, we obtain the transformed load

4-81

$$\bar{P}_0 = -q \begin{bmatrix} 0 \\ 0 \\ 1 \end{bmatrix} \frac{R}{k} J_1(kR)$$

$$\bar{P}_\mu = 0 \quad \mu \neq 0$$

Again, we choose $q = \frac{1}{\pi R^2}$ so that the point load has a magnitude of 1. Then

$$\bar{P}_0 = -\frac{1}{\pi} \begin{bmatrix} 0 \\ 0 \\ 1 \end{bmatrix} \frac{J_1(kR)}{kR} \quad 4-82$$

Taking the limit of \bar{P}_0 as $R \rightarrow 0$ yields

$$\bar{P}_0 = -\frac{1}{2\pi} \begin{bmatrix} 0 \\ 0 \\ 1 \end{bmatrix} \quad 4-83$$

The product $F^{mn} \bar{P}_0$ is

$$-\frac{1}{2\pi} \begin{bmatrix} f^{mn} \\ 0 \\ f^{mn} \\ f^{mn} \end{bmatrix} \quad 4-84$$

Substituting 4-84 into the integral 2-56 yields the displacement vector

$$u_\rho^{mn} = \frac{1}{2\pi} \left[-\int_0^\infty \frac{d}{d(k\rho)} J_0(k\rho) k f_{zz}^{mn} dk \right]$$

$$u_\theta^{mn} = 0 \quad 4-85$$

$$u_z^{mn} = \frac{1}{2\pi} \left[\int_0^\infty k J_0(k\rho) f_{zz}^{mn} dk \right]$$

Substituting the flexibilities 4-68 into 4-85 and applying the integrals 4-76 gives the vector

$$\frac{1}{2\pi} \left[\frac{\alpha_r^2}{2\rho G_r (1 - \alpha_r^2)} + \sum_{l=3}^{4N} \phi_x^{ml} \phi_z^{nl} \int_0^\infty a_l^R k J_1(k\rho) dk \right]$$

0 4-86

$$\frac{1}{2\pi} \left[\frac{1}{2\rho G_r(1-\alpha_r^2)} + \sum_{l=3}^{4N} \phi_z^{ml} \phi_x^{nl} \int_0^\infty a_l^R k J_0(k\rho) dk \right]$$

Changing to the notation defined in Equation 4-78, we obtain

$$u_\rho^{mn} = \frac{1}{2\pi} \left[\frac{\alpha_r^2}{2\rho G_r(1-\alpha_r^2)} + \sum_{l=3}^{4N} \phi_x^{ml} \phi_z^{nl} I_{2l}^R \right]$$

$$u_\theta^{mn} = 0$$

4-87

$$u_z^{mn} = \frac{1}{2\pi} \left[\frac{1}{2\rho G_r(1-\alpha_r^2)} + \sum_{l=3}^{4N} \phi_z^{ml} \phi_x^{nl} I_{1l}^R \right]$$

By comparing the term u_ρ^{mn} of 4-87 to u_z^{mn} of 4-79, we can see that these terms by definition satisfy reciprocity. The displacement u_z at elevation m due to a radial point load applied at elevation n is identically equal in absolute value to the displacement u_ρ at elevation n due to a vertical point load at elevation m . The constant terms in the displacements are the Boussinesq solutions for displacements on the surface of a halfspace due to a vertical point load on the surface. Again, our solution is consistent with the known solution for a halfspace.

4.4.3 Examples

The closed-form solutions to the integrals I_{1l} , I_{2l} and I_{3l} are given in Table 4-I. Notice that when k_l is a positive real number, the term a_l in the integrands becomes singular and the integrals are undefined. In the complex domain, the positive real axis is the branch cut. The branch cut does not concern us since the real eigenvalues for both the in-plane and the anti-plane cases are always negative. The derivation of the solutions to these integrals is in Appendix D. Algorithms for the evaluation of the Struve and Neuman functions are presented in Appendix E.

The accuracy of this scheme was tested by computing displacements in a homogeneous halfspace subjected to static point loads. The geometry of the discretization is shown in Figure 4-3. The material properties are $\rho = \lambda = G = C_s = 1$. The overlying layer has depth $H = 1$ and is

Table 4-I: Integrals Used to Compute Static Displacements

$$I_{1l} = \frac{1}{2k_l} \int_0^\infty \frac{k J_0(k\rho) dk}{(k - k_l)} = \frac{1}{2} \left[\frac{1}{\rho k_l} + \frac{\pi}{2} (\mathbf{H}_0(-\rho k_l) - \mathbf{Y}_0(-\rho k_l)) \right]$$

$$| \arg(-k_l) | < \pi$$

$$I_{2l} = \frac{1}{2k_l} \int_0^\infty \frac{k J_1(k\rho) dk}{(k - k_l)} = \frac{1}{2} \left[1 - \frac{\pi}{2} (\mathbf{H}_1(-\rho k_l) - \mathbf{Y}_1(-\rho k_l)) \right]$$

$$| \arg(-k_l) | < \pi$$

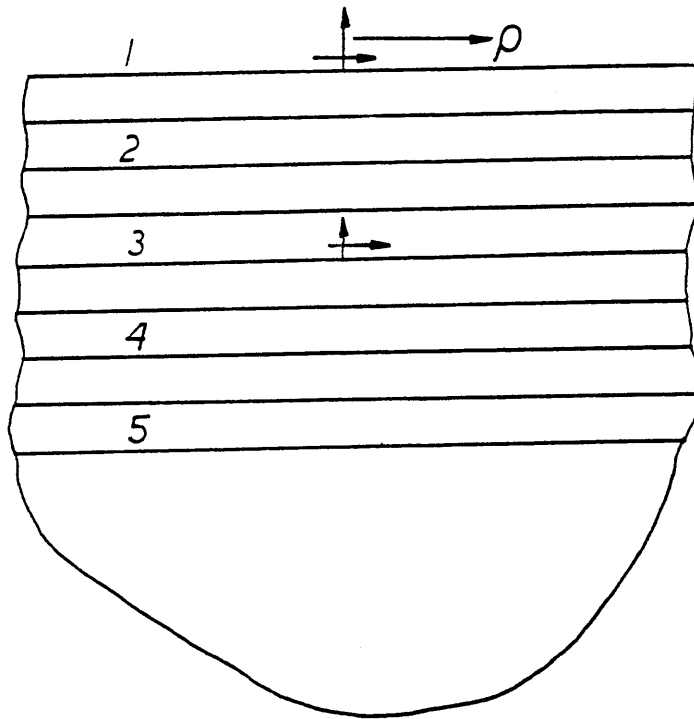
$$I_{3l} = \frac{1}{2k_l} \int_0^\infty \frac{J_1(k\rho) dk}{(k - k_l)} = \frac{1}{2k_l} \left[1 - \frac{1}{\rho k_l} - \frac{\pi}{2} (\mathbf{H}_1(-\rho k_l) - \mathbf{Y}_1(-\rho k_l)) \right]$$

$$| \arg(-k_l) | < \pi$$

Note: $I_{2l} = k_l I_{3l} + \frac{1}{2\rho k_l}$ $\frac{d}{d\rho} I_{3l} = I_{1l} - \frac{1}{\rho} I_{3l}$

discretized into 8 sublayers. Elevations 1 through 5 correspond to depths $z = 0.0, 0.25, 0.5, 0.75,$ and 1.0 . Figures 4-4 through 4-9 show displacements versus distance ρ from the point of application of the load.

Figure 4-3: Geometry of Homogeneous Halfspace Subjected to Static Point Loads



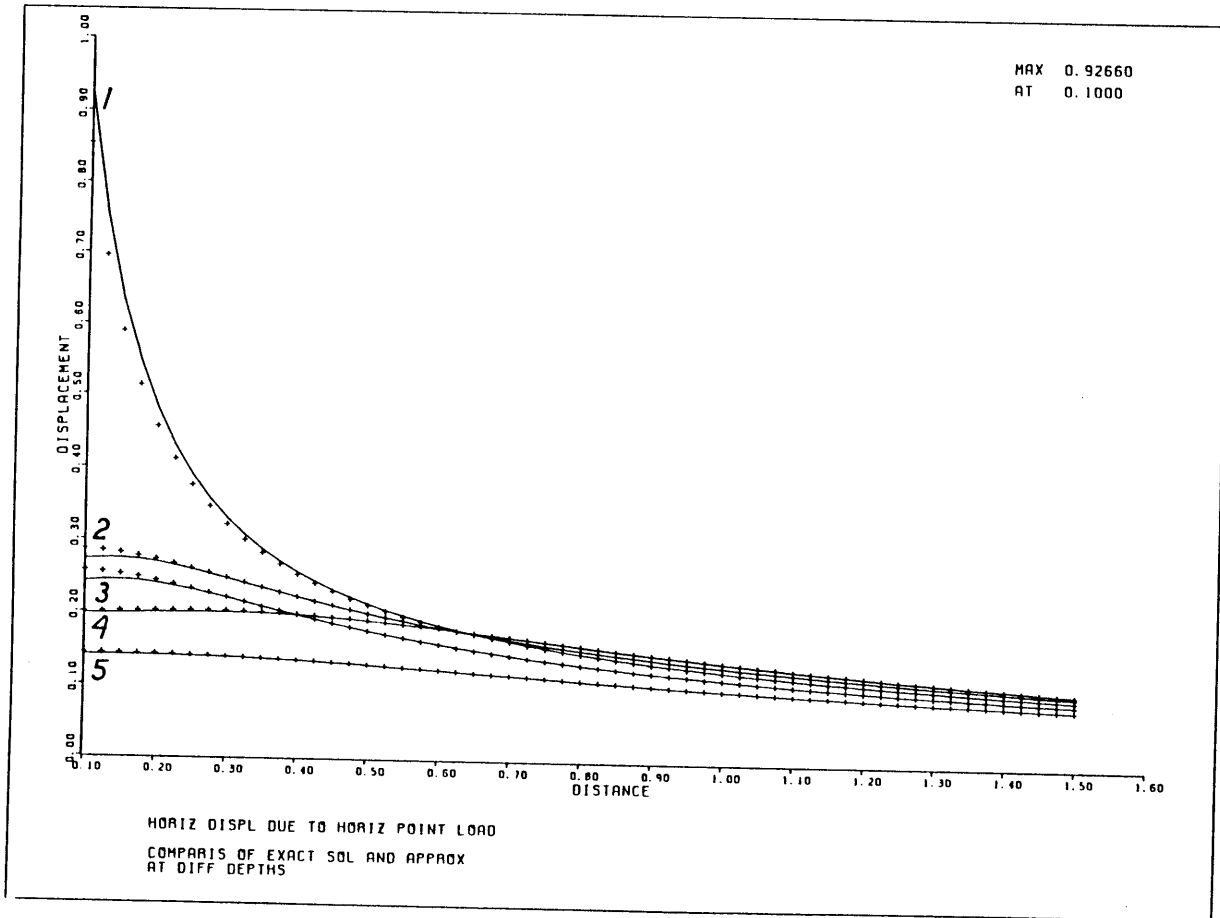
The solid lines are displacements computed with the approximation, the dashed lines are displacements computed with the analytical solutions of Mindlin, Cerutti and Boussinesq which are compiled by Poulos and Davis (1974). The plots all show displacements beginning at $\rho = 0.1$, since both the analytical solutions and the approximations have a $\frac{1}{\rho}$ singularity. Each pair of solid and dashed lines is labeled with the number of the elevation where the displacements were computed.

Figures 4-4 and 4-5 show displacements u_ρ and u_θ at the five elevations due to a horizontal (or radial) unit point load applied at the surface. Agreement with the analytical solution is excellent everywhere. Figure 4-6 shows vertical displacements u_z due to a vertical point load at the surface. Again, agreement with the analytical solution is excellent everywhere. Figure 4-7 shows the "cross term", the displacement u_ρ due to a vertical point load at the surface. In the analytical solution, the displacement u_ρ goes to zero when $\rho = 0$ at every elevation beneath the surface. At the surface, $u_\rho \rightarrow \infty$ due to the singularity of the point load. The approximation has excellent agreement with the analytical solution beneath the surface. At the surface, near the origin, the cross term does not duplicate this singular behavior.

Figures 4-8 and 4-9 show displacements due to point loads applied at elevation 3. In Figure 4-8, u_z due to a buried vertical point load is plotted. In Figure 4-9, u_ρ due to a buried radial load is plotted. Agreement with the analytical solution is excellent at all elevations.

Figures 4-4 through 4-9 are presented to demonstrate the accuracy of this method by comparing approximate displacements to those for which the analytical solution is known. Of course, the advantage of the approximation is that it can be applied to solve for displacements when the analytical solution is not known. As an example of an irregular geometry, the approximation was used to obtain displacements in a Gibson solid. A Gibson solid (see Gibson (1967)) is an elastic half space in which the shear modulus G increases linearly with depth according to $G(z) = G(0) + mz$. (The behavior of a Gibson solid subjected to dynamic loads has been described by Awojobi (1972,1974) and Gazetas (1980).) The layer overlying the halfspace has depth $H = 1$ and is discretized into 10 sublayers. The poisson modulus $\nu = \frac{1}{3}$ is constant

Figure 4-4: Radial Displacements due to Radial Point Load at the Surface



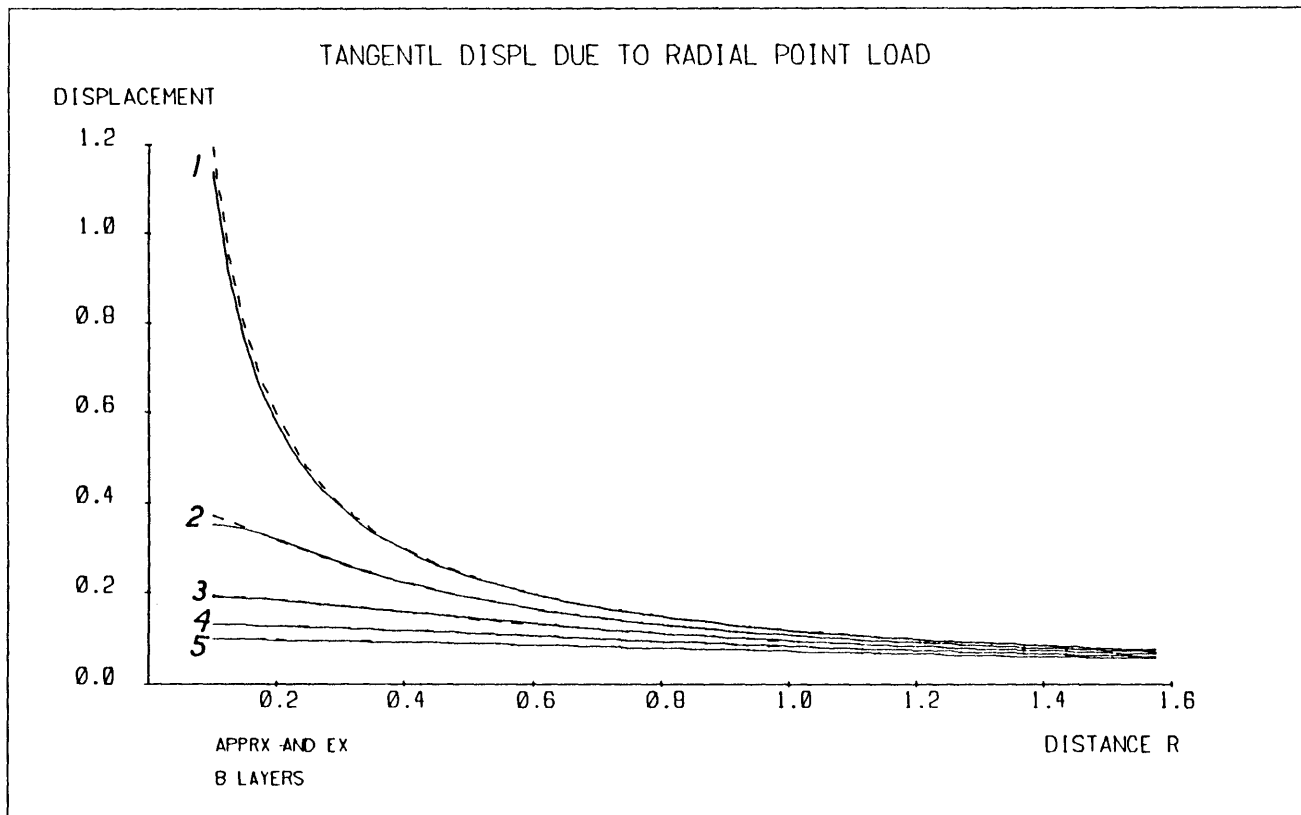


Figure 4-5: Tangential Displacements due to Radial Point Load at the Surface

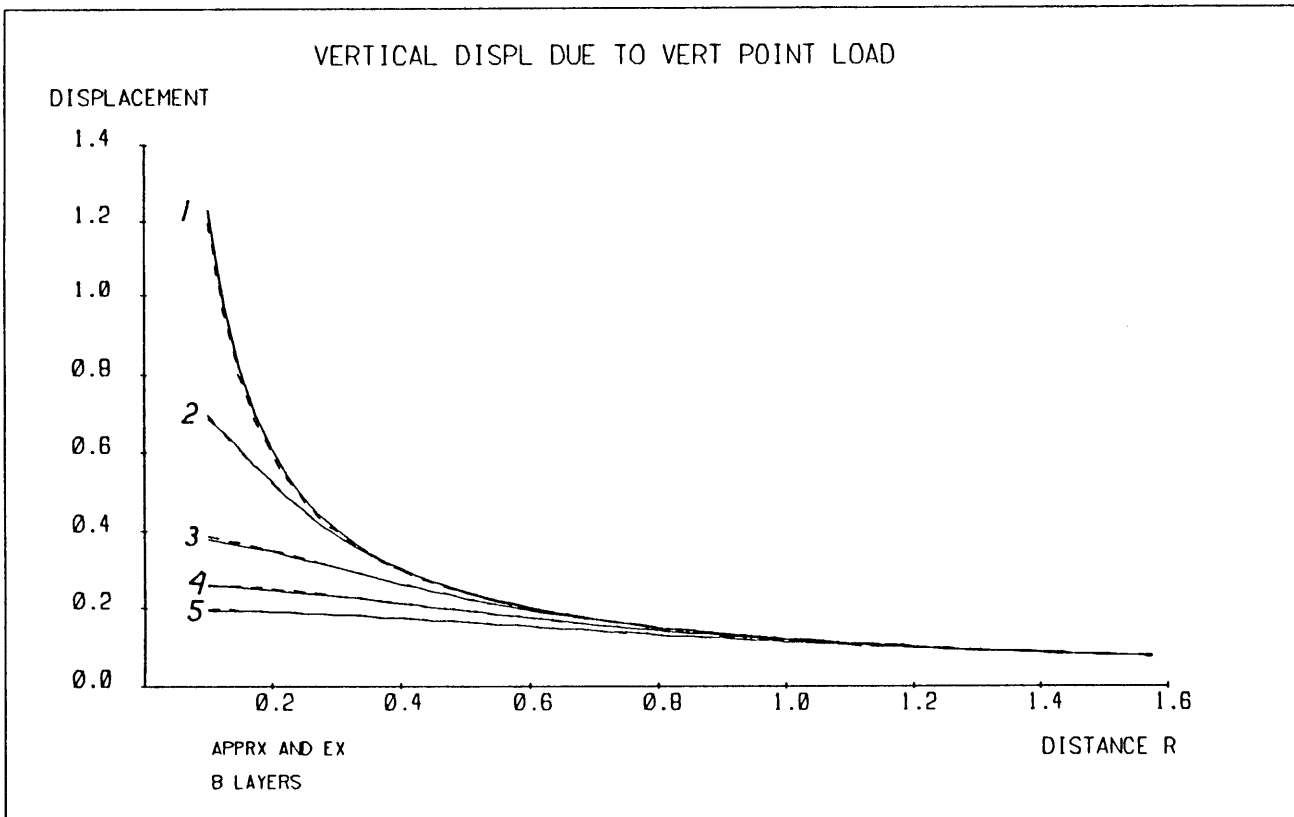


Figure 4-6: Vertical Displacements due to Vertical Point Load at the Surface

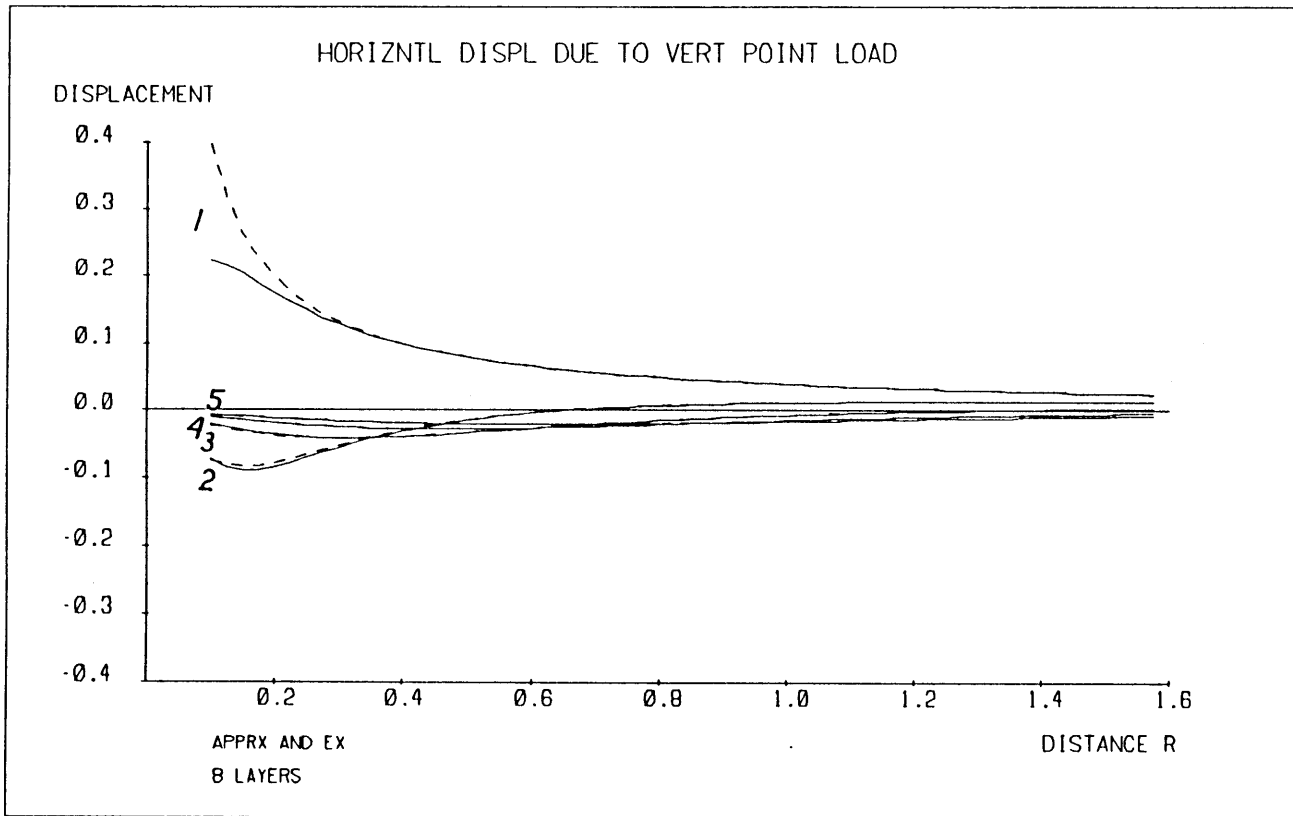


Figure 4-7: Radial Displacements due to Vertical Point Load at the Surface

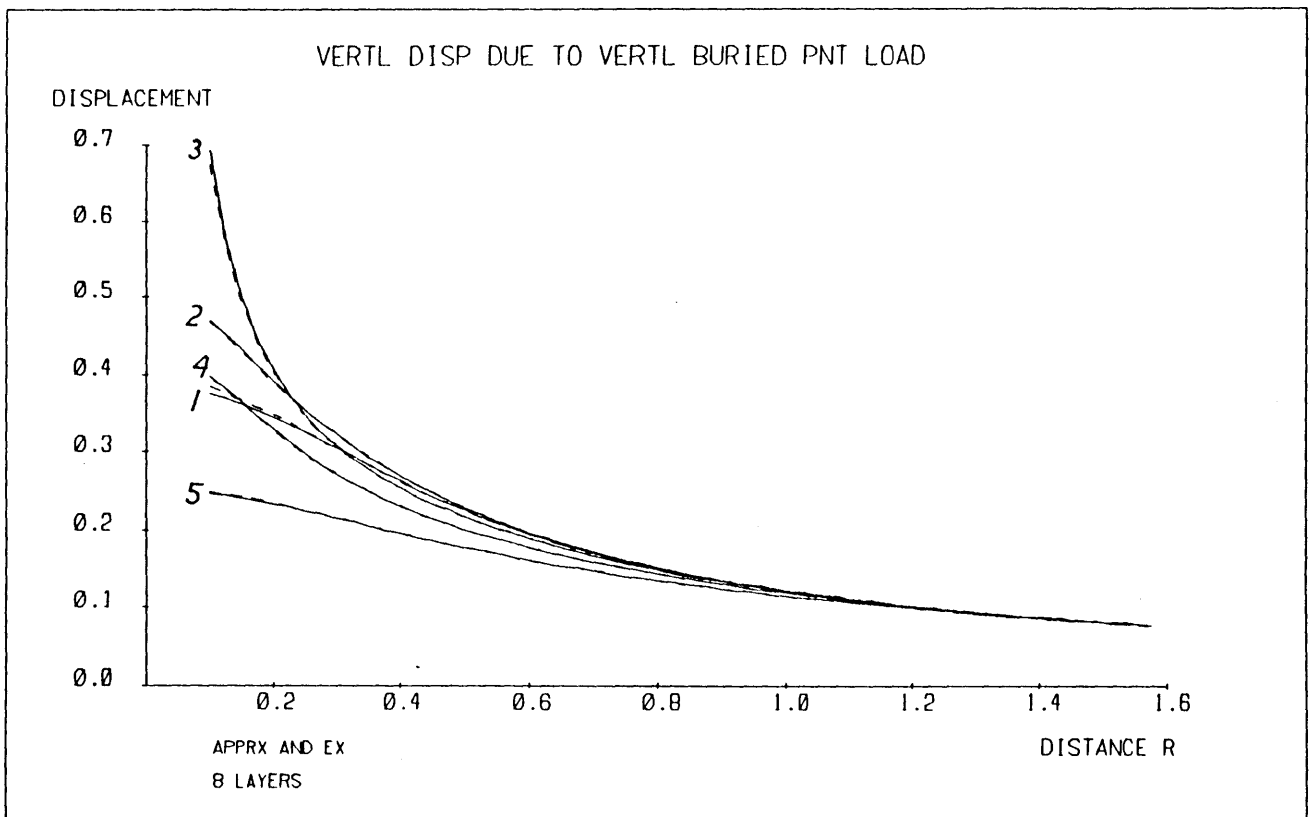


Figure 4-8: Vertical Displacements due to
Vertical Buried Point Load

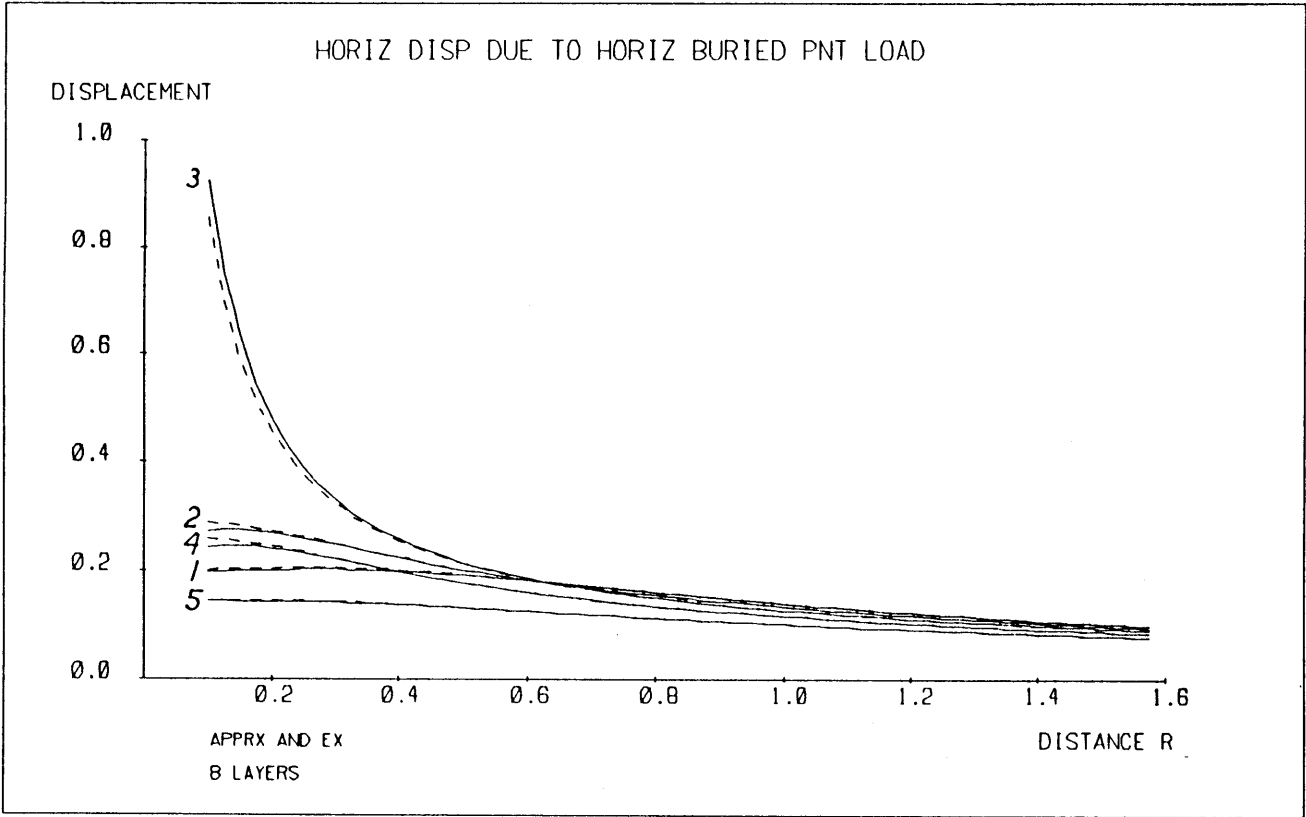


Figure 4-9: Radial Displacements due to Radial Buried Point Load

throughout the halfspace. The shear modulus in the top layer is $G_1 = 1.0$, the shear modulus in each subsequent layer is 0.1 larger than that of the previous layer, and the shear modulus of the halfspace is $G_r = 2.0$.

Figure 4-10 shows displacements u_ρ and u_z at the surface due to a vertical point load at the surface of the Gibson solid. Figure 4-11 shows displacements u_ρ , u_θ and u_z at the surface due to a radial point load at the surface. The magnitudes of the displacements are less than for the homogeneous halfspace, and the displacements drop off more quickly. This is as expected, due to the increased stiffness of the underlying layers.

Another solid of interest to engineers is an "upside-down" Gibson solid, where the upper layers have greater shear moduli than the underlying halfspace. An example of this type is a layered pavement. The approximation was used to obtain displacements in an "upside-down" Gibson solid. The layer overlying the halfspace has depth $H = 1$ and is discretized into 10 sublayers. The poisson modulus $\nu = \frac{1}{3}$ is constant throughout the halfspace. The shear modulus in the top layer is $G_1 = 2.0$, the shear modulus in each subsequent layer is 0.1 smaller than that of the previous layer, and the shear modulus of the halfspace is $G_r = 1.0$

Figure 4-12 shows displacements u_ρ and u_z at the surface due to a vertical point load at the surface of the solid. Figure 4-13 shows displacements u_ρ , u_θ and u_z at the surface due to a radial point load at the surface. Comparison with Figures 4-10 and 4-11 shows that the displacements at the surface are smaller in magnitude than for the regular Gibson solid. This is as expected, since the increased stiffness is concentrated near the surface.

4.5 Displacements due to Static Disk Loads

The application of a static disk load eliminates the singularity at the origin induced by a point load. The transforms of the disk loads are given by 4-71 and 4-81. When these load vectors are applied in the transform 2-56 to obtain displacements, the integrals of 4-78 become

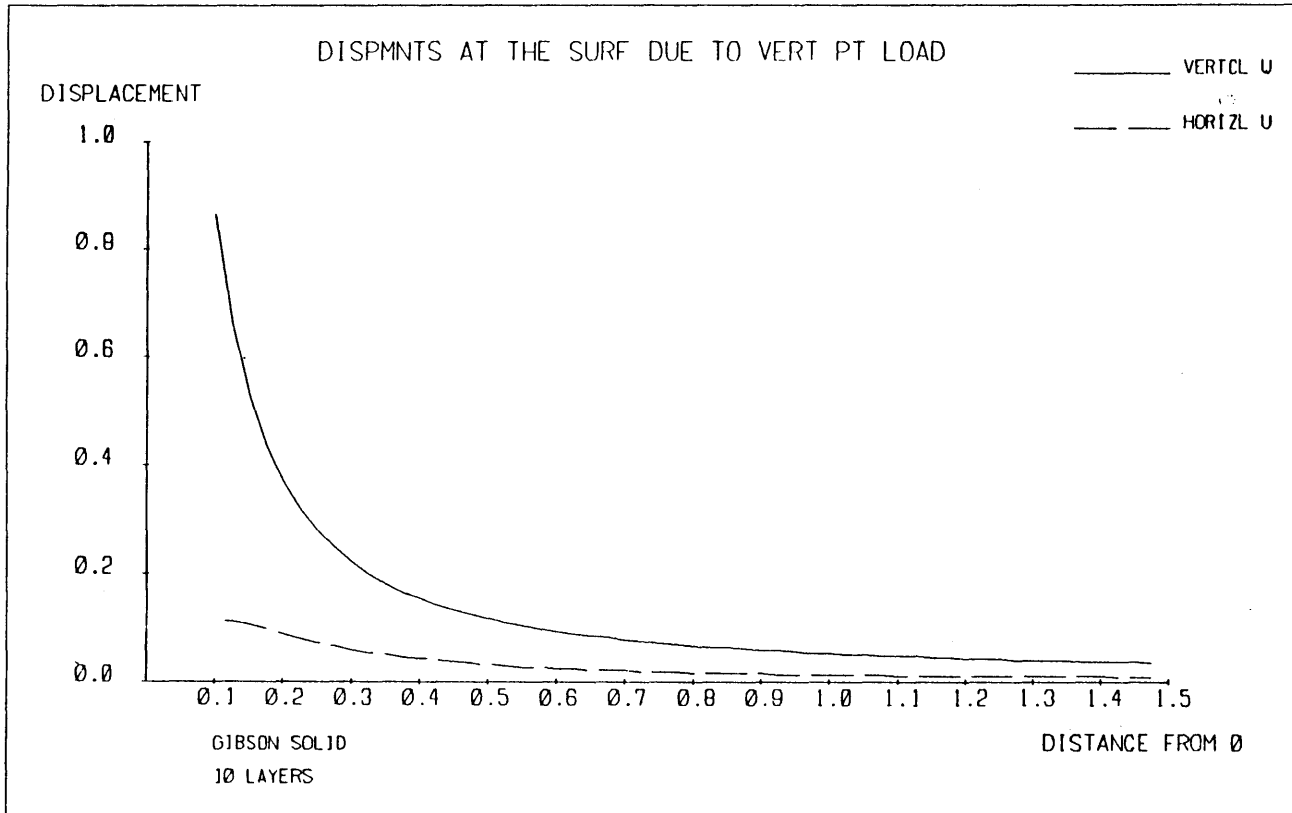


Figure 4-10: Displacements at the Surface due to
Vertical Point Load, $G_p = 2.0$

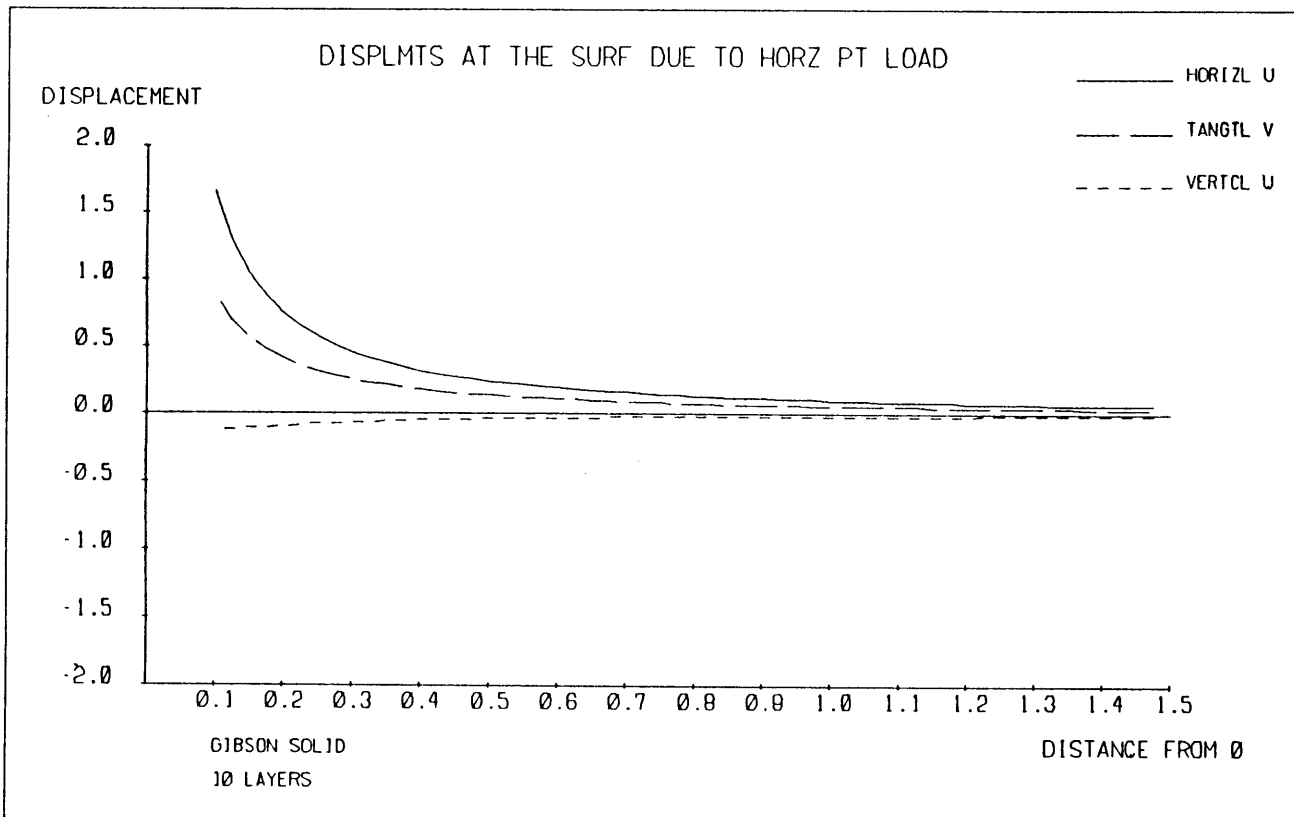


Figure 4-11: Displacements at the Surface due to Radial Point Load, $G_r = 2.0$

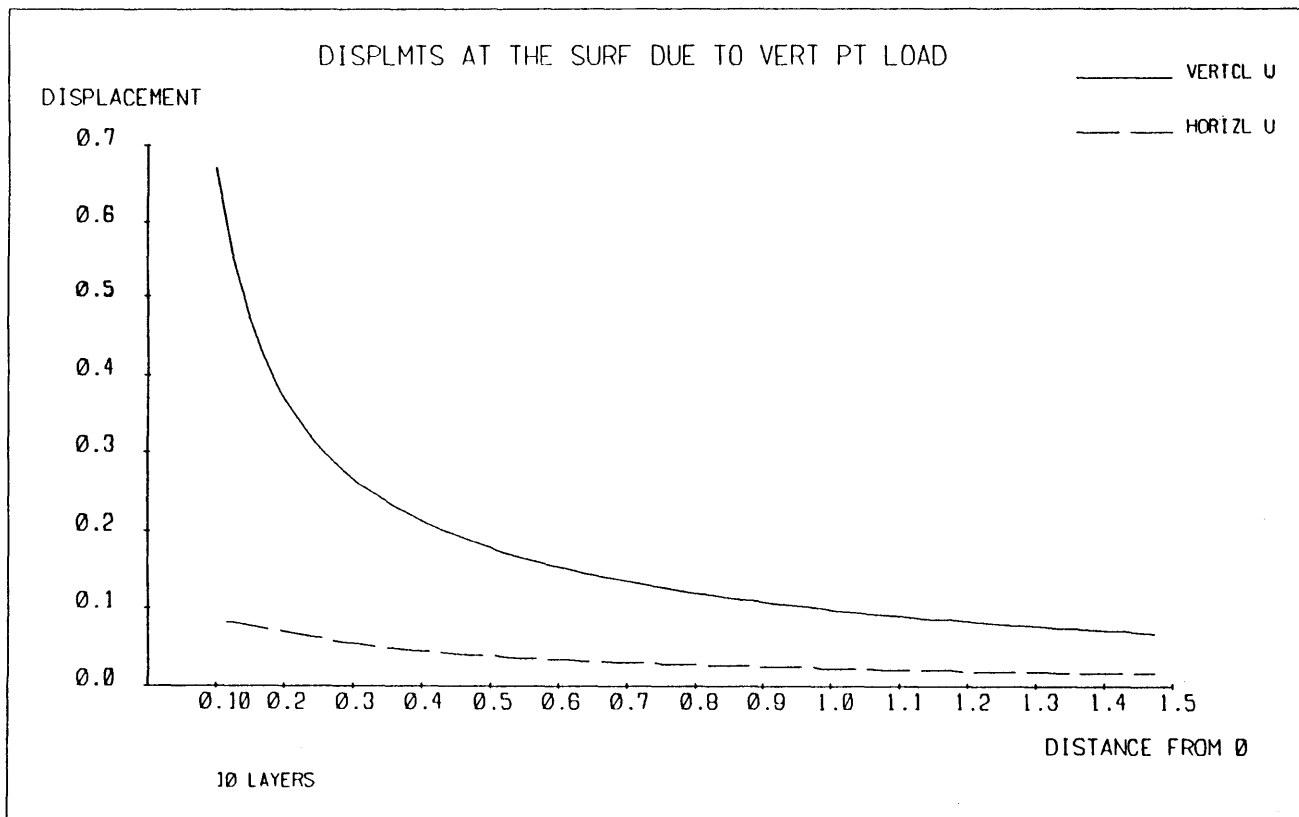


Figure 4-12: Displacements at the Surface due to
Vertical Point Load, $G_1 = 2.0$

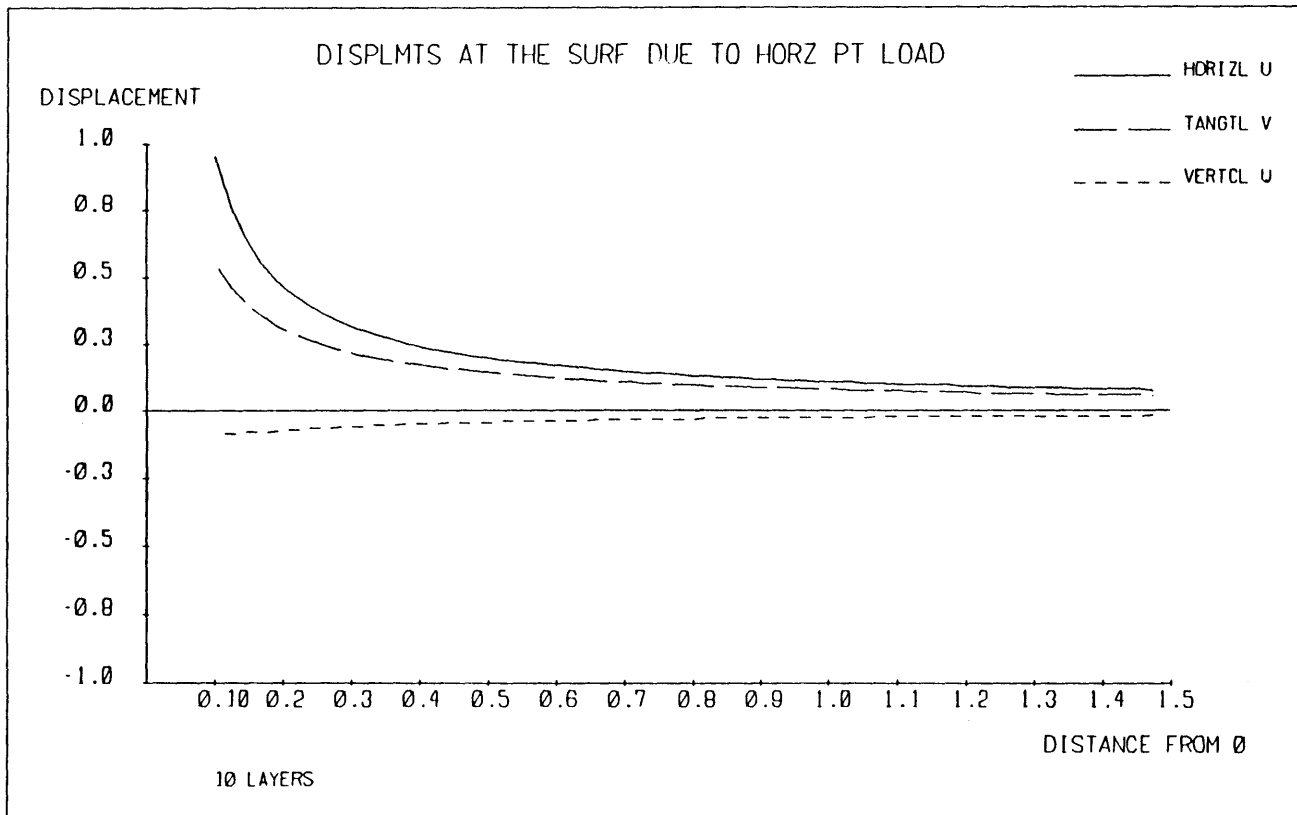


Figure 4-13: Displacements at the Surface due to Radial Point Load, $G_1 = 2.0$

$$I_{3l} = \int_0^\infty a_l \frac{J_1(k\rho)J_1(kR)}{k} dk$$

4-88

$$I_{2l} = \int_0^\infty a_l J_1(k\rho)J_1(kR) dk$$

$$I_{1l} = \int_0^\infty a_l J_0(k\rho)J_1(kR) dk$$

Unfortunately, these integrals do not exist in closed form. Approximate solutions are presented in Appendix D. In the limit when $\rho \rightarrow 0$, the integrals in 4-88 have the same form as 4-78, except that the argument of the Bessel functions is kR rather than $k\rho$. Thus we can obtain displacements along $\rho = 0$ due to static disk loads. The displacement vector at the origin due to a horizontal disk load is

$$u_\rho^{mn} = \frac{1}{2\pi R} \left[\frac{2 - \alpha_r^2}{2G_r(1 - \alpha_r^2)} + \sum_{l=3}^{4N} \phi_z^{ml} \phi_z^{nl} I_{3l}^R(k_l R) + \sum_{l=2}^{2N} \phi_y^{ml} \phi_y^{nl} I_{3l}^L(k_l R) \right]$$

$$u_\theta^{mn} = u_\rho^{mn} \tag{4-89}$$

$$u_z^{mn} = 0$$

The displacement vector at the origin due to a vertical disk load is

$$u_\rho^{mn} = 0$$

$$u_\theta^{mn} = 0 \tag{4-90}$$

$$u_z^{mn} = \frac{1}{\pi R} \left[\frac{1}{2G_r(1 - \alpha_r^2)} + \sum_{l=3}^{4N} \phi_z^{ml} \phi_z^{nl} I_{3l}^R(k_l R) \right]$$

The integral I_{3l} is given in Table 4-1, the argument $k_l\rho$ is replaced by $k_l R$.

Vertical displacements along $\rho = 0$ were computed for the homogeneous halfspace of Section 4.4.3. The halfspace was subjected to a vertical disk load of radius $R = 0.25$. Figure 4-14 shows displacements versus depth. The continuous line is the analytical solution found in Poulos and

Davis (1974). The displacements at the layer interfaces are marked with x's. Again, we see that this method yields very accurate displacements with a relatively small number of layers.

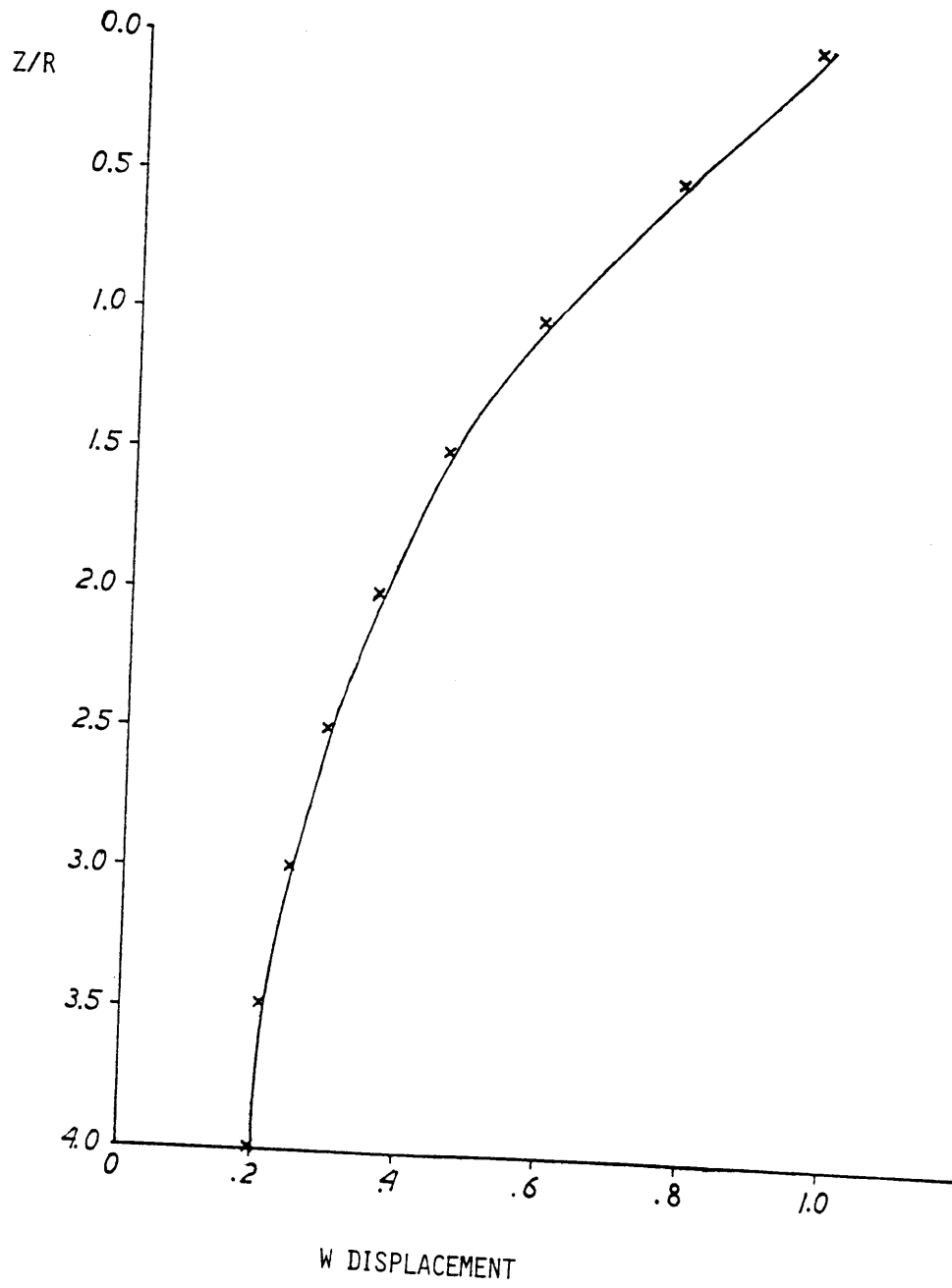
4.6 Conclusions

The method presented above for the calculation of displacements in layered soils is a significant improvement upon existing methods. The technique is efficient in that the stiffness matrices are relatively small, symmetric and banded. We have shown that with a discretization of few layers, the results are very accurate. Since discretization occurs in only the vertical direction and the stiffness of the halfspace is added directly to the system of equations, there is no need to apply artificial boundary conditions to the directions of infinite extent such as would be required for a finite element model of a halfspace.

The Green's functions obtained here have applications to several areas of engineering. In particular, they would be used for the Boundary Element Method, which requires displacements due to point loads on the boundary of a solid. The Green's functions can also be applied to problems in geophysics where earthquake rupture is modeled as the sudden slip of a crack. The slip distribution, or displacement along the crack induced by tractions applied to its face, is used to obtain stresses in the material surrounding the crack. Stresses within the layers can be obtained by differentiating the displacements. Differentiating once with respect to z yields a constant within the layer, since the displacements are piecewise linear in the z direction. Point loads can be added to form double couple sources, the displacement solutions of the individual point loads are then added together. The static displacements may be applied to problems in geotechnical engineering, such as the calculation of equivalent material properties for a layered soil deposit. The integral of point loads applied over a surface area can be used to represent the pressure load of a footing on a layered soil.

An outstanding feature of the method described in this Chapter is its simplicity. Integral

Figure 4-14: Vertical Displacements versus Depth



Transform techniques require the use of conformal mapping, elaborate contour integration and numerical integration. The stiffness method has three steps:

- 1) Assemble global stiffness matrices 4-3 and 4-44.
- 2) Extract eigenvalues and eigenvectors.
- 3) Compute displacements 4-79 and 4-87.

In essence, displacements are computed with a linear combination of the natural modes of propagation, a concept which is familiar from structural dynamics.

Chapter 5

Dynamic Loads in Cross-Anisotropic Layered Halfspaces

5.1 Introduction

The analyses described in this paper have been limited to the loading of isotropic halfspaces. Isotropic materials are the simplest to handle analytically since the stress-strain relations are described by only two elastic constants. However, many materials are not isotropic, in that they do not exhibit elastic symmetry about every reference plane. Materials that are not isotropic are referred to as anisotropic. The number of elastic constants required to describe an anisotropic material is determined by the symmetry of the material. Love (1944) classified anisotropic crystals according to their symmetry systems.

Seismologists have long been interested in the influence of the anisotropy of geological materials on the propagation of seismic waves. There is much seismological evidence that Earth materials are anisotropic. A review of the current state of research on seismic anisotropy has been provided by Crampin et al. (1984). In this work, Crampin discussed possible sources of anisotropy, such as the fracture of large masses of rock, and the influence of anisotropy on wave propagation. In the general case, Rayleigh and Love surface waves are coupled and shear waves travel at different velocities depending on the direction of propagation. Crampin (1984a) calculated equivalent elastic constants for fractured rock.

A particular type of anisotropy is cross-anisotropy, which is characterized by five elastic constants (equivalent to the hexagonal crystal described by Love (1944)). In a cross-anisotropic solid with vertical axis z , all vertical planes are planes of elastic symmetry. Thus all $x-y$ planes,

parallel to $z = 0$, are planes of isotropy. The solid exhibits radial elastic symmetry in that all quantities are independent of the azimuth θ . This property gives cross-anisotropy the alternative name of transverse isotropy. Many materials that are formed with a vertical orientation exhibit cross-anisotropy. This category includes rolled metals, laminated solids, floating lake ice and sediments deposited in layers. It has also been shown (Mitchell (1984)) that a solid composed of many thin isotropic layers can be modeled by a homogeneous cross-anisotropic solid. The gross anisotropic behavior of layered materials is of particular significance to the study of seismology.

The matrix of elastic constants for cross-anisotropy is

$$\begin{array}{ccccccc}
 c_{11} & c_{12} & c_{13} & & & & \\
 c_{12} & c_{11} & c_{13} & & & & \\
 c_{13} & c_{13} & c_{33} & & & & \\
 & & & c_{44} & & & \\
 & & & & c_{44} & & \\
 & & & & & c_{66} &
 \end{array} \tag{5-1}$$

where $c_{66} = \frac{c_{11} - c_{12}}{2}$

An alternative notation, introduced by Love (1944), is

$$\begin{array}{ccccccc}
 A & A-2N & F & & & & \\
 A-2N & A & F & & & & \\
 F & F & C & & & & \\
 & & & L & & & \\
 & & & & L & & \\
 & & & & & N &
 \end{array} \tag{5-2}$$

In the isotropic case, $A = C = \lambda + 2G$, $F = A - 2N = \lambda$ and $L = N = G$. This notation is commonly used in the literature and is used in this paper to avoid the confusion of carrying subscripts.

5.2 Wave Propagation in Cross-Anisotropic Halfspaces

A general technique for obtaining body waves in anisotropic media has been presented by Crampin (1984b). This method involves rotating the elastic tensor so that a harmonic wave is propagating with phase velocity c in the x direction. The values of c are then extracted from the eigenvalue problem generated by the wave equations. In general, wave motion in an anisotropic medium is very complicated. Crampin (1984b) pointed out that the group velocity of a wave in a general anisotropic medium is a vector. Thus energy is propagated into the medium in a different direction than the direction of phase. On the other hand, the symmetry of cross-anisotropy uncouples the anti-plane from the in-plane motions. Thus cross-anisotropy considerably simplifies the analysis of wave propagation.

Mitchell (1984) discussed the inversion of surface waves to obtain material properties of the Earth. Traditionally, data from primary-mode Love and Rayleigh waves are fit to an isotropic model of the Earth and elastic constants are computed. However, often this leads to incompatible Love and Rayleigh velocities. A possible explanation is the anisotropy of the Earth. Mitchell attempted to fit the Rayleigh and Love wave data to a layered cross-anisotropic model and found that the inversion is non-unique. Stoneley (1949) discussed the role of anisotropy in the Earth in contributing to false measurements of the focal depth of earthquakes. He also described how anisotropy would lead to a discrepancy between the time of the event generating P and S waves and how an explosive source would generate S waves as well as P waves.

Solutions for plane waves in cross-anisotropic media are well known. The distinguishing feature of plane wave propagation in cross-anisotropic media is that in general the solution cannot be separated into pure shear and compression waves. In other words, for in-plane waves, the particle motion is not polarized into a compression wave in the direction of phase and a shear wave with motion perpendicular to phase. This polarization does exist in degenerate cases. Stoneley (1949) used displacement potentials to obtain the solution for plane waves in cross-anisotropic

media. He then applied stress-free boundary conditions to obtain the Rayleigh wave equation. White (1965, 1982) also derived the plane wave solution with potentials and used a numerical Fourier transform to compute waveforms for a variety of cross-anisotropic media subjected to a vertical point force. Kirkner (1979) applied the potential solution for surface waves to obtain the dynamic stiffness of a cross-anisotropic halfspace. He constrained the elastic constants so that the in-plane wave is polarized into SV and P components of motion. Anderson (1961) obtained the plane wave motion and applied it to the solution of surface waves in a cross-anisotropic free plate and a plate in contact with a fluid halfspace. He then generalized the single layer solution to the problem of a layered medium with appropriate alterations to the Haskell-Thomson matrix. Crampin (1970) presented the Haskell-Thomson matrix for a general anisotropic solid. Biot (1965, 1983) applied the potential solution for plane waves to the solution of stiffness matrices for orthotropic plates. The stiffness matrices were used in stability problems of plates subjected to horizontal compression and not for the purposes described herein.

As with the isotropic case, we wish to derive stiffness matrices that are algebraic in the horizontal wavenumber k . Once we have obtained the elements of these matrices in terms of the anisotropic elastic constants, the matrix algebra and Hankel transforms required to solve for displacements are the same as described in the previous chapters. In other words, cross-anisotropy affects only the elements of the stiffness matrices and we already have the machinery in place to solve for dynamic and static displacements. Thus the stiffness method presented in this paper is uniquely well suited to problems of cross-anisotropic media, since the anisotropy adds no further complications to the mathematics.

Although the references described above represent a large body of literature on the solutions to wave propagation in cross-anisotropic media, the notation in general is too bulky for the purposes of deriving stiffness matrices. In particular, potential solutions for plane waves are unnecessarily complicated, since the form of the plane wave can be assumed at the outset. Also, we can bypass the plane wave solution and the Haskell-Thomson matrix to obtain the algebraic

layer matrix with a finite element approach. The simplified plane wave solution and the derivation of the stiffness matrices are presented below.

5.2.1 Anti-plane Motion

As in Chapter 2, we make the plane strain assumption that all displacements are independent of the y coordinate. Then the anti-plane motion uncouples from the in-plane motion. Consider a body in anti-plane shear subjected to a harmonic load. The displacement in the y direction is

$$v = a e^{i(\omega t - kx - qz)} \quad 5-3$$

Substituting Equation 5-3 into the equilibrium equation, we obtain

$$\rho \frac{\partial^2 v}{\partial t^2} = N \frac{\partial^2 v}{\partial x^2} + L \frac{\partial^2 v}{\partial z^2} \quad 5-4$$

$$\rho \omega^2 = N k^2 + L q^2$$

Solving Equation 5-4 for q gives

$$q = \frac{\pm i}{\sqrt{L}} \sqrt{Nk^2 - \rho\omega^2} = \pm i q^* \quad 5-5$$

and the full solution is

$$v = \{a_1 e^{q^* z} + a_2 e^{-q^* z}\} e^{i(\omega t - kx)} \quad 5-6$$

We discard the part of the solution that grows with $-z$

$$v = a e^{q^* z} e^{i(\omega t - kx)} \quad 5-7$$

To obtain the stiffness matrix, we compute the shear stress

$$\tau_{yz} = L \frac{\partial v}{\partial z} = L q^* v \quad 5-8$$

Then the exact anti-plane stiffness is

$$k_{yy}(k) = L q^* = \sqrt{L} \sqrt{Nk^2 - \rho\omega^2} \quad 5-9$$

5.2.2 In-plane motion

This section follows (in two dimensions) the notation that Kausel (1984) used to derive the algebraic layer stiffness matrices (these matrices are presented in the following section). In the analysis below, the stiffness matrix is formulated for waves that propagate in the $+z$ direction, rather than away from the surface of the halfspace in the $-z$ direction. This has the effect of reversing the signs of the diagonal elements of the stiffness matrix. This discrepancy is corrected when the stiffness elements are obtained.

Assume a wave of the form

$$U = \begin{bmatrix} u \\ w \end{bmatrix} = \begin{bmatrix} a \\ c \end{bmatrix} e^{-kqz} e^{i(\omega t - kz)} \quad 5-10$$

In matrix form, the equilibrium equation is

$$\begin{aligned} \rho U - \mathcal{L}^T \sigma &= 0 \\ \rho U - \mathcal{L}^T D L U &= 0 \end{aligned} \quad 5-11$$

where

$$\begin{aligned} \mathcal{L}^T &= \begin{bmatrix} \partial/\partial x & 0 & \partial/\partial z \\ 0 & \partial/\partial z & \partial/\partial x \end{bmatrix} \\ \sigma^T &= \{ \sigma_x \quad \sigma_z \quad \tau_{xz} \} \end{aligned} \quad 5-12$$

and D is the matrix of elastic constants. The operator \mathcal{L} is expanded into

$$\mathcal{L} = \mathcal{L}_x \frac{\partial}{\partial x} + \mathcal{L}_z \frac{\partial}{\partial z} \quad 5-13$$

so that the product $\mathcal{L}^T D \mathcal{L}$ becomes

$$\mathcal{L}^T D \mathcal{L} = D_{xx} \frac{\partial^2}{\partial x^2} + 2D_{xz} \frac{\partial^2}{\partial x \partial z} + D_{zz} \frac{\partial^2}{\partial z^2} \quad 5-14$$

where

$$D_{ij} = \frac{1}{2} (\mathcal{L}_i^T D \mathcal{L}_j + \mathcal{L}_j^T D \mathcal{L}_i) \quad i, j = x, z \quad 5-15$$

For the cross-anisotropic halfspace, the D_{ij} are

$$\begin{aligned} D_{xx} &= \begin{bmatrix} A & 0 \\ 0 & L \end{bmatrix} \\ D_{zz} &= \frac{1}{2} \begin{bmatrix} 0 & F+L \\ F+L & 0 \end{bmatrix} \\ D_{zz} &= \begin{bmatrix} L & 0 \\ 0 & C \end{bmatrix} \end{aligned} \tag{5-16}$$

Substituting Equations 5-16, 5-10 and 5-14 into Equation 5-11 gives the matrix equation

$$\begin{bmatrix} -\rho\omega^2 + k^2A - k^2q^2L & -ik^2q(F+L) \\ -ik^2q(F+L) & -\rho\omega^2 + k^2L - k^2q^2C \end{bmatrix} \begin{bmatrix} a \\ c \end{bmatrix} = \begin{bmatrix} 0 \\ 0 \end{bmatrix} \tag{5-17}$$

The roots q are found by taking the determinant of 5-17:

$$(-\rho\omega^2 + k^2A - k^2q^2L)(-\rho\omega^2 + k^2L - k^2q^2C) + k^4q^2(F+L)^2 = 0 \tag{5-18}$$

Expanding Equation 5-18 and substituting $\omega = ck$, we obtain

$$q^4CL + q^2[(F+L)^2 + \rho c^2(C+L) - AC - L^2] + (\rho c^2 - A)(\rho c^2 - L) = 0 \tag{5-19}$$

which is quadratic in q^2 . Let Equation 5-19 be expressed as

$$a^*q^4 + b^*q^2 + c^* = 0 \tag{5-20}$$

where

$$\begin{aligned} a^* &= CL \\ b^* &= (F+L)^2 + \rho c^2(C+L) - AC - L^2 \\ c^* &= (\rho c^2 - A)(\rho c^2 - L) \end{aligned} \tag{5-21}$$

The solution to Equation 5-20 is

$$q^2 = \frac{-b^* \pm \sqrt{b^{*2} - 4a^*c^*}}{2a^*} \tag{5-22}$$

Let r^2 be the + root and s^2 be the - root of Equation 5-22. Then r^2 and s^2 reduce to the values in Equation 2-13 in the isotropic case. Now we can solve for the ratio of the amplitudes a and c from the eigenvalue problem 5-17. For the r root,

$$c = \frac{(-\rho c^2 + A - r^2 L) a}{ir(F + L)} = \frac{-i}{r} f(r) a \quad 5-23$$

where

$$f(r) = \frac{-\rho c^2 + A - r^2 L}{F + L} \quad 5-24$$

In the limit of isotropy, f becomes r^2 . Likewise, for the s root,

$$c = \frac{-i}{s} g(s) a \quad 5-25$$

where

$$g(s) = \frac{-\rho c^2 + A - s^2 L}{F + L} \quad 5-26$$

In the limit of isotropy, g becomes 1. The full solution for displacements is

$$U = \left[\begin{array}{c} 1 \\ -if/r \end{array} \right] a'_1 e^{-krz} + \left[\begin{array}{c} 1 \\ -ig/s \end{array} \right] a'_2 e^{-ksz} + \quad 5-27$$

$$\left[\begin{array}{c} 1 \\ if/r \end{array} \right] a''_1 e^{krz} + \left[\begin{array}{c} 1 \\ ig/s \end{array} \right] a''_2 e^{ksz} \right] e^{i(\omega t - kz)}$$

where a'_1 and a'_2 are amplitudes of waves traveling in the $+z$ direction and a''_1 and a''_2 are amplitudes of waves traveling in the $-z$ direction. The full matrix expression of 5-27 is

$$\begin{bmatrix} u \\ iw \end{bmatrix} = \begin{bmatrix} 1 & 1 & 1 & 1 \\ f & g & -f & -g \\ r & s & -r & -s \end{bmatrix} \text{diag} \{ e^{-krz}, e^{-ksz}, e^{krz}, e^{ksz} \} \begin{bmatrix} a'_1 \\ a'_2 \\ a''_1 \\ a''_2 \end{bmatrix} f_{x,t} \quad 5-28$$

where $f_{x,t} = e^{i(\omega t - kz)}$.

Since we are interested only in waves that travel in the $+z$ direction, we discard the a''_1 and a''_2 parts of the solution. Dropping the primes from the amplitudes, Equation 5-28 reduces to

$$\begin{bmatrix} u \\ iw \end{bmatrix} = \begin{bmatrix} 1 & 1 \\ f & g \\ r & s \end{bmatrix} \begin{bmatrix} e^{-krz} \\ e^{-ksz} \end{bmatrix} \begin{bmatrix} a_1 \\ a_2 \end{bmatrix} f_{x,t} \quad 5-29$$

The displacements are

$$u = \{ a_1 e^{-krz} + a_2 e^{-ksz} \} e^{i(\omega t - kz)} \quad 5-30$$

$$iw = \left\{ \frac{f}{r} a_1 e^{-krz} + \frac{g}{s} a_2 e^{-ksz} \right\} e^{i(\omega t - kz)}$$

The stresses are given by

$$\tau_{xz} = L \left[\frac{\partial u}{\partial z} + \frac{\partial w}{\partial x} \right] \quad 5-31$$

$$\sigma_{zz} = F \frac{\partial u}{\partial x} + C \frac{\partial w}{\partial z}$$

Substituting Equation 5-30 into Equation 5-31, we obtain

$$\tau_{xz} = -Lk \left[\left[r + \frac{f}{r} \right] a_1 e^{-krz} - \left[s + \frac{g}{s} \right] a_2 e^{-ksz} \right] f_{x,t} \quad 5-32$$

$$i\sigma_{zz} = k \left[(F - Cf) a_1 e^{-krz} + (F - Cg) a_2 e^{-ksz} \right] f_{x,t}$$

Now we need to solve for a_1 and a_2 in terms of the displacements. At the surface ($z = 0$),

$$\begin{bmatrix} u \\ iw \end{bmatrix} = \begin{bmatrix} 1 & 1 \\ \frac{f}{r} & \frac{g}{s} \end{bmatrix} \begin{bmatrix} a_1 \\ a_2 \end{bmatrix} f_{x,t} \quad 5-33$$

Inverting the above matrix gives

$$\begin{bmatrix} a_1 \\ a_2 \end{bmatrix} f_{x,t} = \frac{rs}{gr - fs} \begin{bmatrix} g/s & -1 \\ -f/r & 1 \end{bmatrix} \begin{bmatrix} u \\ iw \end{bmatrix} \quad 5-34$$

Substituting Equations 5-34 into Equations 5-32 yields

$$\tau_{xz} = \frac{Lk}{gr - fs} \{ (-r^2g + s^2f) u + (r^2s + fs - s^2r - rs) iw \} \quad 5-35$$

$$i\sigma_{zz} = \frac{k}{gr - fs} \{ (F(gr - fs) + Cgf(s - r)) u + Crs(f - g) iw \}$$

Then, reversing the signs of the diagonal elements, we obtain the stiffness matrix

$$\begin{bmatrix} \tau_{xz} \\ i\sigma_{zz} \end{bmatrix} = \frac{k}{gr - fs} \begin{bmatrix} L(r^2g - s^2f) & L(r^2s + fs - s^2r - gr) \\ F(gr - fs) + Cgf(s - r) & Crs(g - f) \end{bmatrix} \begin{bmatrix} u \\ iw \end{bmatrix} \quad 5-36$$

It can be proved that $k_{xz} = k_{zx}$. In the limit of isotropy, $L = G$, $F = \lambda$, $C = \lambda + 2G$, $f = r^2$, $g = 1$ and r and s reduce to their definitions in Chapter 2. Substituting these values into the expression for the shear stress yields

$$\begin{aligned} \tau_{xz} &= \frac{Gk}{r(1-rs)} [r^2(1-s^2) u + (r^2s + rs - s^2r - r) iw] = \\ &= \frac{Gk}{1-rs} [r(1-s^2) u + (2rs - 2 + 1 - s^2) iw] = \\ &= \frac{Gk(1-s^2)}{1-rs} [r u + iw] - 2Gk iw \end{aligned} \quad 5-37$$

Thus

$$\begin{aligned} k_{xx} &= \frac{Gk(1-s^2)r}{1-rs} \\ k_{xz} &= \frac{Gk(1-s^2)}{1-rs} - 2Gk \end{aligned} \quad 5-38$$

which agree with the elements given by Kausel and Roësset (1981). Likewise, substituting into the expression for the normal stress,

$$\begin{aligned} i\sigma_{zz} &= \frac{k}{1-rs} [\lambda(1-rs) u + (\lambda + 2G)(rs - r^2) u + (\lambda + 2G)s(1-r^2) iw] = \\ &= \frac{k}{1-rs} [(\lambda + 2G)(1-r^2) u - 2G(1-rs) u + (\lambda + 2G)s(1-r^2) iw] = \\ &= \frac{k}{1-rs} [G(1-s^2) u - 2G(1-rs) u + Gs(1-s^2) iw] \end{aligned} \quad 5-39$$

Thus

$$\begin{aligned} k_{zx} &= \frac{Gk(1-s^2)}{1-rs} - 2Gk \\ k_{zz} &= \frac{Gk(1-s^2)s}{1-rs} \end{aligned} \quad 5-40$$

which also agree with Kausel and Roësset (1981).

5.3 Algebraic Stiffness Matrices

In this section, the layer matrices derived by Kausel (1984) are presented and the matrices obtained in the previous section are expanded in a Taylor series for use as algebraic halfspace stiffness matrices.

5.3.1 Layer Matrices

The stiffness matrices for the discrete layers are derived with a finite element solution employed by Kausel (1974) for isotropic materials. In Kausel (1984), the method is generalized for anisotropic materials. A brief summary of the technique is presented here, along with the resulting layer matrices.

The vector of displacements $U (= \{u, v, w\}^T)$ is approximated within a soil layer by a linear expansion

$$U = \frac{z}{h} U_1 + \left[1 - \frac{z}{h} \right] U_2 \quad 5-41$$

The wave equation (presented here in matrix form)

$$W = \rho U - \mathcal{L}^T D \mathcal{L} U \quad 5-42$$

is no longer satisfied within the layer. Then we balance the internal forces in an energy sense:

$$\delta V^T T = \delta V^T S + \int_0^h \delta U^T W dz \quad 5-43$$

where $\delta V^T = \{\delta U_1^T \delta U_2^T\}$, T is the vector of applied external tractions and S is the vector of interface stresses. Equation 5-43 states that the virtual work performed by the external tractions is equal to the virtual work performed by the interface stresses and the unbalanced forces within the layer. In matrix form, Equation 5-41 is

$$U = NV = \begin{bmatrix} \frac{z}{h} I & \left[1 - \frac{z}{h} \right] I \end{bmatrix} \begin{bmatrix} U_1 \\ U_2 \end{bmatrix} \quad 5-44$$

Substituting 5-44 and 5-42 into 5-43 gives

$$\delta V^T T = \delta V^T S + \left\{ \int_0^h \rho N^T N dz \nabla - \int_0^h N^T L^T D L N dz V \right\} \quad 5-45$$

We assume a harmonic form for U

$$U = \bar{U} e^{i(\omega t - kx)} \quad 5-46$$

where $\bar{U} = \bar{U}(z)$. The displacements at the interface are

$$V = \bar{V} e^{i(\omega t - kx)} = \begin{bmatrix} \bar{U}_1 \\ \bar{U}_2 \end{bmatrix} e^{i(\omega t - kx)} \quad 5-47$$

and similar relation exist for S and T in terms of \bar{S} and \bar{T} . Derivatives of V are

$$\frac{\partial^2 V}{\partial t^2} = -\omega^2 V \quad \frac{\partial^2 V}{\partial x^2} = -k^2 V \quad 5-48$$

and $\partial^2 V / \partial t^2$ is zero since the displacements are linear in z . Substituting the expressions for the displacements and the interface stresses into Equation 5-45, integrating over the thickness of the layer and requiring that the equation be satisfied for arbitrary δV leads to the stiffness relation

$$\bar{T} = (Ak^2 + Bk + G - \omega^2 M) \bar{V} \quad 5-49$$

The A , B and G matrices obtained for the cross-anisotropic case are presented in Table 5-I. The M matrix is unchanged by anisotropy since it is a function of only the depth and the mass density of the layers.

5.3.2 Halfspace Matrices

In order to obtain the algebraic stiffness of the halfspace, we proceed as in Chapter 3. The first three terms of the Taylor's series expansion about $k = 0$ of the true stiffness are computed. For the anti-plane case, the derivatives of the stiffness can be computed and evaluated by hand.

Table 5-I: Algebraic Layer Stiffness Matrices *A*, *B* and *G*

$$A_j = \frac{h}{6} \begin{bmatrix} 2A & & & A & & \\ & 2N & & & N & \\ & & 2L & & & L \\ A & & & 2A & & \\ & N & & & 2N & \\ & & L & & & 2L \end{bmatrix}$$

$$B_j = \frac{1}{2} \begin{bmatrix} & & F-L & & & -(F+L) \\ & F-L & & & F+L & \\ & & & F+L & & -(F-L) \\ & & & & & \\ -(F+L) & & & & -(F-L) & \end{bmatrix}$$

$$G_j = \frac{1}{h} \begin{bmatrix} L & & & & -L & \\ & L & & & & -L \\ & & C & & & -C \\ -L & & & L & & \\ & -L & & & L & \\ & & -C & & & C \end{bmatrix}$$

For the in-plane case, derivatives of the stiffness elements and their limits when $k \rightarrow 0$ are computed with the MACSYMA computer program.

Recall the anti-plane stiffness

$$k_{yy}(k) = \sqrt{L} \sqrt{Nk^2 - \rho\omega^2} \quad 5-50$$

At $k = 0$,

$$k_{yy}(0) = \sqrt{L} \sqrt{-\rho\omega^2} = i\omega \sqrt{\rho L} \quad 5-51$$

The first derivative of k_{yy} is

$$k'_{yy}(k) = \frac{\sqrt{L} Nk}{\sqrt{Nk^2 - \rho\omega^2}} = \frac{LNk}{k_{yy}(k)} \quad 5-52$$

which is zero when $k = 0$. The second derivative of the stiffness is

$$k''_{yy}(k) = \frac{LNk_{yy}(k) - k'_{yy}(k)LNk}{k_{yy}^2(k)} = \frac{LN(k_{yy}(k) - k k'_{yy}(k))}{k_{yy}^2(k)} \quad 5-53$$

At $k = 0$,

$$k''_{yy}(0) = \frac{LN}{i\omega\sqrt{\rho L}} = -i\frac{N}{\omega} \sqrt{\frac{L}{\rho}} \quad 5-54$$

Then the paraxial approximation of the anti-plane stiffness is

$$k_{yy}(k) \simeq i\omega\sqrt{\rho L} - i\frac{N}{\omega} \sqrt{\frac{L}{\rho}} \quad 5-55$$

It can easily be verified that this reduces to the paraxial approximation of the isotropic halfspace.

For the in-plane case, only the results obtained from MACSYMA are provided below. For

$k_{xx}(k)$:

$$k_{xx}(0) = i\omega\sqrt{\rho L}$$

$$k'_{xx}(0) = 0 \quad 5-56$$

$$k''_{xz}(0) = \frac{i\sqrt{CL}}{\omega\sqrt{\rho}(L-C)^2} \left\{ -2L^{5/2} - 4FL^{3/2} - 2F^2L^{1/2} + C^{-1/2}L^3 + \right. \\ \left. 2C^{-1/2}FL^2 + C^{1/2}L^2 - AC^{-1/2}L^2 + F^2C^{-1/2}L + \right. \\ \left. 2C^{1/2}FL + 2AC^{1/2}L + C^{1/2}F^2 - AC^{3/2} \right\}$$

For $k_{xz}(k)$:

$$k_{xz}(0) = 0$$

$$k'_{xz}(0) = \frac{(L(F+C) - \sqrt{CL}(L+F))}{L-C} \quad 5-57$$

$$k''_{xz}(0) = 0$$

For $k_{zz}(k)$:

$$k_{zz}(0) = i\omega\sqrt{\rho C}$$

$$k'_{zz}(0) = 0 \quad 5-58$$

$$k''_{zz}(0) = \frac{i\sqrt{CL}}{\omega\sqrt{\rho}(L-C)^2} \left\{ 2FL^{3/2} + 3CL^{3/2} + L^{1/2}(F^2 + 2CF - C^2) + \right. \\ \left. CF^2L^{-1/2} - 2C^{1/2}L^2 - 4C^{1/2}FL - 2C^{1/2}F^2 \right\}$$

It can also be verified that these reduce to the isotropic matrices by appropriate substitutions. With these stiffness matrices, the procedure for computing displacements is the same as described in Chapter 2.

5.4 Dynamic Displacements

Displacements were computed for a cross-anisotropic stratum resting on a rigid base and on a cross-anisotropic halfspace. The stratum has depth $H = 1.0$, density $\rho = 1.0$ and damping $\beta = 0.05$. The elastic constants used for calculations are those of the rock beryl, taken from Anderson (1961):

$$\begin{aligned}
 A &= 4.13 \\
 C &= 3.62 \\
 F &= 1.01 \\
 N &= 1.33 \\
 L &= 1.00
 \end{aligned}$$

The stratum is subjected to disk loads with radius $R = 0.25$. Displacements were computed at the surface for the stratum discretized into 1, 4 and 12 layers.

Displacements for the stratum on a rigid base, plotted versus dimensionless frequency $f_0 = fH\sqrt{L/\rho}$, are shown in Figures 5-1 through 5-4. Figure 5-1 shows the real part of the vertical displacement at the origin due to a vertical disk load. This plot shows a clear resonant peak around $f_0 \simeq 0.45$. This resonance occurs at the shear beam frequency of the vertically propagating compression wave. The velocity of this wave is $C_p = \sqrt{C/\rho} \simeq 1.9026$. Resonance occurs at the frequencies $f = C_p(2j-1)/4H$. The first two compression resonant frequencies in this example are $f_1 = 0.4756$ and $f_2 = 1.42697$. Both of these peaks are evident in Figure 5-1. Figure 5-2 shows the real part of the horizontal displacement at the origin due to a horizontal disk load. Resonance occurs at the shear beam frequencies $f = C_s(2j-1)/4H$ where here $C_s = \sqrt{L/\rho}$ for vertically propagating shear waves. In this example, $C_s = 1.0$ and resonance occurs at $f_1 = 0.25$, $f_2 = 0.75$ and $f_3 = 1.25$. The 12 layer case shows all these peaks and a smaller peak appears around the compression wave resonance frequency. Figures 5-3 and 5-4 show the vertical and horizontal displacements at $\rho = 1.0$ (four times the disk load radius) due to a vertical and a horizontal disk load. These plots illustrate that the static displacements at $\rho = 1.0$ are essentially maintained until the respective resonant frequencies are reached. The motion between the resonant peaks is complicated and not easily interpreted.

Figures 5-5 through 5-8 show the same displacements plotted in Figures 5-1 through 5-4, only the stratum is resting on an anisotropic halfspace with the same properties. Figures 5-5 and 5-6 show displacements that decrease smoothly as frequency increases. The shape of these curves is similar to those of the isotropic case shown in Chapter 3. In Figures 5-7 and 5-8, at $\rho = 1$, the displacements oscillate with frequency. An exact solution for dynamic displacements in cross-

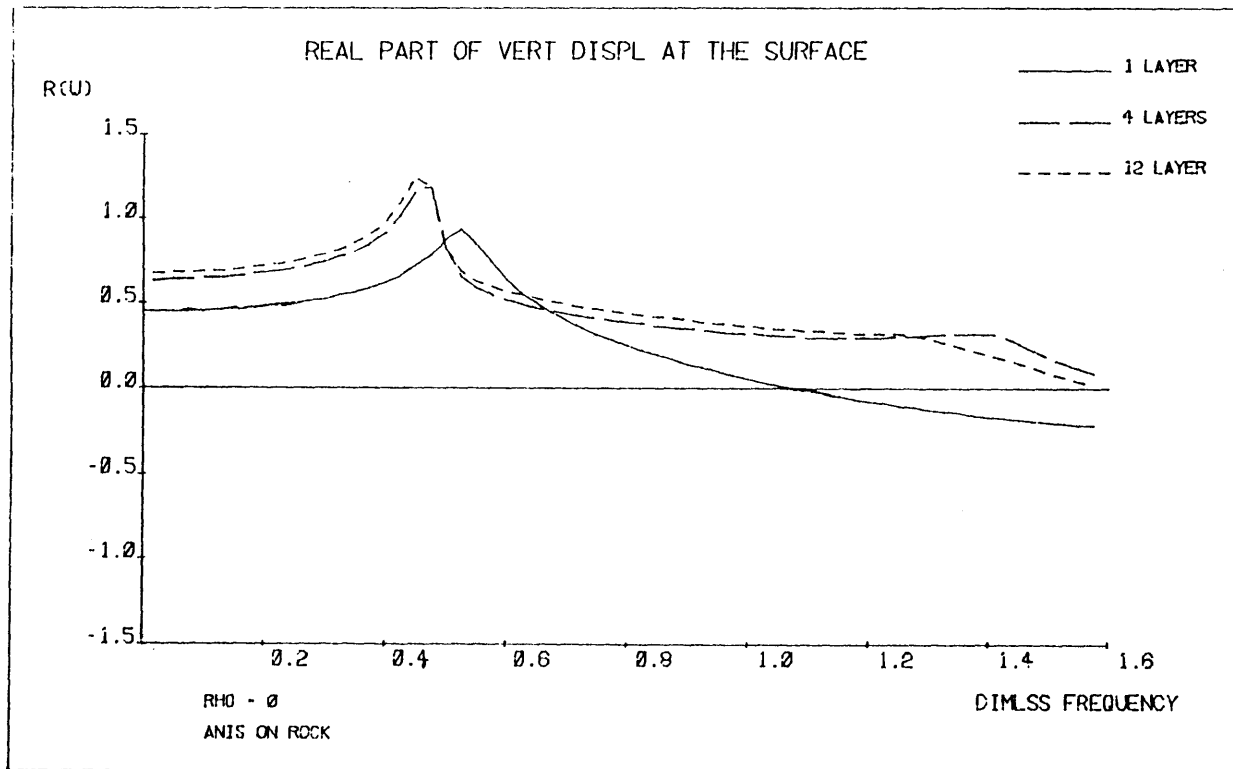


Figure 5-1: Real Part of the Vertical Displacement at $\rho = 0$, Anisotropic Stratum

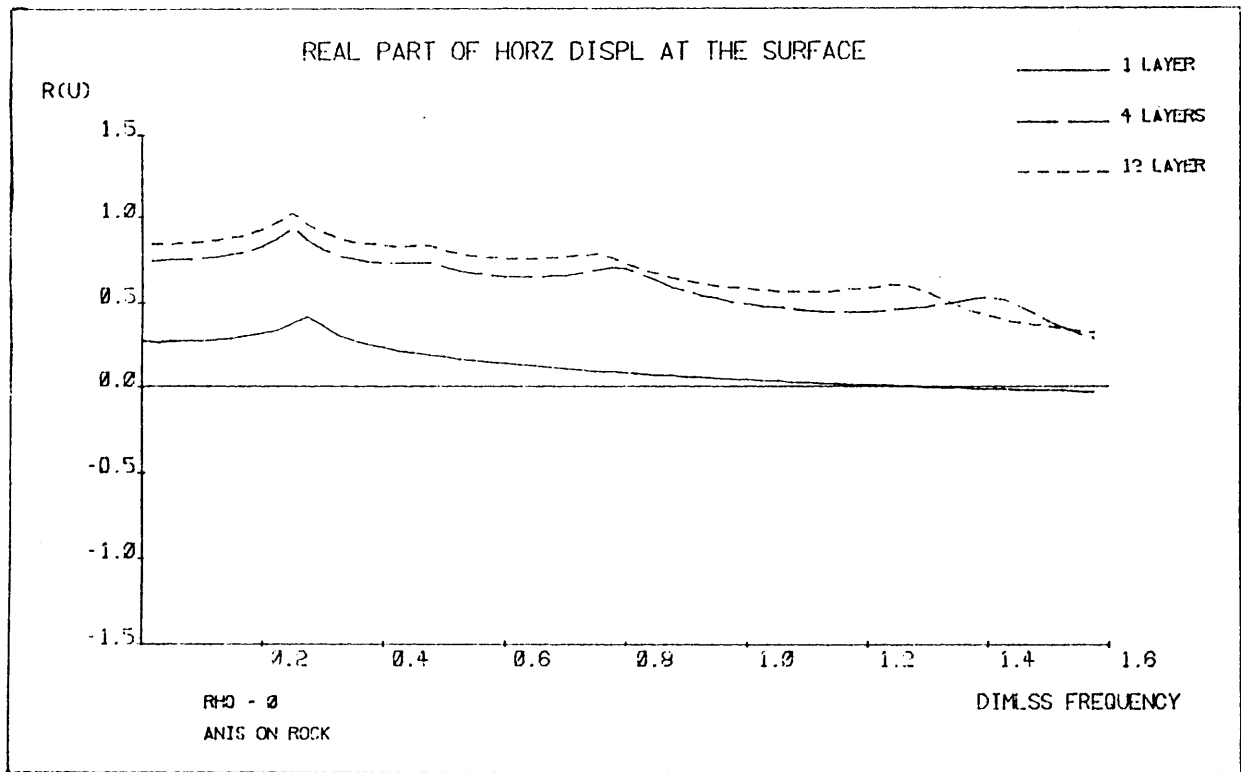


Figure 5-2: Real Part of the Horizontal Displacement at $\rho = 0$, Anisotropic Stratum

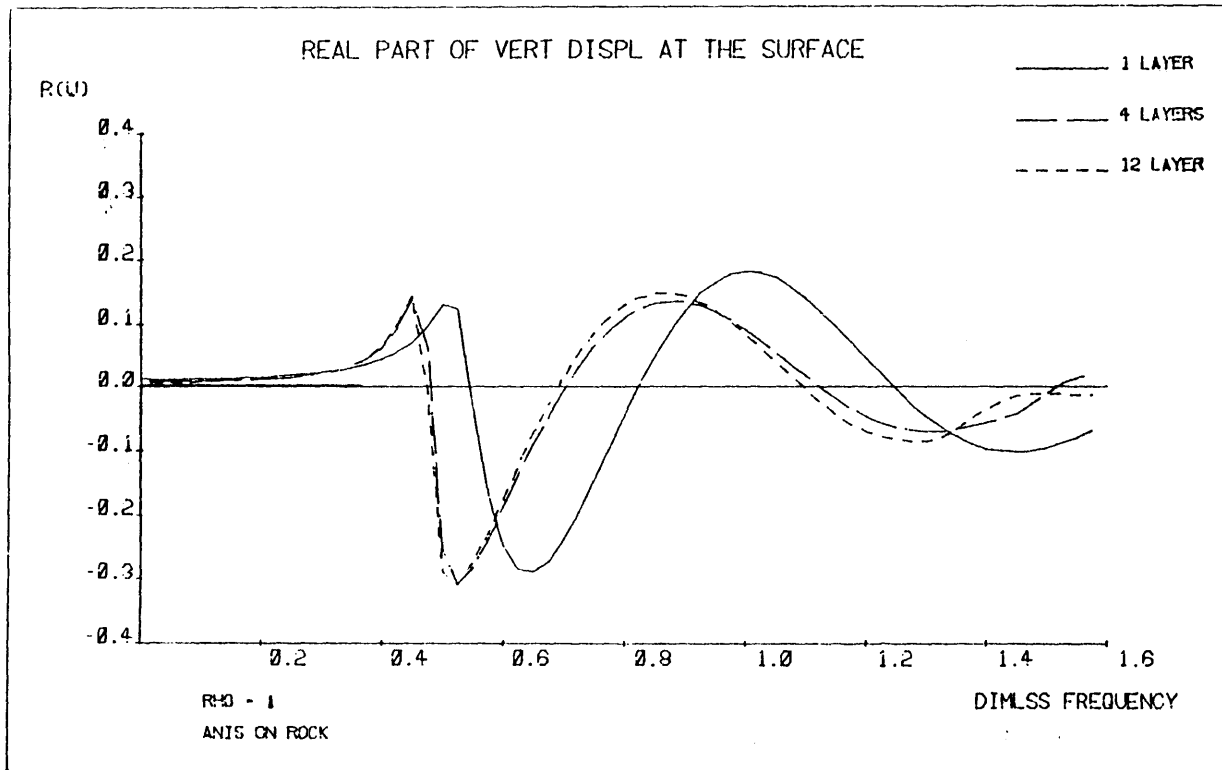


Figure 5-3: Real Part of the Vertical Displacement at $\rho = 1$, Anisotropic Stratum

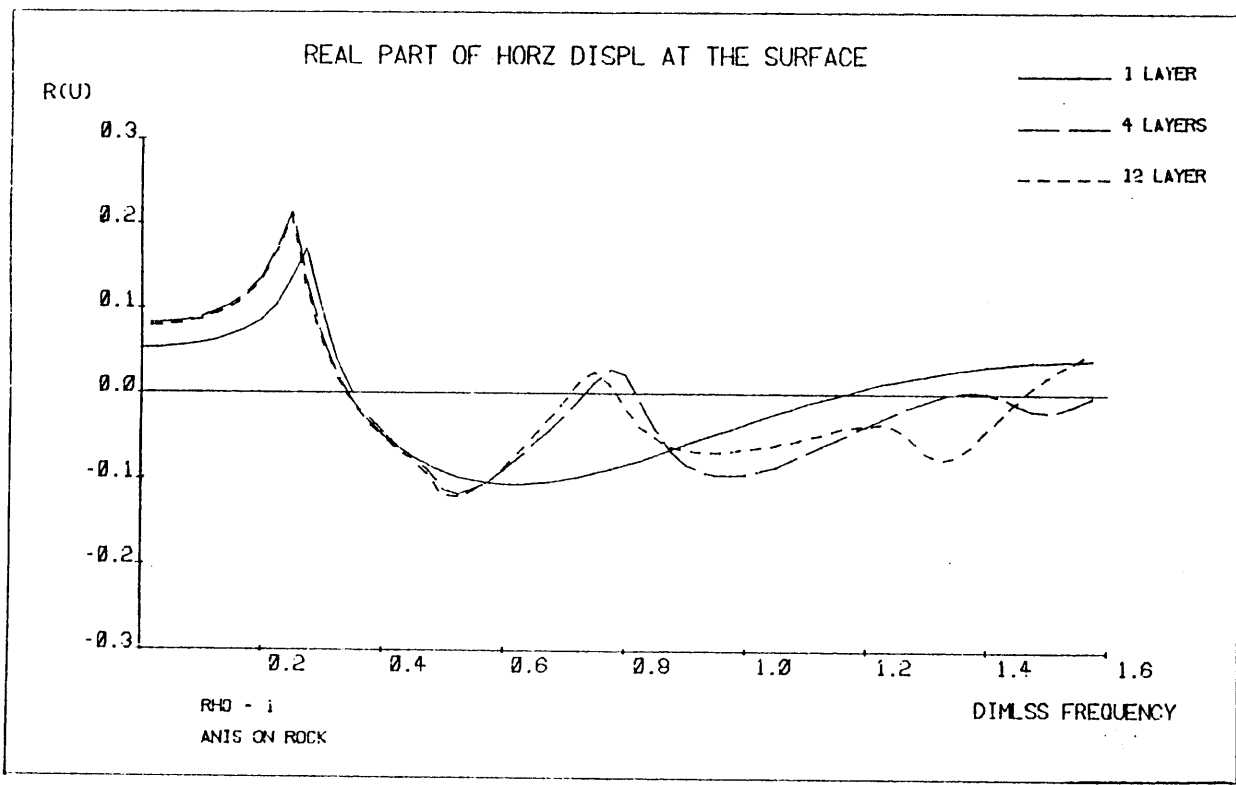


Figure 5-4: Real Part of the Horizontal Displacement at $\rho = 1$, Anisotropic Stratum

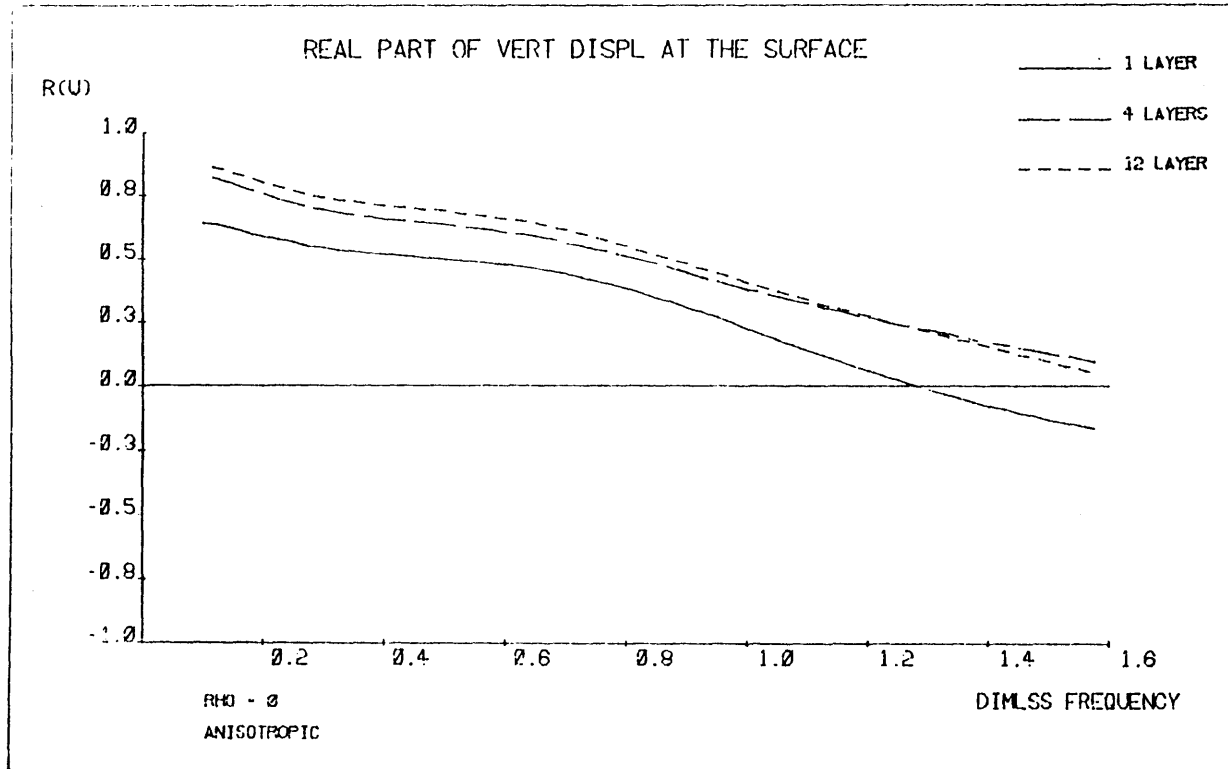


Figure 5-5: Real Part of the Vertical Displacement at $\rho = 0$, Anisotropic Halfspace

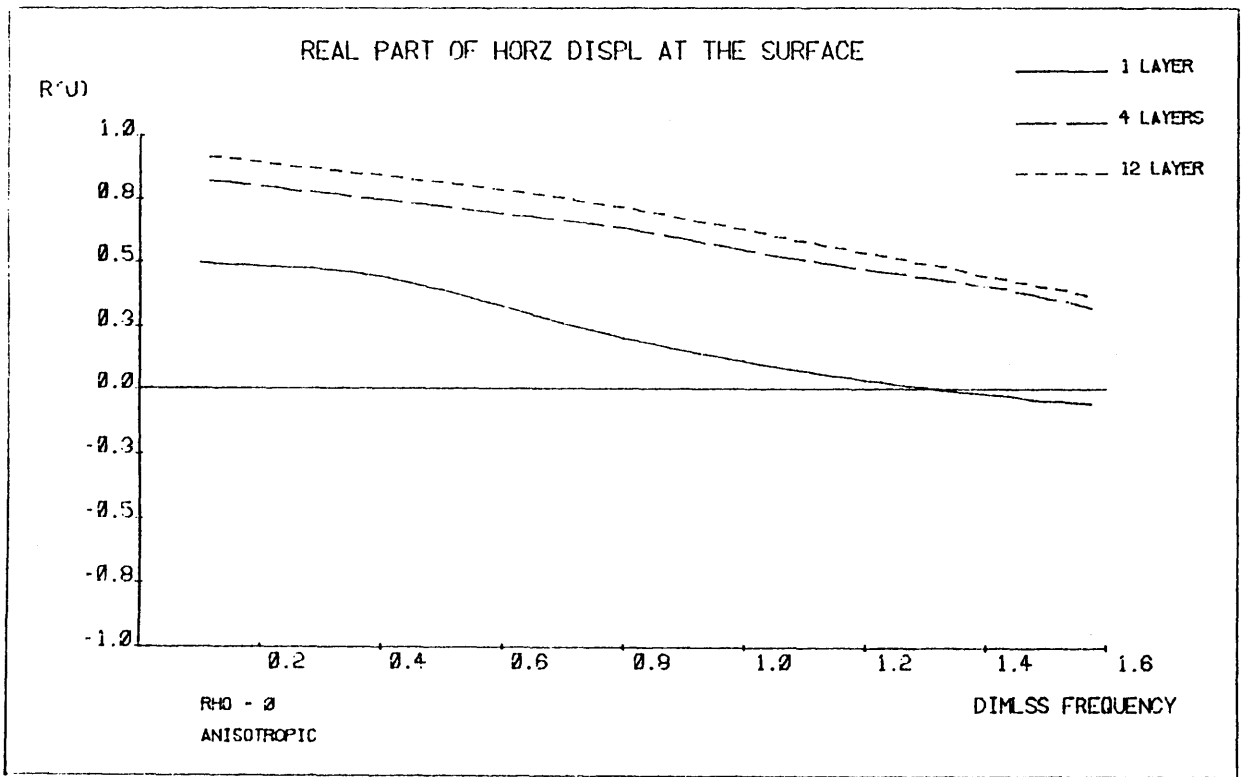


Figure 5-6: Real Part of the Horizontal Displacement at $\rho = 0$, Anisotropic Halfspace

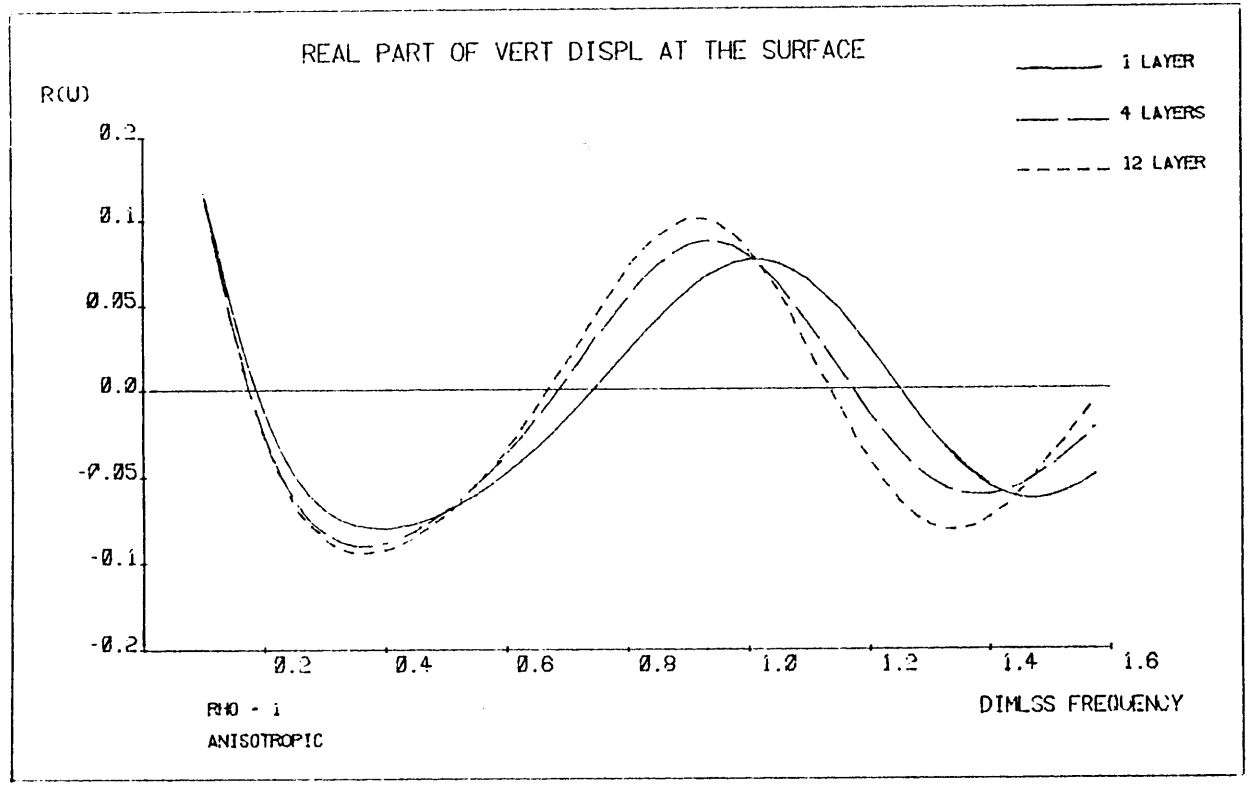


Figure 5-7: Real Part of the Vertical Displacement at $\rho = 1$, Anisotropic Halfspace

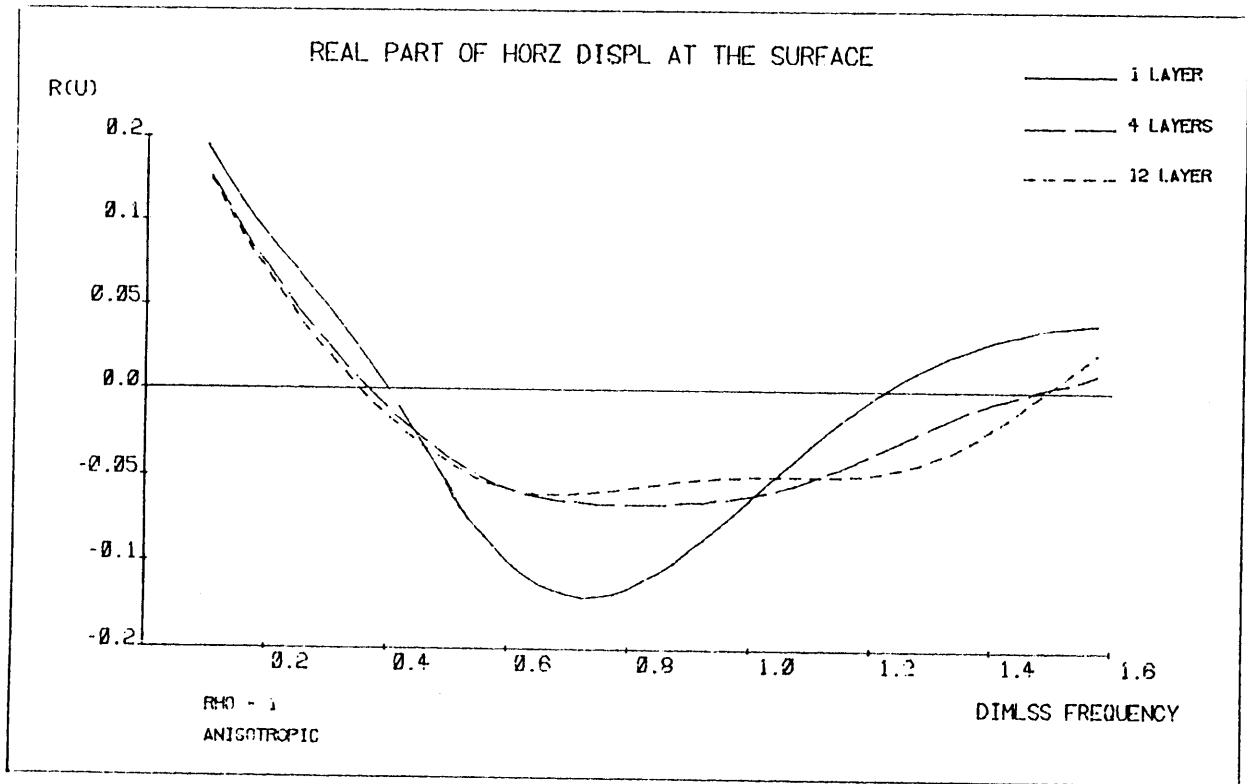


Figure 5-8: Real Part of the Horizontal Displacement at $\rho = 1$, Anisotropic Halfspace

anisotropic media is not readily available for comparison with the approximate solution.

5.5 Static Loads in Cross-Anisotropic Layered Halfspaces

Several analytical solutions for displacements and stresses due to static loads in homogeneous cross-anisotropic media have been published. Barden (1963) presented a solution for stresses and displacements in a cross-anisotropic halfspace subjected to a vertical point load at the surface. Calculations presented in this reference illustrate how increasing the vertical elastic modulus (increasing the degree of anisotropy) decreases the surface displacements. A discussion of the effects of anisotropy on soil behavior is provided at the the end of Barden's work. Pan and Chou (1976, 1979) obtain the solutions for displacements due to point loads in infinite and semi-infinite cross-anisotropic bodies. Their solutions are constructed by assuming a potential function for the point source and then substituting it into the equilibrium equations and enforcing boundary conditions. In general, the solutions for displacements are very complicated and unwieldy. At the surface of a halfspace, they reduce to a more tractable form.

Approximate solutions for layered cross-anisotropic halfspaces subjected to static loads have also been proposed. Gerrard (1967) applied a Fourier series to the solution of stresses and displacements in a layered cross-anisotropic soil deposit subjected to a load symmetrically distributed about the vertical axis. He calculated stresses as a function of depth in a two-layer stratum subjected to a uniform vertical strip loading. Rowe and Booker (1982, 1983) used a stiffness matrix method with numerical inverse transforms to calculate settlement in layered cross-anisotropic halfspaces. They assumed that the elastic modulus varies exponentially with depth within each layer.

The method for the analysis of layered halfspaces subjected to static point loads presented in Chapter 4 can also be applied to cross-anisotropic halfspaces. Again, the solution technique remains the same, only the elements of the stiffness matrix are changed by anisotropy. The exact

stiffness matrix of the cross-anisotropic halfspace is linear in wavenumber k . The stiffness matrix elements are obtained by taking the limit of the dynamic stiffness when ω goes to zero.

For the anti-plane case, setting ω to zero in Equation 5-9 gives the stiffness

$$k_{yy}(k) = \sqrt{NL} k \quad 5-60$$

In the isotropic limit, $N = L = G$ and $k_{yy}(k)$ becomes kG .

For the in-plane case, the quadratic coefficients of Equation 5-20 become

$$\begin{aligned} a^* &= CL \\ b^* &= F(F + 2L) - AC \\ c^* &= AL \end{aligned} \quad 5-61$$

and we have the roots

$$\begin{aligned} r^2 &= \frac{-b^* + \sqrt{b^{*2} - 4a^*c^*}}{2a^*} \\ s^2 &= \frac{-b^* - \sqrt{b^{*2} - 4a^*c^*}}{2a^*} \end{aligned} \quad 5-62$$

Then the functions f and g become

$$\begin{aligned} f &= \frac{A - r^2L}{F + L} \\ g &= \frac{A - s^2L}{F + L} \end{aligned} \quad 5-63$$

and the stiffness elements are (from Equation 5-36)

$$\begin{aligned} k_{xx} &= \frac{Lk}{gr - fs} (r^2g - s^2f) \\ k_{zz} &= k_{zx} = \frac{Lk}{gr - fs} (r^2s + fs - s^2r - gr) \\ k_{zz} &= \frac{Crsk}{gr - fs} (f - g) \end{aligned} \quad 5-64$$

In the static case, r , s , f and g are independent of k .

The inverse of the stiffness matrix 5-64 is

$$K^{-1} = \frac{1}{k_{xx}k_{zz} - k_{xz}^2} \begin{bmatrix} k_{zz} & -k_{xz} \\ -k_{xz} & k_{xx} \end{bmatrix} \quad 5-65$$

As described in Chapter 4, the elements of K^{-1} are the contributions of the rigid body modes to the global flexibility matrix. The flexibilities are substituted into the expressions for displacements due to point loads from Chapter 4 and the inverse transform is performed. The halfspace terms in the displacements due to a horizontal point load are

$$u_{\rho} = \frac{1}{2\pi k_{yy}\rho}$$

$$u_{\theta} = \frac{k_{zz}}{2\pi(k_{xx}k_{zz} - k_{xz}^2)\rho} \quad 5-66$$

$$u_z = \frac{-k_{xz}}{2\pi(k_{xx}k_{zz} - k_{xz}^2)\rho}$$

The halfspace terms in the displacements due to a vertical point load are

$$u_{\rho} = \frac{-k_{xz}}{2\pi(k_{xx}k_{zz} - k_{xz}^2)\rho} \quad 5-67$$

$$u_z = \frac{k_{xx}}{2\pi(k_{xx}k_{zz} - k_{xz}^2)\rho}$$

The displacements in Equations 5-66 and 5-67 are the exact solutions for displacements at the surface of a halfspace due to static loads at the surface.

Displacements were computed for a cross-anisotropic halfspace subjected to unit point loads at the surface. The layer overlying the halfspace has depth $H = 1.0$. The entire halfspace has density $\rho = 1.0$. The elastic constants used for calculations are those of freshwater ice, taken from Anderson (1961):

$$\begin{aligned} A &= 4.60 \\ C &= 4.96 \\ F &= 1.60 \\ N &= 1.215 \\ L &= 1.0 \end{aligned} \quad 5-68$$

Displacements were computed at the surface for the overlying layer discretized into 1 and 4 sublayers.

Figure 5-9 shows the horizontal displacement at the surface due to a horizontal point load. The solid line is the analytical solution. The 4 sublayer solutions is an excellent approximation of the true solution. Figure 5-10 shows the vertical displacement at the surface due to a vertical point load. This single layer solution is excellent, the 4 sublayer solution is indistinguishable from the analytic solution. Note also that the vertical displacements are less than those of the isotropic solid (Figure 4-6) due to the increased vertical stiffness. The discrete layer method obtains excellent results for the static cross-anisotropic halfspace with relatively few layers.

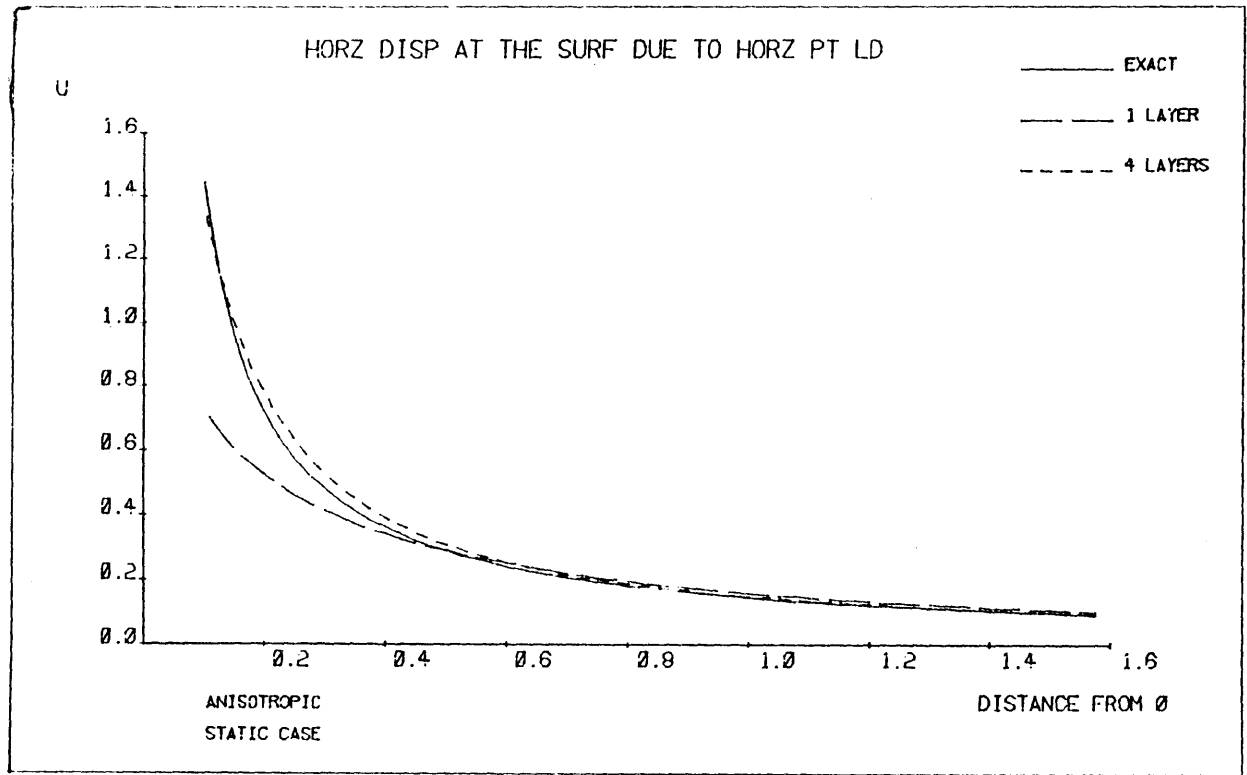


Figure 5-9: Horizontal Displacement due to Static Horizontal Point Load at the Surface

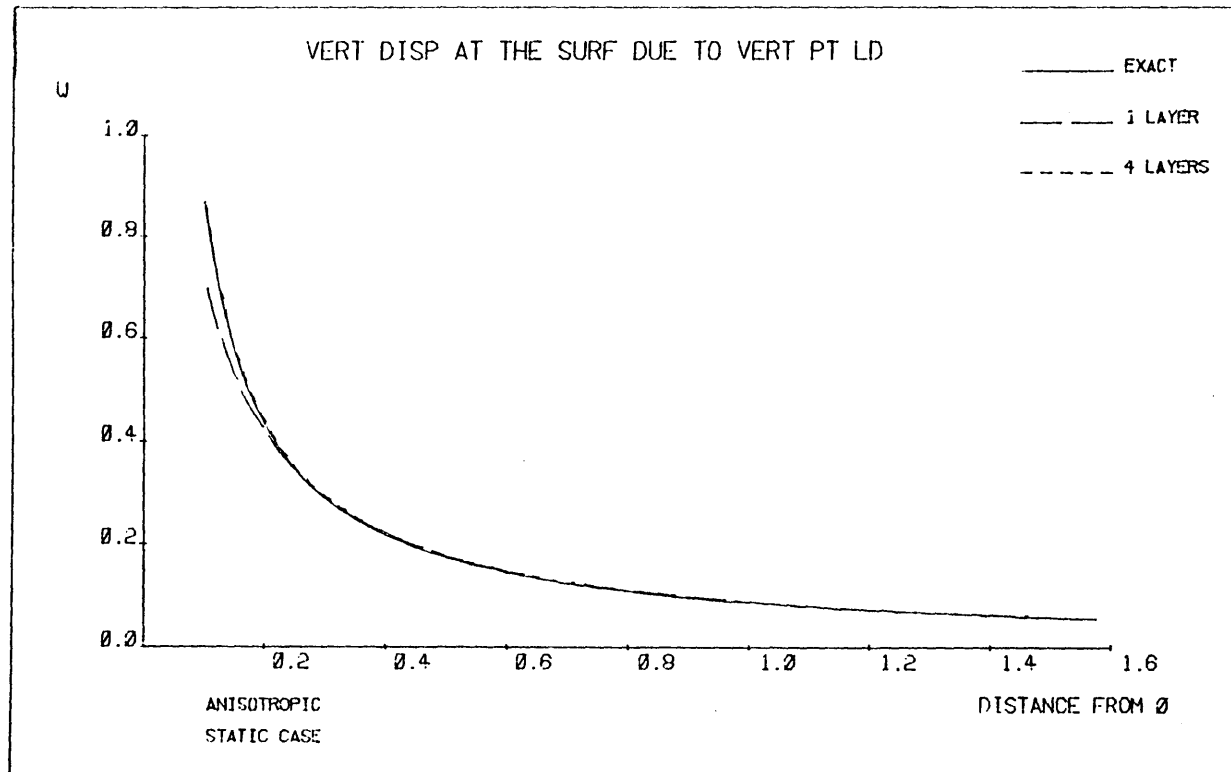


Figure 5-10: Vertical Displacement due to Static Vertical Point Load at the Surface

Chapter 6

Conclusions

A method for obtaining displacements in layered isotropic or anisotropic halfspaces subjected to static or dynamic loads has been presented. The technique involves solving the wave equations in the transformed frequency-wavenumber domain. The displacements are approximated by a linear expansion in the direction of depth. Then the stress-displacement relations of a soil layer are expressed by a stiffness matrix that is algebraic in the horizontal wavenumber. The stiffness of the entire soil system is formed by overlapping the layer matrices at common degrees of freedom. The matrix inversion is accomplished by extracting the eigenvectors and eigenvalues of the global stiffness matrix and applying orthogonality conditions. The inverse wavenumber transform is then performed in closed form. Thus the final expressions for displacements consist of sums of functions of the wavenumbers and eigenvectors. The displacements are computed at discrete frequencies. Solutions in the time domain can be computed with a numerical Fourier transform in the frequency domain. Stresses can be computed in the center of each soil layer, since displacements are linear in the direction of depth and continuous in the radial direction.

The fundamentals of this technique have been developed by Kausel. New developments described in this paper include: the algebraic stiffness matrix for a halfspace, the solution for static point loads in a halfspace and the layer and halfspace stiffness matrices for cross-anisotropic materials. The algebraic halfspace matrix was obtained with the Taylor series expansion of the true stiffness. The ability of the approximate stiffness elements to match the true stiffness has less impact on the accuracy of the solution than does the ability of the approximate stiffness to match the energy absorbing characteristics of the true stiffness. The characteristics of the algebraic halfspace stiffness place limitations on the physical parameters. The accuracy of calculated displacements decays at low frequencies. Some ranges of Poisson ratios give less accurate results,

this can be overcome by increasing the number of sublayers in the model.

The stiffness matrix for static loads in the halfspace is algebraic in the wavenumber and thus does not need to be approximated. However, the exact stiffness of the halfspace alters the structure of the global stiffness matrix so that alternate techniques of linear algebra are required to extract the eigenmodes. The analysis of anisotropic media proved to be simple with the stiffness method. The anisotropic elastic constants appear in the elements of the stiffness matrix, the essential mathematics remain unchanged. Examples of displacements are computed for many cases and compared to known solutions when they exist. Comparison with known solutions illustrates that the stiffness method is very accurate for a soil deposit modeled with relatively few layers.

The work can be extended to other topics of research. Distributed loads covering rectangular areas could be treated with a Fourier transform over the spatial variables. The transform of the loads itself and the inverse transform of the flexibility would be required in closed form. The influence of a viscoelastic halfspace that behaves as a spring and dashpot in parallel could be investigated. This might be accomplished by multiplying the static stiffness by a factor $(1 + 2i\beta)$, where here β is a measure of the strength of the physical dashpot. This solution could be used to study the long term effects of the viscosity of the halfspace. Another modification to the method would be to alter the stiffness matrices to include the effects of pore fluid flow. This work has already been done for the Haskell-Thomson transfer matrix. Starting with the differential equations of motion that include pore fluid, algebraic layer matrices could be obtained by applying the finite element method described above.

Finally, the application of this method on a digital computer must be discussed. The static and dynamic analysis programs are written in FORTRAN 77. The calculations behind the illustrations in this paper were performed on an IBM 370 and a VAX 11/780. On the VAX, the static and dynamic analysis programs each occupy about 85 kilobytes of memory. The space required to run these programs, for a 12 layer problem, is about 175k. The small core requirements for these programs make them ideally suited to applications on microcomputers. The static

analysis program has been compiled and run on an IBM AT Personal Computer. The only drawback to microcomputer applications is that mathematical calculations are an order of magnitude slower than on a minicomputer. Since the calculation capacity of microcomputers is growing rapidly, this problem is expected to diminish in importance. Eventually, distribution of these programs on desktop computers would allow quick calculations for settlement, foundation, vibration and many other geotechnical problems.

Appendix A

Proof that Orthogonality Conditions and Flexibilities For the Static Halfspace Reduce to Those of the Rigid Base Case

A.1 Anti-plane Case

In the rigid base case, $G_r \rightarrow \infty$ and therefore $B = 0$. Displacement at the bedrock interface is zero, thus the last degree of freedom is removed from the system, making the C matrix non-singular. The rigid body mode is no longer part of the system and the real root goes to ∞ (see Appendix B). In fact, for the rigid base case

$$X = [\phi_y \phi_y]$$

and

$$K = \begin{bmatrix} K_L \\ -K_L \end{bmatrix} \tag{A-1}$$

where X is now of dimension $N-1 \times 2N-2$ and K_L is $N-1 \times N-1$. The notation is consistent with that used by Kausel (1982b). Substituting A-1 in the orthogonality condition 4-15 gives

$$\begin{aligned} KX^TAXK - X^TCX &= \begin{bmatrix} K_L \\ -K_L \end{bmatrix} \begin{bmatrix} \phi_y^T \\ \phi_y^T \end{bmatrix} A_y [\phi_y \phi_y] \begin{bmatrix} K_L \\ -K_L \end{bmatrix} - \begin{bmatrix} \phi_y^T \\ \phi_y^T \end{bmatrix} C_y [\phi_y \phi_y] \\ &= \begin{bmatrix} K_L \phi_y^T A_y \phi_y K_L & -K_L \phi_y^T A_y \phi_y K_L \\ -K_L \phi_y^T A_y \phi_y K_L & K_L \phi_y^T A_y \phi_y K_L \end{bmatrix} - \begin{bmatrix} \phi_y^T C_y \phi_y & \phi_y^T C_y \phi_y \\ \phi_y^T C_y \phi_y & \phi_y^T C_y \phi_y \end{bmatrix} \end{aligned} \tag{A-2}$$

But from Kausel (1982b) we know that $\phi_y^T A_y \phi_y = I$ and $\phi_y^T C_y \phi_y = -K_L^2$, so that A-2 equals

$$\begin{bmatrix} K_L^2 + K_L^2 & -K_L^2 + K_L^2 \\ -K_L^2 + K_L^2 & K_L^2 + K_L^2 \end{bmatrix} = 2 \begin{bmatrix} K_L^2 & \\ & K_L^2 \end{bmatrix} = 2 \begin{bmatrix} K_L^2 & \\ & (-K_L)^2 \end{bmatrix} = 2 K^2 \tag{A-3}$$

Hence, our choice of normalization is consistent with the rigid base case.

Expressions 4-30 can be shown to reduce to the rigid base case, where $B = 0$ and $M = I$

$$A_y^{-1} = \frac{1}{2} [\Phi_y \Phi_y] \begin{bmatrix} \Phi_y^T \\ \Phi_y^T \end{bmatrix} = \frac{1}{2} [\Phi_y \Phi_y^T + \Phi_y \Phi_y^T] = \Phi_y \Phi_y^T$$

$$0 = -\frac{1}{2} X K X^T = -\frac{1}{2} [\Phi_y \Phi_y] \begin{bmatrix} K_L \\ -K_L \end{bmatrix} \begin{bmatrix} \Phi_y^T \\ \Phi_y^T \end{bmatrix} = -\frac{1}{2} [\Phi_y K_L \Phi_y^T - \Phi_y K_L \Phi_y^T] = 0 \quad A-4$$

Since $\overline{K} = K$ in the rigid base case, the last two equations of 4-30 are the same. Since \overline{C} is singular for the halfspace case, we cannot develop the corresponding orthogonality conditions that parallel the rigid base case, i.e., $C_y^{-1} = -\Phi_y K_L^{-2} \Phi_y^T$

To prove that the flexibilities reduce to the rigid base case, we substitute A-1 into 4-38

$$\frac{1}{2} X (kI - K)^{-1} \overline{K}^{-1} X^T =$$

$$\frac{1}{2} [\Phi_y \Phi_y] \begin{bmatrix} kI - K_L & \\ & kI + K_L \end{bmatrix}^{-1} \begin{bmatrix} K_L^{-1} & \\ & -K_L^{-1} \end{bmatrix} \begin{bmatrix} \Phi_y^T \\ \Phi_y^T \end{bmatrix} =$$

$$\frac{1}{2} [\Phi_y (kI - K_L)^{-1} K_L^{-1} \Phi_y^T - \Phi_y (kI + K_L)^{-1} K_L^{-1} \Phi_y^T] = \quad A-5$$

$$\frac{1}{2} \Phi_y [(kI - K_L)^{-1} K_L^{-1} - (kI + K_L)^{-1} K_L^{-1}] \Phi_y^T$$

Expanding A-5 gives

$$\frac{1}{2} [(kI - K_L)^{-1} K_L^{-1} - (kI + K_L)^{-1} K_L^{-1}] = \text{diag} \left[\frac{1}{2k_j(k - k_j)} - \frac{1}{2k_j(k + k_j)} \right] =$$

$$\text{diag} \frac{1}{2k_j} \left[\frac{k + k_j - k + k_j}{(k^2 - k_j^2)} \right] = \text{diag} \left[\frac{1}{k^2 - k_j^2} \right] = D_L \quad j = 1, \dots, 2N-2 \quad A-6$$

Thus $F_{yy} = \Phi_y D_L \Phi_y^T$ as given by Kausel(1982b).

A.2 In-plane case

In the rigid base case, $B_x = B_z = 0$. Displacements at the bedrock interface are zero, thus the last degree of freedom in the x and z directions are removed from the system, making C_x and C_z non-singular. For the rigid base case,

$$X = \begin{bmatrix} \phi_x & \phi_x \\ \phi_z & -\phi_z \end{bmatrix}$$

and

$$K = \begin{bmatrix} K_R \\ -K_R \end{bmatrix} \tag{A-7}$$

where X is dimension $2N-2 \times 4N-4$ and K_R is $2N-2 \times 2N-2$. Substituting A-8 into the orthogonality condition 4-15 gives

$$\begin{aligned} & \begin{bmatrix} K_R \\ -K_R \end{bmatrix} \begin{bmatrix} \phi_x^T & \phi_z^T \\ \phi_x^T & -\phi_z^T \end{bmatrix} \begin{bmatrix} A_x \\ A_z \end{bmatrix} \begin{bmatrix} \phi_x & \phi_x \\ \phi_z & -\phi_z \end{bmatrix} \begin{bmatrix} K_R \\ -K_R \end{bmatrix} - \\ & \begin{bmatrix} \phi_x^T & \phi_z^T \\ \phi_x^T & -\phi_z^T \end{bmatrix} \begin{bmatrix} C_x \\ C_z \end{bmatrix} \begin{bmatrix} \phi_x & \phi_x \\ \phi_z & -\phi_z \end{bmatrix} = \\ & \begin{bmatrix} K_R (\phi_x^T A_x \phi_x + \phi_z^T A_z \phi_z) K_R & K_R (-\phi_x^T A_x \phi_x + \phi_z^T A_z \phi_z) K_R \\ K_R (-\phi_x^T A_x \phi_x + \phi_z^T A_z \phi_z) K_R & K_R (\phi_x^T A_x \phi_x + \phi_z^T A_z \phi_z) K_R \end{bmatrix} - \\ & \begin{bmatrix} \phi_x^T C_x \phi_x + \phi_z^T C_z \phi_z & \phi_x^T C_x \phi_x - \phi_z^T C_z \phi_z \\ \phi_x^T C_x \phi_x - \phi_z^T C_z \phi_z & \phi_x^T C_x \phi_x + \phi_z^T C_z \phi_z \end{bmatrix} \end{aligned} \tag{A-8}$$

Although it is not readily apparent, the normalization of Equations 17a and 17b of Kausel (1982b) can be expanded and manipulated to give

$$K_R (\phi_x^T A_x \phi_x + \phi_z^T A_z \phi_z) K_R - (\phi_x^T C_x \phi_x + \phi_z^T C_z \phi_z) = 2K_R^2$$

and

$$K_R \phi_x^T A_x \phi_x K_R + \phi_x^T C_x \phi_x = 0 \quad K_R \phi_z^T A_z \phi_z K_R + \phi_z^T C_z \phi_z = 0 \tag{A-9}$$

Thus A-8 equals

$$2 \begin{bmatrix} K_R^2 & \\ & K_R^2 \end{bmatrix} \quad \text{A-10}$$

When Equations A-9 are substituted into A-8, we see that both the diagonal and the off-diagonal elements are satisfied. This, our normalization is again consistent with the rigid base case.

The inverse of \overline{A} can be shown to reduce to the rigid base case, where $M=I$ and $K=\overline{K}=K_R$. Substituting A-7 into 4-63 gives

$$\begin{aligned} \begin{bmatrix} A_x^{-1} & \\ & A_z^{-1} \end{bmatrix} &= \frac{1}{2} \begin{bmatrix} \phi_x & \phi_x \\ \phi_z & -\phi_z \end{bmatrix} I \begin{bmatrix} \phi_x^T & \phi_z^T \\ \phi_x^T & -\phi_z^T \end{bmatrix} = \\ \frac{1}{2} \begin{bmatrix} \phi_x \phi_x^T + \phi_x \phi_x^T & \phi_x \phi_z^T - \phi_x \phi_z^T \\ \phi_z \phi_x^T - \phi_z \phi_x^T & \phi_z \phi_z^T + \phi_z \phi_z^T \end{bmatrix} &= \begin{bmatrix} \phi_x \phi_x^T & \\ & \phi_z \phi_z^T \end{bmatrix} \end{aligned} \quad \text{A-11}$$

$$\begin{aligned} \begin{bmatrix} A_x^{-1} & \\ & A_z^{-1} \end{bmatrix} \begin{bmatrix} B_{xz}^T & B_{xz} \end{bmatrix} \begin{bmatrix} A_x^{-1} & \\ & A_z^{-1} \end{bmatrix} &= \\ -\frac{1}{2} \begin{bmatrix} \phi_x & \phi_x \\ \phi_z & -\phi_z \end{bmatrix} \begin{bmatrix} K_R & \\ & -K_R \end{bmatrix} \begin{bmatrix} \phi_x^T & \phi_z^T \\ \phi_x^T & -\phi_z^T \end{bmatrix} &= \\ \begin{bmatrix} A_z^{-1} B_{xz}^T A_x^{-1} & A_x^{-1} B_{xz} A_z^{-1} \end{bmatrix} &= \end{aligned} \quad \text{A-12}$$

$$\begin{aligned} -\frac{1}{2} \begin{bmatrix} \phi_x K_R \phi_x^T - \phi_x K_R \phi_x^T & \phi_x K_R \phi_z^T + \phi_x K_R \phi_z^T \\ \phi_z K_R \phi_x^T + \phi_z K_R \phi_x^T & \phi_z K_R \phi_z^T - \phi_z K_R \phi_z^T \end{bmatrix} &= \\ \begin{bmatrix} -\phi_x K_R \phi_z^T \\ -\phi_z K_R \phi_x^T \end{bmatrix} &= \\ \begin{bmatrix} \phi_x & \phi_x \\ \phi_z & -\phi_z \end{bmatrix} \begin{bmatrix} K_R^{-1} & \\ & K_R^{-1} \end{bmatrix} \begin{bmatrix} \phi_x^T & \phi_z^T \\ \phi_x^T & -\phi_z^T \end{bmatrix} &= \begin{bmatrix} 2\phi_x K_R^{-1} \phi_z^T \\ 2\phi_z K_R^{-1} \phi_x^T \end{bmatrix} = 0 \end{aligned} \quad \text{A-13}$$

These all agree with Equation 21 of Kausel (1982b). Since the \overline{C} matrix is singular, we cannot invert it.

Now we examine the flexibility 4-65. Let the flexibility matrix be given by

$$\frac{1}{2} X (kI - K)^{-1} \overline{K}^{-1} X^T = \frac{1}{2} X D \overline{K}^{-1} X^T \quad \text{A-14}$$

where

$$D = \begin{bmatrix} D_1 & \\ & D_2 \end{bmatrix} = \begin{bmatrix} \frac{1}{k-k_j} & \\ & \frac{1}{k+k_j} \end{bmatrix} \quad j = 1, \dots, 4N-4 \quad A-15$$

Substituting A-7 into A-14 yields

$$\begin{aligned} & \frac{1}{2} \begin{bmatrix} \Phi_x & \Phi_x \\ \Phi_z & -\Phi_z \end{bmatrix} \begin{bmatrix} D_1 & \\ & D_2 \end{bmatrix} \begin{bmatrix} K_R^{-1} & \\ & -K_R^{-1} \end{bmatrix} \begin{bmatrix} \Phi_x^T & \Phi_z^T \\ \Phi_x^T & -\Phi_z^T \end{bmatrix} = \\ & \frac{1}{2} \begin{bmatrix} \Phi_x D_1 K_R^{-1} \Phi_x^T - \Phi_x D_2 K_R^{-1} \Phi_x^T & \Phi_x D_1 K_R^{-1} \Phi_z^T + \Phi_x D_2 K_R^{-1} \Phi_z^T \\ \Phi_z D_1 K_R^{-1} \Phi_x^T + \Phi_z D_2 K_R^{-1} \Phi_x^T & \Phi_z D_1 K_R^{-1} \Phi_z^T - \Phi_z D_2 K_R^{-1} \Phi_z^T \end{bmatrix} = \\ & \frac{1}{2} \begin{bmatrix} \Phi_x (D_1 - D_2) K_R^{-1} \Phi_x^T & \Phi_x (D_1 + D_2) K_R^{-1} \Phi_x^T \\ \Phi_z (D_1 + D_2) K_R^{-1} \Phi_x^T & \Phi_z (D_1 - D_2) K_R^{-1} \Phi_z^T \end{bmatrix} \end{aligned} \quad A-16$$

Substituting the definition of D from A-15 into A-16 gives

$$\begin{aligned} & \frac{1}{2} (D_1 - D_2) K_R^{-1} = \text{diag} \left[\frac{1}{2k_j} \left[\frac{1}{k-k_j} - \frac{1}{k+k_j} \right] \right] = \frac{1}{2k_j} \left[\frac{k+k_j-k+k_j}{(k^2-k_j^2)} \right] = \\ & \text{diag} \left[\frac{1}{k^2-k_j^2} \right] = D_R \\ & \frac{1}{2} (D_1 + D_2) K_R^{-1} = \text{diag} \left[\frac{1}{2k_j} \left[\frac{1}{k-k_j} + \frac{1}{k+k_j} \right] \right] = \frac{1}{2k_j} \left[\frac{k-k_j+k+k_j}{(k^2-k_j^2)} \right] = \\ & \text{diag} \left[\frac{k}{k_j(k^2-k_j^2)} \right] = kK_R^{-1} D_R \end{aligned} \quad A-17$$

Thus

$$\begin{aligned} F_{xx} &= \Phi_x D_R \Phi_x^T \\ F_{xz} &= k \Phi_x K_R^{-1} D_R \Phi_z^T \\ F_{zz} &= \Phi_z D_R \Phi_z^T \end{aligned} \quad A-18$$

which are the same expressions given by Kausel (1982b).

Appendix B

Static Eigenvalues for the Anti-plane Case of a Homogeneous Stratum on an Elastic Halfspace

B.1 Discrete Case

The analytic solution for the static anti-plane eigenvalues of a homogeneous stratum overlying an elastic halfspace is derived below. The analytic solution for the discrete case is difficult to evaluate numerically, but is useful for examining the behavior of the eigenvalues. The analytic solution for the continuum case (the "exact" solution) is undefined when the halfspace is homogeneous. The geometry of the problem is shown in Figure B-1.

B.1.1 Roots of the Eigenvalue Problem

To begin, we rewrite the eigenvalue problem, Equation 4-3, for the N-layer anti-plane case

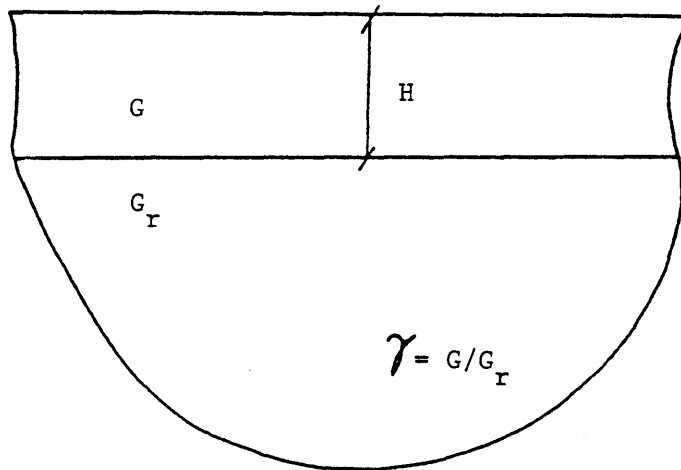
$$(Ak^2 + Bk + C)X = 0 \tag{B-1}$$

in the dimensionless form

$$(\overline{A}\kappa^2 + \overline{B}\kappa + \overline{C})X = 0 \tag{B-2}$$

with $\kappa^2 = \frac{1}{8}(kh)^2$ and

Figure B-1: Homogenous Layer Overlying an Elastic Halfspace



$$\begin{array}{l}
 \overline{A} = \left[\begin{array}{cccc} 2 & 1 & & \\ 1 & 4 & 1 & \\ & 1 & 4 & 1 \\ & & 1 & 4 \\ & & & 1 & 2 \end{array} \right] \\
 \overline{B} = \left[\begin{array}{c} 0 \\ \cdot \\ \cdot \\ \cdot \\ \frac{\sqrt{6}}{\gamma} \end{array} \right] \\
 \overline{C} = \left[\begin{array}{cccc} 1 & -1 & & \\ -1 & 2 & -1 & \\ & -1 & 2 & \\ & & & -1 \\ & & & -1 & 1 \end{array} \right] \\
 X = \left[\begin{array}{c} x_1 \\ \cdot \\ x_l \\ \cdot \\ x_N \\ x_{N+1} \end{array} \right]
 \end{array} \quad B-3$$

where

$$\gamma = \frac{G}{G_r} \quad x_{N+1} \equiv x_r$$

and the subscript r refers to the halfspace (rock).

Then all equations, except the first and last, are of the form of a difference equation

$$(\kappa^2 - 1) x_{l-1} + (4\kappa^2 + 2) x_l + (\kappa^2 - 1) x_{l+1} = 0 \quad B-4$$

while the first and last, which constitute the boundary conditions of the difference equation, are

$$\begin{array}{l}
 (1 + 2\kappa^2) x_1 + (-1 + \kappa^2) x_2 = 0 \\
 (-1 + \kappa^2) x_N + \left(2\kappa^2 + \frac{\sqrt{6}}{\gamma} \kappa + 1\right) x_r = 0
 \end{array} \quad B-5$$

Assume a solution of the form

$$x_l = c z^{l-1} \tag{B-6}$$

Then, after dividing by z^{l-2} , we obtain

$$-(1 - \kappa^2) + 2(1 + 2\kappa^2)z - (1 - \kappa^2)z^2 = 0 \tag{B-7}$$

which has the solution

$$z = \frac{1 + 2\kappa^2}{1 - \kappa^2} \pm \sqrt{\left[\frac{1 + 2\kappa^2}{1 - \kappa^2}\right]^2 - 1} \tag{B-8}$$

Making the substitution

$$\cos \theta = \frac{1 + 2\kappa^2}{1 - \kappa^2} \tag{B-9}$$

we obtain

$$z = \cos \theta \pm \sqrt{\cos^2 \theta - 1} = \cos \theta \pm i\sqrt{1 - \cos^2 \theta} = \cos \theta \pm i \sin \theta \tag{B-10}$$

Therefore $z = e^{\pm i\theta}$. The complete solution is then

$$x_l = A e^{i(l-1)\theta} + B e^{-i(l-1)\theta} \tag{B-11}$$

with A , and B being arbitrary constants.

Now rewrite the boundary conditions in terms of θ :

$$x_1 \cos \theta - x_2 = 0 \tag{B-12}$$

$$-x_N + \left[\cos \theta + \frac{\sqrt{6}}{\gamma} \frac{\kappa}{1 - \kappa^2} \right] x_r = 0$$

Solving for κ from Equation B-9 gives

$$1 + 2\kappa^2 - \cos \theta + \kappa^2 \cos \theta = 0 \tag{B-13}$$

That is

$$\kappa^2 = -\frac{1 - \cos \theta}{2 + \cos \theta} = -\frac{2 \sin^2 \frac{\theta}{2}}{3 - 2 \sin^2 \frac{\theta}{2}} = -\frac{2}{3} \frac{\sin^2 \frac{\theta}{2}}{1 - \frac{2}{3} \sin^2 \frac{\theta}{2}}$$

and

B-14

$$1 - \kappa^2 = 1 + \frac{2}{3} \frac{\sin^2 \frac{\theta}{2}}{1 - \frac{2}{3} \sin^2 \frac{\theta}{2}} = \frac{1}{1 - \frac{2}{3} \sin^2 \frac{\theta}{2}}$$

Hence

$$\frac{\sqrt{6}\kappa}{1 - \kappa^2} = 2i \sin \frac{\theta}{2} \sqrt{1 - \frac{2}{3} \sin^2 \frac{\theta}{2}} \quad B-15$$

Define

$$s_j = \sqrt{1 - \frac{2}{3} \sin^2 \frac{\theta}{2}} \quad B-16$$

Then

$$\frac{\sqrt{6}\kappa}{1 - \kappa^2} = 2i s_j \sin \frac{\theta}{2} \quad B-17$$

The boundary conditions are then (from B-12 and B-17)

$$\begin{aligned} x_1 \cos \theta - x_2 &= 0 \\ -x_N + \left[\cos \theta + \frac{2i}{\gamma} s_j \sin \frac{\theta}{2} \right] x_r &= 0 \end{aligned} \quad B-18$$

Substituting the solution B-11 into the difference equation B-18, we obtain

$$\begin{aligned} (A + B) \cos \theta - (A e^{i\theta} + B e^{-i\theta}) &= 0 \\ -\left[A e^{i(N-1)\theta} + B e^{-i(N-1)\theta} \right] + \left[\cos \theta + \frac{2i s_j}{\gamma} \sin \frac{\theta}{2} \right] \left[A e^{iN\theta} + B e^{-iN\theta} \right] &= 0 \end{aligned} \quad B-19$$

Factoring out A and B gives

$$\begin{aligned} A (\cos \theta - e^{i\theta}) + B (\cos \theta - e^{-i\theta}) &= 0 \\ e^{iN\theta} A \left[\cos \theta - e^{-i\theta} + \frac{2i s_j}{\gamma} \sin \frac{\theta}{2} \right] + e^{-iN\theta} B \left[\cos \theta - e^{i\theta} + \frac{2i s_j}{\gamma} \sin \frac{\theta}{2} \right] &= 0 \end{aligned} \quad B-20$$

Apply the identities

$$\begin{aligned} \cos \theta - e^{i\theta} &= -i \sin \theta \\ \cos \theta - e^{-i\theta} &= i \sin \theta \end{aligned} \quad B-21$$

Then B-20 can be expressed as a matrix equation

$$\begin{bmatrix} -i \sin \theta & i \sin \theta \\ e^{iN\theta} \left[i \sin \theta + \frac{2i s_j}{\gamma} \sin \frac{\theta}{2} \right] & e^{-iN\theta} \left[-i \sin \theta + \frac{2i s_j}{\gamma} \sin \frac{\theta}{2} \right] \end{bmatrix} \begin{bmatrix} A \\ B \end{bmatrix} = \begin{bmatrix} 0 \\ 0 \end{bmatrix} \quad B-22$$

For a non-trivial solution for A and B , the determinant of the matrix must be zero. This gives

$$-i \sin \theta \left[e^{-iN\theta} \left[-i \sin \theta + \frac{2i s_j}{\gamma} \sin \frac{\theta}{2} \right] + e^{iN\theta} \left[i \sin \theta + \frac{2i s_j}{\gamma} \sin \frac{\theta}{2} \right] \right] = 0 \quad B-23$$

The above equation implies that either $\sin \theta = 0$ or the term in brackets is zero. The two possibilities are explored below.

If $\sin \theta = 0$, then $\theta = j\pi$ and $\cos \theta = \cos j\pi = (-1)^j = \pm 1$. This gives (from B-14)

$$\kappa^2 = -\frac{2}{3} \frac{\sin^2 j \frac{\pi}{2}}{1 - \frac{2}{3} \sin^2 j \frac{\pi}{2}} = \begin{cases} -2 & \text{for } j = \text{odd} \\ 0 & \text{for } j = \text{even} \end{cases} \quad B-24$$

Since $x_l = A e^{i(l-1)\theta} + B e^{-i(l-1)\theta}$, then for even values of j , we have

$$x_l = A + B \quad B-25$$

which looks like the rigid body mode. On the other hand, for odd values of j , we have

$$e^{i\theta} = e^{-i\theta} = -1 \quad B-26$$

and

$$x_l = (A + B) (-1)^{l-1}$$

As we shall see, both of the above are spurious solutions. Solving for A and B from the second equation of B-19, we have

$$\frac{2i s_j}{\gamma} \left[A e^{iN\theta} + B e^{-iN\theta} \right] \sin \frac{\theta}{2} = 0$$

with

B-27

$$\frac{2i s_j}{\gamma} \neq 0, \sin \frac{\theta}{2} = \sin \frac{j\pi}{2} \neq 0, e^{iN\theta} = e^{-iN\theta} = \pm 1$$

Thus

$$A + B = 0 \rightarrow A = -B \rightarrow x_l = 0 \text{ for } j \text{ both odd and even}$$

Hence, the assumption that $\sin \theta = 0$ is false.

If $\sin \theta \neq 0$, then

$$e^{-iN\theta} \left[-i \sin \theta + \frac{2i s_j}{\gamma} \sin \frac{\theta}{2} \right] + e^{iN\theta} \left[i \sin \theta + \frac{2i s_j}{\gamma} \sin \frac{\theta}{2} \right] = 0$$

$$i \sin \theta (e^{iN\theta} - e^{-iN\theta}) + \frac{2i s_j}{\gamma} \sin \frac{\theta}{2} (e^{iN\theta} + e^{-iN\theta}) = 0$$

$$2i \sin \frac{\theta}{2} \cos \frac{\theta}{2} \cdot 2i \sin N\theta + \frac{2i s_j}{\gamma} \sin \frac{\theta}{2} \cdot 2 \cos N\theta = 0 \quad B-28$$

$$\sin \frac{\theta}{2} \left[i \cos \frac{\theta}{2} \sin N\theta + \frac{s_j}{\gamma} \cos N\theta \right] = 0$$

For $\sin \frac{\theta}{2} = 0, \frac{\theta}{2} = j\pi$ and $\kappa^2 = 0$, we obtain the true rigid body mode (this implies that $A = B$).

On the other hand, the non-rigid body modes follow from the transcendental equation

$$i \cos \frac{\theta}{2} \sin N\theta + \frac{s_j}{\gamma} \cos N\theta = 0$$

or

B-29

$$\cot N\theta = -\frac{i \gamma \cos \frac{\theta}{2}}{s_j}$$

For purely real θ , the above equation cannot be satisfied.

B.1.2 Real Roots

For purely imaginary $\theta = 2i\alpha$, we have

$$\sin N\theta = \sin 2iN\alpha = i \sinh 2N\alpha$$

$$\cos N\theta = \cos 2iN\alpha = \cosh 2N\alpha$$

$$\begin{aligned}\sin \frac{\theta}{2} &= i \sinh \alpha \\ \cos \frac{\theta}{2} &= \cosh \alpha\end{aligned}\tag{B-30}$$

Substituting B-30 into B-29 gives

$$\coth 2N\alpha = \frac{\gamma \cosh \alpha}{\sqrt{1 + \frac{2}{3} \sinh^2 \alpha}}\tag{B-31}$$

Applying the definition of κ and Equation B-14, we obtain

$$kh = -\frac{2 \sinh \alpha}{\sqrt{1 + \frac{2}{3} \sinh^2 \alpha}}\tag{B-32}$$

Figure B-2 shows the root α of Equation B-31 for $N = \gamma = 1$ and kh as a function of α . Figure B-2 illustrates some of the features of these roots. Note that as α increases, $\coth 2N\alpha$ approaches 1 and the right-hand side of B-31 approaches $\gamma \sqrt{\frac{3}{2}}$ from below. Thus these two curves will intersect at finite α only if $\gamma \sqrt{\frac{3}{2}} > 1$, or $\gamma > \sqrt{\frac{2}{3}}$. The solution for kh given by Equation B-32 is only valid for $\gamma > \sqrt{\frac{2}{3}}$. Note also that as α increases, kh approaches $-\sqrt{6}$. This is a bound on the magnitude of kh which is independent of the number of layers

Finally, the first equation of B-19 requires that $A = B$ (since $i \sin \theta \neq 0$). Choose arbitrarily $A = B = \frac{1}{2}$. Then

$$x_l = \cos (l-1) \theta = \cosh 2(l-1) \alpha\tag{B-33}$$

This is the modal shape.

It is also possible to find real roots for the wavenumber k for complex values of θ or α . Assume, for example

$$\alpha = x + iy\tag{B-34}$$

Then

$$\sinh \alpha = \sinh x \cosh iy + \cosh x \sinh iy = \sinh x \cos y + i \cosh x \sin y =$$

$$\sqrt{\sinh^2 x \cos^2 y + \cosh^2 x \sin^2 y} e^{i\phi} = r e^{i\phi}$$

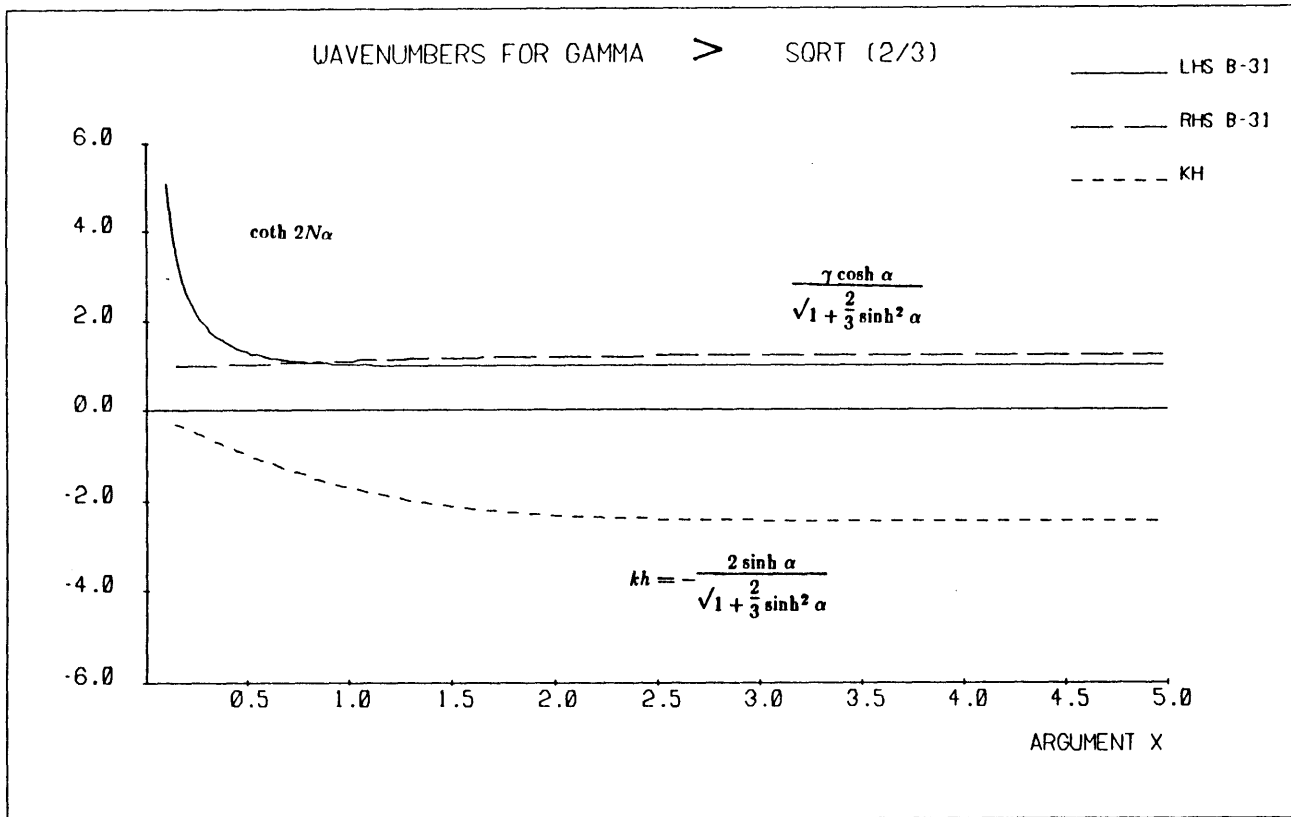


Figure B-2: The Root α of Equation B-31 and kh versus α

with

B-35

$$\tan \phi = \frac{\cosh x \sin y}{\sinh x \cos y} = \frac{\sin \phi}{\cos \phi}$$

For arbitrary values of x and y , we can reach any point r and ϕ in the complex plane. Hence, using the form of kh from B-32, we obtain

$$\begin{aligned} \frac{\sinh \alpha}{\sqrt{1 + \frac{2}{3} \sinh^2 \alpha}} &= \frac{r e^{i\phi}}{\sqrt{1 + \frac{2}{3} r^2 e^{2i\phi}}} = \\ &= \frac{r e^{i\phi}}{\sqrt{\left[1 + \frac{2}{3} r^2 \cos 2\phi\right] + i \left[\frac{2}{3} r^2 \sin 2\phi\right]}} = \\ &= \frac{r e^{i\phi}}{4 \sqrt{\left[1 + \frac{2}{3} r^2 \cos 2\phi\right]^2 + \left[\frac{2}{3} r^2 \sin 2\phi\right]^2}} e^{i \frac{\psi}{2}} \end{aligned} \tag{B-36}$$

with

$$\tan \psi = \frac{\frac{2}{3} r^2 \sin 2\phi}{1 + \frac{2}{3} r^2 \cos 2\phi}$$

The phase of the above ratio is $e^{i(\phi - \psi/2)}$. For a purely real k , we must have

$$e^{i(\phi - \frac{\psi}{2})} = \pm 1, \text{ squaring gives } e^{i(2\phi - \psi)} = 1$$

Then

B-37

$$2\phi - \psi = 2j\pi \quad 2\phi = \psi + 2j\pi$$

$$\tan 2\phi = \tan \psi$$

This implies that (from B-37 and B-36)

$$\frac{\sin 2\phi}{\cos 2\phi} = \frac{\frac{2}{3} r^2 \sin 2\phi}{1 + \frac{2}{3} r^2 \cos 2\phi}$$

Hence

B-38

$$\sin 2\phi \left[\frac{1}{\cos 2\phi} - \frac{\frac{2}{3} r^2}{1 + \frac{2}{3} r^2 \cos 2\phi} \right] = 0$$

This can be satisfied only if $\sin 2\phi = 0$, that is

$$\sin \phi \cos \phi = 0 \tag{B-39}$$

There are two solutions of B-39 to investigate.

If $\sin \phi = 0$, then $\cosh x \sin y = 0$ and $y = j\pi$, so that $\cos y = \cos j\pi = (-1)^j$ and $\alpha = x + ij\pi$. Hence

$$\begin{aligned} \sinh \alpha &= \sinh x (-1)^j \\ \cosh \alpha &= \cosh x (-1)^j \end{aligned} \tag{B-40}$$

and

$$\begin{aligned} \cosh 2N\alpha &= \cosh 2Nx \\ \sinh 2N\alpha &= \sinh 2Nx \end{aligned} \tag{B-41}$$

Substituting B-40 and B-41 in B-31 gives

$$\coth 2Nx = \frac{\gamma \cosh x (-1)^j}{\sqrt{1 + \frac{2}{3} \sinh^2 x}} \tag{B-42}$$

and substituting in B-32 gives

$$kh = -\frac{2 \sinh x (-1)^j}{\sqrt{1 + \frac{2}{3} \sinh^2 x}} \tag{B-43}$$

Since an odd j leads to $x < 0$ (from B-42), this is exactly the same solution that we had before with $\alpha \rightarrow x(-1)^j$. Hence, the assumption that $\sin \phi = 0$ is not interesting.

The other possible solution to B-39 is $\cos \phi = 0$. This leads to $\sinh x \cosh y = 0$ and either $x = 0$ or $y = \pi/2(2j-1)$. $x = 0$ is not a root because it makes θ real and the characteristic equation B-29 is not satisfied. The solution $y = \pi/2(2j-1)$ gives $\alpha = x + i\pi/2(2j-1)$ and $\sin y = (-1)^{j-1}$. Hence

$$\begin{aligned} \sinh \alpha &= i \cosh x (-1)^{j-1} \\ \cosh \alpha &= i \sinh x (-1)^{j-1} \end{aligned} \tag{B-44}$$

and

$$\cosh 2N\alpha = \cosh 2Nx (-1)^{N(2j-1)} \quad B-45$$

$$\sinh 2N\alpha = \sinh 2Nx (-1)^{N(2j-1)}$$

Finally,

$$\sqrt{1 + \frac{2}{3} \sinh^2 \alpha} = \sqrt{1 - \frac{2}{3} \cosh^2 x} = i \sqrt{\frac{2}{3} \cosh^2 x - 1} \quad B-46$$

Substituting in B-31 and B-32 gives

$$\coth 2Nx = \frac{\gamma \sinh x (-1)^{j-1}}{\sqrt{\frac{2}{3} \cosh^2 x - 1}} \quad B-47$$

and

$$kh = -\frac{2 \cosh x (-1)^{j-1}}{\sqrt{\frac{2}{3} \cosh^2 x - 1}} \quad B-48$$

We choose $j = 1$, so that

$$\coth 2Nx = \frac{\gamma \sinh x}{\sqrt{\frac{2}{3} \cosh^2 x - 1}} \quad B-49$$

and

$$kh = -\frac{2 \cosh x}{\sqrt{\frac{2}{3} \cosh^2 x - 1}} \quad B-50$$

These equations provide the real root for $\gamma < \sqrt{\frac{2}{3}}$. The two sides of Equation B-49 are plotted in Figure B-3. The $\cosh x$ must be greater than $\sqrt{\frac{3}{2}}$ in order for the denominator of B-49 to be real. Thus x is greater than 0.6584. Again, the limit of $\coth 2Nx$ is 1 as x becomes large. The limit of the right-hand side (from above) is $\gamma\sqrt{\frac{3}{2}}$. Thus γ must be less than $\sqrt{\frac{2}{3}}$ in order for there to be a root x . The eigenvalue kh from Equation B-50 is plotted in Figure B-4. Again, kh approaches $-\sqrt{6}$, but from $-\infty$ at $x = 0.6584$. The modal shape is

$$\begin{aligned} x_l &= \cosh (2 (l - 1) (x + i\pi/2)) = \cosh (l - 1) (2x + i\pi) = \\ &\cosh 2(l-1)x (-1)^{l-1} \end{aligned} \quad B-51$$

The modal shape grows exponentially with depth and alternates in sign.

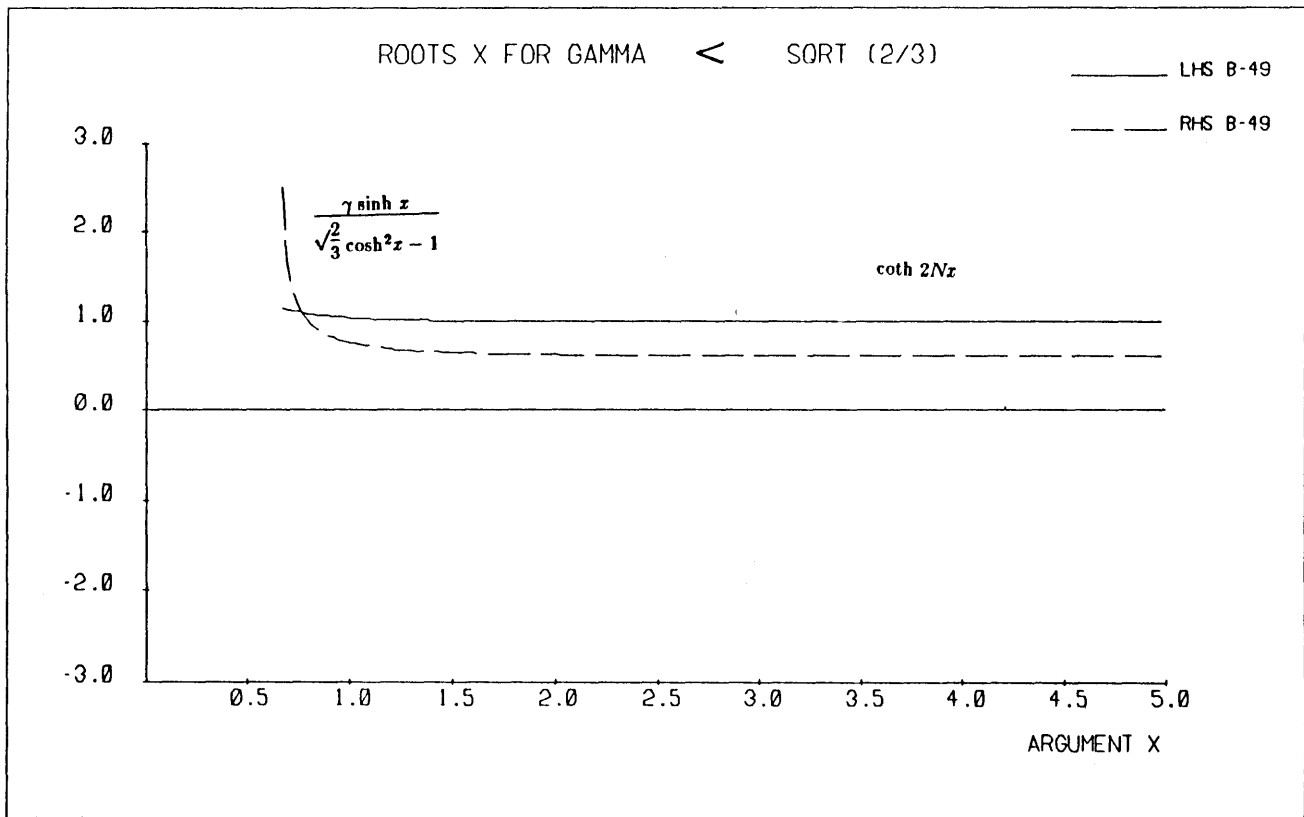


Figure B-3: The Root of Equation B-49

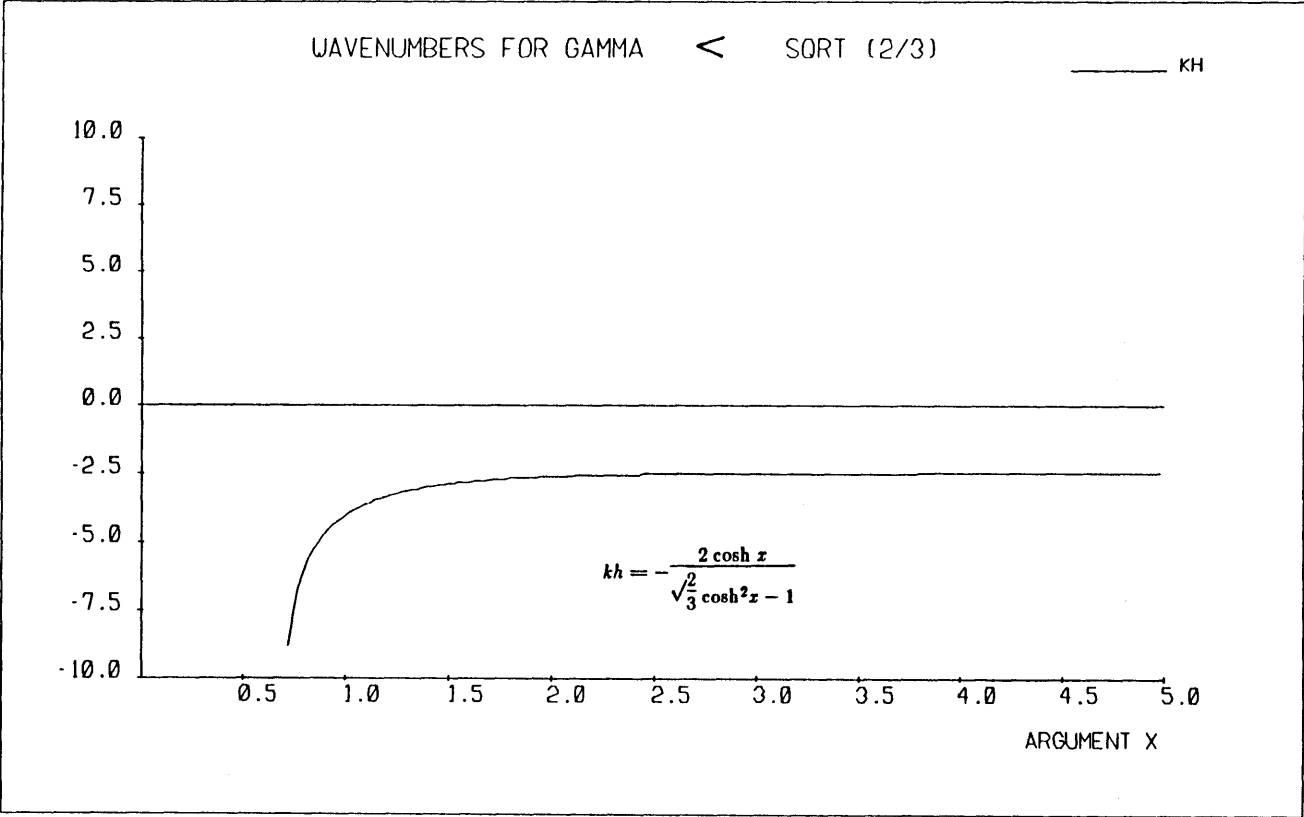


Figure B-4: Wavenumber kh

To illustrate the effect of the soil properties on the real root, Figure B-5 is presented below. This is a plot of $-kh$ as a function of γ . As γ goes toward 0 (the halfspace becomes stiffer), the eigenvalue kh approaches ∞ .

B.2 Continuum Solution

B.2.1 Eigenvalues

The eigenvalues for the continuum case can be obtained directly from the transcendental stiffness matrices for the single layer and the halfspace. The transcendental anti-plane stiffness of the layer is

$$K_1 = \frac{kG}{\sinh kH} \begin{bmatrix} \cosh kH & -1 \\ -1 & \cosh kH \end{bmatrix} \quad B-52$$

The stiffness of the halfspace is

$$K_r = kG_r = \left[\frac{kG}{\sinh kH} \right] \frac{\sinh kH}{\gamma} \quad B-53$$

The sum of B-52 and B-53 gives the global stiffness matrix

$$K = \frac{kG}{\sinh kH} \begin{bmatrix} \cosh kH & -1 \\ -1 & \cosh kH + \frac{1}{\gamma} \sinh kH \end{bmatrix} \quad B-54$$

To obtain the eigenvalues, we set the determinant of the global matrix to zero and solve the resulting equation for k . By inspection, we can see that $k = 0$ is a root, this is the rigid body mode.

For $k \neq 0$, we obtain

$$\cosh^2 kH + \frac{1}{\gamma} \cosh kH \sinh kH - 1 = 0 \quad B-55$$

Applying the identity

$$\cosh^2 kH - 1 = \sinh^2 kH \quad B-56$$

to B-55 gives the eigenvalue solution

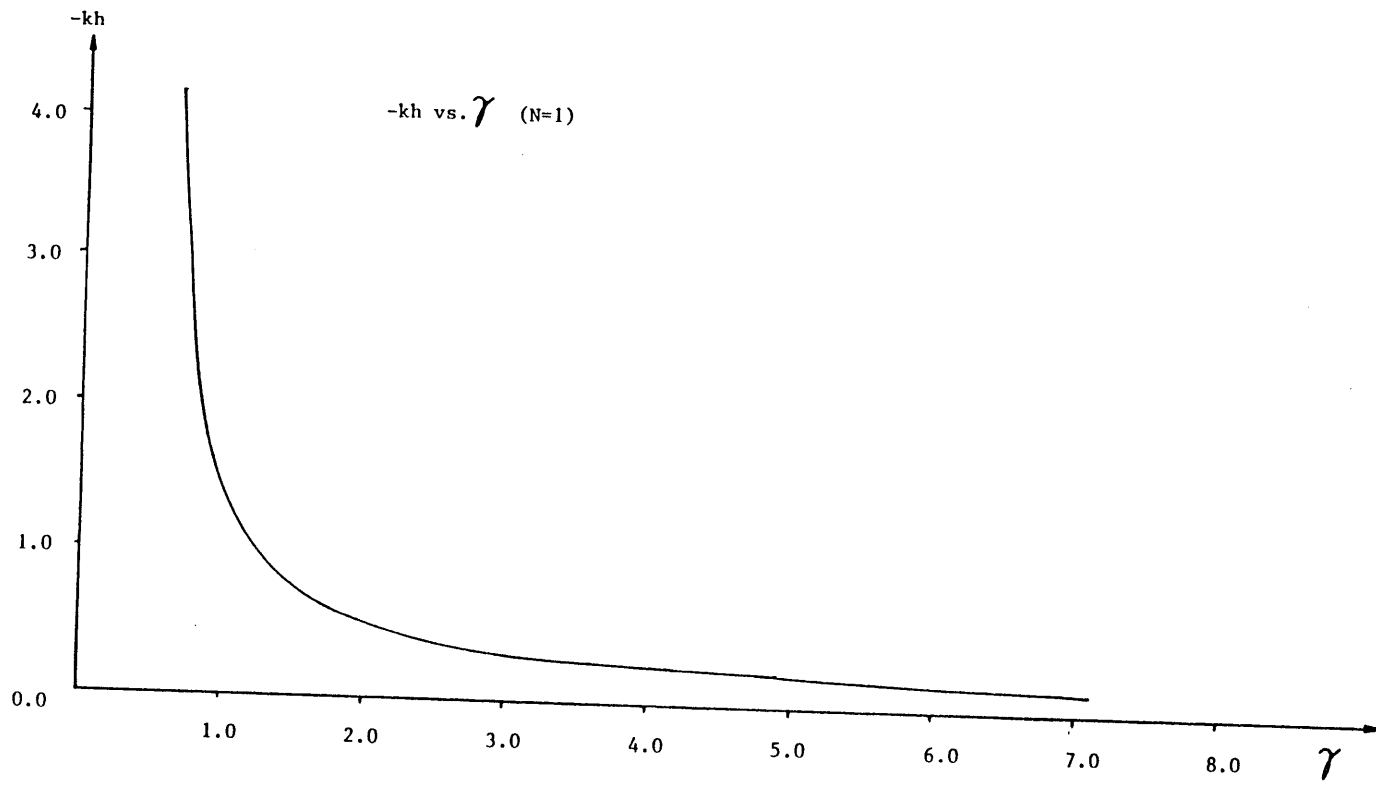


Figure B-5: Wavenumber kh versus γ

$$\coth kH = -\gamma \tag{B-57}$$

In general, $\gamma < 1$, and the above equation has no real roots. In this respect, it differs from the discrete solution, which admits one real root. For $\gamma > 1$, we do have real roots.

Assume a complex root of the form $kH = -(x + iy)$. Substituting this root in B-57 gives

$$\coth (x+iy) = \gamma \tag{B-58}$$

Expanding the hyperbolic cotangent

$$\coth (x+iy) = \frac{\cosh (x+iy)}{\sinh (x+iy)} = \frac{\cosh x \cos y + i \sinh x \sin y}{\sinh x \cos y + i \cosh x \sin y} \tag{B-59}$$

Substituting this expansion into B-58 and separating the real and imaginary parts results in two governing equations

$$\begin{aligned} \cos y (\cosh x - \gamma \sinh x) &= 0 \\ \sin y (\sinh x - \gamma \cosh x) &= 0 \end{aligned} \tag{B-60}$$

If $\cos y \neq 0$ and $\sin y \neq 0$, then the above system of equations is incompatible. When $\cos y = 0$, the first equation is satisfied and $\sin y = \pm 1$. The second equation becomes

$$\tanh x = \gamma \tag{B-61}$$

which only has a root for $\gamma < 1$. The solution for x and y is then

$$\begin{aligned} x &= \operatorname{arctanh} \gamma \\ y &= \frac{\pi}{2} (2j-1) \end{aligned} \tag{B-62}$$

The eigenvalue is

$$kH = -\left[\operatorname{arctanh} \gamma + i \frac{\pi}{2} (2j-1) \right] \quad \text{for } \gamma < 1 \tag{B-63}$$

When $\sin y = 0$, the second equation of B-60 is satisfied and $\cos y = \pm 1$. Thus the roots for x and y are

$$\begin{aligned} \coth x = \gamma, \quad x &= \operatorname{arccoth} \gamma \\ y &= \pi j \end{aligned} \tag{B-64}$$

A root for x exists only if $\gamma > 1$. The eigenvalue is

$$kH = -\left[\operatorname{arccoth} \gamma + i \pi j \right] \quad \text{for } \gamma > 1 \quad B-65$$

B.2.2 Modal Shapes for $\gamma < 1$

From the first equation of B-54, we have

$$u_1 \cosh kH - u_r = 0 \quad B-66$$

Arbitrarily selecting $u_1 = 1$ gives $u_r = \cosh kH$.

For intermediate points, we decompose the stratum into two sublayers of thicknesses z and $H-z$. The first equation of the overlapped stiffness matrix is $u_1 \cosh kz - u_2 = 0$, which leads to

$$u_2 = \cosh kz = \cosh kH \frac{z}{H} = \cosh \xi (kH) \quad \text{where } \xi = \frac{z}{H} \quad B-67$$

Then the mode shape is

$$\phi_j = \cosh \left[-\xi \left[\operatorname{arctanh} \gamma + i \frac{\pi}{2} (2j-1) \right] \right] \quad B-68$$

Define $\tanh \beta = \gamma$, then $\beta = \operatorname{arctanh} \gamma$, and

$$\phi_j = \cosh \beta \xi \cos \frac{\pi}{2} (2j-1) \xi + i \sinh \beta \xi \sin \frac{\pi}{2} (2j-1) \xi \quad B-69$$

Note that no root exists when $\gamma = 1$ (a homogeneous halfspace) other than the rigid body mode. These "exact" eigenvalues are easy to compute and can be used as starting values in a search for the discrete eigenvalues.

Appendix C

Solution of the Discrete Static Eigenvalue Problem

The procedures used to extract the eigenvalues and eigenvectors of the static problem described in Chapter 4 are explained below. Section C.1 presents an algorithm for obtaining complex conjugate pairs of eigenvalues and eigenvectors. Section C.2 describes a method called "cleaning" that improves the accuracy of the eigenvectors. In Section C.3, the application of these techniques to the problem of Chapter 4 is discussed.

C.1 Iteration for Proximal and/or Complex Conjugate Pairs of Eigenvalues

The technique described below is an adaptation of one given by Zurmühl (1964). The method can be applied to obtain pairs of proximal or complex conjugate pairs of eigenvalues from a non-symmetric real matrix. No complex algebra is required to obtain the complex conjugate modes, which makes this algorithm extremely efficient for the purposes described in this paper.

A real, non-symmetric matrix A has right eigenvectors X , left eigenvectors Y , and eigenvalues λ given by

$$A X = \lambda X \quad \text{right eigenvectors} \quad C-1$$

$$A^T Y = \lambda Y \quad \text{or} \quad Y^T A = \lambda Y^T \quad \text{left eigenvectors}$$

Assume that the starting vector contains contributions from all N modes (N is an even number for this case).

$$\begin{aligned} X_0 &= c_1 \phi_1 + c_2 \phi_2 + \dots + c_n \phi_n = \Phi C \\ Y_0 &= d_1 \psi_1 + d_2 \psi_2 + \dots + d_n \psi_n = \Psi D \end{aligned} \quad C-2$$

After direct iteration, $X_{k+1} = A X_k$ and $Y_{k+1} = A^T Y_k$, then, if the modes are not normalized

$$\begin{aligned} X_k &= c_1 \lambda_1^k \phi_1 + c_2 \lambda_2^k \phi_2 + \dots = \Phi A^k C \\ Y_k &= d_1 \lambda_1^k \psi_1 + d_2 \lambda_2^k \psi_2 + \dots = \Psi A^k D \end{aligned} \quad C-3$$

If $|\lambda_1| \simeq |\lambda_2|$, which is the case when $\lambda_2 = \lambda_1^*$, then $|\lambda_1^k| \simeq |\lambda_2^k|$ and the vectors approach a linear combination of the modes ϕ_1, ϕ_2

$$\begin{aligned} X_k &\simeq c_1 \lambda_1^k \phi_1 + c_2 \lambda_2^k \phi_2 \\ X_{k+1} &\simeq c_1 \lambda_1^{k+1} \phi_1 + c_2 \lambda_2^{k+1} \phi_2 \\ X_{k+2} &\simeq c_1 \lambda_1^{k+2} \phi_1 + c_2 \lambda_2^{k+2} \phi_2 \end{aligned} \quad C-4$$

The results are similar for Y_k, Y_{k+1}, Y_{k+2} . Notice that X_k and Y_k are not eigenvectors, i.e., they do not satisfy the equations in C-1. The above implies that the three vectors are linear combinations, i.e. they satisfy an equation of the form

$$X_{k+2} - 2 a_1 X_{k+1} + a_0 X_k = 0 \quad C-5$$

Substituting C-4 into C-5, we obtain

$$(\lambda_1^2 - 2 a_1 \lambda_1 + a_0) c_1 \lambda_1^k \phi_1 + (\lambda_2^2 - 2 a_1 \lambda_2 + a_0) c_2 \lambda_2^k \phi_2 = 0 \quad C-6$$

Since ϕ_1 and ϕ_2 are independent, it follows that the terms in parentheses must be zero. Hence, λ_1 and λ_2 are the roots of the equation

$$\lambda^2 - 2 a_1 \lambda + a_0 = 0 \quad C-7$$

with solutions $\lambda = a_1 \pm \sqrt{a_1^2 - a_0}$. We know that our solutions will be complex, thus

$$\lambda = a_1 \pm i \sqrt{a_0 - a_1^2} \quad C-8$$

To determine a_0, a_1 , we return to Equation C-5, which we write in matrix form as

$$(X_k - 2 X_{k+1}) \begin{bmatrix} a_0 \\ a_1 \end{bmatrix} = -X_{k+2} \quad C-9$$

Multiplying C-9 by $\{ Y_k^T, -\frac{1}{2} Y_{k+1}^T \}$, we obtain

$$\begin{bmatrix} Y_k^T X_k & -2Y_k^T X_{k+1} \\ -\frac{1}{2}Y_{k+1}^T X_k & Y_{k+1}^T X_{k+1} \end{bmatrix} \begin{bmatrix} a_0 \\ a_1 \end{bmatrix} = \begin{bmatrix} -Y_k^T X_{k+2} \\ \frac{1}{2}Y_{k+1}^T X_{k+2} \end{bmatrix} \quad C-10$$

The inverse of the matrix in C-10 is

$$\frac{1}{(Y_k^T X_k)(Y_{k+1}^T X_{k+1}) - (Y_k^T X_{k+1})^2} \begin{bmatrix} Y_{k+1}^T X_{k+1} & 2Y_k^T X_{k+1} \\ \frac{1}{2}Y_{k+1}^T X_k & Y_k^T X_k \end{bmatrix} \quad C-11$$

Letting the denominator of the constant term be given by D and making the substitution

$Y_k^T X_{k+2} = Y_k^T A X_{k+1} = Y_{k+1}^T X_{k+1}$, we obtain the solution for a_0, a_1

$$\begin{bmatrix} a_0 \\ a_1 \end{bmatrix} = \frac{1}{D} \begin{bmatrix} (Y_k^T X_{k+1})(Y_{k+1}^T X_{k+2}) - (Y_{k+1}^T X_{k+1})^2 \\ \frac{1}{2}[(Y_k^T X_k)(Y_{k+1}^T X_{k+2}) - (Y_{k+1}^T X_k)(Y_{k+1}^T X_{k+1})] \end{bmatrix} \quad C-12$$

After finding a_0, a_1 and λ_1, λ_2 , we determine the eigenvectors as (omitting a constant normalization factor)

$$\begin{aligned} \phi_1 &= X_{k+1} - \lambda_2 X_k \\ \phi_2 &= X_{k+1} - \lambda_1 X_k \end{aligned} \quad C-13$$

In practice, the three iterations X_k, X_{k+1}, X_{k+2} will retain a residual contribution of the other eigenvectors. Thus Equation C-5 translates into

$$\begin{aligned} S &= a_0 X_k - 2 a_1 X_{k+1} + X_{k+2} \neq 0 \\ Q &= a_0 Y_k - 2 a_1 Y_{k+1} + Y_{k+2} \neq 0 \end{aligned} \quad C-14$$

Note the S and Q have the same coefficients a_0, a_1 , since they must lead to the same characteristic polynomial for λ . We now require the product $q = Q^T S$ to be a minimum in the least squares sense, i.e.

$$\frac{\partial q}{\partial a_0} = 0 \quad \frac{\partial q}{\partial a_1} = 0 \quad C-15$$

The product for q is expanded

$$\begin{aligned} q &= a_0^2 Y_k^T X_k - 2 a_0 a_1 (Y_k^T X_{k+1} + Y_{k+1}^T X_k) + \\ & a_0 (Y_k^T X_{k+2} + Y_{k+2}^T X_k) + 4 a_1^2 Y_{k+1}^T X_{k+1} - \\ & 2 a_1 (Y_{k+1}^T X_{k+2} + Y_{k+2}^T X_{k+1}) + Y_{k+2}^T X_{k+2} \end{aligned} \quad C-16$$

Taking derivatives gives

$$\frac{\partial q}{\partial a_0} = 2 a_0 Y_k^T X_k - 2 a_1 (Y_k^T X_{k+1} + Y_{k+1}^T X_k) + (Y_k^T X_{k+2} + Y_{k+2}^T X_k) = 0 \quad C-17$$

$$\begin{aligned} \frac{\partial q}{\partial a_1} &= -2 a_0 (Y_k^T X_{k+1} + Y_{k+1}^T X_k) + 8 a_1 Y_{k+1}^T X_{k+1} - \\ &2 (Y_{k+1}^T X_{k+2} + Y_{k+2}^T X_{k+1}) = 0 \end{aligned}$$

In matrix form, C-17 is

$$\begin{bmatrix} Y_k^T X_k & -(Y_k^T X_{k+1} + Y_{k+1}^T X_k) \\ -\frac{1}{4}(Y_k^T X_{k+1} + Y_{k+1}^T X_k) & Y_{k+1}^T X_{k+1} \end{bmatrix} \begin{bmatrix} a_0 \\ a_1 \end{bmatrix} = \begin{bmatrix} -\frac{1}{2}(Y_k^T X_{k+2} + Y_{k+2}^T X_k) \\ \frac{1}{4}(Y_{k+1}^T X_{k+2} + Y_{k+2}^T X_{k+1}) \end{bmatrix} \quad C-18$$

Now, when we apply these identities to C-18,

$$\begin{aligned} Y_{k+1}^T X_k &= Y_k^T A X_k = Y_k^T X_{k+1} \\ Y_k^T X_{k+2} &= Y_{k+1}^T X_{k+1}, Y_{k+2}^T X_k \\ Y_{k+2}^T X_{k+1} &= Y_{k+1}^T X_{k+2} \end{aligned} \quad C-19$$

the above equations reduce to our original system C-10. Thus we have shown this solution to be optimal in the least squares sense. It can also be shown that the eigenvalues λ_1, λ_2 from Equation C-8 have errors of the order $(|\lambda_j| / |\lambda_1|)^2$, as in Rayleigh's quotient.

C.2 Cleaning Eigenvectors

The "cleaning" procedure described in this section is adapted from Zurmühl (1964). The method takes advantage of the orthogonality of right and left eigenvectors to sweep out residual components of other modes from a particular eigenvector. The three possible combinations of modes are discussed: complex conjugate with complex conjugate, complex conjugate with distinct, and distinct with distinct.

C.2.1 Distinct Eigenvalues

First, we make a change of notation

$$\begin{aligned} X_k &\rightarrow \phi_j'' & X_{k+1} &\rightarrow \phi_j' \\ Y_k &\rightarrow \psi_j'' & Y_{k+1} &\rightarrow \psi_j' \end{aligned} \quad C-20$$

The eigenvectors obtained from direct iteration are given by

$$\begin{aligned} \phi_j'' &= c_1^j \phi_1 + c_2^j \phi_2 + \dots = \phi_j + \sum_{l \neq j} c_l^j \phi_l \\ \psi_j'' &= d_1^i \psi_1 + d_2^i \psi_2 + \dots = \psi_j + \sum_{l \neq i} d_l^i \psi_l \end{aligned} \quad C-21$$

where d_j^i and c_j^i are small coefficients. Our objective is to compute these coefficients so that the residual components of other modes can be removed. For eigenvalues that are not repeated, the orthogonality conditions are

$$\begin{aligned} \psi_i^T A \phi_j &= 0 & \text{for } i \neq j \\ &\neq 0 & \text{for } i = j \end{aligned}$$

and

C-22

$$\begin{aligned} \psi_i^T \phi_j &= 0 & \text{for } i \neq j \\ &\neq 0 & \text{for } i = j \end{aligned}$$

Then we can expand the product

$$\begin{aligned} \psi_i''^T \phi_j'' &= \left[\psi_i^T + \sum_{k \neq i} d_k^i \psi_k^T \right] \left[\phi_j + \sum_{l \neq j} c_l^j \phi_l \right] = \\ &= \psi_i^T \phi_j + \sum_{l \neq j} c_l^j \psi_i^T \phi_l + \sum_{k \neq i} d_k^i \psi_k^T \phi_j + \sum_{k \neq i} \sum_{l \neq j} d_k^i c_l^j \psi_k^T \phi_l \end{aligned} \quad C-23$$

The application of the orthogonality conditions C-22 to the summations in C-23 gives

$$\sum_{l \neq j} c_l^j \psi_i^T \phi_l = \begin{cases} c_i^j \psi_i^T \phi_i & \text{for } i \neq j \\ 0 & \text{for } i = j \end{cases}$$

$$\sum_{k \neq i} d_k^i \psi_k^T \phi_j = \begin{cases} d_j^i \psi_j^T \phi_j & \text{for } i \neq j \\ 0 & \text{for } i=j \end{cases} \quad C-24$$

$$\sum_{k \neq i} \sum_{l \neq j} d_k^i c_l^j \psi_k^T \phi_l = \sum_{k \neq i, k \neq j} d_k^i c_k^j \psi_k^T \phi_k$$

The last expression of C-24 is quadratic in the error terms. For $i \neq j$, we have

$$\psi_i''^T \phi_j'' = c_i^j \psi_i^T \phi_i + d_j^i \psi_j^T \phi_j + \text{quadratic error} \quad C-25$$

For $i = j$, we have

$$\psi_i''^T \phi_i'' = \psi_i^T \phi_i + \text{quadratic error} \quad C-26$$

Since the quadratic error is very small, we can write

$$\psi_i''^T \phi_i'' \simeq \psi_i^T \phi_i \quad C-27$$

$$\psi_i''^T \phi_j'' \simeq c_i^j \psi_i^T \phi_i'' + d_j^i \psi_j^T \phi_j''$$

We define the constants

$$\psi_i''^T \phi_i'' = \beta_i \quad C-28$$

$$\psi_i''^T \phi_j'' = \beta_{ij} = c_i^j \beta_i + d_j^i \beta_j$$

From the second orthogonality condition, we can write in a similar fashion

$$\alpha_{ij} = \lambda_i c_i^j \beta_i + \lambda_j d_j^i \beta_j$$

with

C-29

$$\alpha_{ij} = \psi_i''^T A \phi_j'' = \psi_i'^T \phi_j'' = \psi_i''^T \phi_j'$$

Combining the results of C-28 and C-29, we obtain the system

$$\begin{bmatrix} \alpha_{ij} \\ \beta_{ij} \end{bmatrix} = \begin{bmatrix} \lambda_i & \lambda_j \\ 1 & 1 \end{bmatrix} \begin{bmatrix} c_i^j \beta_i \\ d_j^i \beta_j \end{bmatrix} \quad C-30$$

This has the solution

$$\begin{bmatrix} \beta_i c_i^j \\ \beta_j d_j^i \end{bmatrix} = \frac{1}{\lambda_i - \lambda_j} \begin{bmatrix} 1 & -\lambda_j \\ -1 & \lambda_i \end{bmatrix} \begin{bmatrix} \alpha_{ij} \\ \beta_{ij} \end{bmatrix} \quad C-31$$

from which we can obtain the correction coefficients, with $\lambda_i \simeq \lambda'_i$ and $\lambda_j \simeq \lambda'_j$ (eigenvalues with second order error). The above coefficients correspond to the corrections of ϕ_j'' and ψ_i''

$$\begin{aligned} \psi_i'' &= \psi_i'' - d_j^i \psi_j'' \\ \phi_j'' &= \phi_j'' - c_i^j \phi_i'' \end{aligned} \quad C-32$$

The correction coefficients for ϕ_i'' and ψ_j'' are obtained simply by interchanging the indices i and j

$$\begin{bmatrix} \beta_j c_j^i \\ \beta_i d_i^j \end{bmatrix} = \frac{1}{\lambda_j - \lambda_i} \begin{bmatrix} 1 & -\lambda_i \\ -1 & \lambda_j \end{bmatrix} \begin{bmatrix} \alpha_{ji} \\ \beta_{ji} \end{bmatrix} \quad C-33$$

The new coefficients α_{ji} and β_{ji} are

$$\begin{aligned} \alpha_{ji} &= \psi_j''^T A \phi_i'' = \psi_j'^T \phi_i'' = \psi_j''^T \phi_i' \\ \beta_{ji} &= \psi_j''^T \phi_i'' \end{aligned} \quad C-34$$

In general, $\alpha_{ij} \neq \alpha_{ji}$ and $\beta_{ij} \neq \beta_{ji}$.

C.2.2 Complex Conjugate Eigenvalues

In this case, the i^{th} and j^{th} eigenvalues are both complex conjugate pairs. The iterations on the j^{th} right eigenvector and i^{th} left eigenvector converge to

$$\begin{aligned} X_j'' &= c_1^j \phi_1 + c_2^j \phi_2 + \dots + c_i^j \phi_i + c_i^{*j} \phi_i^* + \dots + \phi_j + \phi_j^* + \dots \\ Y_i'' &= d_1^i \psi_1 + d_2^i \psi_2 + \dots + \psi_i + \psi_i^* + \dots + d_j^i \psi_j + d_j^{i*} \psi_j^* + \dots \end{aligned} \quad C-35$$

with small coefficients c_i^j and d_j^i . The starred quantities correspond to complex conjugate quantities. In the expressions above, both the i^{th} and j^{th} modes are shown as multiple modes, but this is not necessary in the general case. One additional iteration yields

$$\begin{aligned} X_j' &= A X_j'' = \lambda_1 c_1^j \phi_1 + \dots + \lambda_i c_i^j \phi_i + \lambda_i^* c_i^{*j} \phi_i^* + \dots \\ Y_i' &= A^T Y_i'' = \lambda_1 d_1^i \psi_1 + \lambda_2 d_2^i \psi_2 + \dots + \lambda_i \psi_i + \lambda_i^* \psi_i^* \end{aligned} \quad C-36$$

Applying the orthogonality condition and ignoring the quadratic error terms, we have the products

$$\begin{aligned}\beta''_{ij} &= Y_i''^T X_j'' = c_i^j \psi_i^T \phi_i + c_i^{*j} \psi_i^{*T} \phi_i^* + d_j^i \psi_j^T \phi_j + d_j^{*i} \psi_j^{*T} \phi_j^* \\ \beta''_{ij} &= p + q + r + s\end{aligned}\tag{C-37}$$

Similarly,

$$\begin{aligned}\beta'_{ij} &= Y_i'^T X_j' = \lambda_i^2 c_i^j \psi_i^T \phi_i + \lambda_i^{*2} c_i^{*j} \psi_i^{*T} \phi_i^* + \lambda_j^2 d_j^i \psi_j^T \phi_j + \lambda_j^{*2} d_j^{*i} \psi_j^{*T} \phi_j^* \\ \beta'_{ij} &= \lambda_i^2 p + \lambda_i^{*2} q + \lambda_j^2 r + \lambda_j^{*2} s\end{aligned}\tag{C-38}$$

For the second orthogonality condition, we have (as above)

$$\begin{aligned}\alpha''_{ij} &= Y_i''^T A X_j'' = Y_i'^T X_j' = \\ &\lambda_i c_i^j \psi_i^T \phi_i + \lambda_i^* c_i^{*j} \psi_i^{*T} \phi_i^* + \lambda_j d_j^i \psi_j^T \phi_j + \lambda_j^* d_j^{*i} \psi_j^{*T} \phi_j^* \\ \alpha''_{ij} &= \lambda_i p + \lambda_i^* q + \lambda_j r + \lambda_j^* s\end{aligned}\tag{C-39}$$

Similarly,

$$\alpha'_{ij} = Y_i'^T A X_j' = \lambda_i^3 p + \lambda_i^{*3} q + \lambda_j^3 r + \lambda_j^{*3} s\tag{C-40}$$

Combining the previous results, we obtain the system of equations

$$\begin{aligned}\begin{bmatrix} 1 & 1 & 1 & 1 \\ \lambda_i & \lambda_i^* & \lambda_j & \lambda_j^* \\ \lambda_i^2 & \lambda_i^{*2} & \lambda_j^2 & \lambda_j^{*2} \\ \lambda_i^3 & \lambda_i^{*3} & \lambda_j^3 & \lambda_j^{*3} \end{bmatrix} \begin{bmatrix} p \\ q \\ r \\ s \end{bmatrix} &= \begin{bmatrix} \beta''_{ij} \\ \alpha''_{ij} \\ \beta'_{ij} \\ \alpha'_{ij} \end{bmatrix}\end{aligned}\tag{C-41}$$

from which we can solve for p , q , r and s . Writing the vector of unknowns in the form given below alters the coefficient matrix so that all elements are real.

$$\begin{aligned} & \left[\begin{array}{l} (p+q) \\ (r+s) \end{array} \right] \\ & \left| (p-q)(\lambda_i - \lambda_i^*) \right| \\ & \left[\begin{array}{l} (r-s)(\lambda_j - \lambda_j^*) \end{array} \right] \end{aligned} \tag{C-42}$$

After finding p, q, r and s , we determine c_i^j and d_j^i and correct the eigenvectors as

$$\begin{aligned} X_j'' &= X_j'' - c_i^j \phi_i - c_i^{j*} \phi_i^* \\ Y_i'' &= Y_i'' - d_j^i \psi_j - d_j^{i*} \psi_j^* \end{aligned} \tag{C-43}$$

To obtain d_i^j and c_j^i we repeat the procedure, exchanging indices and computing α_{ji}'' , etc.

C.2.3 One Complex Conjugate Eigenvalue and One Distinct Eigenvalue

In this case, the j^{th} eigenvalue is a complex conjugate pair and the i^{th} eigenvalue is distinct.

The iteration converges to

$$\begin{aligned} X_j'' &= c_1^j \phi_1 + c_2^j \phi_1 + \dots + c_i^j \phi_i + \dots + \phi_j + \phi_j^* + \dots \\ \psi_i'' &= d_1^i \psi_1 + d_2^i \psi_2 + \dots + \psi_i + \dots + d_j^i \psi_j + d_j^{i*} \psi_j^* + \dots \end{aligned} \tag{C-44}$$

and similar expressions for Y_j'' and ϕ_i'' . Then the orthogonality conditions give (ignoring quadratic error terms)

$$\begin{aligned} \beta_{ij}'' &= \psi_i''^T X_j'' = c_i^j \psi_i^T \phi_i + d_j^i \psi_j^T \phi_j + d_j^{i*} \psi_j^{*T} \phi_j^* \\ \beta_{ij}'' &= p + r + s \end{aligned} \tag{C-45}$$

Also,

$$\begin{aligned} \alpha_{ij}'' &= \psi_i''^T A X_j'' = \psi_i'^T x_j'' = \lambda_i c_i^j \psi_i^T \phi_i + \lambda_j d_j^i \psi_j^T \phi_j + \lambda_j^* d_j^{i*} \psi_j^{*T} \phi_j^* \\ \alpha_{ij}'' &= \lambda_i p + \lambda_j r + \lambda_j^* s \end{aligned} \tag{C-46}$$

Finally,

$$\beta'_{ij} = \psi'_i{}^T X'_j = \lambda_i^2 p + \lambda_j^2 r + \lambda_j^{*2} s \quad C-47$$

The matrix expression of the above is

$$\begin{bmatrix} 1 & 1 & 1 \\ \lambda_i & \lambda_j & \lambda_j^* \\ \lambda_i^2 & \lambda_j^2 & \lambda_j^{*2} \end{bmatrix} \begin{bmatrix} p \\ r \\ s \end{bmatrix} = \begin{bmatrix} \beta''_{ij} \\ \alpha''_{ij} \\ \beta'_{ij} \end{bmatrix} \quad C-48$$

Again, we can make the coefficient matrix real by writing the vector of unknowns as

$$\begin{bmatrix} p \\ (r+s) \\ (r-s)(\lambda_j - \lambda_j^*) \end{bmatrix} \quad C-49$$

The remainder of the procedure is as described in the two sections above.

C.3 The Static Eigenvalue Problem

The technique described here is applied to the solutions of both the in-plane and the anti-plane eigenvalue problems. In the static problem, we first normalize the matrices by a reference thickness h so that the eigenvalue problem becomes

$$(A(kh)^2 + B(kh) + C)X = 0 \quad C-50$$

This improves numerical stability and gives constant dimensionality

For the static problem, the double dimension matrix \bar{A} is

$$\bar{A} = \begin{bmatrix} 0 & I \\ -A^{-1}C & -A^{-1}B \end{bmatrix} \quad C-51$$

The right and left eigenvectors are defined by

$$\begin{bmatrix} 0 & I \\ -A^{-1}C & -A^{-1}B \end{bmatrix} \begin{bmatrix} \phi_j \\ k_j \phi_j \end{bmatrix} = k_j \begin{bmatrix} \phi_j \\ k_j \phi_j \end{bmatrix} \quad C-52$$

$$\begin{bmatrix} 0 & -CA^{-1} \\ I & -BA^{-1} \end{bmatrix} \begin{bmatrix} \psi_{1j} \\ \psi_{2j} \end{bmatrix} = k_j \begin{bmatrix} \psi_{1j} \\ \psi_{2j} \end{bmatrix}$$

The relationship between the right and left eigenvectors is

$$\begin{bmatrix} \psi_{1j} \\ \psi_{2j} \end{bmatrix} = \begin{bmatrix} -C\phi_j \\ kA\phi_j \end{bmatrix} \quad C-53$$

The orthogonality of the double dimension vectors gives the result described in Chapter 4

$$k_i k_j \phi_j^T A \phi_i - \phi_j^T C \phi_i = 0 \quad \text{for } i \neq j \quad C-54$$

For the numerical method, the starting vectors for mode j are $Y_0 = X_0 = \{ U_0^T, U_0^T \}$ where

$$U_0 = \cosh \frac{i-1}{N} \cos \frac{\pi}{2} (2j-1) \frac{i-1}{N} \quad C-55$$

is the continuum solution of Appendix B. To begin, we do not need to sweep components of the rigid body mode out of the starting vector, since one iteration removes all components ($\lambda = 0$). We define the $2N$ vectors X_k and Y_k as

$$X_k = \begin{bmatrix} U_k \\ V_k \end{bmatrix} \quad Y_k = \begin{bmatrix} W_k \\ Z_k \end{bmatrix} \quad C-56$$

One iteration on X_k gives

$$X_{k+1} = A X_k = \begin{bmatrix} V_k \\ A^{-1} (-C U_k - B V_k) \end{bmatrix} \quad C-57$$

One iteration on Y_k gives

$$Y_{k+1} = A^T Y_k = \begin{bmatrix} -C A^{-1} Z_k \\ W_k - B A^{-1} Z_k \end{bmatrix} \quad C-58$$

One more iteration is performed to obtain X_{k+2} and Y_{k+2} . Then the cross products of C-10 and C-12 are computed. The constants a_0 and a_1 are computed and then convergence is checked. If they have not converged, then X_{k+2} and Y_{k+2} are normalized by their largest values and another

two iterations are performed.

When the eigenvalues have converged to sufficient accuracy, the wavenumbers and modes are stored and cleaning is performed with the eigenvectors previously obtained. Also, components of each mode are swept from the starting vector C-55 with the Gram-Schmidt orthogonalization procedure.

Since this method uses direct iteration, the remaining eigenvalue with the largest magnitude is obtained. Convergence is rapid as long as two roots are not close in magnitude. One way to avoid convergence problems is to obtain real roots with a search procedure. For the anti-plane case, a search is conducted beginning at $k = 0$. For the in-plane case, the anti-plane real root is used as a starting point for searches in both directions. Our experience has shown that the anti-plane real root lies between the in-plane roots, although we have no proof that this observation is always the case.

Appendix D

Solutions of Integrals for Static Displacements

D.1 Integrals for Static Point Loads

Recall the definitions of these integrals from Chapter 4:

$$I_{1l} \equiv \int_0^{\infty} a_l k J_0(k\rho) dk$$

$$I_{2l} \equiv \int_0^{\infty} a_l k J_1(k\rho) dk \tag{D-1}$$

$$I_{3l} \equiv \int_0^{\infty} a_l J_1(k\rho) dk$$

where

$$a_l = \frac{1}{2 k_l (k - k_l)} \tag{D-2}$$

Note also that

$$\frac{d}{d\rho} I_{3l} = I_{1l} - \frac{1}{\rho} I_{3l} \tag{D-3}$$

since

$$\frac{d}{d\rho} J_1(k\rho) = k J_0(k\rho) - \frac{1}{\rho} J_1(k\rho) \tag{D-4}$$

The solutions of these integrals are found in Erdelyi et. al. (1944). This reference contains the solution of the generic Hankel transform

$$\int_0^{\infty} f(x) J_\nu(xy) (xy)^{1/2} dx \tag{D-5}$$

For the case where

$$f(x) = x^{\nu-1/2} (x + a)^{-1} \tag{D-6}$$

The solution of the Hankel transform is

$$\int_0^\infty J_\nu(xy) x^\nu (x + a)^{-1} dx = \tag{D-7}$$

$$\frac{\pi}{2} a^\nu \sec(\nu\pi) \left[\mathbf{H}_{-\nu}(ay) - Y_{-\nu}(ay) \right] \quad | \arg(a) | < \pi$$

where \mathbf{H} is the Struve function and Y is the Neumann function, or Bessel function of the second kind. This formula allows us to solve for all three of the integrals in D-1.

D.1.1 Solution of I_{2l}

Evaluate D-7 for the case where $\nu = 1$.

$$\int_0^\infty \frac{J_1(xy) x dx}{x + a} = -\frac{\pi}{2} a \left[\mathbf{H}_{-1}(ay) - Y_{-1}(ay) \right] \tag{D-8}$$

Now substitute $a = -k_l$, $x = k$, and $y = \rho$ into D-8

$$\int_0^\infty \frac{J_1(k\rho) k dk}{k - k_l} = \frac{\pi}{2} k_l \left[\mathbf{H}_{-1}(-\rho k_l) - Y_{-1}(-\rho k_l) \right] \quad | \arg(-k_l) | < \pi \tag{D-9}$$

We apply these identities to the right hand side of D-9

$$Y_{-1}(x) = -Y_1(x) \tag{D-10}$$

$$\mathbf{H}_{-1}(x) = -\mathbf{H}_1(x) + \frac{2}{\pi}$$

to obtain

$$\frac{\pi}{2} k_l \left[\frac{2}{\pi} - \mathbf{H}_1(-\rho k_l) - Y_1(-\rho k_l) \right] \tag{D-11}$$

Therefore

$$I_{2l} = \frac{1}{2} \left[1 - \frac{\pi}{2} (\mathbf{H}_1(-\rho k_l) - Y_1(-\rho k_l)) \right] \quad D-12$$

This solution is valid for all k_l which are not positive real numbers.

D.1.2 Solution of I_{3l}

First we must express I_{3l} in a form to which we can apply D-7.

$$\begin{aligned} I_{3l} &= \frac{1}{2k_l} \int_0^\infty \frac{J_1(k\rho) dk}{k - k_l} = \frac{1}{2k_l} \times -\frac{1}{k_l} \int_0^\infty \frac{(k - k_l - k) J_1(k\rho) dk}{k - k_l} = \\ & \frac{1}{2k_l} \left[-\frac{1}{k_l} \int_0^\infty J_1(k\rho) dk + \frac{1}{k_l} \int_0^\infty \frac{J_1(k\rho) k dk}{k - k_l} \right] \end{aligned} \quad D-13$$

This is the sum of two integrals which we already know. Substituting 4-76 and D-11 into D-13 gives

$$\frac{1}{2k_l} \left[-\frac{1}{k_l} \times \frac{1}{\rho} + \frac{1}{k_l} \times k_l \left[1 - \frac{\pi}{2} (\mathbf{H}_1(-\rho k_l) - Y_1(-\rho k_l)) \right] \right] \quad D-14$$

Rearranging terms gives

$$I_{3l} = \frac{1}{2k_l} \left[1 - \frac{1}{\rho k_l} - \frac{\pi}{2} (\mathbf{H}_1(-\rho k_l) - Y_1(-\rho k_l)) \right] \quad D-15$$

Comparing the two integrals above, we can see the relationship

$$I_{2l} = k_l I_{3l} + \frac{1}{2\rho k_l} \quad D-16$$

D.1.3 Solution of I_{1l}

First we expand I_{1l}

$$I_{1l} = \frac{1}{2k_l} \int_0^\infty \frac{J_0(k\rho) k dk}{k - k_l} = \frac{1}{2k_l} \int_0^\infty \frac{(k - k_l + k_l) J_0(k\rho) dk}{k - k_l} = \quad D-17$$

$$\frac{1}{2k_l} \int_0^\infty J_0(k\rho) dk + \frac{1}{2} \int_0^\infty \frac{J_0(k\rho) dk}{k - k_l}$$

We apply D-7 to obtain

$$\int_0^\infty \frac{J_0(k\rho) dk}{k - k_l} = \frac{\pi}{2} (\mathbf{H}_0(-\rho k_l) - Y_0(-\rho k_l)) \quad D-18$$

Substituting in D-17 gives

$$I_{1l} = \frac{1}{2} \left[\frac{1}{\rho k_l} + \frac{\pi}{2} (\mathbf{H}_0(-\rho k_l) - Y_0(-\rho k_l)) \right] \quad D-19$$

D.2 Approximations of Integrals for Static Disk Loads

The solutions to the integrals of 4-88 can not be found in integral tables. An approximate solution for I_{2l} is described below. First, we introduce the notation

$$\begin{aligned} J_1(k\rho) &\rightarrow J_{1\rho} \\ J_1(kR) &\rightarrow J_{1R} \end{aligned} \quad D-20$$

For an integral of the form of I_{2l} , we choose an *ansatz*

$$\begin{aligned} \int_0^\infty \frac{J_{1\rho} J_{1R} dk}{k + a} &= C J_1(a\rho) (\mathbf{H}_{-1}(aR) - Y_{-1}(aR)) & \rho \leq R \\ |\arg(a)| < \pi & C J_1(aR) (\mathbf{H}_{-1}(a\rho) - Y_{-1}(a\rho)) & \rho \geq R \end{aligned} \quad D-21$$

$$\begin{aligned} \int_0^\infty \frac{J_{1\rho} J_{1R} dk}{k - a} &= C J_1(-a\rho) (\mathbf{H}_{-1}(-aR) - Y_{-1}(-aR)) & \rho \leq R \\ |\arg(-a)| < \pi & C J_1(-aR) (\mathbf{H}_{-1}(-a\rho) - Y_{-1}(-a\rho)) & \rho \geq R \end{aligned}$$

where C is an arbitrary constant. When the two integrals above are added together, the result is an integral from Table 2-III.

$$\frac{1}{2} \int_0^\infty \left[\frac{J_{1\rho} J_{1R}}{k - a} + \frac{J_{1\rho} J_{1R}}{k + a} \right] dk = \int_0^\infty \frac{k J_{1\rho} J_{1R}}{k^2 - a^2} dk = \frac{\pi}{2i} J_1(a\rho) H_1^{(2)}(aR) \quad D-22$$

We apply these identities

$$\begin{aligned}
 \mathbf{H}_{-1}(-aR) &= \mathbf{H}_{-1}(aR) \\
 J_1(-a\rho) &= -J_1(a\rho) \\
 Y_{-1}(aR) &= -Y_1(aR) \\
 Y_{-1}(-aR) &= Y_1(aR) + 2i J_1(aR)
 \end{aligned}
 \tag{D-23}$$

Substituting D-23 into D-22 and summing, we obtain for $\rho \leq R$

$$\begin{aligned}
 &\frac{1}{2} C \left[J_1(a\rho) (\mathbf{H}_{-1}(aR) + Y_1(aR)) - J_1(a\rho) (\mathbf{H}_{-1}(aR) - Y_1(aR) - 2i J_1(aR)) \right] = \\
 &\frac{1}{2} C J_1(a\rho) (2 Y_1(aR) + 2i J_1(aR)) = i C J_1(a\rho) (J_1(aR) - i Y_1(aR)) = \\
 &i C J_1(a\rho) H_1^{(2)}(aR)
 \end{aligned}
 \tag{D-24}$$

By equating the results of D-24 and D-22, we can solve for C

$$\begin{aligned}
 i C J_1(a\rho) H_1^{(2)}(aR) &= \frac{\pi}{2i} J_1(a\rho) H_1^{(2)}(aR) \\
 C &= -\frac{\pi}{2}
 \end{aligned}
 \tag{D-25}$$

Thus, we obtain

$$\begin{aligned}
 \int_0^\infty \frac{J_{1\rho} J_{1R} dk}{k+a} &= -\frac{\pi}{2} J_1(a\rho) (\mathbf{H}_{-1}(aR) - Y_{-1}(aR)) \quad \rho \leq R \\
 |\arg(a)| < \pi &\quad -\frac{\pi}{2} J_1(aR) (\mathbf{H}_{-1}(a\rho) - Y_{-1}(a\rho)) \quad \rho \geq R
 \end{aligned}
 \tag{D-26}$$

Numerical evaluation shows that this integral estimate is accurate for real values of a when a is of the same magnitude as ρ and R . However, complex values of a introduce larger errors. When a has a large imaginary part, there is no correspondence between the numerical values of this integral and the integral estimate. For applications to static displacements, when the imaginary part of wavenumbers are often many times larger than the real parts, this integral estimate is not useful. It seems that terms are missing from the integral estimate. The true solution to this integral is probably an infinite series of Bessel functions.

Appendix E

Numerical Evaluation of Struve and Neumann Functions

The integrals presented in Tables 2-III and 4-I are evaluated numerically. Algorithms for functions in Table 4-I are presented here. Functions in Table 2-III can be found in the references cited in Chapter 2. The Struve and Neumann functions are evaluated with ascending series for small arguments and with asymptotic expansions for large arguments. The absolute value of the argument at which evaluation goes from series to asymptotic expansion is determined by convergence considerations. The ascending series are valid for all complex arguments z . The asymptotic expansions are valid for arguments in the right half of the complex plane (positive real part). For arguments with a negative real part, the functions are evaluated for the negative of the argument; and the result for the true argument is then obtained with an analytic continuation. The series and expressions given below are taken from Abromowitz and Stegun (1972), Spiegel (1968) and Boas (1966).

E.1 Struve Functions

The functions appearing in Table 4-I are the differences between the Struve functions and the Neumann functions (Bessel functions of the second kind). Since the numerical evaluations of these functions have different convergence properties, they must be evaluated separately and then summed. For large arguments, the difference between the Struve and Neumann functions has an asymptotic expansion.

E.1.1 Ascending Series

The ascending series of the Struve function is

$$\mathbf{H}_n(z) = \sum_{k=0}^{\infty} (-1)^k \frac{(z/2)^{2k+n+1}}{\Gamma(k+3/2)\Gamma(n+k+3/2)} \quad E-1$$

The product of the gamma functions is

$$\begin{aligned} \Gamma(k+3/2)\Gamma(n+k+3/2) &= \frac{\sqrt{\pi}}{2^{k+1}}(2k+1)!! \frac{\sqrt{\pi}}{2^{n+k+1}}(2(n+k)+1)!! = \\ &= \frac{\pi}{2^n 2^{2(k+1)}}(2k+1)!!(2n+2k+1)!! \end{aligned} \quad E-2$$

where !! indicates the odd factorial,

$$(2k+1)!! = 1 \cdot 3 \cdot 5 \cdots (2k+1) \quad E-3$$

Substituting E-2 into E-1 gives the ascending series

$$\mathbf{H}_n = z^{n+1} \frac{2}{\pi} \sum_{k=0}^{\infty} \frac{(-z^2)^k}{(2k+1)!!(2n+2k+1)!!} \quad E-4$$

In particular, for orders 0 and 1:

$$\mathbf{H}_0(z) = \frac{2}{\pi} \left[z - \frac{z^3}{1^2 \cdot 3^2} + \frac{z^5}{1^2 \cdot 3^2 \cdot 5^2} - \cdots \right] \quad E-5$$

$$\mathbf{H}_1(z) = \frac{2}{\pi} \left[\frac{z^2}{1^2 \cdot 3} - \frac{z^4}{1^2 \cdot 3^2 \cdot 5} + \frac{z^6}{1^2 \cdot 3^2 \cdot 5^2 \cdot 7} - \cdots \right]$$

We want to find the limit on the absolute value of the argument that can be used in this series by first finding the largest term in the summation. The order of magnitude of this term determines how many digits of precision there are in the series evaluation. For \mathbf{H}_0 , the series takes this form,

$$\mathbf{H}_0 = z \frac{2}{\pi} \sum_{k=0}^{\infty} \frac{(-z^2)^k}{[(2k+1)!!]^2} \quad E-6$$

We express the denominator as

$$(2k + 1)!! = \frac{(2k + 1)!}{(2k)!} = \frac{(2k + 1)!}{2^k k!} \tag{E-7}$$

For large k , we apply Stirling's formula to E-7:

$$\frac{(2k + 1)!}{2^k k!} \simeq \frac{((2k + 1)/e)^{2k+1} \sqrt{2\pi (2k + 1)}}{2^k (k/e)^k \sqrt{2\pi k}} \tag{E-8}$$

From here, we neglect the 1 in $(2k + 1)$ to obtain, for E-8,

$$\left[\frac{2k}{e} \right]^{(k+1)} \sqrt{2} \tag{E-9}$$

Then the denominator of E-6 is given by

$$[(2k + 1)!!]^2 \simeq \left[\frac{2k}{e} \right]^{(2k+2)} \times 2 \tag{E-10}$$

Now we examine the k^{th} term in the series, substituting for z its absolute value R

$$\frac{R^{2k}}{[(2k + 1)!!]^2} \simeq \frac{R^{2k+2}}{(2k/e)^{2k+2} \cdot 2} \times \frac{1}{R^2} = \left[\frac{R e}{2k} \right]^{(2k+2)} \frac{1}{2R^2} \tag{E-11}$$

In order to find the maximum, we want to find the k for which the derivative of the series term with respect to k vanishes. Equation E-11 is of the form

$$y = u^v \text{ where } u = u(k) = \left[\frac{R e}{2k} \right]^{2k+2} \text{ and } v = v(k) = 2k + 2 \tag{E-12}$$

Differentiating with respect to k gives

$$\begin{aligned} \frac{dy}{dk} &= \frac{\partial y}{\partial u} \frac{du}{dk} + \frac{\partial y}{\partial v} \frac{dv}{dk} = \\ v u^{v-1} u' + \ln(u) u^v v' &= 0 \\ v u' + \ln(u) u v' &= 0 \end{aligned} \tag{E-13}$$

Substituting E-12 into E-13, we obtain

$$-(2k + 2) \frac{u}{k} + 2u \ln \left[\frac{R e}{2k} \right] = 0 \tag{E-14}$$

If we approximate the logarithm term as being of order 1, then

$$\ln \left[\frac{R e}{2k} \right] \simeq 1 \quad \rightarrow \quad \frac{R e}{2k} = e \quad \rightarrow \quad R = 2k \quad E-15$$

Then the maximum term is

$$\frac{R^{2k}}{[(2k+1)!!]^2} \simeq \left[\frac{R e}{2k} \right]^{2k+2} \times \frac{1}{2R^2} \simeq \frac{e^{R+2}}{2R^2} \quad E-16$$

For a double precision computer program with 14 available digits, if the desired precision is 8 digits, then no more than 6 digits are available for the largest term in the series. Then we can compute the maximum radius

$$\frac{e^{R+2}}{2R^2} = 10^6 \quad E-17$$

The solution of E-17 gives a maximum radius of $R = 18$. A test of the ascending series with a quadruple precision program verified that for $R > 18$, the asymptotic expansion is more accurate than the ascending series.

E.1.2 Asymptotic Expansion

We define the function $F_n(z)$ as the difference between the Struve and Neumann functions:

$$F_n(z) = H_n(z) - Y_n(z) \quad E-18$$

The asymptotic representation of this function is

$$F_n(z) = \frac{1}{\pi} \sum_{k=0}^{p-1} \frac{\Gamma(k+1/2) (z/2)^{-2k+n-1}}{\Gamma(n-k+1/2)} \quad E-19$$

The series is truncated before the p^{th} term, where the terms begin to grow in absolute value. For the expression in E-19, this occurs when the index p equals the absolute value of the argument R .

When $n = 0$, E-19 becomes

$$F_0(z) = \frac{1}{\pi} \left[\frac{2}{z} + \sum_{k=1}^{p-1} \frac{\sqrt{\pi} (2k-1)!! (2k-1)!!}{2^k \sqrt{\pi} (-1)^k 2^k} \left[\frac{2}{z} \right]^{(2k+1)} \right] \quad E-20$$

By defining $(-1)!! = 1$, we can simplify E-20

$$F_0(z) = \frac{2}{\pi z} \sum_{k=0}^{p-1} (-1)^k \left[\frac{(2k-1)!!}{z^k} \right]_2 \quad E-21$$

When $n = 1$,

$$F_1(z) = \frac{1}{\pi} \left[\frac{\sqrt{\pi}}{\sqrt{\pi/2}} + \frac{\sqrt{\pi/2} (z/2)^2}{\sqrt{\pi}} + \sum_{k=2}^{p-1} \frac{\sqrt{\pi/2^k} (2k-1)!! (2/z)^{2k}}{(-1)^{k-1} \sqrt{\pi} 2^{k-1} / (2k-3)!!} \right] \quad E-22$$

Simplified, E-22 becomes

$$F_1(z) = \frac{2}{\pi} \left[1 + \frac{1}{z^2} - \sum_{k=2}^{p-1} \frac{(2k-1)!! (2k-3)!!}{(-z^2)^k} \right] \quad E-23$$

As stated previously, the asymptotic expansion is valid for arguments z with a positive real part.

When z has a negative real part we must apply analytic continuation.

E.1.3 Analytic Continuation

Mapping a point z from the right half plane to the left half plane, without crossing the negative real axis, is shown in Figure E-1. In going from the first quadrant to the third, z is multiplied by $e^{-i\pi}$. In going from the fourth quadrant to the second, z is multiplied by $e^{i\pi}$.

The continuation rule for the Struve function is

$$\begin{aligned} \mathbf{H}_n(z e^{\pm i\pi}) &= e^{\pm i\pi(n+1)} \mathbf{H}_n(z) = (-1)^{n+1} \mathbf{H}_n(z) \\ \mathbf{H}_n(-z) &= -(-1)^n \mathbf{H}_n(z) \end{aligned} \quad E-24$$

For orders 0 and 1,

$$\begin{aligned} \mathbf{H}_0(-z) &= -\mathbf{H}_0(z) \\ \mathbf{H}_1(-z) &= \mathbf{H}_1(z) \end{aligned} \quad E-25$$

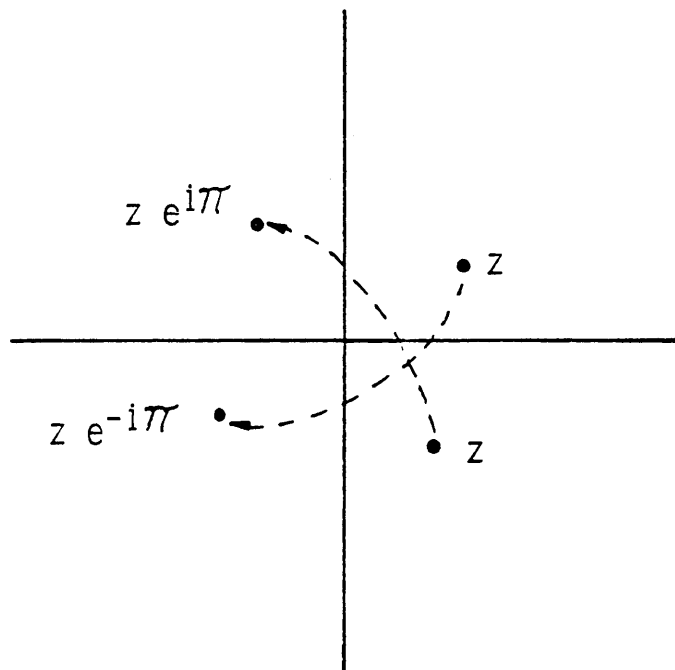
The continuation rule for the Neumann function is

$$Y_n(z e^{\pm i\pi}) = (-1)^n [Y_n(z) \pm 2i J_n(z)] \quad E-26$$

Then

$$\begin{aligned} Y_0(-z) &= [Y_0(z) \pm 2i J_0(z)] \\ Y_1(-z) &= -[Y_1(z) \pm 2i J_1(z)] \end{aligned} \quad E-27$$

Figure E-1: Mapping z from the Right Half Plane to the Left



Substituting E-26 and E-24 into the expression for $F_n(z)$, we obtain

$$\begin{aligned}
 F_n(z e^{\pm i\pi}) &= \mathbf{H}_n(z e^{\pm i\pi}) - Y_n(z e^{\pm i\pi}) = & E-28 \\
 &= -(-1)^n \mathbf{H}_n(z) - (-1)^n [Y_n(z) \pm 2i J_n(z)] = \\
 &= -(-1)^n [\mathbf{H}_n(z) + Y_n(z) \pm 2i J_n(z)] = \\
 &= -(-1)^n [\mathbf{H}_n(z) - Y_n(z) + 2\{Y_n(z) \pm i J_n(z)\}] = \\
 &= -(-1)^n [F_n(z) \pm 2i \{J_n(z) \mp i Y_n(z)\}] \\
 F_n(z e^{\pm i\pi}) &= -(-1)^n [F_n(z) \pm 2i H_n^{2,1}(z)]
 \end{aligned}$$

where the Hankel function $H_n(z)$ are defined by

$$\begin{aligned}
 H_n^1(z) &= J_n(z) + i Y_n(z) & E-29 \\
 H_n^2(z) &= J_n(z) - i Y_n(z)
 \end{aligned}$$

In summary, when mapping from the first to the third quadrant, the appropriate expression is

$$F_n(-z) = -(-1)^n [F_n(z) - 2i H_n^1(z)] \quad E-30$$

When going from the fourth to the second quadrant, we use

$$F_n(-z) = -(-1)^n [F_n(z) + 2i H_n^2(z)] \quad E-31$$

Numerical evaluation of the Hankel function is given in Section E.3 below.

A plot of the functions $F_0(x)$ and $F_1(x)$ is shown in Figure E-2. The argument of the function is real and the function is singular at $x = 0$ due to the singularity of the Neumann function. Figure E-3 to E-6 show contours in the complex plane of the F function. Contours are shown for $\text{imag}(z) \geq 1.0$ due to numerical difficulties of calculation near the branch cut. Contour lines are plotted for increments of .02 and dotted lines are negative contours. Figure E-3 shows contours of the real part of $F_0(z)$ and Figure E-4 shows contours of the imaginary part of $F_0(z)$. Figures E-5 and E-6 show the real and imaginary parts of $F_1(z)$. The outstanding feature of these plots is the waviness of the functions near the negative real axis. For the purposes described in this paper, we know from Chapter 4 that the functions are never evaluated near the negative real axis.

E.2 Neumann Functions

E.2.1 Ascending Series

The Neumann functions must be evaluated numerically for addition to the Struve functions.

The ascending series for the Neumann function is

$$Y_n(z) = \frac{-n! (z/2)^{-n}}{\pi} \sum_{k=0}^{n-1} \frac{(z/2)^k J_k(z)}{(n-k) k!} + \frac{2}{\pi} \{ \ln(z/2) - \psi(n+1) \} J_n(z) \quad E-32$$

$$- \frac{2}{\pi} \sum_{k=1}^{\infty} (-1)^k \frac{(n+2k) J_{n+2k}(z)}{k(n+k)}$$

where

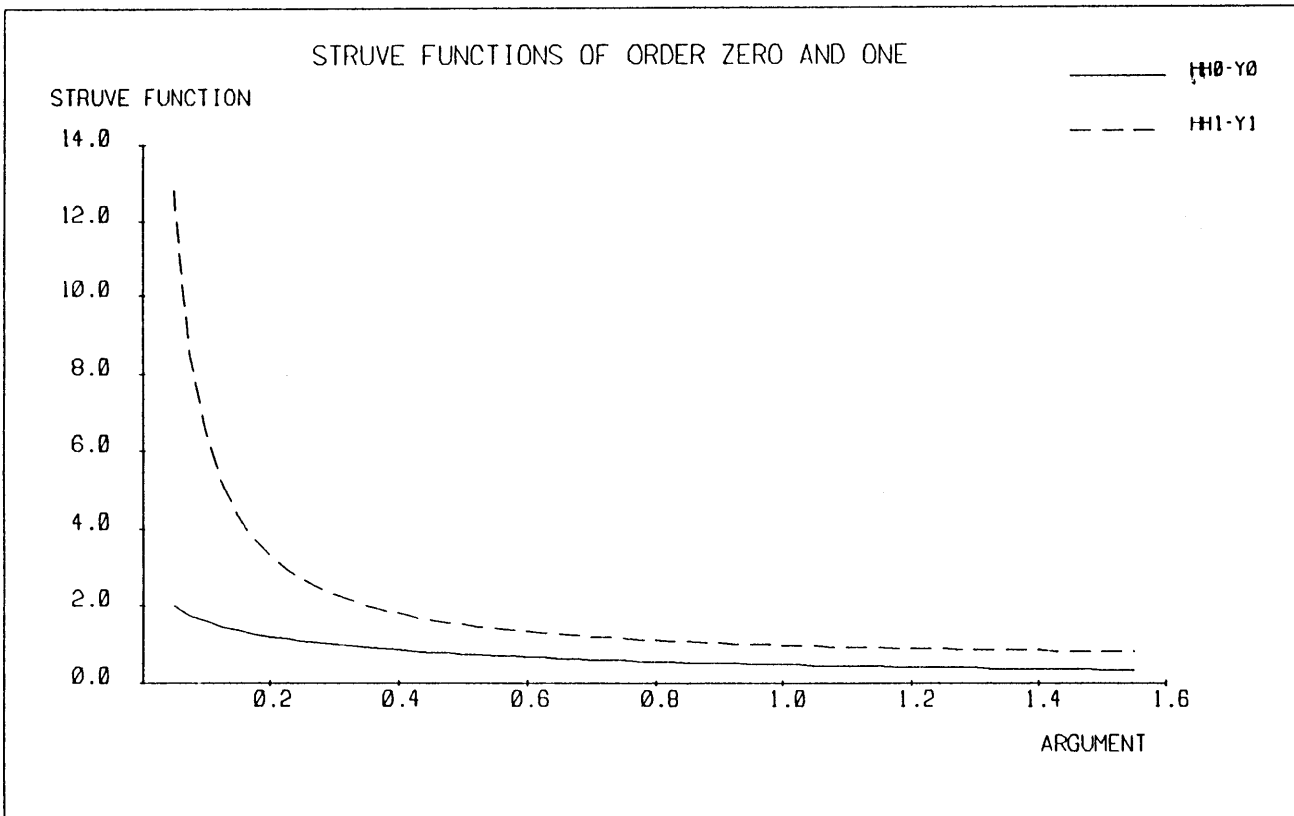


Figure E-2: The Functions $F_0(x)$ and $F_1(x)$ for Real Argument

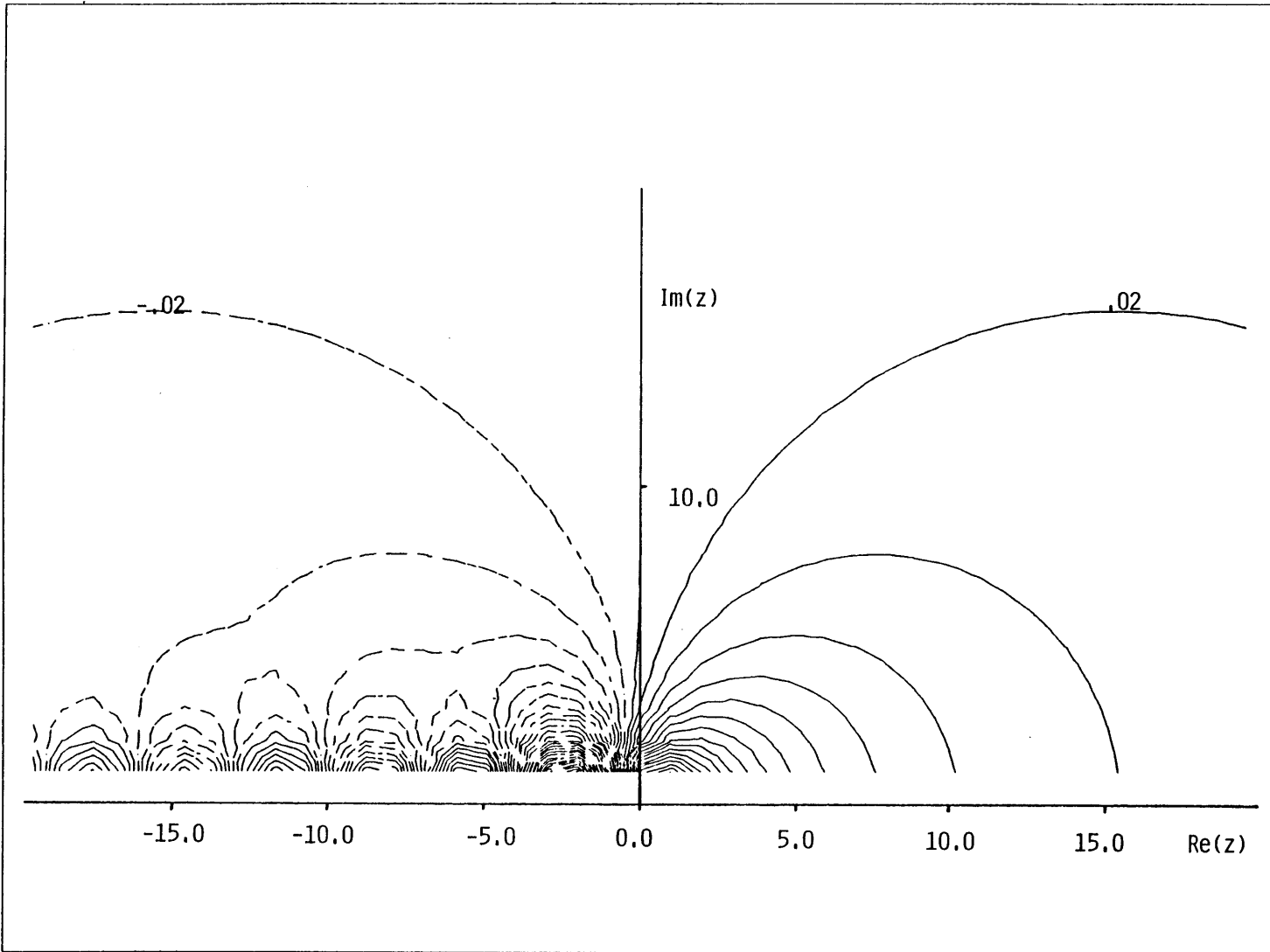


Figure E-3: Contours of the Real Part of $F_0(z)$

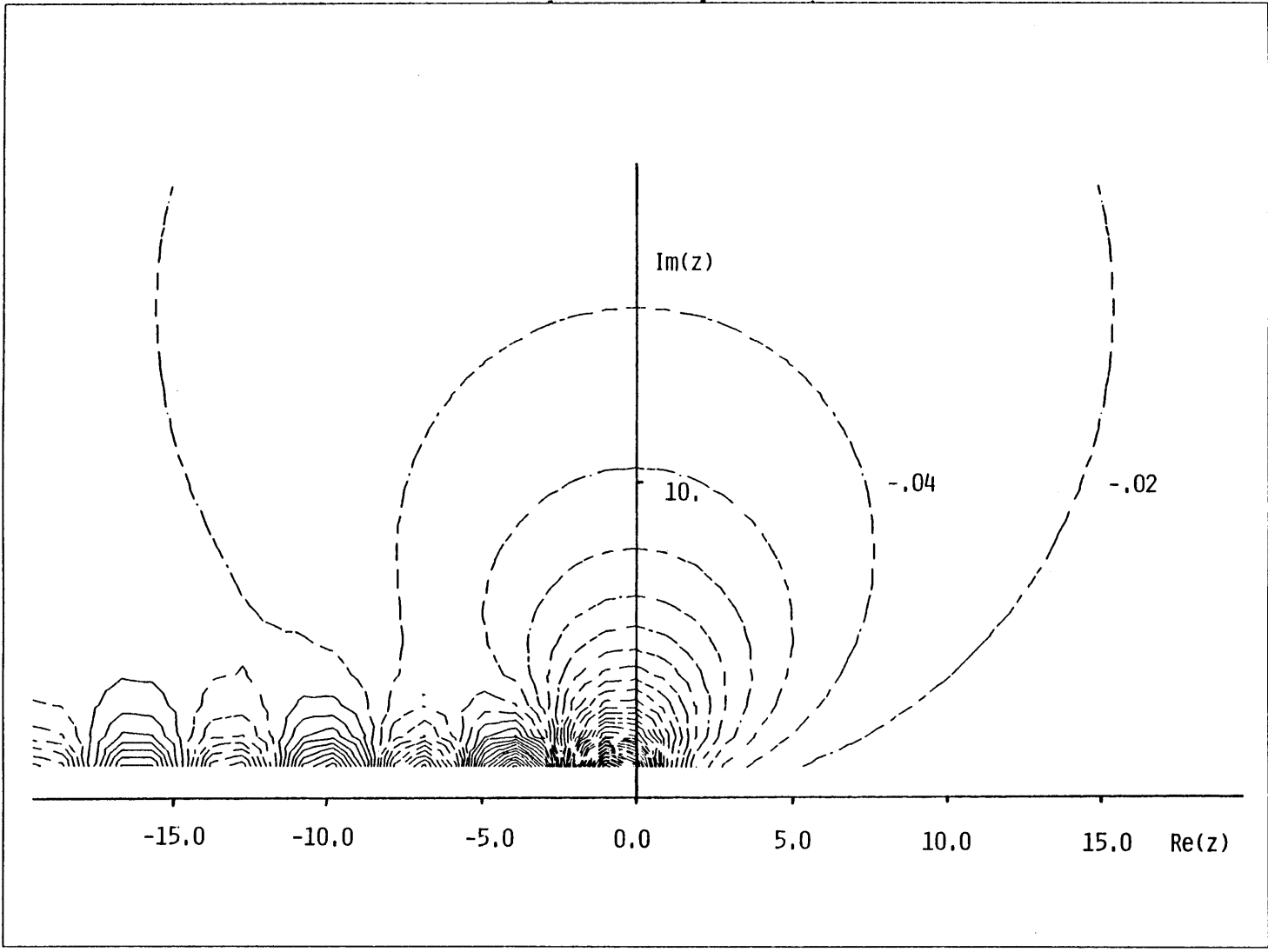


Figure E-4: Contours of the Imaginary Part of $F_0(z)$

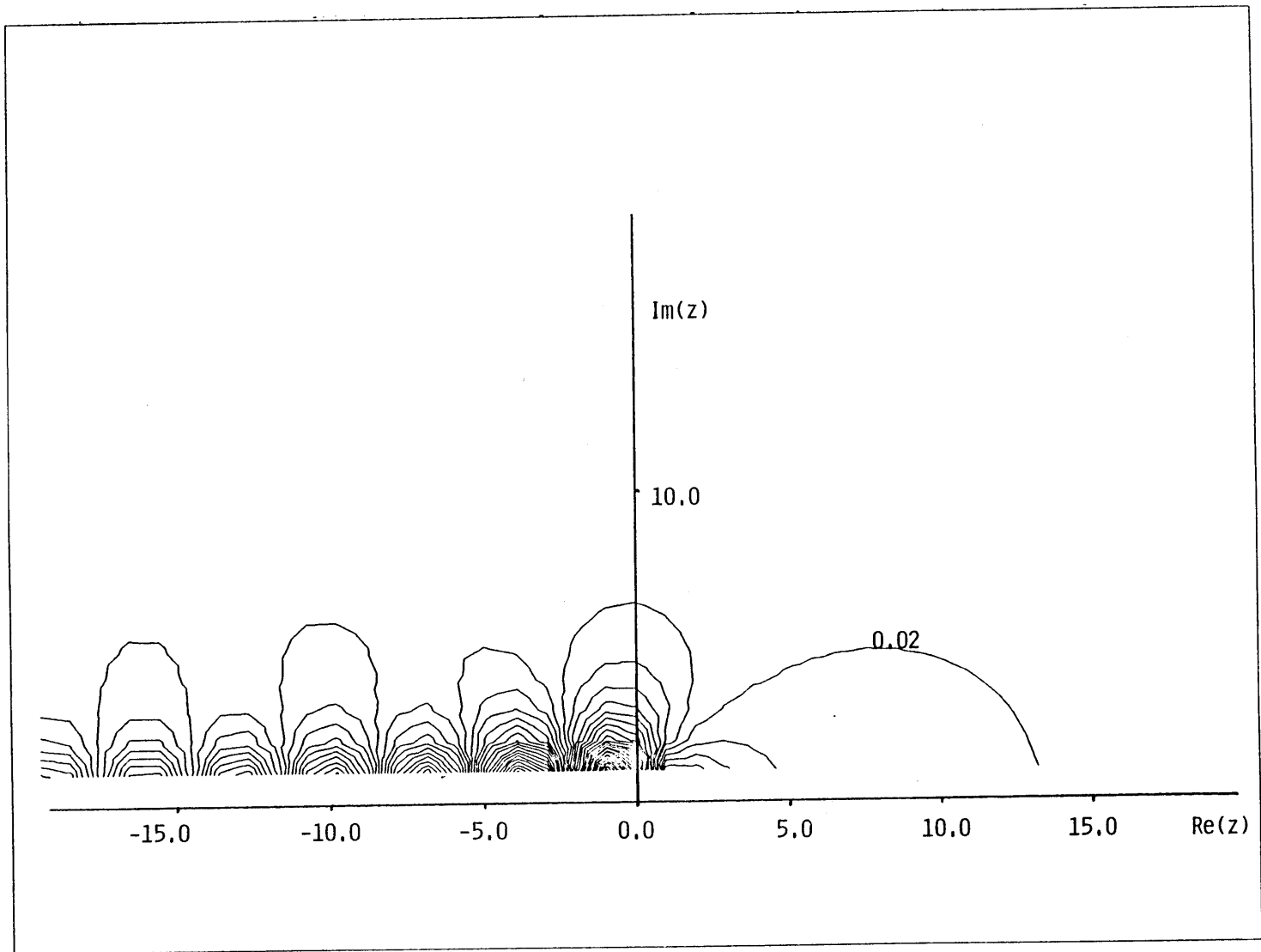


Figure E-5: Contours of the Real Part of $F_1(z)$

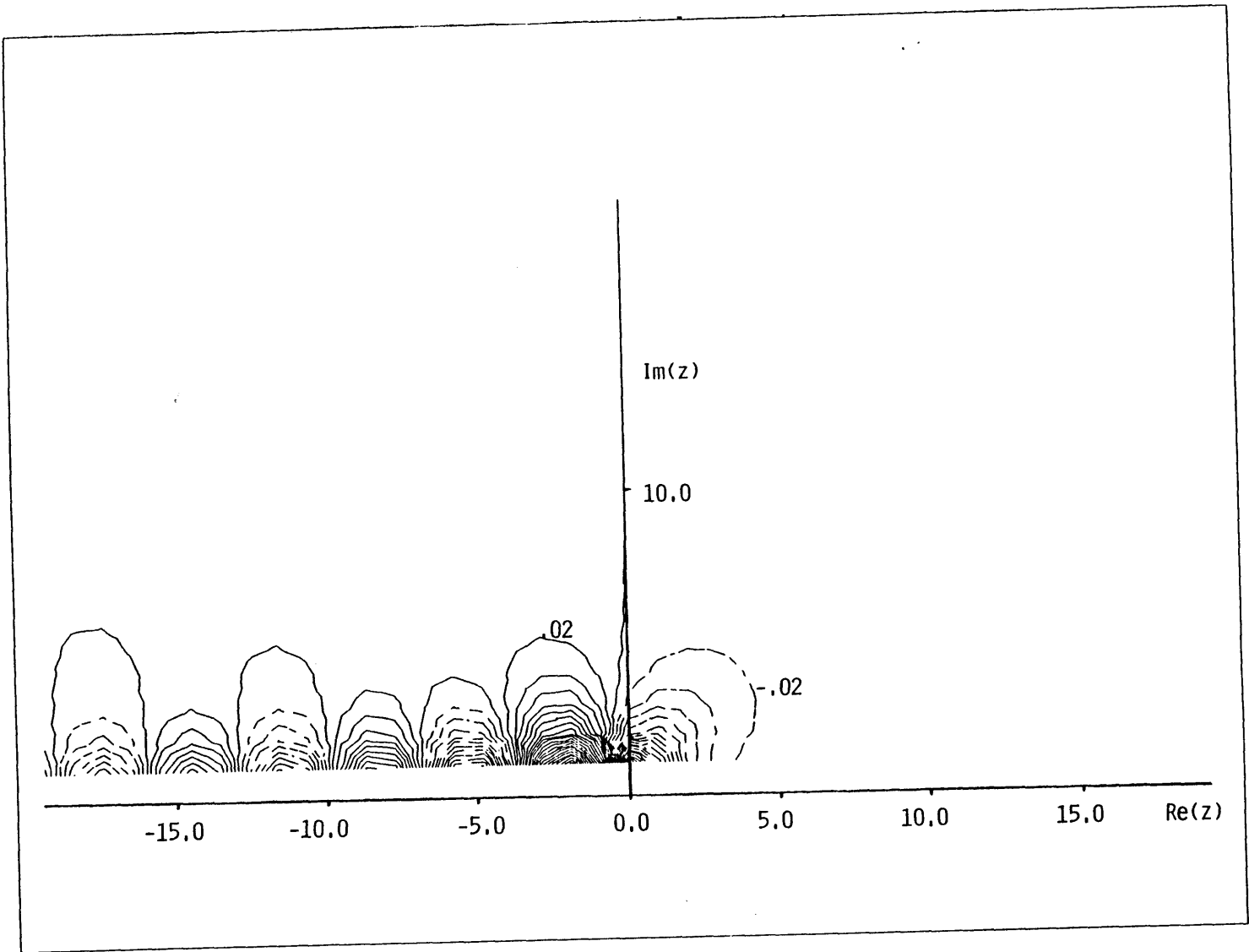


Figure E-6: Contours of the Imaginary Part of $F_1(z)$

$$\psi(n) = -\gamma + \sum_{k=1}^{n-1} \frac{1}{k} \quad n \geq 2 \quad E-33$$

and γ is Euler's constant ($\simeq 0.577216$). We define these coefficients

$$\begin{aligned} b_k &= \left[\frac{iz}{2} \right]^{(k)} \frac{1}{k!} \\ s_k &= \frac{2i}{\pi} \sum_{j=1}^k \frac{1}{j} \\ c &= \frac{2i}{\pi} (\ln(z/2) + \gamma) \end{aligned} \quad E-34$$

Applying the coefficients in E-34 to the ascending series E-32, we obtain these simplified series

$$\begin{aligned} Y_0(z) &= -i \left(c + \sum_{k=1}^{\infty} b_k^2 (c - s_k) \right) \\ Y_1(z) &= -i(z/2) \left[c - \frac{i}{\pi} \left[1 + \left[\frac{2}{z} \right]^{(2)} \right] \right] - i(z/2) \sum_{k=1}^{\infty} \frac{b_k^2}{k+1} \left[c - s_k - \frac{i}{\pi(k+1)} \right] \end{aligned} \quad E-35$$

These series are valid for complex arguments with absolute values less than 10. For $R \geq 10$, we use the asymptotic expansion.

E.2.2 Asymptotic Expansion

The asymptotic expansion of $Y_n(z)$ for large argument is

$$Y_n(z) = \sqrt{\frac{2}{\pi z}} \{ P(n,z) \sin \chi + Q(n,z) \cos \chi \} \quad E-36$$

where $\chi = z - (n/2 + 1/4) \pi$ and, with $4n^2$ denoted by μ ,

$$\begin{aligned} P(n,z) &= 1 - \frac{(\mu-1)(\mu-9)}{2!(8z)^2} + \frac{(\mu-1)(\mu-9)(\mu-25)(\mu-49)}{4!(8z)^4} - \dots \\ Q(n,z) &= i \frac{(\mu-1)}{8z} - i \frac{(\mu-1)(\mu-9)(\mu-25)}{3!(8z)^3} + \dots \end{aligned} \quad E-37$$

This series is truncated before the terms begin to increase, approximately when $k = R$. This asymptotic expansion for the Neumann functions is valid for $\text{Re}(z) > 0$. The analytic

continuation is given by E-26. The Bessel functions required for the continuation have this asymptotic expansion

$$J_n(z) = \sqrt{\frac{2}{\pi z}} \{ P(n,z) \cos \chi - Q(n,z) \sin \chi \} \quad E-38$$

which only differs from E-36 by the exchange of $\cos \chi$ and $\sin \chi$. Thus the continuation is computed without the explicit evaluation of E-38.

E.3 Hankel Functions

Hankel functions appear in the analytic continuation of the $F_n(z)$ function, E-28. Since the Hankel function is only required when $R > 18$, we only need the asymptotic expansion. The expansions contain the polynomials $P(n,z)$ and $Q(n,z)$ given in E-37

$$\begin{aligned} H_n^1(z) &= \sqrt{\frac{2}{\pi z}} \{ P(n,z) + i Q(n,z) \} e^{i\chi} \\ H_n^2(z) &= \sqrt{\frac{2}{\pi z}} \{ P(n,z) - i Q(n,z) \} e^{-i\chi} \end{aligned} \quad E-39$$

The analytic continuation of the Hankel functions is given by

$$\begin{aligned} H_0^1(z e^{i\pi}) &= -H_0^2(z) \\ H_0^2(z e^{i\pi}) &= H_0^1(z) + 2 H_0^2(z) \\ H_1^1(z e^{i\pi}) &= H_1^2(z) \\ H_1^2(z e^{i\pi}) &= -[H_1^1(z) + 2 H_1^2(z)] \\ H_0^1(z e^{-i\pi}) &= 2 H_0^1(z) + H_0^2(z) \\ H_0^2(z e^{-i\pi}) &= -H_0^1(z) \\ H_1^1(z e^{-i\pi}) &= -[2 H_1^1(z) + H_1^2(z)] \\ H_1^2(z e^{-i\pi}) &= H_1^1(z) \end{aligned} \quad E-40$$

Appendix F

Calculation of the Paraxial Approximation

The first and second derivatives of the exact stiffness of the halfspace and their limits as $k \rightarrow 0$ are given in this appendix.

F.1 Anti-plane Case

Recall from Chapter 3 the anti-plane stiffness,

$$K(k) = k s G = kG \sqrt{1 - (\omega/kC_s)^2} = G \sqrt{k^2 - (\omega/C_s)^2} \quad F-1$$

At $k = 0$, Equation F-1 is

$$K(0) = i \frac{G \omega}{C_s} \quad F-2$$

The first derivative of F-1 with respect to k is

$$K'(k) = \frac{k G}{\sqrt{k^2 - (\omega/C_s)^2}} \quad F-3$$

It is clear from Equation F-3 that $K'(k) = 0$. The second derivative of F-1 with respect to k is

$$K''(k) = \frac{G (\omega/C_s)^2}{(k^2 - (\omega/C_s)^2)^{3/2}} \quad F-4$$

At $k = 0$, Equation F-4 is

$$K''(0) = -i \frac{G C_s}{\omega} \quad F-5$$

The second-order approximation of the stiffness is then

$$K(k) \simeq i \frac{G \omega}{C_s} - \frac{k^2}{2} i \frac{G C_s}{\omega} \quad F-6$$

F.2 In-plane Case

The exact in-plane stiffness is

$$K(k) = G \left[\frac{1-s^2}{1-rs} \begin{bmatrix} kr & k \\ k & ks \end{bmatrix} - \begin{bmatrix} & 2k \\ 2k & \end{bmatrix} \right] \quad F-7$$

where

$$s = \sqrt{1 - (\omega/C_s k)^2} \quad F-8$$

$$r = \sqrt{1 - (\omega/C_p k)^2}$$

The first derivative of s with respect to k is

$$\frac{ds}{dk} = \frac{(\omega/C_s k)^2}{k \sqrt{1 - (\omega/C_s k)^2}} \quad F-9$$

$$\frac{ds}{dk} = \frac{1-s^2}{ks}$$

Similarly,

$$\frac{dr}{dk} = \frac{1-r^2}{kr} \quad F-10$$

Also, we calculate

$$\frac{d(ks)}{dk} = s + k \frac{ds}{dk} = s + \frac{1-s^2}{s} \quad F-11$$

$$\frac{d(ks)}{dk} = \frac{1}{s}$$

and likewise,

$$\frac{d(kr)}{dk} = \frac{1}{r} \quad F-12$$

Now consider the first factor

$$F(k) = \frac{1-s^2}{1-rs} \quad F-13$$

We take the first derivative

$$\frac{dF}{dk} = \frac{-2s \frac{ds}{dk}(1-rs) + (1-s^2) \frac{d(rs)}{dk}}{(1-rs)^2} \quad F-14$$

The derivative of rs is

$$\frac{d(rs)}{dk} = s \frac{dr}{dk} + r \frac{ds}{dk} = s \frac{1-r^2}{kr} + r \frac{1-s^2}{ks} \quad F-15$$

$$\frac{d(rs)}{dk} = \frac{1}{krs} [s^2(1-r^2) + r^2(1-s^2)]$$

Substituting F-9 and F-15 into F-14 gives

$$\frac{dF}{dk} = \frac{-2s \frac{1-s^2}{ks} (1-rs) + (1-s^2) \frac{1}{krs} [s^2(1-r^2) + r^2(1-s^2)]}{(1-rs)^2} \quad F-16$$

$$\frac{dF}{dk} = \frac{(1-s^2)(r-s)^2}{krs(1-rs)^2}$$

Now we can complete the derivative of the stiffness matrix.

For the first diagonal term:

$$\frac{dF}{dk}(kr) + F \frac{d(kr)}{dk} = \frac{(1-s^2)(r-s)^2}{krs(1-rs)^2} kr + \frac{1-s^2}{r(1-rs)} = \quad F-17$$

$$\frac{1-s^2}{rs(1-rs)^2} \{ r(r-s)^2 + s(1-rs) \}$$

For the second diagonal term:

$$\frac{dF}{dk}(ks) + F \frac{d(ks)}{dk} = \frac{(1-s^2)(r-s)^2}{krs(1-rs)^2} ks + \frac{1-s^2}{s(1-rs)} = \quad F-18$$

$$\frac{1-s^2}{rs(1-rs)^2} \{ s(r-s)^2 + r(1-rs) \}$$

For the off-diagonal term:

$$\frac{dF}{dk} k + F - 2 = \frac{(1-s^2)(r-s)^2 k}{krs(1-rs)^2} + \frac{1-s^2}{1-rs} - 2 = \quad F-19$$

$$\frac{1-s^2}{rs(1-rs)^2} \{ (r-s)^2 + rs(1-rs) \} - 2$$

The first derivative of the stiffness matrix is

$$K' = G \frac{1-s^2}{1-rs} \left[\frac{(r-s)^2}{1-rs} \begin{bmatrix} 1/s & 1/rs \\ 1/rs & 1/r \end{bmatrix} + \begin{bmatrix} 1/r & 1 \\ 1 & 1/s \end{bmatrix} \right] - \begin{bmatrix} 2G \\ 2G \end{bmatrix} \quad F-20$$

We must now evaluate this expression in the limit when $k \rightarrow 0$. For s and r , as k goes to zero,

$$s \rightarrow i \frac{\omega}{C_s k} \quad F-21$$

$$r \rightarrow i \frac{\alpha \omega}{C_s k}$$

The limiting values of these quotients are

$$\lim_{k \rightarrow 0} \frac{1-s^2}{1-rs} \rightarrow \frac{-i^2}{-i^2 \alpha} = \frac{1}{\alpha} \quad F-22$$

$$\lim_{k \rightarrow 0} \frac{(r-s)^2}{1-rs} \rightarrow \frac{i^2(\alpha-1)^2}{-i^2 \alpha} = -\frac{(1-\alpha)^2}{\alpha}$$

Since

$$\lim_{k \rightarrow 0} \frac{1}{s} = \lim_{k \rightarrow 0} \frac{1}{r} = \lim_{k \rightarrow 0} \frac{1}{rs} = 0 \quad F-23$$

then the first matrix and the diagonal elements of the second matrix of F-20 vanish. Hence, the derivative of K when $k \rightarrow 0$ is

$$K'(0) = G \frac{1-2\alpha}{\alpha} \begin{bmatrix} & 1 \\ 1 & \end{bmatrix} \quad F-24$$

Now we evaluate the second derivative. We define the factor H :

$$H = \frac{(r-s)^2}{1-rs} \quad F-25$$

The derivative of H is

$$\begin{aligned} \frac{dH}{dk} &= \frac{2(r-s) \left[\frac{dr}{dk} - \frac{ds}{dk} \right] (1-rs) + \frac{drs}{dk} (r-s)^2}{(1-rs)^2} = & F-26 \\ &= \frac{-2(r-s)^2(1+rs)(1-rs) + (r-s)^2 [s(1-r^2) + r^2(1-s^2)]}{krs(1-rs)^2} = \\ \frac{dH}{dk} &= \frac{(r-s)^2 [(r-s)^2 - 2(1-rs)]}{krs(1-rs)^2} \end{aligned}$$

Other derivatives that we need are

$$\begin{aligned} \frac{d(1/s)}{dk} &= -\frac{1-s^2}{ks^3} & F-27 \\ \frac{d(1/r)}{dk} &= -\frac{1-r^2}{kr^3} \\ \frac{d(1/rs)}{dk} &= -\frac{r^2+s^2-2r^2s^2}{k(rs)^3} \end{aligned}$$

We now want to take the first derivative of the first derivative of the stiffness matrix given by

$$K' = GF \left[H \begin{bmatrix} 1/s & 1/rs \\ 1/rs & 1/r \end{bmatrix} + \begin{bmatrix} 1/r & 1 \\ 1 & 1/s \end{bmatrix} \right] - \begin{bmatrix} 2G \\ 2G \end{bmatrix} \quad F-28$$

For the first diagonal term:

$$\begin{aligned} \frac{F'H}{s} + \frac{FH'}{s} + FH(1/s)' + \frac{F'}{r} + F(1/r)' &= \\ \frac{(1-s^2)(r-s)^2}{krs(1-rs)^2} \left[\frac{(r-s)^2}{s(1-rs)} + \frac{1}{r} \right] + & F-29 \\ \frac{1-s^2}{1-rs} \left[\frac{(r-s)^2(r^2+s^2-2)}{krs^2(1-rs)^2} - \frac{(r-s)^2(1-s^2)}{(1-rs)ks^3} - \frac{(1-r^2)}{kr^3} \right] \end{aligned}$$

In the limit when $k \rightarrow 0$, several terms vanish, since r and s appear with higher powers in the denominator. The only terms that survive are

$$\begin{aligned} -\frac{(1-s^2)}{1-rs} \left[\frac{(r-s)^2(1-s^2)}{(1-rs)ks^3} + \frac{1-r^2}{kr^3} \right] &= \\ -\frac{C_s}{\omega} \frac{1}{\alpha^2} i^3 (-(1-\alpha)^2 + 1) &= & F-30 \end{aligned}$$

$$i \frac{C_s \alpha^2 - 2\alpha}{\omega \alpha^2} = -i \frac{C_s (2 - \alpha)}{\omega \alpha}$$

Then

$$K''_{11}(0) = -i\rho C_s \omega \left[\left[\frac{C_s}{\omega} \right]^2 \left[\frac{2 - \alpha}{\alpha} \right] \right] \quad F-31$$

For the second diagonal term:

$$\begin{aligned} F'H \frac{1}{r} + FH' \frac{1}{r} + FH \left[\frac{1}{r} \right]' + F' \frac{1}{s} + F \left[\frac{1}{s} \right]' = \\ \frac{(1-s^2)(r-s)^2}{krs(1-rs)^2} \left[\frac{(r-s)^2}{1-rs} \frac{1}{r} + \frac{1}{s} \right] + \\ \frac{1-s^2}{1-rs} \left[\frac{(r-s)^2(r^2+s^2-2)}{kr^2s(1-rs)^2} - \frac{(r-s)^2(1-r^2)}{kr^3(1-rs)} - \frac{1-s^2}{ks^3} \right] \end{aligned} \quad F-32$$

Again, in the limit, only the last two terms survive:

$$\begin{aligned} -\frac{1}{\alpha} \left[\frac{i^2(\alpha-1)^2}{-i^2\alpha} \frac{(-\alpha^2 i^2)}{\alpha^3 i^3 \omega / C_s} + \frac{-i^2}{i^3 \omega / C_s} \right] = \\ -\frac{C_s}{\alpha \omega i^3} \left[-\frac{(1-\alpha)^2}{\alpha^2} + 1 \right] = -\frac{i C_s}{\alpha^3 \omega} (\alpha^2 - (1-\alpha)^2) = \\ -\frac{i C_s}{\alpha^3 \omega} (2\alpha - 1) = \frac{i C_s}{\alpha^3 \omega} (1 - 2\alpha) \end{aligned} \quad F-33$$

Then

$$K''_{22}(0) = i\omega\rho C_s \left[\left[\frac{C_s}{\omega} \right]^2 \frac{1}{\alpha^3} (1 - 2\alpha) \right] \quad F-34$$

The off-diagonal term is

$$F'H \frac{1}{rs} + FH' \frac{1}{rs} + FH \left[\frac{1}{rs} \right]' + F' \quad F-35$$

It can be shown that in the limit of $k \rightarrow 0$ all terms vanish. Hence

$$K''(0) = i\rho\omega C_s \left[\frac{C_s}{\omega} \right]^2 \frac{1}{\alpha^3} \begin{bmatrix} -\alpha^2(2-\alpha) \\ 1-2\alpha \end{bmatrix} \quad F-36$$

The paraxial approximation to the halfspace impedance matrix is then

$$K(k) \simeq i\omega\rho C_s \begin{bmatrix} 1 & \\ & 1/\alpha \end{bmatrix} + G \frac{(1-2\alpha)}{\alpha} k \begin{bmatrix} & 1 \\ 1 & \end{bmatrix} + i \frac{G C_s}{2\alpha\omega} k^2 \begin{bmatrix} -(2-\alpha) & \\ & (1-2\alpha)/\alpha^2 \end{bmatrix} \quad F-37$$

Appendix G

Proof that the Paraxial Approximation is Consistent with the Clayton-Engquist Approximation

In this appendix, it is shown that the paraxial approximation of the halfspace stiffness derived in Chapter 3 is consistent with the paraxial approximation of the wave equation employed as an absorbing boundary by Clayton and Engquist (1977). The paper cited above shall be referred to as C-E in the following sections.

G.1 Anti-plane Case

G.1.1 Clayton-Engquist Method

The differential equation for anti-plane motion is

$$\frac{\partial^2 v}{\partial x^2} + \frac{\partial^2 v}{\partial z^2} = \frac{1}{C_s^2} v \quad G-1$$

If we assume a solution of the form

$$v = A e^{i(\omega t - k_x x - k_z z)} \quad G-2$$

then the dispersion relation is

$$\omega = C_s (k_x^2 + k_z^2)^{1/2} \quad G-3$$

Solving Equation G-3 for k_z gives

$$k_z = \pm (\omega/C_s) (1 - (C_s^2 k_x^2/\omega^2))^{1/2} \quad G-4$$

When $|C_s k_x/\omega| > 1$, k_z is imaginary. This corresponds to evanescent waves, which are physically impossible in the undamped halfspace. In C-E, solutions to the wave equation are restricted to

paraxial waves by expanding the right-hand side of Equation G-4 about small $C_s k_x/\omega$. This can be accomplished with any rational expansion, including a Taylor series. Approximation A2 of C-E is the second-order Taylor series expansion (here we choose the negative root of G-4 for consistency with the coordinate system of this paper):

$$\frac{C_s k_z}{\omega} = -\left[1 - \frac{1}{2}(C_s k_x/\omega)^2\right] \quad G-5$$

G.1.2 Stiffness Method

Now consider the paraxial approximation of the stiffness presented in this paper for the anti-plane case:

$$\tau_{yz} = G \frac{\partial v}{\partial z} = i\omega\rho C_s \left[1 - \frac{1}{2}(C_s k_x/\omega)^2\right] \quad G-6$$

The exponential dependence of v on z implies that the derivative of v with respect to z is equivalent to multiplication by $-ik_z$:

$$\frac{\partial v}{\partial z} = -ik_z v \quad G-7$$

Substituting G-7 into the paraxial approximation gives:

$$G(-ik_z)v = i\omega\rho C_s \left[1 - \frac{1}{2}(C_s k_x/\omega)^2\right] \quad G-8$$

Simplifying this expression gives

$$G k_z = -\omega\rho C_s \left[1 - \frac{1}{2}(C_s k_x/\omega)^2\right]$$

$$\frac{G}{\omega\rho C_s} k_z = -\left[1 - \frac{1}{2}(C_s k_x/\omega)^2\right] \quad G-9$$

$$\frac{C_s k_z}{\omega} = -\left[1 - \frac{1}{2}(C_s k_x/\omega)^2\right]$$

which is identical to Equation G-5.

G.2 In-plane Case

G.2.1 Clayton-Engquist Method

Let the vector of displacements be denoted by $U (= \{u, w\}^T)$. In matrix form, the wave equation is

$$\frac{\partial^2 U}{\partial t^2} = D_1 \frac{\partial^2 U}{\partial x^2} + H \frac{\partial^2 U}{\partial x \partial z} + D_2 \frac{\partial^2 U}{\partial z^2} \quad G-10$$

where

$$\begin{aligned} D_1 &= \begin{bmatrix} C_p^2 & \\ & C_s^2 \end{bmatrix} \\ D_2 &= \begin{bmatrix} C_s^2 & \\ & C_p^2 \end{bmatrix} \\ H &= (C_p^2 - C_s^2) \begin{bmatrix} 0 & 1 \\ 1 & 0 \end{bmatrix} \end{aligned} \quad G-11$$

The Fourier transform of Equation G-10 is

$$[I - D_1(k_x/\omega)^2 - H(k_x/\omega)(k_z/\omega) - D_2(k_z/\omega)^2] U(\omega, k_x, k_z) = 0 \quad G-12$$

Consider this form of an approximation:

$$\frac{\partial^2 U}{\partial t \partial z} + C_1 \frac{\partial^2 U}{\partial t^2} + C_2 \frac{\partial^2 U}{\partial t \partial x} + C_3 \frac{\partial^2 U}{\partial x^2} = 0 \quad G-13$$

The Fourier transform of the approximation is

$$U(k_z/\omega) = [C_1 - C_2(k_x/\omega) + C_3(k_x/\omega)^2] U \quad G-14$$

Substituting Equation G-14 into G-13 gives

$$[I - D_1(k_x/\omega)^2 - (k_x/\omega)H[C_1 - C_2(k_x/\omega) + C_3(k_x/\omega)^2] - D_2[C_1 - C_2(k_x/\omega) + C_3(k_x/\omega)^2]^2] U = 0 \quad G-15$$

We can solve for the matrices in the approximation by matching the powers of (k_x/ω) . Matching the constant terms gives

$$I - D_2 C_1^2 = 0 \quad G-16$$

$$C_1 = D_2^{-1/2} = \begin{bmatrix} 1/C_s \\ 1/C_p \end{bmatrix}$$

Matching the linear terms gives

$$-HC_1 + D_2 (C_1 C_2 + C_2 C_1) = 0$$

$$C_1 C_2 + C_2 C_1 = D_2^{-1} H C_1 \quad G-17$$

$$C_1 C_2 C_1^{-1} + C_2 = D_2^{-1} H = (C_p^2 - C_s^2) \begin{bmatrix} 0 & 1/C_s^2 \\ 1/C_p^2 & 0 \end{bmatrix}$$

Assume that

$$C_2 = \begin{bmatrix} a & b \\ c & d \end{bmatrix} \quad G-18$$

Then substituting G-18 into G-17 gives

$$C_1 C_2 C_1^{-1} + C_2 = \begin{bmatrix} 1/C_s \\ 1/C_p \end{bmatrix} \begin{bmatrix} a & b \\ c & d \end{bmatrix} \begin{bmatrix} C_s & \\ & C_p \end{bmatrix} + \begin{bmatrix} a & b \\ c & d \end{bmatrix} \quad G-19$$

$$\begin{bmatrix} a & C_p b/C_s \\ C_s c/C_p & d \end{bmatrix} + \begin{bmatrix} a & b \\ c & d \end{bmatrix} = (C_p^2 - C_s^2) \begin{bmatrix} 1/C_s^2 \\ 1/C_p^2 \end{bmatrix}$$

It follows then that

$$2a = 0 \quad \rightarrow \quad a = 0 \quad 2d = 0 \quad \rightarrow \quad d = 0$$

$$(C_p/C_s + 1) b = \frac{C_p^2 - C_s^2}{C_s^2} \quad \rightarrow \quad b = \frac{C_p - C_s}{C_s} \quad G-20$$

$$(C_s/C_p + 1) c = \frac{C_p^2 - C_s^2}{C_p^2} \quad \rightarrow \quad c = \frac{C_p - C_s}{C_p}$$

Then

$$C_2 = (C_p - C_s) \begin{bmatrix} 0 & 1/C_s \\ 1/C_p & 0 \end{bmatrix} \quad G-21$$

which differs in sign from the C_2 matrix of C-E. Matching terms in $(k/\omega)^2$ gives

$$-D_1 + HC_2 - D_2 (C_2^2 + C_1C_3 + C_3C_1) = 0 \quad G-22$$

$$C_1C_3 + C_3C_1 = D_2^{-1} (HC_2 - D_1) - C_2^2$$

The right-hand side of the equation above is

$$\begin{aligned} & \left[\frac{C_s^2 - C_p C_s - C_p^2}{C_p C_s} \quad \frac{C_p^2 - C_s C_p - C_s^2}{C_p C_s} \right] - \\ & \left[\frac{C_p^2 - 2C_p C_s + C_s^2}{C_p C_s} \quad \frac{C_p^2 - 2C_s C_p + C_s^2}{C_p C_s} \right] = \\ & \left[\frac{C_s - 2C_p}{C_s} \quad \frac{C_p - 2C_s}{C_p} \right] \end{aligned} \quad G-23$$

Since C_1 is diagonal, C_3 must also be diagonal. Then

$$C_3 = \frac{1}{2} \begin{bmatrix} C_s - 2C_p & \\ & C_p - 2C_s \end{bmatrix} \quad G-24$$

Substituting $\alpha = C_s/C_p$, we have the matrices

$$\begin{aligned} C_1 &= \frac{1}{C_s} \begin{bmatrix} 1 & \\ & \alpha \end{bmatrix} \\ C_2 &= \frac{1-\alpha}{\alpha} \begin{bmatrix} 1 & \\ & \alpha \end{bmatrix} \\ C_3 &= \frac{C_p}{2} \begin{bmatrix} \alpha - 2 & \\ & 1 - 2\alpha \end{bmatrix} \end{aligned} \quad G-25$$

G.2.2 Stiffness Method

The paraxial approximation of this paper was derived with a coordinate system where the z axis is positive upwards, away from the halfspace. On the other hand, the C-E approximation was derived with the reverse coordinate system, with the z coordinate increasing into the halfspace (i.e. "down"). Thus the diagonal elements of the stiffness matrix must be reversed in sign. The

paraxial approximation of the stiffness is then

$$\begin{aligned} \begin{bmatrix} \tau_{xz} \\ \sigma_z \end{bmatrix} &= \begin{bmatrix} -i\omega\rho C_p \\ \alpha & 1 \end{bmatrix} + ikG \frac{1-2\alpha}{\alpha} \begin{bmatrix} & 1 \\ -1 & \end{bmatrix} \\ &\quad - \frac{ik^2GC_s}{2\alpha\omega} \begin{bmatrix} \alpha-2 & \\ & (1-2\alpha)/\alpha^2 \end{bmatrix} \end{bmatrix} U \end{aligned} \quad G-26$$

In terms of the displacement vector U , the stress vector is

$$\begin{bmatrix} \tau_{xz} \\ \sigma_z \end{bmatrix} = \begin{bmatrix} G \\ \lambda \end{bmatrix} \frac{\partial U}{\partial x} + \begin{bmatrix} G \\ \lambda+2G \end{bmatrix} \frac{\partial U}{\partial z} \quad G-27$$

We substitute Equation G-27 for the stress vector in Equation G-26 and multiply through by $i\omega$.

Then we interpret $i\omega$ as derivation with respect to t and $-ik$ as derivation with respect to x .

$$\begin{aligned} \begin{bmatrix} G \\ \lambda \end{bmatrix} \frac{\partial^2 U}{\partial x \partial t} + \begin{bmatrix} G \\ \lambda+2G \end{bmatrix} \frac{\partial^2 U}{\partial z \partial t} &= \\ \begin{bmatrix} -\rho C_p \\ \alpha & 1 \end{bmatrix} \frac{\partial^2 U}{\partial t^2} - G \frac{1-2\alpha}{\alpha} \begin{bmatrix} & 1 \\ -1 & \end{bmatrix} \frac{\partial^2}{\partial x \partial t} & \\ - \frac{GC_p}{2} \begin{bmatrix} \alpha-2 & \\ & (1-2\alpha)/\alpha^2 \end{bmatrix} \frac{\partial^2 U}{\partial x^2} & \end{aligned} \quad G-28$$

Then, rearranging terms and dividing by $\lambda+2G$, we obtain

$$\begin{aligned} \begin{bmatrix} \alpha^2 \\ & 1 \end{bmatrix} \frac{\partial^2 U}{\partial z \partial t} &= -\frac{1}{C_p} \begin{bmatrix} \alpha \\ & 1 \end{bmatrix} \frac{\partial^2 U}{\partial t^2} - \\ (1-\alpha) \begin{bmatrix} & \alpha \\ & 1 \end{bmatrix} \frac{\partial^2 U}{\partial x \partial t} - \frac{C_p}{2} \begin{bmatrix} \alpha^2(\alpha-2) & \\ & 1-2\alpha \end{bmatrix} \frac{\partial^2 U}{\partial x^2} & \end{aligned} \quad G-29$$

The approximation of the differential equation is

$$\frac{\partial^2 U}{\partial z \partial t} = -\frac{1}{C_s} \begin{bmatrix} 1 & \\ & \alpha \end{bmatrix} \frac{\partial^2 U}{\partial t^2} - \frac{(1-\alpha)}{\alpha} \begin{bmatrix} & 1 \\ \alpha & \end{bmatrix} \frac{\partial^2 U}{\partial x \partial t} - \frac{C_p}{2} \begin{bmatrix} \alpha-2 & \\ & 1-2\alpha \end{bmatrix} \frac{\partial^2 U}{\partial x^2} \quad G-30$$

Comparing Equation G-30 with Equation G-13 and the matrices give in Equation G-25, we can see that these paraxial approximations are identical.

References

- Abramowitz, A. and I.A. Stegun. *Handbook of Mathematical Functions*. New York: Dover, 1972.
- Aki, K. and P.G. Richards. *Quantitative Seismology, Theory and Methods*. San Francisco: W.H. Freeman and Company, 1980.
- Alekseyev, A.S. and B.G. Mikhaylenko. Solution of Lamb's Problem for a Vertically Inhomogeneous Elastic Halfspace. *Akad. Nauk Izu. Physics of the Solid Earth*, 1976/1977, 12(1) 748-755.
- Anderson, D.L. Elastic Wave Propagation in Layered Anisotropic Media. *J. Geophys. Res.*, 1961, 66(9) 2953-2963.
- Apse, R.J. and J.E. Luco. On the Green's Functions for a Layered Halfspace, Part II. *Bull. Seism. Soc. Am.*, 1983, 73(4) 931-951.
- Awojobi, A.O. Vertical Vibration of a Rigid Circular Foundation on Gibson Soil. *Géotechnique*, 1972, 22(2) 333-343.
- Awojobi, A.O. The Invariance of Gibson's Law for a Stratum on a Frictionless Base. *Géotechnique*, 1974, 24(3) 359-366.
- Båth. *Introduction to Seismology*. Boston: Birkhäuser Verlag, 1979. 2nd edition.
- Barden, L. Stresses and Displacements in a Cross-anisotropic Soil. *Géotechnique*, 1963, 13(1) 198-210.
- Biot, M.A. *Mechanics of Incremental Deformations*. New York: John Wiley & Sons, 1965.
- Biot, M.A. Fundamentals of Generalized Rigidity Matrices for Multi-layered Media. *Bull. Seism. Soc. Am.*, 1983, 73(3) 749-763.
- Boas, M.L. *Mathematical Methods in the Physical Sciences*. New York: John Wiley & Sons, 1966.
- Bouchon, M. A Simple Method to Calculate Green's Functions for Elastic Layered Media. *Bull. Seism. Soc. Am.*, 1981, 71(4) 959-971.
- Brekovskih, L.M. *Waves in Layered Media*. New York: Academic Press, 1980. 2nd edition. Translated by R.T. Beyer.
- Bullen, K.E. *An Introduction to the Theory of Seismology*. Cambridge, England: Cambridge Press, 1963.
- Burminster, D.M. The General Theory of Stresses and Displacements in Layered Systems. *J. Appl. Phys.*, 1945, 16(1) 89-94, 126-127, 296-302.

- Cagniard, L. *Reflection and Refraction of Progressive Seismic Waves*. New York: McGraw-Hill, 1962. Translated by E.A. Flinn and C.H. Dix.
- Clayton, R. and B. Engquist. Absorbing Boundary Conditions for Acoustic and Elastic Wave Equations. *Bull. Seism. Soc. Am.*, 1977, 67(6) 1529-1540.
- Crampin, S. The Dispersion of Surface Waves in Multilayered Anisotropic Media. *Geophys. J. R. astr. Soc.*, 1970, 21(1) 387-402.
- Crampin, S. and E.M. Chesnokov and R.G. Hipkin. Seismic Anisotropy--the State of the Art: II. *Geophys. J. R. astr. Soc.*, 1984, 76(1) 1-16.
- Crampin, S. Effective Anisotropic Elastic Constants for Wave Propagation through Cracked Solids. *Geophys. J. R. astr. Soc.*, 1984, 76(1) 135-145.
- Crampin, S. An Introduction to Wave Propagation in Anisotropic Media. *Geophys. J. R. astr. Soc.*, 1984, 76(1) 17-28.
- Davies, T.G. and P.K. Banerjee. The Displacement Field due to a Point Load at the Interface of a Two Layer Elastic Half-space. *Géotechnique*, 1978, 28(1) 43-56.
- Davies, T.G. and P.K. Banerjee. *Elasto-Dynamic Green's Functions for a Halfspace*. Technical Report GT/1983/1, Department of Civil Engineering, SUNY/Buffalo, 1983.
- deHoop, A.T. A Modification of Cagniard's Method of Solving Seismic Pulse Problems. *Appl. Sci. Res.*, 1960, 8(1) 349-356.
- Dix, C.H. The Method of Cagniard in Seismic Pulse Problems. *Geophys.*, 1954, 19(4) 722-738.
- Drake, L.A. Love and Rayleigh Waves in Non-horizontally Layered Media. *Bull. Seism. Soc. Am.*, 1972, 62(5) 1241-1258.
- Dunkin, J.W. Computation of Modal Solutions in Layered Elastic Media at High Frequencies. *Bull. Seism. Soc. Am.*, 1965, 55(2) 335-358.
- Erdélyi, A. (Editor). *Tables of Integral Transforms*. New York: McGraw-Hill, 1954. Bateman Manuscript Project.
- Ewing, W., W.S. Jardetzky and F. Press. *Elastic Waves in Layered Media*. New York: McGraw-Hill, 1957.
- Gazetas, G. Static and Dynamic Displacements of Foundations on Heterogeneous Multilayered Soils. *Géotechnique*, 1967, 30(2) 159-177.
- Gerrard, C.M. Stresses and Displacements in Layered Cross-anisotropic Elastic Systems. *Proceedings of the Fifth Australia-New Zealand Conference on Soil Mechanics and Foundation Engineering*, 1967, 187-197.
- Gibson, R.E. Some Results Concerning Displacements and Stresses in a Non-homogeneous Elastic Half-space. *Géotechnique*, 1967, 17(1) 58-67.
- Graff, K.F. *Wave Motion in Elastic Solids*. Ohio State University Press, 1975.

- Harkrider, D.G. Surface Waves in Multilayered Elastic Media, Rayleigh and Love Waves from Buried Sources in a Multilayered Elastic Half-space. *Bull. Seism. Soc. Am.*, 1964, 54(2) 627-679.
- Haskell, N.A. The Dispersion of Surface Waves on Multilayered Media. *Bull. Seism. Soc. Am.*, 1953, 4317-34.
- Haskell, N.A. Radiation Pattern of Surface Waves from Point Sources in a Multi-layered Medium. *Bull. Seism. Soc. Am.*, 1964, 54(1) 377-393.
- Hull, S.W. and E. Kausel. Dynamic Loads in Layered Halfspaces. *Proceedings of the Fifth ASCE EMD Specialty Conference*, 1984, 201-204. University of Wyoming, Laramie, Wyoming.
- Johnson, L.R. Green's Function for Lamb's Problem. *Geophys. J. R. astr. Soc.*, 1974, 37(1) 99-131.
- Kausel, E. *Forced Vibrations of Circular Foundations on Layered Media*. Technical Report R74-11, Soil Publication No. 336, Department of Civil Engineering, M.I.T., 1974.
- Kausel, E. *An Explicit Solution for the Green's Functions for Dynamic Loads in Layered Media*. Technical Report R81-13, Department of Civil Engineering, M.I.T., May 1981.
- Kausel, E. and J.M. Roësset. Stiffness Matrices for Layered Soils. *Bull. Seism. Soc. Am.*, 1981, 71(6) 1743-1761.
- Kausel, E. and R. Peek. *Boundary Integral Method for Stratified Soils*. Technical Report R82-50, Department of Civil Engineering, M.I.T., June 1982.
- Kausel, E. and R. Peek. Dynamic Loads in the Interior of a Layered Stratum: an Explicit Solution. *Bull. Seism. Soc. Am.*, 1982, 72(5) 1459-1481.
- Kausel, E. Wave Propagation in Anisotropic Layered Media. Unpublished manuscript, 1984.
- Kirkner, D.J. *Steady State Response of a Circular Foundation on a Transversely Isotropic Medium*. PhD thesis, Case Western Reserve University, 1979.
- Knopoff, L. A Matrix Method for Elastic Wave Problems. *Bull. Seism. Soc. Am.*, 1964, 54(1) 431-438.
- Love, A.E.H. *A Treatise on the Mathematical Theory of Elasticity*. New York: Dover, 1944. 4th edition.
- Love, A.E.H. *Some Problems of Geodynamics*. New York: Dover, 1967.
- Luco, J.E. and R.J. Apsel. On the Green's Functions for a Layered Halfspace, Part I. *Bull. Seism. Soc. Am.*, 1983, 73(4) 909-929.
- Lysmer, J. and G. Waas. Shear Waves in Plane Infinite Structures. *J. Eng. Mech. Div., ASCE*, 1972, 18(1) 85-105.
- Mitchell, B.J. On the Inversion of Love- and Rayleigh-wave Dispersion and Implications for Earth Structure and Anisotropy. *Geophys. J. R. astr. Soc.*, 1984, 76(1) 233-241.

- Pan, Y.-C. and T.-W. Chou. Point Force Solution for an Infinite Transversely Isotropic Solid. *J. Appl. Mech.*, 1976, 48(1) 608-612.
- Pan, Y.-C. and T.-W. Chou. Green's Function Solutions for Semi-infinite Transversely Isotropic Materials. *Int. J. Engng. Sci.*, 1979, 17(5) 545-551.
- Pao, Yih-Hsing. Elastic Waves in Solids. *Trans. of the ASME Jour. of Appl. Mech.*, 1983, 50(1) 1152-1164.
- Pinney, E. Surface Motion due to a Point Source in a Semi-infinite Elastic Medium. *Bull. Seism. Soc. Am.*, 1954, 44(1) 571-596.
- Poulos, H.G. and E.H. Davis. *Elastic Solutions for Soil and Rock Mechanics*. New York: John Wiley & Sons, 1974.
- Roësset, J.M. and E. Kausel. *Fundamentals of Wave Propagation*. Class notes, 1980.
- Rowe, R.K. and J.R. Booker. Finite Layer Analysis of Nonhomogeneous Soils. *J. Eng. Mech. Div., ASCE*, 1982, 108(1) 115-132.
- Rowe, R.K. and J.R. Booker. *Deformation Analysis for Periodically Layered Soil*. Technical Report R455, School of Civil and Mining Engineering, The University of Sydney, July 1983.
- Schlue, J.W. Finite Element Matrices for Seismic Surface Waves in Three-dimensional Structures. *Bull. Seism. Soc. Am.*, 1979, 69(5) 1425-1437.
- Spiegel, M.R. *Schaum's Outline Series. Mathematical Handbook of Formulas and Tables*. New York: McGraw-Hill, 1968.
- Stoneley, R. The Seismological Implications of Anisotropy in Continental Structure. *Monthly Notices of the Roy. astr. Soc.*, 1949, 5(1) 343-353.
- Tassoulas, J.L. *Elements for the Numerical Analysis of Wave Motion in Layered Media*. Technical Report R81-2, Department of Civil Engineering, M.I.T., February 1981.
- Thomson, W.T. Transmission of Elastic Waves through a Stratified Solid Medium. *J. Appl. Phys.*, 1950, 21(1) 89-93.
- Ueshita, K. and G.G. Meyerhof. Deflection of Multilayer Soil Systems. *Jour. of Soil Mech. and Found. Div., ASCE*, 1967, SM5257-282.
- Waas, G. *Linear Two-dimensional Analysis of Soil Dynamics Problems in Semi-infinite Layered Media*. PhD thesis, University of California, Berkeley, 1972.
- White, J.E. *Seismic Waves: Radiation, Transmission and Attenuation*. New York: McGraw-Hill, 1965.
- White, J.E. Computed Waveforms in Transversely Isotropic Media. *Geophysics*, 1982, 47(5) 771-783.
- Whittaker, W.L. and P. Christiano. *Dynamic Response of Flexible Plates Bearing on an Elastic Half-space*. Technical Report RP-125-9-79, Department of Civil Engineering, Carnegie-Mellon

University, 1979.

Zurmühl, R. *Matrizen und ihre technischen Anwendungen*. Berlin: Springer-Verlag, 1964.